Stockholm University

Delving in the Dark

Searching for Signatures of Non-Standard Physics in Cosmological and Astropyhsical Observables

Janina J. Renk

Doctoral Thesis in Theoretical Physics at Stockholm University, Sweden 2020

Delving in the Dark

Searching for Signatures of Non-Standard Physics in Cosmological and Astrophysical Observables

Janina. J. Renk

Academic dissertation for the Degree of Doctor of Philosophy in Theoretical Physics at Stockholm University to be publicly defended on Friday 11 September 2020 at 13.00 in sal FB42, AlbaNova universitetscentrum, Roslagstullsbacken 21.

Abstract

The dark sectors of our Universe, *dark matter* and *dark energy*, together constitute about 96 % of the total energy content of the Universe. To date, we only have observational evidence for their existence. What is still lacking is a complete theoretical framework consistent with all observational data to embed a dark matter particle or component into the standard models of particle physics and cosmology, as well as an explanation for the nature or origin of dark energy.

Since the discovery of these dark components decades ago, a variety of different theories have been proposed to overcome the shortcomings of our current standard models. To assess the viability of these non-standard theories, they ideally should be tested against all relevant available datasets. In this thesis, I show two examples of how cosmological and astrophysical observables are used to constrain or even rule out non-standard cosmological models. Further, I present the first software tool that provides a general framework to test non-standard physics with global fits to data from particle physics and cosmology simultaneously.

The first example is minimally coupled covariant Galileons, a modification of General Relativity to explain dark energy without the need for a fine-tuned cosmological constant. I demonstrate how the combination of constraints arising from the integrated Sachs-Wolf effect and the propagation speed of gravitational waves can rule out all three branches of the theory.

The second example shows how the existence and parameter space of cosmic superstrings can be constrained. These are the hypothesised fundamental building blocks of Type IIb Superstring theory, stretched out to cosmological scales during the phase of inflation. The theory can be tested through the unique microlensing signature of cosmic superstrings when crossing the line of sight of an observer monitoring a point-like source. I show how, based on simulations, we can estimate the expected detection rates from observations of distant Type Ia Supernovae and stars in Andromeda; from these estimates I assess the implications for the theory.

Finally, I present CosmoBit, a new module for the Global and Modular Beyond-Standard Model Inference Tool (GAMBIT). \gambit allows the user to test a variety of extensions to the Standard Model of particle physics against data from, e.g. collider searches, dark matter direct and indirect detection experiments, as well as laboratory measurements of neutrino properties. CosmoBit augments this with the inclusion of cosmological likelihoods. This addition opens up the possibility to test a given model against data from, e.g. the Big Bang Nucleosynthesis proceeding minutes after the Big Bang, probes of the Cosmic Microwave Background ~ 380,000 years later, and (laboratory) measurements from the present day, 13.8 billion years after the Big Bang. Including measurements that span several different epochs and orders of magnitude in energy, the combination of CosmoBit with other GAMBIT modules provides a promising tool for shedding light on the dark sectors of the Universe.

Keywords: *cosmology, gravitation, Galileon, dark energy, dark matter, cosmic superstrings, neutrino mass, parameter inference.*

Stockholm 2020
http://urn.kb.se/resolve?urn=urn:nbn:se:su:diva-182445

ISBN 978-91-7911-108-3
ISBN 978-91-7911-109-0

Department of Physics

Stockholm University, 106 91 Stockholm

DELVING IN THE DARK

Janina J. Renk

Stockholm
University

Delving in the Dark

Searching for Signatures of Non-Standard Physics in Cosmological and Astropyhsical Observables

Janina J. Renk

ISBN print 978-91-7911-108-3
ISBN PDF 978-91-7911-109-0

Cover Illustration by Basset & Baki Kouba
Printed in Sweden by Universitetsservice US-AB, Stockholm 2020

To everyone who's
been told
"*You can't make it*"
a thousand times.

You can.

Abstract

The dark sectors of our Universe, *dark matter* and *dark energy*, together constitute about 96% of the total energy content of the Universe. To date, we only have observational evidence for their existence. What is still lacking is a complete theoretical framework consistent with all observational data to embed a dark matter particle or component into the standard models of particle physics and cosmology, as well as an explanation for the nature or origin of dark energy.

Since the discovery of these dark components decades ago, a variety of different theories have been proposed to overcome the shortcomings of our current standard models. To assess the viability of these non-standard theories, they ideally should be tested against all relevant available datasets. In this thesis, I show two examples of how cosmological and astrophysical observables are used to constrain or even rule out non-standard cosmological models. Further, I present the first software tool that provides a general framework to test non-standard physics with global fits to data from particle physics and cosmology simultaneously.

The first example is minimally coupled covariant Galileons, a modification of General Relativity to explain dark energy without the need for a fine-tuned cosmological constant. I demonstrate how the combination of constraints arising from the integrated Sachs-Wolf effect and the propagation speed of gravitational waves can rule out all three branches of the theory.

The second example shows how the existence and parameter space of cosmic superstrings can be constrained. These are the hypothesised fundamental building blocks of Type IIb Superstring theory, stretched out to cosmological scales during the phase of inflation. The theory can be tested through the unique microlensing signature of cosmic superstrings when crossing the line of sight of an observer monitoring a point-like source. I show how, based on simulations, we can estimate the expected detection rates from observations of distant Type Ia Supernovae and stars in Andromeda; from these estimates I assess the implications for the theory.

Finally, I present CosmoBit, a new module for the Global and Modular Beyond-Standard Model Inference Tool (GAMBIT). GAMBIT allows the user to test a variety of extensions to the Standard Model of particle physics against data from, e.g. collider searches, dark matter direct and indirect detection experiments, as well as laboratory measurements of neutrino properties. CosmoBit augments this with the inclusion of cosmological likelihoods. This addition opens up the possibility to test a given model against data from, e.g. the Big Bang Nucleosynthesis proceeding minutes after the Big Bang, probes of the Cosmic Microwave Background $\sim 380,000$ years later, and (laboratory) measurements from the present day, 13.8 billion years after the Big Bang. Including measurements that span several different epochs and orders of magnitude in energy, the combination of CosmoBit with other GAMBIT modules provides a promising tool for shedding light on the dark sectors of the Universe.

Svensk Sammanfattning

De mörka sektorerna i vårt universum, mörk materia och mörk energi, utgör tillsammans ungefär 96% av universums totala energiinnehåll. Hittills har vi bara observationella bevis för deras existens. Det som fortfarande saknas är en fullständig teoretisk ram som överensstämmer med alla observationsdata för att inbegripa en partikel eller komponent av mörk materia i standardmodeller av partikelfysik och kosmologi, samt en förklaring till naturen eller ursprunget av mörk energi.

Sedan dessa mörka komponenter upptäcktes för årtionden sedan, har en mängd olika teorier föreslagits för att övervinna bristerna i våra nuvarande standardmodeller. För att bedöma användbarheten hos dessa icke-standardteorier bör de helst testas mot alla relevanta tillgängliga data. I denna avhandling visar jag två exempel på hur kosmologiska och astrofysiska observationer kan användas för att begränsa eller till och med utesluta teorier bortom standardmodellen. Dessutom presenterar jag för första gången mjukvara som kan ge en allmän ram som testar icke-standardfysik med globala anpassningar för data från partikelfysik och kosmologi.

Det första exemplet är minimalt kopplade kovarianten Galileons, en modifiering av allmänna relativitetsteorin för att modellera mörk energi utan behov av en fininställd kosmologisk konstant. Jag demonstrerar hur kombinationen av begränsningar från den integrerade Sachs-Wolf effekten och utbredningshastigheten av gravitationsvågor kan utesluta alla tre grenar av teorin.

Det andra exemplet visar hur existensen och parametern som rymmer kosmiska supersträngar kan begränsas. Dessa är de grundläggande byggstenarna i Type IIb supersträngteori som sträckte sig till kosmologiska skalor under inflationsfasen. Teorin kan testas genom den unika mikrolinsningssignaturen för kosmiska supersträngar när de passerar siktlinjen för en observatör som övervakar en punktliknande källa. Baserat på simuleringar uppskattas förväntade antal detektioner från observationer av de avlägsna typ Ia supernovor och av stjärnor i Andromeda och från dessa uppskattningar bedömer jag konsekvenserna för teorin.

Slutligen presenterar jag CosmoBit, en ny modul för GAMBIT, the Global and Modular Beyond-Standard-Model Inference Tool. GAMBIT tillåter användaren att testa en mängd olika utvidgningar till standardmodeller för partikelfysik mot data från till exempel accelerator sökningar, direkta och indirekta detektionsförsöker efter mörk materia, liksom laboratorie mätningar av neutrinoegenskaper. CosmoBit har utvidgat detta genom att inkludera den kosmologiska sannolikheten. Denna utökning öppnar upp möjligheten att testa en given modell mot data från till exempel Big Bang Nukleosyntes som fortsätter minuter efter Big Bang, sonder för kosmiska bakgrundsstrålningen $380,000$ år senare och laboratorie mätningar från idag, 13.8 miljarder år efter Big Bang. Inklusive mätningar som sträcker sig över flera storleksordningar i energi och olika epoker, CosmoBit visar sig vara ett lovande verktyg för att belysa universums mörka sektorer.

List of Included Papers

The following papers are included in the thesis. They are referred to by the corresponding letter in the text.

A *Galileon Gravity in Light of ISW, CMB, BAO and H_0 Data*
Janina Renk, Miguel Zumalacárregui, Francesco Montanari, Alexandre Barreira, *JCAP*, **1710**, 20 (2017).
DOI: 10.1088/1475-7516/2017/10/020, [arXiv: 1707.02263].

B *Prospects of Cosmic Superstring Detection through Microlensing of Extragalactic Point-Like Sources*
David F. Chernoff, Ariel Goobar, Janina J. Renk *MNRAS*, **491** (2020) no. 1, 596-614.
DOI: 10.1093/mnras/stz2855, [arXiv: 1905.03796].

Acknowledgements

I would like to thank Katherine Freese for giving me the freedom to work on a topic I am passionate about and for financially supporting my studies and this work. I am very grateful to my supervisors Pat Scott, Felix Kahlhöfer, and Joakim Edsjö for unexpectedly taking me up as their student. Thank you for your guidance and support during the last years and for always having looked out for my interests. I am deeply indebted to Pat, thank you for your invaluable support during the process of writing this thesis. Furthermore, I want to thank all my collaborators and all members of the GAMBIT community and SNOVA group. Thank you, Alexandre Barreira, Ariel Goobar, Francesco Montanari and Miguel Zumalacárregui for our great collaborations. I have learned a lot from you, and really appreciate your time, guidance, and patience.

Working on a PhD is not all roses. So I am incredibly grateful to my mentor Kerstin Jon-And for being there for me during the challenging times. Thank you for your counsel, for encouraging me, and for believing in me. I am also deeply grateful to all my collaborators who have always treated me with respect, heard my voice, and, when others didn't, encouraged me. My special thanks goes to Miguel Zumalacárregui. Thank you for being a great mentor, teacher and friend. Without your enthusiasm in mentoring me during my master's project and without your encouragement I never would have thought about starting a PhD. And Sanjay. Thank you for always being there for me, cheering me up, and for never getting tired of listening to me complain. You have been way better than any army of penguins could ever be. Thank you.

I would further like to thank all my colleges in the Oscar Klein Centre at Stockholm University, as well as all members of the Astrophysics groups at Imperial College and the University of Queensland for providing a fun and stimulating work environment. Many thanks to Alex for distracting me by planning (fun) events, Anders for the great culture nights, Eliel for making working late hours fun, Suhail for all the delicious chai fikas (*namaste behan ch..ai*), and of course, all members of the SKUIRROLL collaboration. Especially to Sémili, thank you very much for your help with the Svensk Sammanfattning. And of course, a special thanks to all my office mates along the way: Adri and Sunny (may Gaunt rest in piece), Binnie, Conor, Marjia, Sanjay, Sebastian, and Selim, it's been a pleasure sharing 1109 and the bit with you, and Gian, Jace, and Oli, thank you for the delicious Thursday cakes and Tim Tam slams!

While working on my PhD I moved to four different countries on three continents, with a gigantic tea mug as my only steady companion. The circumstances haven't always been easy, so I am incredibly grateful to have a family and friends who have put up with me despite rarely being around. Thank you, Laura, for all our adventures! Our travels have been the best breaks of all. Of course, a huge thanks also goes to Destiny Lions (and old juice lady) for watching out for us and for making it rain in the right places. Daniel and

Erik, it's been an honour to share an office, loads of Friday chocolate, Swedish lessons, cakes, and dinner nights with you. *Tack så mycket!*

Last but not least, die Leute, die mich schon am längsten kennen. Danke Dome, fürs Asyl im Paradies gewähren, wenn ich gestresst oder obdachlos war, und für die Notfall Computerreparatur via Ferndiagnose. Danke Janine, für all die Hilfspakete, den Motivationsgesang, und den essenziellen Monster Treibstoff für diese Arbeit. Lisa und Nina. Danke, dass ihr mich schon die Hälfte meines Lebens begleitet, und mich selbst am anderen Ende der Welt besucht habt. Mein besonderer Dank gilt meiner Familie. Ich kann nicht in Worte fassen, wie dankbar ich euch für eure Unterstützung, euren Rückhalt, und euer Verständnis in den letzten Jahren bin – ich weiß, man hat es nicht leicht mit so einem Physiker.

Janina J. Renk
Frankfurt, 16-07-2020

Preface

This doctoral thesis consists of three major parts: Part I is a general introduction to the relevant research topics. It contains a summary of two published scientific papers, which are included in Part III.

Part II contains the description of CosmoBit, a GAMBIT module for computing cosmological observables and likelihoods. GAMBIT, the Global and Modular Beyond-the-Standard Model Inference Tool, is a software tool designed to test various theories of physics beyond the Standard Model of particle physics. The addition of CosmoBit opens up the possibility to simultaneously test models against observations from particle physics and cosmology. My contributions to GAMBIT presented in this thesis are centred around cosmological aspects and problems. I will, therefore, not aim to give an introduction to nor review of theories beyond the Standard Model of particle physics. Instead, I will focus the discussion on cosmology. The paper associated with the release of CosmoBit has not been submitted for publication at the time of writing. Hence, Part II of this thesis is devoted to presenting the details of the project.

Parts of this thesis have been adopted from my Licentiate thesis 'Invalidation of Minimally Coupled Covariant Galileon Cosmologies'. This applies to section 2.3 − 2.7, and section 3.4 as well as 4.1.

I use the metric convention $(-,+,+,+)$ and natural units, in which $k_b = \hbar = c = 1$. The Planck mass is given by $M_{\rm Pl}^{-2} = 8\pi G$ and Greek indices run from 0 to 3, while Latin indices run from 1 to 3. Bars over quantities denote space averages except where otherwise indicated. The subscript 0 indicates the present value of a time-dependent quantity, i.e. $x(t_0) = x_0$.

Contents

Part II Project Summary

Part III Papers

The Author's Contribution

Paper A I led this analysis. I set up the pipeline to compare theoretical predictions of the integrated Sachs-Wolfe effect to various existing datasets. Francesco Montanari wrote section 2, the introduction on the spectra and observables we mainly used. Alexandre Barreira and Miguel Zumalacárregui are the main contributors to section 3 on covariant Galileons. Miguel Zumalacárregui ran and analysed the Monte Carlo Markov Chains leading to Table 1 and Figure 3. I produced the results from post-processing the Markov Chains and all remaining figures and tables, where Alexandre Barreira contributed to the computation of the likelihood from Baryonic Acoustic Oscillation data.

Paper B The idea for the project came from Ariel Goobar. The contact authors of the article are David F. Chernoff and me. David F. Chernoff provided a set of codes to carry out the simulations to estimate the microlensing events sourced by cosmic superstrings of stars in M31. I set up the pipeline to combine these codes and extended it to compute the lensing rates of SNe Ia. I produced all figures but the right panel of Figure 2. All results presented in the paper, except the simulations leading to Figure 6, have been produced by me. David F. Chernoff wrote the major part of the introductory chapters, $1-3$, as well as appendix A, B and E. The main contributions to chapter 4 and 5 came from Ariel Goobar. I was the main contributor to chapter 6 and 7 in the main text, and to Appendix C and D.

CosmoBit I lead this project together with Patrick Stöcker. Being a module of GAMBIT, CosmoBit was developed as a collaborative effort of the GAMBIT Cosmology Working group, consisting of Csaba Balasz, Sanjay Bloor, Torsten Bringmann, Tomas Gonzalo, Will Handley, Sebastian Hoof, Selim Hotinli, Felix Kahlhöfer, Pat Scott, Patrick Stöcker, Aaron Vincent, Martin White, and myself.

I joined the project at the stage where a basic version of CosmoBit includ-

ing an interface to CLASS, the Planck likelihoods (plc), the MultiModeCode, and DarkAges had already been implemented by Selim Hotinli and Patrick Stöcker. I re-designed the first three of these interfaces to enable a consistent treatment of different models and consistent communication between the codes. This re-design enabled the possibility to use MontePython likelihoods as a further external library. The implementation of the new interfaces to CLASS and MontePython were carried out by Sanjay Bloor and me. I implemented the interface to AlterBBN; the treatment of the relative covariance matrices was contributed by Patrick Stöcker. Sanjay Bloor, Sebastian Hoof, and Patrick Stöcker solved technicalities concerning the installation of the different external libraries on different systems. Decisions which physics models to include were the result of group discussions. The implementation was carried out by Patrick Stöcker and me. Patrick Stöcker ran the validation scans. The presentation of CosmoBit in Part II of this thesis is drawn upon the draft for the paper in preparation 'CosmoBit: A GAMBIT module for computing cosmological observables and likelihoods' authored by the GAMBIT Cosmology Working group. Further, section 3.1 closely follows the discussion from the paper draft.

Abbreviations

ΛCDM	Λ Cold Dark Matter, the concordance model of cosmology
νGal_3	cubic covariant Galileon with massive neutrinos
νGal_4	quartic covariant Galileon with massive neutrinos
νGal_5	quintic covariant Galileon with massive neutrinos
BAO	Baryonic Acoustic Oscillations
BBN	Big Bang Nucleosynthesis
BSM	Beyond the Standard Model
CDF	Cumulative Probability Distribution Function
CMB	Cosmic Microwave Background
CSS	Cosmic Superstring
DE	Dark Energy
DM	Dark Matter
EMC	Electromagnetic Counterpart
FLRW	Friedmann-Lemaître-Robertson-Walker
GAMBIT	The Globular and Modular Beyond-the-Standard-Model Inference Tool
GNCs	Galaxy Number Counts
GR	General Relativity
GUT	Grand Unified Theory
GW	Gravitational Wave
IGM	Intergalactic Medium
ISW	Integrated Sachs-Wolfe effect
MCMC	Markov Chain Monte Carlo
M31	Andromeda
MCMC	Monte Carlo Markov Chain
ML	Microlensing
MW	Milky Way

SNe Ia	Supernova Type Ia
SM	Standard Model of particle physics
UV	Ultraviolet
WISE	Wide-Field Infrared Survey Explorer

Chapter 1

Introduction

According to our current understanding the constituents of the Standard Model of particle physics only contribute 4% to the total energy content of our Universe. To account for the other 96% additional energy components labelled *dark matter* and *dark energy* are incorporated into the concordance model of cosmology. Dark matter (DM) is introduced to explain, e.g. the shape of galaxy rotation curves, gravitational lensing effects and structure formation. The inclusion of dark energy, on the other hand, is necessary to incorporate the observed late-time acceleration of the Universe into the concordance model of cosmology, ΛCDM. The model of ΛCDM stands for a Universe filled with collisionless cold dark matter (CDM) and a cosmological constant Λ driving the accelerated late-time expansion, where General Relativity (GR) governs the laws of gravity.[1]

To date the concordance model of cosmology has been extremely successful: with only six free parameters the model can fit measurements from three independent high-precision measurements yielding consistent result for the inferred parameter values [8, 9]. These datasets are the temperature anisotropy power spectrum of the Cosmic Microwave Background (CMB), distance measures from Type Ia Supernovae (SNe Ia), and the scale of Baryonic Acoustic Oscillations (BAO).[2] This agreement is especially remarkable when considering that the CMB spectrum probes epochs from $\sim 380,000$ years after the Big Bang, while SNe Ia are observed in the late Universe.

From an observational point of view, ΛCDM has received a slight setback in the past years: a tension emerged between different techniques to determine

[1] For textbook introductions and reviews on dark matter refer to Refs. [1–5]. See, e.g. Refs. [6, 7] for reviews on dark energy.

[2] See Ref. [10] for the constraints on ΛCDM including the latest measurements of the CMB from the Planck satellite.

the value of the present expansion rate of the Universe, the Hubble rate H_0. Different results have been obtained through either local measurements [11–16] or by means of the CMB power spectrum detected by the Planck satellite [10, 17]. Possible sources for this inconsistency between early- and late-time measurements can be systematics in the locally measured value of H_0, internal inconsistencies in Planck data, or a hint for new physics beyond the assumptions and parameters of ΛCDM.

Turning to a theoretical perspective, the concordance model of cosmology also leaves a few open questions: What *is* dark energy? If the cosmological constant was simply to be interpreted as the vacuum energy density of empty space, why is it several orders of magnitudes smaller than theoretically predicted? As GR is not quantisable, how can we describe gravity on a quantum level? Besides being cold and collision-less, are there other properties of DM affecting the evolution of the Universe?

The last question relates to an open question of the Standard Model of particle physics: if DM is composed of particles, how can these be incorporated into the Standard Model? The lack of any convincing observational evidence for the detection of a DM particle poses stringent constraints on possible underlying theories.

Even beyond the question of the existence and identity of the DM particle, the Standard Model (SM) of particle physics is not complete. The most compelling evidence for the need for beyond-the-standard-model (BSM) physics is the mystery of neutrino masses. The SM includes three massless neutrino flavour eigenstates, ν_e, ν_μ, and ν_τ. However, oscillations between the different flavour eigenstates have been observed in solar and atmospheric neutrinos, leading to the conclusion that at least two of the eigenstates must be massive [18–20]. This observation has direct implications for cosmology: massive neutrinos interact gravitationally and therefore affect structure formation and – depending on their mass – can contribute to the energy budget of non-relativistic matter in today's Universe.

The unsolved questions regarding the foundations of the standard models of cosmology and particle physics have led to much activity in proposing and building new BSM models. At the same time advancing experimental methods and technologies are giving us access to more and more datasets investigating different aspects of fundamental physics. While it is essential to advance both theoretical and experimental progress in these areas, one crucial part should not be forgotten: testing the viability of new models against all available data to assess whether the new theories can match the success of the current standard models.[3]

[3]A brief comment to clarify the naming conventions: the term 'Standard Model' always

This concern lies at the heart of this thesis: the test of various non-standard models against different datasets to determine whether they can be seen as a viable alternative to the standard model. This endeavour can be relatively straight forward if one can find a prediction of a given non-standard theory that is in clear contradiction with available data and the predictions of the standard model. In this case, one can rule out the theory.

Assessing the viability of an alternative model gets more difficult when experiments to detect distinct signatures of the specific non-standard theory need to be designed. While a detection of such a signal has the potential to confirm *a prediction* of the theory, a non-detection can often only set constraints on the parameter space of the model.[4] In this case, an analysis comparing a model to different datasets – that separately only have constraining power – can give more conclusive results.

The practice of combining different datasets to perform parameter estimates is generally referred to as performing 'global fits'. The importance of combining not only datasets from one but several fields can be seen by considering the example of a specific DM model: it might not only be constrained by data from direct or indirect DM detection experiments but also from missing energy searches at the large hadron collider (LHC), as well as cosmological observables sensitive to properties of DM and its relic density in the Universe. Hence, to extract the full wealth of information experimental data offer, the results from different research fields need to be combined. Further, to decide if one model is superior to others in predicting and describing observed phenomena, all relevant datasets must be taken into account. Consequently, to answer the question of whether a given model provides a better alternative to another, global fits of both models need to be performed.

In this work I present three examples in which my collaborators and I apply different strategies to test non-standard physics:

- *Ruling out a theory with a conflicting dataset.* I show how minimally coupled covariant Galileons, a modified gravity model, can be ruled out using cosmological and astrophysical observables. Covariant Galileons are a modification of gravity that extend the standard scenario of GR by adding a scalar degree of freedom [21–23]. The kinematics of this scalar

refers to the Standard Model of particle physics. On the contrary, I will refer to ΛCDM as the 'concordance model (of cosmology)' to avoid any confusion between the two. When referring to model extensions or generalisations, the term 'BSM theories' always stands for theories beyond the Standard Model of particle physics. The term 'non-standard physics' is applied to extensions of both models.

[4]Note that confirming a prediction of a theory is not the same as confirming a theory itself. While the former can be achieved with a single measurement, the latter is a much more complex.

field drive the late-time acceleration such that no fine-tuned cosmological constant needs to be included. The theory is divided into three different branches with increasing numbers of parameters and complexity: a cubic, quartic and quintic branch. All three branches of the covariant Galileons naturally solve the Hubble tension [24]. The key phenomenological properties that differ from ΛCDM in Galileon cosmologies are *i)* a non-trivial evolution of the lensing potential after matter domination, and *ii)* an anomalous propagation speed of tensor perturbations. The consequences of *i)* are that the cubic branch of the theory can be ruled out. My collaborators and I showed this in Paper A; I will summarise these results in Sec. 4.1. Property *ii)* leads to the invalidation of the quartic and quintic branch. Even though I did not obtain these results, I will include them in the discussion in Sec. 4.1 for the sake of completeness.

- *Constraining a theory by probing distinct predictions.* The existence and parameter space of cosmic superstrings (CSSs), one-dimensional fundamental building blocks of string theory stretched out to cosmological scales, can be tested using a unique signature: when a CSS crosses the line of sight between an observer and a point-like source, the flux of the source is instantaneously doubled. Once the alignment between observer, string and source is broken, the flux will immediately drop back to its original value. This immediate increase and decrease of the flux makes the lensing events sourced by CSSs clearly distinguishable from lensing events by any other known source. In Paper B, we estimate the lensing rates sourced by CCSs of extragalactic optical sources: stars in Andromeda and Supernovae Type Ia. Our results show that current datasets can independently confirm constraints on the theory obtained by other means. While current data are not sufficient to put more stringent constraints on the theory, we show that targeted surveys can increase the constraints on the theory and the probability of a detection.

- *Testing the viability of a theory with global fits.* We extend the framework of GAMBIT, the Globular and Modular Beyond-the-Standard-Model Inference Tool, with a new module, CosmoBit. This extension allows the user to perform parameter scans of a variety of BSM models, testing the theory against particle physics as well as cosmological observations. The cosmology-related non-standard models are extensions of standard ΛCDM that include, e.g. a treatment of neutrino masses consistent with results from particle physics, non-standard neutrino temperatures, inflationary models, and annihilating or decaying DM models. CosmoBit makes various cosmological likelihoods available through interfaces with external libraries; these likelihoods range from the abundance of

light elements produced in the early Universe, to observations of the CMB, and late-time observables like galaxy clustering. As a first application, I use CosmoBit to constrain the mass of the lightest neutrino to be $m_{\nu,\,\text{light}} \lesssim 0.058$ eV ($m_{\nu,\,\text{light}} \lesssim 0.056$ eV) at 95% confidence level assuming a normal (inverted) mass hierarchy. I present details of the implementation, validation and results in Part II of this work.

This thesis is structured as follows: In **Part I**, chapter 2 briefly reviews the concordance model of cosmology along with its central assumptions and equations. I introduce the observables that support the cosmological concordance model, open questions and unsolved problems. An introduction to the extensions of ΛCDM relevant to this thesis is given in Chapter 3; in particular these are inflationary models setting the initial conditions of the Universe (3.1), the effect of neutrino masses in cosmology (3.2), the addition of non-standard radiation contents (3.3), modifications to GR focusing on Galileon Gravity (3.4), and cosmology with cosmic superstrings (3.5). I briefly discuss how these different extensions connect in Sec. 3.6

I provide a summary of the results from the included papers in chapter 4. How minimally-coupled covariant Galileons can be invalidated by cosmological and astrophysical observables is shown in Sec. 4.1. I discuss the constraints on the parameter space of the models arising from CMB, BAO and ISW data (summarising the results of Paper A), as well as from a gravitational wave event with the observation of the associated gamma-ray burst. I summarise the prospects of the detection of CCSs through the observation of microlensing events of extragalactic point-like sources, the results of Paper B, in Sec. 4.2.

Part II starts with Chapter 5 introducing statistical methods for parameter inference and GAMBIT, the Globular and Modular Beyond-the-Standard-Model Inference Tool. In Chapter 6, I present the new module CosmoBit. I will first provide an executive summary of the module in Sec. 6.1. Sec. 6.2 serves to introduce the implemented models, and Sec. 6.3 gives an overview of the implemented likelihoods. Details about the implementation and the usage of the tool are given in 6.4. I present validation plots and first physics results in 6.5. I close this part with a conclusion and outlook in Chapter 7.

Part III contains Papers A and B.

The topics covered in this work are quite broad. They range from a phenomenological aspect of string theory to a modified gravity model and simultaneous global fits of particle physics and cosmology. An in-depth introduction to all of these fields is not withing the scope of this thesis. Instead, the focus of Part I is to introduce the broad underlying concepts and context to the reader. I refer the interested reader to the included papers and the provided references for more details.

Chapter 2

The Evolution of the Universe in ΛCDM

The concordance model of cosmology, ΛCDM, is based on several major assumptions:

- the Universe is **isotropic** and **homogeneous** on large scales ($\gtrsim 100$ Mpc),
- the Universe was born in a **Big Bang** and the initial conditions for structure formation are scale-free Gaussian scalar perturbations,
- the **Standard Model of particle physics** describes the standard matter and radiation content,
- an additional matter species, called **cold dark matter** (CDM), which only interacts weakly with Standard Model particles is introduced to, e.g. allow observed structures to form,
- **General Relativity** (GR) governs the laws of gravity, and
- the late-time acceleration is sourced by the constant energy density of the **cosmological constant**, Λ.

In this chapter, I briefly review some aspects of ΛCDM, focusing on the theory of gravity, the central equations for the background evolution of the Universe, and key parameters and observables.[1] The first section, 2.1, focuses on the initial conditions for the evolution of the Universe in the concordance model. I discuss the principles of light element formation in the early Universe during the epoch of Big Bang Nucleosynthesis in Sec. 2.2. Sec. 2.3 introduces the

[1] This chapter serves only as a brief introduction to the concordance model of cosmology. For textbook introductions to the topics refer to, e.g. Refs. [25–32]. Examples of comprehensive lecture notes are Refs. [33–36].

basic principles of General Relativity; the fundamental background equations of cosmology are presented in Sec. 2.4. After that, I introduce some of the key observables used to test and constrain the model of ΛCDM in Sec. 2.5. The model parameters of ΛCDM are discussed in Sec. 2.6. I conclude this chapter by commenting on present observational tensions in Sec. 2.7.

2.1 Initial Conditions

The cosmological principle states that the Universe is isotropic and homogeneous on large scales. However, the fact that solar systems and galaxies like the one we live in exist show that this is not true on small scales. The predictions of the concordance model, therefore, must include the formation of structures, such as the ones we can observe today. The key to this lies in the first $1/10^{32}$ fraction of a second after the birth of the Universe: in the most popular theory of the early Universe density fluctuations appearing on a quantum level were amplified to classical scales in a phase of a rapid accelerated expansion, called *inflation*. These small density fluctuations produced during inflation act as the seeds for the formation of structures that we observe today.[2]

In ΛCDM one is usually agnostic about whether a phase of inflation took place, and if so, how exactly it proceeded. No specific assumptions about the underlying theory causing the beginning of the accelerated expansion, its end, or how its energy is converted to the standard radiation or matter contents (the mechanism of *reheating*), are made. Instead, one assumes that the density perturbations providing the seeds for structure formation are given in the form of the parametrised *primordial power spectrum* (PPS).

A power spectrum quantifies the variance of the deviation of a random variable from its mean in Fourier space. Consider, e.g. density fluctuations with respect to the mean density field $\bar{\rho}$,

$$\delta(\vec{x}) \equiv \frac{\rho(\vec{x}) - \bar{\rho}}{\bar{\rho}} = \int \hat{\delta}(\vec{x})\, e^{-i\vec{k}\vec{x}}\, \frac{\mathrm{d}^3\, k}{(2\pi)^3}\,, \tag{2.1}$$

with $\hat{\delta}(\vec{k})$ being the Fourier transform of $\delta(\vec{x})$. The dimensionless power spectrum $\mathcal{P}(k)$ is then given by

$$\langle \hat{\delta}(\vec{k})\, \hat{\delta}^*(\vec{k'}) \rangle \equiv \frac{2\pi^2}{k^3}\, \mathcal{P}(k)\, \delta_D(\vec{k} - \vec{k'})\,, \tag{2.2}$$

where δ_D is the Dirac delta function. Both homogeneity and isotropy are ensured by this form: the term $\delta_D(\vec{k} - \vec{k'})$ manifests homogeneity by forbidding

[2] For details on perturbations in the early Universe refer to Refs. [37–40].

the correlation of different wave vectors $\vec{k}$ in Fourier space. Isotropy is ensured as $P(k)$ does not depend on the direction of $\vec{k}$. The variance of the power spectrum within a volume characterised by the window function $W_R(k)$,

$$\sigma_R^2 = 4\pi \int_0^\infty \frac{\mathrm{d}\, k}{k(2\pi)^3} \mathcal{P}_\delta(k)\, W_R^2(k)\,, \tag{2.3}$$

is commonly used as a measure of the amplitude of the power spectrum at a given scale. If one was to consider the fluctuations within a sphere of given radius R, the window function $W_R^2(k)$ would take the form of a top-hat filter for a three dimensional sphere.

The PPS $\mathcal{P}_\mathcal{R}(k)$ quantifies the variations of the curvature fluctuations ξ in the early Universe. These can be related to fluctuations in the density field. In ΛCDM the dimensionless PPS is assumed to be scale-free and takes the form

$$\mathcal{P}_\mathcal{R}(k) = A_s \left(\frac{k}{k_\star}\right)^{n_s - 1}\,, \tag{2.4}$$

where $k_\star$ gives the pivot scale, and the two parameters A_s and n_s parametrise the amplitude and tilt of the PPS respectively. The parameters A_s and n_s are fundamental model parameters of ΛCDM (see Sec. 2.6). Note that $\mathcal{P}_\mathcal{R}(k)$ is scale invariant for $n_s = 1$.

As mentioned above, this specific parametrised form of the PPS is an assumption of ΛCDM. It is, however, motivated by the shape of the PPS derived from specific inflation theories. I will comment more on the motivations for inflation and concrete examples of inflation models in Sec. 3.1. In the context of the standard ΛCDM scenario, however, only the form of the PPS given in Eq. (2.4) and the parameters defining the shape are important.

2.2 The Early Universe and Big Bang Nucleosynthesis

Having set the stage for the evolution of the Universe by defining the initial conditions, we move on to the physics in the early Universe and the phase of Big Bang Nucleosynthesis. At early times, the Universe is in a hot, dense state and particle interactions proceed fast enough to keep them in thermal equilibrium. As the Universe expands and cools deviations from this equilibrium will occur. This eventually allows for the onset of Big Bang Nucleosynthesis (BBN). Starting a few minutes after the Big Bang, and lasting for only about 20 minutes, BBN constitutes an important part of the evolution of the Universe: during its course, the first light elements are synthesised from the

primordial plasma. As the abundance of these light elements can be inferred from measurements today, 13.8 billion years later, BBN provides the possibility to test the physics of the very early Universe.[3]

An important concept during the evolution of the Universe is the concept of the *freeze out* of an interaction. It can be understood as follows: the rate Γ of any reaction,

$$\Gamma \propto \langle \sigma v \rangle n \,, \tag{2.5}$$

depends on the interaction cross-section σ, the particle velocity v, and the number density of particles available for the reaction n. As the Universe expands, the temperature and number density of particles decrease, reducing the interaction rate. Once the reaction rate drops below the expansion rate, the reaction will not take place any longer, i.e. it will freeze out.

In the early Universe neutrinos are kept in thermal equilibrium with the primordial plasma[4] via the weak interaction,

$$\nu + \bar{\nu} \leftrightarrow e^+ + e^- \,. \tag{2.6}$$

Once the temperature drops below ~ 2.7 MeV a few seconds after the Big Bang, the weak interaction freezes out and neutrinos *decouple* from the photon-electron gas. Hence, their temperature will evolve independently from the other components.[5] In the absence of any other reaction, neutrinos will cool and dilute as the Universe expands.

Photons and electrons are kept in thermal equilibrium until electron-positron annihilation

$$e^+ + e^- \leftrightarrow 2\,\gamma \tag{2.7}$$

becomes suppressed. This happens as soon as the photon energy becomes too low to produce electron-positron pairs at $T \sim 2\,m_e \sim 1$ MeV, with m_e being the electron mass. The annihilations transfer energy to the photon gas. The temperature of the already decoupled neutrinos will remain unaffected by this.

The temperature ratio between neutrinos and photons, T_ν/T_γ, can be estimated with a simple calculation: entropy conservation before and after electron-positron annihilation requires

$$s'_{e^+} + s'_{e^-} + s'_\gamma = \tilde{s}_\gamma \tag{2.8}$$

[3]For textbook introductions, see the relevant chapters of Refs. [31, 41, 42]; for pedagogical reviews and lecture notes refer to Refs. [43–46].

[4]Thermal equilibrium of the primordial plasma means that the neutrino temperature, T_ν, is equal to the electron and photon temperature, i.e. $T_\nu = T_e = T_\gamma$.

[5]That is, except for the dilution due to the expansion of the Universe that all species experience.

to hold. Here, s'_x denotes the entropy of x before annihilation, $\tilde{s}_\gamma$ is the entropy of photons after $e^\pm$ annihilation. The entropy of a relativistic particle scales with their internal degrees of freedom, g, and their temperature T as $\propto g\,T^3$. Fermions receive an additional factor of (7/8) with respect to bosons.[6] The temperature ratio follows from the entropy conservation equation when using the fact that before $e^\pm$ annihilation all involved particles were in thermal equilibrium, hence $T_{e^+} = T_{e^-} = T_\gamma = T'$. Thus $s'_{e^+} = s'_{e^-} = (7/8)\,s'_\gamma$, and Eq. (2.8) leads to

$$\frac{T'}{\tilde{T}} = \left(\frac{4}{11}\right)^{1/3} = \frac{T_\nu}{T_\gamma}\,. \tag{2.9}$$

The last equation holds as $\tilde{T}$ represents the photon temperature after $e^\pm$ annihilation, and $T' = T_\nu$ under the assumption that neutrinos decoupled instantaneously once the weak interaction froze out. This means that neutrinos did not receive any energy injection from the $e^\pm$ annihilations. In reality, precise decoupling calculations show that this is not exactly true, as neutrinos do not decouple instantaneously: electrons and positrons start annihilating before neutrinos are completely decoupled and inject some of their energy into neutrinos. Hence, the neutrino-photon temperature ratio is in fact slightly higher than the analytical expression given in Eq. (2.9), see Refs. [48, 49].

In the SM there is no other decay or reaction that adds to or removes energy from photons or neutrinos after $e^\pm$ annihilation. Under this assumption, the temperature ratio T_ν/T_γ, therefore, remains constant until the present day.

After neutrino decoupling and the annihilation of electron-positron pairs, neutron-proton collisions and interconversion through the weak force still take place. As neutrons are heavier than protons the neutron to proton ratio, n/p, will decrease as the Universe expands. The exact value of n/p depends on the interplay between expansion rate of the Universe, the strength of the weak interaction, and the age of the Universe as the neutron is unstable and decays with a lifetime of $\tau_n = 880.2 \pm 1.0$ [50]. As we will see below, the ratio n/p is an important quantity for calculating the predictions of element abundances from the BBN. Hence, any modifications to the expansion rate, or changes of the neutron lifetime will affect the predictions for the abundance of light elements.

[6] The entropy and energy density of ultra-relativistic species can be derived from their temperature using Bose-Einstein or Fermi-Dirac statistics for bosons and fermions respectively. For bosons the entropy is given by $s_B = g\,\frac{2\pi^2}{45}\,T^3$ and the energy density by $\rho_B = g\,\frac{\pi^2}{30}\,T^4$. The number of internal degrees of freedom of photons, electrons, and positrons is 2. For the derivation of the expressions for the entropy and energy density in the context of cosmology, refer to Refs. [28, 31, 42]; see Ref. [47] for a clear and explicit summary.

The chain reaction of the synthesis of light elements is started by the formation of deuterium (^{2}H) through neutron-proton collisions,

$$n + p \rightarrow {}^2\mathrm{H} + \gamma\,, \tag{2.10}$$

starting at a temperature of about 80 keV. The exact temperature depends not only on the proton-to-neutron ratio, but also on the baryon-to-photon ratio η, as high-energy photons can photodissociate the newly formed deuterium. Hence, a higher abundance of photons will delay the onset of BBN. The synthesis of deuterium is followed by the formation of ^{3}He, ^{4}He, ^{3}H and ^{7}Li through

$$\begin{aligned} {}^2\mathrm{H} + {}^2\mathrm{H} &\rightarrow {}^3\mathrm{He} + n\,, \\ {}^2\mathrm{H} + {}^2\mathrm{H} &\rightarrow {}^3\mathrm{H} + p\,, \\ {}^3\mathrm{He} + {}^2\mathrm{H} &\rightarrow {}^4\mathrm{He} + p\,, \\ {}^4\mathrm{He} + {}^3\mathrm{H} &\rightarrow {}^7\mathrm{Li} + \gamma\,. \end{aligned} \tag{2.11}$$

The production of subsequent elements heavier than the stable ^{4}He is highly suppressed, as there is no stable element with atomic mass 5. The stable atomic mass gap at 8 essentially prevents the efficient synthesis of any other heavier element.

The epoch of BBN ends once the temperature falls below $T \sim 30$ keV. After that, the production of heavier nuclei ceases owing to a lack of available energy. The only mechanism to affect the number densities until stars form and nuclear fusions start in their interiors, is the decay of unstable elements.

The observation of element abundances today offers a test for the physics of the early Universe.[7] The theoretical predictions for the light element abundances depend on

- the expansion rate in the early Universe during the epoch of BBN,
- the baryon-to-photon ratio η at the epoch of BBN,
- the neutron lifetime, and
- all relevant nuclear reaction rates.

The latter two are uncertainties that must be taken into account when calculating predictions for the light element abundances. The first two points are, as we shall see in Sec. 2.4, determined by the cosmological model.

[7] I will comment on the observational principle for these measurements in Sec. 2.5

2.3 General Relativity

The simple laws of Newtonian dynamics are sufficient to describe gravitational interactions of objects on Earth. However, they fail to provide a proper description of large, cosmological scales, or in strong gravitational fields. The first hint that a description of gravity beyond Newton's laws might be necessary was discovered in 1856 when the mathematician Urbain LeVerrier observed an anomalous perihelion motion of Mercury [51]. Albert Einstein gave a resolution to this problem in 1916: with the publication of the theory of General Relativity (GR) [52] he presented a replacement of Newton's laws that can correctly describe the anomalous observation [53].

The basis of GR is the realisation of the equality of inertial and gravitational mass, formulated in different equivalence principles:

- *Weak Equivalence Principle.* There is a universality between the free-fall and the gravitational interaction for all particles. It is satisfied if a space-time metric exists to which all matter species are universally coupled. Free-falling objects follow geodesics of this metric.
- *Einstein Equivalence Principle.* The weak equivalence principle holds and the laws of physics reduce to the ones of special relativity in all freely falling local frames, independent of velocity or position.
- *Strong Equivalence Principle.* The validity of the weak equivalence principle extends to massive gravitating objects, and in all freely falling frames one recovers locally the same special relativistic physics, independent of position or velocity.

Imposing the strong equivalence principle has two important consequences: *i)* time passes more slowly in strong gravitational fields and *ii)* the presence of a gravitational mass bends the path of a passing light ray, an effect called *gravitational lensing*. GR incorporates these effects, while the Newtonian limit is correctly recovered in weak gravitational fields. However, the great difference to Newton's theory is that in Einstein's theory gravity is described by a metric that is related to the contents of the Universe via Einstein's equations[8]

$$G_{\mu\nu} + \Lambda g_{\mu\nu} = 8\pi G T_{\mu\nu} \,, \tag{2.12}$$

with the Einstein tensor $G_{\mu\nu} \equiv R_{\mu\nu} - \frac{1}{2} g_{\mu\nu} R$, the Ricci tensor $R_{\mu\nu}$, the Ricci scalar R, the metric tensor $g_{\mu\nu}$ and the cosmological constant Λ. While the left-hand side of the equation describes the curvature of space-time, the right-hand

[8] For a detailed review on how they were originally derived see, e.g. Ref. [54]. For textbook introductions to GR, I refer the reader to Refs. [25, 30, 32, 55].

side describes its content given by the energy-momentum tensor. Modelling the content of the Universe as a perfect fluid, the energy-momentum tensor simplifies to

$$T_{\mu\nu} = (\bar{\rho} + \bar{p}) u_\mu u_\nu + \bar{p} g_{\mu\nu} \,, \tag{2.13}$$

with the isotropic pressure p, the relativistic mass-energy density ρ and the tangent velocity 4-vector u^μ. The explicit time dependence is dropped for simplicity, bars over quantities ($\bar{x}$) denote their space average. The Einstein Equations (Eq. 2.12) assure energy-momentum conservation: as the Einstein tensor is divergence free, the energy-momentum tensor must be as well, leading to $\nabla_\nu T^{\mu\nu} = 0$.

The cosmological constant is added to the left-hand side of Einstein's equations to produce the observed accelerated late-time expansion of the Universe. However, this term can also be moved to the right-hand side and included in the energy-momentum tensor as a fluid with a negative equation of state, $w = p/\rho = -1$. While these two scenarios are equivalent, models with a time-dependent evolution of the equation of state parameter, $w \to w(t)$ yield a different cosmological evolution than ΛCDM, and are commonly referred to as Dark Energy (DE) models.

In addition to Einstein's historical considerations that lead to the formulation of GR [54], one can also derive the field equations of GR from an action-based approach with the Einstein-Hilbert action (S_{EH}) and the action of a matter field (S_{M})

$$S = S_{\mathrm{EH}} + S_{\mathrm{M}} = \frac{M_{\mathrm{Pl}}^2}{2} \int \mathrm{d}^4x \, \sqrt{-g} \, (R - 2\Lambda) + \int \mathrm{d}^4x \, \sqrt{-g} \, \mathcal{L}_{\mathrm{M}}[g_{\mu\nu}, \psi_{\mathrm{m}}] \,, \tag{2.14}$$

with the reduced Planck mass defined via $M_{\mathrm{Pl}}^{-2} = 8\pi G$, and the Lagrangian $\mathcal{L}_M$ describing some matter field ψ_{m}. Varying the action with respect to the metric leads to the field equations given in Eq. (2.12).

Einstein's field equations have a large number of exact solutions [56–58], however, not all of them are physically acceptable or relevant [58–60]. Notable exceptions of great relevance for astrophysics are, e.g. the Schwarzschild solution [61] describing the gravitational field around a massive spherically symmetric body in vacuum, or the Kerr solution describing a rotating axially-symmetric black hole in vacuum [62].

The arguably most relevant solutions for cosmology are Friedmann-Lemaître-Robertson-Walker (FLRW) metrics [63–66], which describe the background of a homogeneous and isotropic expanding universe with the line element

$$\mathrm{d}s^2 = -\mathrm{d}t^2 + a^2(t) \left(\frac{\mathrm{d}r^2}{1 - kr^2} + r^2 (\mathrm{d}\theta^2 + \sin^2\theta \, \mathrm{d}\phi^2) \right) , \tag{2.15}$$

where the scale factor $a(t)$ represents the time evolution of the spatial part of the metric and k sets the geometry of the Universe: closed ($k > 0$), open ($k < 0$) or flat ($k = 0$).

In a completely homogeneous and isotropic Universe described by the FLRW metric, structures like stars, planets or galaxies would never form. To explain their appearance, perturbations to the background evolution must be considered. This is typically done by expanding the metric $g_{\mu\nu}$ around the FLRW background, $g_{\mu\nu}^{\mathrm{FLRW}}$,

$$g_{\mu\nu} = g_{\mu\nu}^{\mathrm{FLRW}} + \delta g_{\mu\nu} \,, \tag{2.16}$$

where $\delta g_{\mu\nu}$ parametrises the metric fluctuations.

Assuming that the Universe is flat and considering only scalar perturbations, the perturbed line element in Newtonian gauge takes the form

$$\mathrm{d}s^2 = -(1+2\Psi)\,\mathrm{d}t^2 + a^2(t)\,(1-2\Phi)\,\mathrm{d}\mathbf{x}^2 \,, \tag{2.17}$$

where $\mathrm{d}\mathbf{x}$ represents the spatial part of the metric and the scalar fields Φ and Ψ are the gravitational, or Bardeen, potentials. The sum of these potentials, $\Phi + \Psi$, is commonly referred to as the lensing potential.

In general, vector and tensor perturbations can also enter Eq. (2.16). Vector perturbations are usually small and decay quickly. Tensor perturbations, on the other hand, manifest as gravitational waves and provide an observational probe.

From fixing the metric in the Einstein Equations to the FLRW metric, and the space-time content to be described by the perfect fluid energy-momentum tensor (Eq. 2.13), we can derive the evolution of the cosmological background. I will outline the results in the next section.

2.4 Background Evolution

The Friedmann equations, describing the background expansion of the Universe, can be derived from the time-time and space-space components of Einstein's field equation for the FLRW metric.[9] This yields

$$H(t)^2 \equiv \left(\frac{\dot{a}}{a}\right)^2 = \frac{8\pi G}{3}\bar{\rho} + \frac{\Lambda}{3} - \frac{k}{a^2} \,, \tag{2.18}$$

$$\frac{\ddot{a}}{a} = -\frac{4\pi G}{3}\,(\bar{\rho} + 3\bar{p}) + \frac{\Lambda}{3} \,, \tag{2.19}$$

[9]The time-time component is derived by choosing the indices $\mu = \nu = 0$ in Eq. (2.12), the space-space component is obtained by setting $\mu = \nu = i$, where i runs from 1 to 3.

including the definition of the Hubble parameter $H(t)$. The present value of the Hubble parameter, $H(t_0) = H_0$, is one of the model parameters of ΛCDM. The value of H_0 is commonly stated via the reduced Hubble rate h, defined via $H_0 = 100\,h$ km/(s Mpc). The scale factor a, measuring the relative expansion of the Universe, is normalised to take the value 1 today. Hence, $a_0 = a(t_0) = 1$, yielding the relation to the redshift z with $a = 1/(1+z)$.[10]

Using the conservation of energy and momentum, $\nabla_\nu T^{\mu\nu} = 0$, the continuity equation takes the form

$$\dot{\bar{\rho}} + 3\frac{\dot{a}}{a}\,(\bar{\rho} + \bar{p}) = \dot{\bar{\rho}} + 3\,\frac{\dot{a}}{a}\bar{\rho}\,(1+w) = 0\,, \tag{2.20}$$

with the equation of state parameter $w = \bar{p}/\bar{\rho}$ parametrising the relation between pressure and density.

The equation of state parameters for relativistic matter, non-relativistic matter and the cosmological constant are given by $w = 1/3$, 0 and -1, respectively. With these relations one can solve the continuity equation to obtain the time evolution of the densities of the species: $\bar{\rho}_\mathrm{r}(t) = \bar{\rho}_\mathrm{r0}\,a^{-4}$, $\bar{\rho}_\mathrm{m}(t) = \bar{\rho}_\mathrm{m0}\,a^{-3}$ and $\bar{\rho}_\Lambda(t) = \Lambda = \text{const}$. Besides the densities of the contents of the Universe, one defines the critical density $\bar{\rho}_\mathrm{c}(t) \equiv 3\,H^2(t)/(8\pi G)$; physically it describes the density of a sphere filled with matter in which the specific kinetic energy exactly balances the gravitational potential.

The Friedmann equation (Eq. (2.18)) can then be re-written in terms of the scale factor and the energy densities of the different species, $\Omega_\mathrm{i0} = \bar{\rho}_\mathrm{i0}/\rho_\mathrm{c0}$, as

$$H^2(a) = H_0^2\left[\Omega_\mathrm{r0}\,a^{-4} + \Omega_\mathrm{m0}\,a^{-3} + \Omega_\mathrm{k0}\,a^{-2} + \Omega_{\Lambda 0}\right] \equiv H_0^2 E^2(a)\,, \tag{2.21}$$

with the definition of the curvature 'density' $\Omega_\mathrm{k0} = -k/H_0^2$. The matter energy density Ω_m0 stands for the sum of the cold dark matter (Ω_cdm0) and baryonic matter (Ω_b0) components, and Ω_r0 for the energy density in radiation. Assuming that the Universe is spatially flat, as in the standard ΛCDM scenario, the Friedmann equation for $t = t_0$ reduces to $\Omega_\mathrm{r0} + \Omega_\mathrm{m0} + \Omega_\Lambda = 1$.

From the form of the Friedmann equation given in Eq. (2.21), it is easy to see that in the early Universe radiation is the dominant contribution to the total energy density. As the Universe expands and a increases, contributions from matter components will take over the leading contribution. Eventually, as

[10] The concept of redshift can be easily understood by considering the emission of a wave with wavelength λ at a given point in time. While the wave travels towards a potential observer, the Universe expands, causing the wavelength to be stretched, i.e. λ is shifted towards the 'red', less energetic part of the spectrum. In line with this picture the redshift at the present day is zero.

a approaches unity, the energy density will be dominated by the contribution from the cosmological constant.

The energy density of radiation after $e^{\pm}$ annihilation only receives contributions from photons and ultra-relativistic neutrinos. It can be formulated in terms of the temperature ratio of photon to neutrino from Eq. (2.9):

$$\rho_r(t) = \left[1 + N_{\rm ur}\frac{7}{8}\left(\frac{T_\nu}{T_\gamma}\right)^4\right]\rho_\gamma(t)\,. \tag{2.22}$$

This equation defines $N_{\rm ur}$ as the effective number of ultra-relativistic fermions with the same temperature as SM neutrinos. In ΛCDM this is fixed to $N_{\rm ur} = 3.045$, slightly higher than the three generations of neutrinos in the SM [48, 49]. This deviation is to account for corrections arising from precise calculations of the neutrino temperature after decoupling. The corrections enter as neutrinos do not decouple instantaneously and therefore receive some energy from annihilating electron-positron pairs. Note that even though from a physical perspective, the temperature ratio T_ν/T_γ is modified, one commonly incorporates the effects into $N_{\rm ur}$, the number of ultra-relativistic neutrino-like species. In ΛCDM these two treatments yield mathematically the same results; it is, however, crucial to realise that modifying the temperature ratio between photons and neutrinos, and introducing an additional ultra-relativistic species are two distinct physical scenarios.

The actual value of the energy density in photons today can be determined by measuring the black body temperature of the photons from the Cosmic Microwave Background (CMB). Using the Stefan-Boltzmann law this yields

$$\Omega_{\gamma 0} = \frac{\rho_{\gamma 0}}{\rho_{\rm crit0}} = \frac{4\,\sigma_{SB}T_{\rm CMB}^4}{3\,H_0^2/(8\pi G)}\,, \tag{2.23}$$

with the Stefan-Boltzmann constant $\sigma_{SB} = \pi^2/60$ (in natural units). A measurement of the CMB photon temperature allows one to calculate the number density of photons today by using Bose-Einstein statistics, this yields

$$n_{\gamma 0} = \frac{2\,\zeta_3 T_{\gamma 0}^3}{\pi^2}\,. \tag{2.24}$$

Another important quantity, especially for the predictions from BBN, is the baryon-to-photon ration η. Assuming all baryons appear in the form of hydrogen, their number density is given by $n_b = \rho_b/m_p$, with the proton mass m_p. In combination with Eq. (2.24), the baryon-to-photon ratio,

$$\eta = n_b/n_\gamma\,, \tag{2.25}$$

can be calculated. By inserting typical values for these quantities today to obtain η_0, one finds that there are about one billion photons per baryon in the present-day Universe. Note that in ΛCDM the value of η remains constant after the conversion of electron-positron pairs into photons freezes out. Hence, η does not change between the epoch of BBN and today, i.e. $\eta_0 = \eta_{\mathrm{BBN}}$.

Cosmological Distance Measures

Measurements of distances are, as we shall see in Sec. 2.5 when discussing observables, of great importance in cosmology. Owing to the expansion of the Universe, the distance between two objects is continuously changing, making it necessary to exactly define what distance one is referring to.[11] I briefly introduce the most important cosmological distances. For more details on distance measures in cosmology refer to Ref. [67], or cosmology textbooks and lecture notes given in Refs. [25–36].

- *Hubble distance.* The distance light could have travelled in one Hubble time $t_H = 1/H_0$, given by $D_{\mathrm{H}} = c/H_0$.

- *Comoving distance.* The distance along the line of sight between observer and source comoving with the mean Hubble flow on a surface of constant time, i.e. the coordinate distance $\mathrm{d}\bar{x}$. Photons travel on null geodesics, $\mathrm{d}s = 0$, therefore, $a\,\mathrm{d}D_{\mathrm{C}} = -c\,\mathrm{d}t = -c\,\mathrm{d}a/\dot{a}$.[12] Hence,

$$D_{\mathrm{C}} = D_{\mathrm{H}} \int_0^z \frac{\mathrm{d}z'}{E(z')}\,. \tag{2.26}$$

  In a spatially flat universe, the transverse comoving distance D_{M} between two objects is equal to the comoving distance, i.e. $D_{\mathrm{M}} = D_{\mathrm{C}}$. The comoving distance from the Big Bang to a given redshift $\tilde{z}$ is used to calculate the event horizon, i.e. the region in space which has been in causal contact up to $\tilde{z}$. Regions outside this horizon could not have exchanged any information due to the finite speed of light.

- *Angular diameter distance.* The relation between the physical transverse size of an object and its angular size. It is calculated with the relation $D_{\mathrm{A}} = D_{\mathrm{M}}/(1+z)$.

[11] For clearness, I will only in this section explicitly write out all factors of c. After that, I will return to natural units in which $c = 1$.

[12] The minus sign in the definition ensures that D_{C} increases away from the observer, while the time and scale factor increase towards the observer.

- *Luminosity distance.* The ratio between bolometric luminosity L and flux S. The definition and its relation to the angular diameter distance are:

$$D_{\mathrm{L}}^2 \equiv L/(4\pi S)\,, \qquad D_{\mathrm{L}} = (1+z)^2\, D_{\mathrm{A}}\,. \tag{2.27}$$

- *Effective projected distance.* It is defined to be

$$D_{\mathrm{V}} \equiv \left[(1+z)^2 D_{\mathrm{A}}^2 \frac{cz}{H(z)}\right]\,. \tag{2.28}$$

  In some analyses of Baryonic Acoustic Oscillations, it is used to increase the signal-to-noise ratio, e.g. in Refs. [68–71].

2.5 Cosmological and Astrophysical Observables

After introducing the key concepts and equations of the evolution of the Universe, we now turn to observational probes of the underlying theory. The three sets of independent observables leading to the current concordance model of cosmology are the Cosmic Microwave Background, Baryonic Acoustic Oscillations and Supernovae Type Ia. I briefly introduce the physical concepts of these observations in the following. Additionally, I will discuss other cosmological and astrophysical probes that are relevant in the context of this thesis. For a dedicated review of cosmological observables, see Ref. [72].

Temperature Anisotropies in the Cosmic Microwave Background (CMB). After the initial conditions for the evolution are set, the Universe expands and cools. At early times baryons and photons in the primordial plasma were coupled via Thomson scattering. Through gravitational attraction the plasma collapsed towards over-dense regions. At the same time, the expansion of the Universe and the radiation pressure of photons counteracted this inwards pull, causing the photon-baryon plasma to undergo acoustic oscillations. These oscillations propagated with the sound speed c_s through the plasma. About $380,000$ years after the Big Bang, the plasma cooled down to a temperature where electrons and protons combined to neutral hydrogen, called the phase of *recombination*; photons decoupled from baryons and could travel almost entirely freely through the Universe. These relic photons are still observable today and form the Cosmic Microwave Background (CMB) radiation. They have an almost perfect black body spectrum with a temperature of $T_{\mathrm{CMB}} = (2.7255 \pm 0.0006)$ K, as determined by the COBE mission [73–76]. However, anisotropies at the level of 10^{-5} were also detected [77, 78]. These

anisotropies carry imprints from the acoustic oscillations, primordial density fluctuations, the evolution of the gravitational potentials and today's structure of the Universe through lensing effects. Thus, we can infer information about structure formation, curvature and the background expansion of the Universe from the CMB temperature anisotropy power spectrum.

One can extract even more information from the CMB by measuring so-called E- and B-mode polarisations of CMB photons. These originate from the anisotropy of CMB photons within the surface of last scattering; when scattering off free electrons via Thomson scattering, this anisotropy leads to a linear polarisation of the resulting radiation field. E modes are sourced by scalar perturbations, i.e. perturbations in the density field. At linear order, B modes are caused by tensor perturbations, i.e. gravitational waves. They can, however, also be sourced by non-linear effects in the late Universe, such as weak gravitational lensing. The overall polarisation signal is sub-dominant compared to the temperature anisotropies and suppressed by several orders of magnitudes. So far only B modes sourced by gravitational lensing have been detected [79]. The detection of B modes from gravitational waves cannot be explained by the standard initial conditions assumed in ΛCDM, and would, therefore, constitute a hint of new physics.[13]

Baryonic Acoustic Oscillation (BAO) scale. The acoustic oscillations in the photon-baryon plasma from the period before decoupling not only left signatures in the photon distribution (and hence the CMB) but also affected the baryon distribution. The largest comoving distance a sound wave could have travelled before the time of baryon kinetic decoupling from photons, i.e. the sound horizon of the oscillation, is ~ 150 Mpc.[14] This scale is still imprinted in today's large scale structure, providing a *'standard ruler'* for measuring the expansion of the Universe: the time evolution of the ratio between the sound horizon at baryon decoupling and the distance of an observed galaxy (via Eq. 2.28) allows one to infer information about the expansion rate

[13]For a review about the search for B modes from tensor perturbations, see Ref. [80]. For detailed reviews on CMB physics, see, e.g. Refs. [81–85].

[14]Note that the redshift of baryon kinetic decoupling from photons is not equal to the redshift of photon decoupling: electrons and protons combine to neutral hydrogen once the interaction rate of the reaction $p^+ + e^- \to \mathrm{H} + \gamma$ becomes smaller than the expansion rate. This happens at redshift $z_\star \sim 1100$. After that, the number density of free electrons decreases; hence, the Thomson scattering rate of photons on electrons decreases and photons decouple. This takes place at redshift $z_{\mathrm{dec}} \sim 1090$. However, owing to the high photon-to-baryon ratio, baryons are affected by the photon drag for a bit longer. The time when baryons are released from the photon pressure is called the epoch of drag and takes place at about $z_{\mathrm{drag}} \sim 1060$.

of the Universe at different redshifts.

Type Ia Supernovae (SNe Ia). Type Ia Supernovae are often referred to as *standardisable candles* as the bolometric luminosity of their explosion is standardisable [86–88]. This property makes them a valuable observable for cosmology. In fact, it was measurements from SNe Ia that led to the discovery of the late-time acceleration of the Universe [8, 9].

The standardisation of the flux allows one to compute the luminosity distance of an observed object via the first relation in Eq. (2.27). The second relation connects the inferred luminosity distance to the expansion history $H(z)$. Hence, cosmological parameters can be constrained by comparing distances of low- and high-redshift SNe Ia.

Gravitational Lensing. An important consequence of GR is the concept of gravitational lensing: photons passing massive objects get deflected from their path, causing an observer to see only distorted images of the source. How severe this distortion is, depends on the geometry of the alignment, and on the mass of the foreground object acting as a gravitational lens. One distinguishes three different types of lensing:[15]

- *Strong Lensing*: The lens is so massive that the distortions of photons emitted from a source behind it can be fully resolved. This leads to one source appearing as either multiple different images or, in case of perfect alignment, even as a ring around the lens. The measurement of the time delay between the appearance of two images of the same source can be used to measure the Hubble rate in the nearby Universe [90] (see Refs. [14, 15, 91] for recent results).

- *Weak Lensing*: The lens is not strong enough to cause deflections leading to distinct observed images. However, the shape of the image of an extended source (typically a galaxy cluster) will appear distorted. The observation of a single, distorted source cannot provide any further information about the lens unless the exact, undistorted intrinsic shape of the source is known. This information is, however, not accessible for us as observers. Nevertheless, information about the lens can be inferred by statistical means: the distortions seen in all images of sources around a given lens will be correlated, allowing us to infer an estimate of the foreground mass [see Refs. 92, 93, for the first detections of the signal].

[15] See Ref. [89] for a textbook introduction fully devoted to the topic of gravitational lensing.

- *Microlensing*: The foreground mass is comparably light, and the distortions of photons are too small to be resolved, leading to an increased measured flux compared to the flux of the unlensed object or a shift in the apparent position of the object.

Integrated Sachs-Wolfe (ISW) Amplitude. The ISW effect probes the time evolution of gravitational potentials [94, 95]. Photons that travel through a gravitational potential well experience a blueshift when falling in and a redshift when climbing out. If the potential stays constant in time, there is no net effect. However, if the potential changes in time, the photon will experience an additional blue- or redshift. The ISW effect on the CMB photons is given by

$$\frac{\Delta T}{T}(\hat{n}) = -\int_{\tilde{\eta}_0}^{\tilde{\eta}_\star} \mathrm{d}\eta \, \frac{\partial(\Psi + \Phi)}{\partial \eta} \,, \tag{2.29}$$

with the conformal time at CMB release $\tilde{\eta}_\star$ and the conformal time at the observer $\tilde{\eta}_0$. In a ΛCDM model with massless neutrinos the gravitational potentials decay at early times, are constant during matter domination and decrease again when the cosmological constant starts to take over. Hence, only contributions from before and after matter domination are expected. Contributions to the ISW effect prior to matter domination are called 'early' ISW and from after 'late' ISW effect.

The late ISW effect contributes to the largest angular scales of the CMB power spectrum. As the late ISW effect is sensitive to gravitational interaction of photons after matter domination, it probes the times where a cosmological constant, dark energy, or modified gravity, become relevant [96, 97]. However, it is only sub-dominant in the CMB temperature spectrum. Further, being an autocorrelation, the CMB temperature anisotropy spectrum is not sensitive to the sign of the ISW effect. Therefore, it cannot discriminate whether the potentials decay or increase.

To probe the sign of the ISW effect, and to increase its signal-to-noise ratio, the cross-correlation between the CMB temperature spectrum and galaxy number counts (GNCs) from foreground galaxies can be considered [98]. When compared to data, the ISW amplitude is usually defined to be the summed signal of this cross-correlation at the measured angular scales (with some appropriate normalisation). This method provides the possibility to obtain information about the sign of the ISW effect. Furthermore, the evolution of the gravitational potentials at different times can be probed by using galaxy catalogues that cover different redshift ranges.

Light Element Abundances. The measurements of light element abundances today allows us to probe the Universe at the phase of BBN when it was

just a few minutes old (see Sec. 2.2). The observational principles are given below, for more details refer to, e.g. Refs. [43, 45, 46, 99].

- *Deuterium* is observed through UV absorption lines within the solar system, young galaxies, or the intergalactic medium. The observed abundance yields a lower bound on the primordial abundance: deuterium is destroyed as it is burnt to helium-3 in stellar interiors, while the abundances generated by astrophysical production mechanisms lie orders of magnitude below the primordial abundance.

- *Helium-3* is produced and destroyed in stellar interiors. Therefore it is difficult to infer the primordial abundance from the one measured today. The abundance is relatively low, and it has so far only been measured in our galaxy. Observations of ^{3}He are made via its hyperfine structure transitions in the galactic interstellar medium in ionised hydrogen regions. The ground state of singly-ionised helium-3 is split into two hyperfine structure states, a singlet and a triplet state. When transiting from the former into the latter a photon with a wavelength of $\sim$3.46 cm is emitted [100].

- *Helium-4* is produced in stars. Measurements of the primordial abundance are therefore made in extragalactic regions with low abundances of heavy elements, indicating little stellar activity. The helium-4 abundance is measured through the emission of its optical recombination line in ionised hydrogen regions.

- *Lithium-7* gets destroyed at relatively low temperature in stellar interiors. It can be produced via nuclear fusion and spallation in the interstellar medium, but also through nuclear fusion in stars with metallicities[16] similar to the Sun's. However, it has been discovered that at the surface of very old, low metallicity galactic stars the lithium abundance is almost constant, providing a possible measure for its primordial abundance [101].

2.6 Cosmological Parameters

In the literature, ΛCDM is usually treated as a six parameter model with the free parameters

$$\{\omega_\mathrm{b}, \omega_\mathrm{cdm}, H_0, \tau_\mathrm{reio}, A_s, n_s\}\,. \tag{2.30}$$

[16]The metallicity gives an indication of the chemical composition of a star. It is quantified via the ratio of the iron and hydrogen number densities.

These are the physical energy densities of baryonic and dark matter today ($\omega_x = \Omega_{x0}\, h^2$), the Hubble constant, the reionisation optical depth, and the amplitude and scalar spectral index of the primordial curvature perturbations (see Eq. 2.4 for a definition of the latter two). Note that in some analyses the angular acoustic scale of the first CMB peak, $\theta_\star$, is used as a model parameter instead of H_0. It is given by

$$\theta_\star = r_s^\star / D_A^\star \,, \tag{2.31}$$

where $r_s^\star$ is the sound horizon at recombination, and $D_A^\star$ is the angular diameter distance to recombination, taking place at redshift $z_\star \sim 1100$. If one uses $\theta_\star$ as a model parameter, H_0 is an inferred quantity. Note that $\theta_\star$ only depends on background quantities. Hence, no perturbations must be evaluated to calculate one of the parameters while the other is given.

In this six-parameter baseline model, the curvature of the Universe Ω_k is assumed to vanish. The reason is that the geometry of the Universe has been measured to be flat up to high accuracy. In the latest Planck analysis, Ω_k was determined to be 0.001 ± 0.002 [10].

Technically, the temperature of the CMB is also a free parameter. However, it is well constrained by COBE/FIRAS mission to be $T_\mathrm{CMB} = (2.7255 \pm 0.0006)$ K [73–76] such that given the precision of current datasets its uncertainty is negligible compared to the other parameters. Therefore it is usually fixed to the central value, see, e.g. Refs. [10, 17, 102]. Nevertheless, it is important to note that this statement only holds for currently available datasets. It has been shown that neglecting the errors of the CMB temperature measurement can lead to a bias of 1% in the best-fit values of the cosmological parameters [103]. Hence, it might be necessary to include it as a cosmological parameter in future studies having access to more precise measurements.

Another *a priori* unknown parameter is the sum of the neutrino masses, $\Sigma\, m_\nu$. In most model analyses, this is commonly fixed to the minimal value of 0.06 eV [104]. The reason for that is that ΛCDM favours massless neutrinos in analyses where the parameter is allowed to vary freely. From the observation of neutrino oscillations, we know that neutrinos are massive [18–20], so the baseline analysis usually fixes $\Sigma\, m_\nu$ to the minimum allowed value (see, e.g. Refs. [10, 17, 102]).

Table 2.1 lists the values of the cosmological parameters as determined by the Planck collaboration with the 2018 data release [105] of the CMB spectra, CMB lensing and BAO data. The results show that the DM abundance is about five times higher than the abundance of baryons. Further, the cosmological constant contributes about 70% of the total energy density of the present-day Universe.

From these six baseline parameter values, quantities such as the age of

Parameter	Value in baseline ΛCDM
ω_b	0.002242 ± 0.00014
ω_{cdm}	0.11933 ± 0.00091
H_0	67.66 ± 0.42 [km/s/Mpc]
$\ln(10^{10} A_s)$	3.047 ± 0.014
n_s	0.9665 ± 0.0038
τ_{reio}	0.0561 ± 0.0071

Table 2.1: Cosmological parameters and their 68% confidence intervals from the Planck 2018 analysis [10] obtained by combining the CMB spectra, CMB lensing reconstruction and BAO data (corresponding to the last column in their Table 2). In the baseline analysis $T_{\rm CMB} = 2.7255$ K, $\Omega_{\rm k} = 0$ and $\Sigma\, m_\nu = 0.06$ eV are fixed parameters. See Ref. [10] for analysis details.

the Universe ($t_U = 13.787 \pm 0.020\,\text{Gyr}$), the energy density in matter ($\Omega_m = 0.3111 \pm 0.0056$), or the cosmological constant ($\Omega_\Lambda = 0.6889 \pm 0.0056$) can be inferred. Another derived parameter is $\sigma_8 = 0.8102 \pm 0.0060$, a measure for the growth of density fluctuations from the early Universe. It is defined as the variance of the matter power spectrum on a scale of $8\,h^{-1}$ Mpc (see Eq. 2.3). As one can also directly measure σ_8 through the observation of galaxy clusters at different redshifts, it provides an important consistency check for the physics of the early and late Universe.

2.7 Observational Challenges and Tensions

Despite its great success, the concordance model of ΛCDM does leave some problems unsolved:

- *Lithium problem.* The lithium problem refers to the tension between the primordial abundance of lithium-7 as theoretically predicted, and the measured abundance. While measurements yield a value $(1.6 \pm 0.3) \times 10^{-10}$ [106] for the abundance of lithium relative to helium, predictions from BBN assuming ΛCDM are $(4.72 \pm 0.72) \times 10^{-10}$ [107]. It is still unclear whether the problem is due to unaccounted-for nuclear reactions during BBN, additional particles not included in the SM of particle physics, the astrophysical observations, or errors in the projection from the lithium abundance today to the primordial abundance. See Refs. [99, 108, 109] for reviews of the problem and Ref. [107] for an assessment with recent data.

- *Small scale problems.* The concordance model has several problems related to small scale structure; the DM distribution observed in the centres of many halos is cored where simulations predict a cusp profile (*core/-cusp problem*) [110], the observed number of satellite structures is lower than the expectation from simulations (*missing satellite problem*) [111], and the substructures which are obtained from simulations are too big to not be seen (*too big to fail problem*) [112]. For more details and possible solutions, see, e.g. Refs. [113–115].

- *CMB anomalies.* Unexpected features exist in the CMB sky [105, 116–119]. These are, for example, a lack of correlation and variance on large scales, a preference for odd parity modes, and an unexpected large cold spot. For a detailed summary, refer to Ref. [120].

- *Growth rate of structure.* Measurements of the growth rate of structure (encoded into σ_8) from different experiments lead to differences in the inferred cosmological parameters. The Planck measurement [10, 17] yields higher values for Ω_m and σ_8 than the results from weak lensing probes by the Kilo-Degree Survey (KiDS) with a $\sim 2.6\,\sigma$ significance [121, 122]. The analysis from the correlation of weak lensing, galaxy lensing and clustering signals from the Dark Energy Survey (DES) is also in tension with the Planck data; Abbott *et al.* [123] found a $\sim 1.7\,\sigma$ tension, which was confirmed by Raveri *et al.* [124], while Troxel *et al.* [125] pointed out it could be relieved it further noise corrections are applied. The latest analysis of cluster counts and weak lensing signal in the DES 1 year data, using a different galaxy sample than Ref. [123], raises the tension to $5.6\,\sigma$ [126]. They perform a careful analysis of potential sources for the discrepancy and find that it is likely caused by their modelling of the lensing signal rather than by model inconsistencies of ΛCDM. The results from the Subaru Hyper Suprime-Cam of galaxy clustering data are in agreement with the values from the Planck CMB analysis [127].

- *Hubble constant.* The value for the Hubble constant inferred from the CMB by measurements of the Planck satellite, $H_0 = 67.66 \pm 0.42$ km/(s Mpc) [10, 17, 102], is lower than the one from SN Ia in the local Universe [11, 16, 128]. Using the latest data, the local measurements of $H_0 = 74.03 \pm 1.42$ yield a tension of $\sim 4.4\,\sigma$ significance [16]. Re-analyses searching for inconsistencies in the SNe Ia and CMB data analyses respectively could not identify errors in either analysis [129–135]. Analyses using only light element abundances from BBN as probes of the early Universe, omitting CMB data, find a similar discrepancy [136, 137]. Beyond consistency tests, many different explanations and models have

been investigated and/or proposed to solve the tension; just a few examples are non-standard neutrino (self-)interactions [e.g. 138–143], early dark energy models [e.g. 144–147], or modifications of GR [e.g. 24, 148–150]. To date, no commonly agreed solution has been found.

Chapter 3

Models Beyond ΛCDM

Motivations to consider models beyond the standard assumptions and parameters of ΛCDM are diverse: they arise not only from trying to solve existing theoretical or observational problems, but also from trying to gain a deeper understanding of the laws that govern our Universe, and of its dominating dark components. Hence, many models and theories that go beyond the concordance model of ΛCDM have been built and tested. Examples are models of inflation [151–158], cosmologies including effects of non-standard particle physics [140, 142, 159–164], non-standard properties like self-interactions or decays of the DM particles [165–168], replacing the cosmological constant with a perfect fluid [169–171], and theories that modify the laws of General Relativity [171–177]. Even though some of these theories succeed in solving one or more of the problems of ΛCDM, none of them has emerged as a serious competitor so far.

In this chapter, I introduce the extensions of ΛCDM important in the context of this thesis: inflation (Sec. 3.1), massive neutrinos (Sec. 3.2), additional energy content in the form of radiation (Sec. 3.3), modifications of gravity (Sec. 3.4), and cosmic superstrings (Sec. 3.5). I conclude this chapter in Sec. 3.6 where I comment on (possible) connections between these different extensions of ΛCDM.

3.1 Non-Standard Initial Conditions: Inflationary Models

In the concordance model of cosmology, the initial conditions for the evolution of perturbations in the Universe are assumed to be given by a perfectly Gaussian distribution. In ΛCDM, one quantifies these perturbations in terms of the primordial power spectrum of curvature fluctuations which follows a sim-

ple power-law; it provides the seeds for the formation of gravitationally bound structures that eventually evolve to form the structures we can observe today. The most widely accepted scenario by which such perturbations would have been generated is a phase of accelerated expansion in the early Universe. The occurrence of this epoch of *inflation* not only provides an explanation for how structures could have formed in an initially homogeneous Universe but also solves other problems faced by ΛCDM: the flatness, horizon and monopole problems. I explain these problems and how inflation can solve these next. After that, I show how inflation can be realised with single-field models in the slow-roll approximation. Finally, I discuss the observable signatures of inflation models. For details going beyond this brief outline, I refer the reader to Refs. [35, 178–181] for introductions in form of lecture notes, and to Refs. [37–40] for textbook introductions.

3.1.1 Motivation

Quantitatively the requirement of an accelerated expansion can be formulated by requiring that the second time derivative of the scale factor is positive, i.e. $\ddot{a} > 0$. Using the second Friedmann equation (Eq. 2.19) and setting $\Lambda = 0$, one can translate the requirement on the evolution of the scale factor into a condition for the pressure and density of the energy content of the Universe, these are:

$$\ddot{a} > 0 \iff \rho + 3p < 0\,. \tag{3.1}$$

As can be seen from (Eq. 2.19) this also implies that $\dot{a} = aH$ increases, while the Hubble radius $1/(aH)$ decreases. The latter is the key feature for solving three other problems that ΛCDM faces in the absence of an inflationary phase:

- *Flatness problem.* The curvature of the Universe today, inferred from observations, is close to zero, $\Omega_k = 0.001 \pm 0.002$ (see Sec. 2.6). A small curvature contribution means that the sum of all other energy components, Ω_{tot}, must be close to unity. This becomes apparent by re-arranging the Friedmann equation (Eq. 2.18) to

$$\Omega_{\text{tot}} - 1 = \frac{k}{a^2 H^2} = \frac{k}{\dot{a}^2}\,. \tag{3.2}$$

  In ΛCDM the expansion of the Universe is decelerating until the cosmological constant takes over and dominates the energy density in the late Universe. During the phase of the decelerated expansion ($\ddot{a} < 0$) the scale factor only increases; hence, unless curvature is vanishing, Ω_{tot} will be driven away from unity. Therefore extremely fine-tuned initial conditions would be required to lead to the observed $\Omega_{\text{tot}} \sim 1$ today.

An inflationary phase can solve this problem: $\dot{a}$ increases during inflation, setting $\Omega_{\rm tot}$ close to unity without the necessity for any fine-tuning. If inflation lasts long enough, one expects the observation of an almost vanishing curvature term.

- *Horizon problem.* Assuming an evolution of the Universe as in ΛCDM, one can calculate the particle horizon at the time of recombination, when the CMB was released. This calculation indicates that only patches of the sky of about 1° could have been in causal contact, which is in direct contradiction to the observed uniform temperature of the CMB photons. The existence of an early inflationary phase solves this contradiction. During inflation, the comoving Hubble radius is reduced, so regions that were in causal contact at early times are pushed outside the horizon. After the inflationary phase ends, the Hubble radius increases. Modes that were disconnected gradually enter the horizon again, explaining why we can observe correlations on much larger scales than expected in a universe without an early inflationary phase.

- *Magnetic monopoles.* At very early times, before the Universe was just fractions of a second old ($t_U < 10^{-11}$), the energies exceeded the ones from any observational tests we have so far, e.g. from high-energy cosmic rays or probes from the LHC. Hence, it is yet unknown how the laws of physics behave at these high energies. Some theories, called Grand Unified Theories (GUT), predict that all known gauge forces – the strong, weak, and electromagnetic forces – can be unified above a certain energy scale. If this is the case, phase transitions may take place when the strong force separates from the other forces, or when other symmetries break. One possible implication of such phase transitions is the production of topological defects. In which form these appear depends on the details of the phase transition; examples would be the existence of magnetic monopoles, one-dimensional strings, or two-dimensional domain walls. The masses of magnetic monopoles are estimated to be around $10^{13} - 10^{18}$ GeV. In combination with their high predicted number density, these objects would completely dominate the energy density of the Universe today. However, the rapid expansion during an inflationary phase would separate these monopoles sufficiently far from each other, diluting their number density beyond current observational limits.

3.1.2 Slow-Roll Single Field Inflation

A simple way to model inflation from a theoretical perspective is by a scalar field ϕ with a slowly-evolving potential. The slow evolution of the field, usually

referred to as the *inflaton*, is required to ensure inflation lasts long enough to solve the horizon, flatness and monopole problem. The inflaton potential then determines the shape and properties of the primordial power spectrum.

The action of the inflaton, assuming a minimal coupling to gravity and a standard kinetic term $X = \frac{1}{2}(\partial_\mu \phi)^2$, takes the form

$$S_\phi = \int \mathrm{d}^4x \sqrt{-g}\,[X - V(\phi)]\ . \tag{3.3}$$

The requirement on the potential $V(\phi)$ is that it dominates over the kinetic energy and other potential contributions to the stress-energy tensor. This condition is equivalent to the requirement that in an expanding FLRW metric ϕ evolves, and keeps evolving, slow compared to the expansion of the Universe. Under these assumptions the continuity equation (Eq. 2.20) and the first Friedmann equation (Eq. 2.18) read

$$\ddot{\phi} + 3H\dot{\phi} + V'(\phi) = 0 \quad \text{and} \quad H^2 = \frac{8\pi G}{3}\left[\frac{1}{2}\dot{\phi}^2 + V(\phi)\right]\ , \tag{3.4}$$

where the prime denotes a partial derivative with respect to the inflaton ϕ.

A reformulation of Eq. (3.4) yields the definition of the so called *slow roll parameters* ϵ_i,

$$\epsilon_1 \equiv -\frac{\dot{H}}{H^2} = \frac{8\pi G}{2}\left(\frac{\mathrm{d}\phi}{\mathrm{d}N}\right)^2 \quad \text{and} \quad \epsilon_{i+1} \equiv \dot{\epsilon}_i/(H\epsilon_i)\,. \tag{3.5}$$

The parameter N gives the number of e-foldings of expansion and is defined via $\mathrm{d}N \equiv H\mathrm{d}t = \mathrm{d}\ln a$. Successful inflation requires that the first and the second slow-roll parameter are much smaller than unity, i.e. $\epsilon_1 \ll 1$ and $\epsilon_2 \ll 1$. Alternatively, one can express the first two slow-roll parameters via the potential of the inflaton as

$$\epsilon_\mathrm{v} \equiv \frac{M_\mathrm{Pl}^2}{2}\left(\frac{V'(\phi)}{V(\phi)}\right)^2 \quad \text{and} \quad \eta_\mathrm{v} \equiv M_\mathrm{Pl}^2\frac{V''(\phi)}{V(\phi)}\,, \tag{3.6}$$

using $M_\mathrm{Pl}^{-2} = 8\pi G$.

The scalar perturbations produced in slow-roll inflation take the form of the primordial power spectrum which is assumed in ΛCDM (Eq. 2.4). Hence, one can express the parameters A_s and n_s in terms of the slow-roll parameters,

$$n_s - 1 = 2\,\eta_\mathrm{v} - 6\,\epsilon_\mathrm{v}, \qquad A_s = \frac{1}{24\,\pi^2\epsilon_\mathrm{v}^\star}\frac{V^\star}{M_\mathrm{Pl}^4}\,. \tag{3.7}$$

The notation $Z^\star$ denotes that the quantity Z is evaluated at the pivot scale $k_\star$. However, the slow-roll parameters (Eq. 3.6) can in general be functions of

the scale k. In that case n_s does not take a constant value, as in ΛCDM, but it is slightly 'running',

$$n_s(k) = n_s^\star + \frac{1}{2}\frac{\mathrm{d}\, n_s(k)}{\mathrm{d}\,\ln\, k}\,\ln(k/k_\star) + \dots\,. \tag{3.8}$$

Slow-roll inflation exhibits another feature that is not included in the simple assumptions for primordial fluctuations made in ΛCDM: beyond scalar perturbations, tensor perturbations are generated. These tensor perturbations can be parametrised via

$$\mathcal{P}_t(k) = \frac{k^3}{2\pi^2}|h_k|^2 = A_t\left(\frac{k}{k_\star}\right)^{n_t}\,, \tag{3.9}$$

with A_t and n_t parametrising the the amplitude and tilt of the spectrum, and where $|h_k|^2$ is the amplitude of tensor perturbations derived from the perturbed FLRW metric, $g_{\mu\nu} = g_{\mu\nu}^{\mathrm{FLRW}} + h_{\mu\nu}$. With this, one defines the scalar-to-tensor ratio:

$$r \equiv \mathcal{P}_t(k_\star)/\mathcal{P}_\mathcal{R}(k_\star) = 16\,\epsilon_{\mathrm{v}}^\star\,. \tag{3.10}$$

For a given form of the potential $V(\phi)$, one can calculate the spectral index (Eq. 3.3) and the scalar-to-tensor ratio (Eq. 3.10). Constraints on these quantities from measurements of the CMB spectra and the BAO scale can then be used to test and rule out concrete inflation models, see, e.g. Refs. [151–153, 182–184]

After the inflationary period, the Universe is assumed to fully thermalise before the evolution according to the (standard) cosmological model sets on. This phase of thermalisation is commonly referred to as *reheating*.[1] The end of reheating, a_{reh}, is given by [182, 185, 186]

$$\frac{k_\star}{a_0 H_0} = \frac{a_\star}{a_{\mathrm{end}}}\frac{a_{\mathrm{end}}}{a_{\mathrm{reh}}}\frac{a_{\mathrm{reh}}}{a_{\mathrm{eq}}}\frac{H_\star}{H_{\mathrm{eq}}}\frac{a_{\mathrm{eq}}H_{\mathrm{eq}}}{a_0 H_0}\,, \tag{3.11}$$

where $k_\star = a_\star H_\star$ is the pivot scale at horizon crossing, a_{end} is the scale factor at the end of inflation, and a_{eq} and H_{eq} are the scale factor and Hubble rate at the time of matter-radiation equality. Observations constrain the values of a and H today and at matter-radiation equality; the values of $H_\star$ and $N_\star \equiv \ln(a_{\mathrm{end}}/a_\star)$, on the other hand, are set by choice of a specific model for inflation. The model for the reheating process dictates the ratio $a_{\mathrm{end}}/a_{\mathrm{reh}}$. If no concrete reheating model is assumed, the redefinition $N_\star \equiv \ln(a_{\mathrm{reh}}/a_\star)$ can absorb the uncertainties concerning the reheating process. In this case, $N_\star$ becomes an independent inflationary model parameter.

[1] For a review on reheating, refer to, e.g. Ref. [155].

3.1.3 Beyond Slow-Roll Single Field Inflation

Generally, inflation models can predict a more complicated form of primordial density and curvature fluctuations than can be captured by a power-law with running spectral index and the slow-roll approximation. If the slow-roll conditions are not fulfilled, one must take perturbations to the FLRW metric into account.

Further generalisations are to either allow for a non-standard kinetic term or to introduce more than one inflaton field, leading to so-called multi-field inflation models. These models can yield different initial conditions: in standard single-field models, density perturbations correspond directly to perturbations of the metric, leading to *adiabatic* initial conditions (adiabatic as the entropy remains constant). In contrast, more complex models can introduce *isocurvature* modes, meaning that different species can be perturbed in different ways. For example, a perturbation in the matter field, $\delta\rho_m$, could be exactly cancelled by a perturbation in the radiation field, $\delta\rho_r$. This cancellation leaves the overall density perturbation zero and breaks the direct correspondence between density and metric perturbations.

Since the original proposal of inflation and first pioneering studies [187–196], a large number of different models have been proposed and investigated. Popular examples are eternal inflation [197–201], natural inflation [202–205], chaotic inflation [196, 199, 200, 206, 207], and hilltop models [208–211]. For reviews of single-field models and comparison against data, refer to Refs. [151–154]. For a review of multi-field inflation models and their observational signatures, see Refs. [155–158].

3.1.4 Observational Signatures

Inflation gives rise to the initial curvature perturbations of the Universe. Having taken place in the very early Universe, long before elements form or photons decouple, there are no direct electromagnetic observables available to probe inflationary theories. Nevertheless, the perturbations generated impact the evolution of the Universe, imprinting signatures on observables today. Examples are:

- *Angular scale of the first CMB peak.* The angular scale of the first peak of the CMB temperature power spectrum is sensitive to the nature of the initial conditions: baryonic acoustic oscillations generated by adiabatic modes follow a cosine. In contrast, purely isocurvature modes would lead to an oscillation described by a sine function. Oscillations following a sine function would shift the angular position of the first peak from $\ell \simeq 220$ in the adiabatic case, to about $\ell \simeq 330$ in the pure isocurvature case.

The Planck measurement of the CMB places the first peak very close to 220, excluding the presence of pure isocurvature initial conditions [105]. The situation becomes more involved when adiabatic and isocurvature modes are mixed. The exact position of the first CMB peak must be evaluated on a case-by-case basis and can be used to constrain or rule out models that generate isocurvature modes.

- *B-mode polarisation of the CMB.* Tensor perturbations in the early Universe would manifest as linear B-mode polarisations in the CMB (see Sec. 2.5). In ΛCDM, assuming a primordial power spectrum with only scalar perturbations, these types of B modes cannot be explained, providing a test for inflationary models. However, the expected amplitude is small and suppressed by several orders of magnitude compared to the temperature fluctuations in the CMB. So far no detection of B modes sourced by gravitational waves has been made. Nevertheless, the non-detection helps to rule out inflationary models by constraining the scalar-to-tensor ratio r. Current limits arising from a combination of CMB and BAO data yield $r < 0.056$ at a pivot scale of $k_\star = 0.002$ Mpc^{-1} at 95% confidence level [184].

- *Primordial gravitational waves.* Tensor perturbations created during inflation would leave a stochastic gravitational wave (GW) background. Estimates from single-field slow-roll inflation models suggest that the energy density of these GWs today would be of the order of $\Omega_{\mathrm{GW0}} \sim 10^{-15}$. A direct detection of these is technically challenging and currently beyond the sensitivity of any ongoing GW observatories [212, 213]. The stochastic GW background could, however, become detectable in the far future by missions like the proposed Big Bang Observer (BBO) [214, 215]. Already in construction and currently planned to launch in 2034 is the Laser Interferometer Space Antenna (LISA) [216], which is expected to probe a frequency range of $(10^{-5} - 0.1)$ Hz. In most scenarios, this is orders of magnitude above the expected stochastic GW background signal. However, some inflationary models predict an amplified signal of this stochastic background which would be in the detectable range of LISA. Examples are the formation of primordial black holes or models that incorporate additional degrees of freedom arising, e.g. from particle production during inflation or spectator fields [217].

3.2 Non-Minimal Neutrino Masses in Cosmology

The treatment of neutrino masses in the concordance model of ΛCDM is usually highly simplified: one massive neutrino with the minimum required mass from oscillation measurements, 0.06 eV [104]. However, this is not a realistic treatment for two reasons. Firstly, two different oscillations between mass eigenstates have been observed, leading to the conclusion that at least two neutrinos have non-zero mass eigenstates. Secondly, laboratory measurements only constrain the absolute neutrino mass scale to be smaller than 1.1 eV [218] at 90% confidence level. Hence, there is no reason to fix the sum of the neutrino masses to their minimal allowed value. Therefore, a straightforward extension of ΛCDM is to include a physical treatment of neutrino masses, in line with the observations from oscillation measurements. I will refer to these models as $\nu\Lambda$CDM to make it explicit that the neutrino mass sum is treated as a free parameter. In this section, I will briefly outline why cosmological observables are sensitive to the sum of neutrino masses. For detailed reviews of neutrino cosmology, see Refs. [219–222].

The fact that neutrinos are massive and their mass is below 1.1 eV has important consequences for the background evolution of the Universe. At early times, when the temperatures are high, neutrinos are ultra-relativistic and, therefore, contribute to the radiation content of the Universe (Ω_r in the Friedmann equation, Eq. 2.21). As the Universe expands and cools, the massive eigenstates will gradually become non-relativistic and start contributing to the matter content (Ω_m). For $m_\nu \lesssim 1.1$ eV this happens after matter-radiation equality. The exact time, however, depends on the neutrino mass: the higher the mass, the earlier they become non-relativistic. Generally, the inclusion of massive neutrinos means that one cannot compute the background evolution analytically and numerical tools are needed. Examples are the Code for Anisotropies in the Microwave Background (CAMB) [223, 224] and the Cosmic Linear Anisotropy Solving System (CLASS) [225, 226].

On the level of background quantities, the energy density in neutrinos today, $\Omega_{\nu 0}$, and the value of the Hubble parameter H_0, are degenerate. Lowering $\Omega_{\nu 0}$ can always be compensated for by increasing H_0 such that the angular acoustic scale of the first CMB peak will not change (see Eq. 2.31). Hence, a direct, local measurement of H_0, independent from the CMB, can help to break this degeneracy and increase the constraints on the sum of the masses, $\Sigma\, m_\nu$. In addition to that, measurements of the BAO scale at different redshifts add information about the time evolution of the Hubble rate. In particular, the combination of CMB and BAO data breaks a degeneracy between H_0 and $\Omega_{\mathrm{m}0}$, allowing for better constraints on $\Sigma\, m_\nu$.

Let us now turn to the effects of neutrino masses on scalar perturbations of

the FLRW metric (Eq. 2.15). Neutrino masses contribute to the gravitational potentials, affecting the evolution of the baryon-photon plasma in the early Universe, and the matter distribution in the late Universe. As neutrinos only interact weakly with other SM particles, they can travel through gravitational potential wells relatively undisturbed whilst relativistic. This *free streaming* leads to a damping of perturbations below a critical scale, set by the size of the horizon when a neutrino species becomes non-relativistic. This free-streaming scale $\lambda_{\rm fs}$ depends on the mass of the neutrino, the temperature at which they become non-relativistic and on the energy density in matter. On scales smaller than the free-streaming scale, neutrinos cannot be bound to gravitational potentials owing to their large velocities. On scales larger than the free-streaming scale, however, neutrinos cluster with baryons and dark matter. Hence, massive neutrinos distribute power from small scales to larger scales. Additionally, the baryon and DM perturbations on small scales will grow more slowly compared to a scenario with massless neutrinos. Hence, the linear growth rate of perturbations becomes scale-dependent. This also leads to a decrease of the gravitational potentials even during matter domination.

The effects of massive neutrinos on the matter power spectrum are observable: lensing of the CMB and galaxy clusters is sensitive to neutrino masses, as the matter distribution along the line of sight, acting as a lens, is changed. Beyond that, the modified time evolution of the gravitational potentials has effects on the integrated Sachs-Wolf effect (see Sec. 2.5).

There are, however, complications when using cosmological data to constrain neutrino masses: the regimes in which observables add most constraining power on massive neutrinos come from small, non-linear scales of the matter power spectrum. Therefore results rely on the accurate modelling of these non-linearities. This modelling is usually done with N-body simulations, for example, the 'halofit' model [227, 228]. A complication that arises is the precise modelling of baryonic feedback from ongoing galaxy formation processes on small scales, see, e.g. Refs. [229–232]. The unknowns in these processes set a lower limit on the matter power spectrum scales that provide reliable predictions. Hence, the range of the data most sensitive to the mass of neutrinos cannot be used to obtain constraints so far.

Besides the challenges in obtaining theoretical predictions of the matter power spectrum on small scales, further complications in the process of the comparison to data arise. The density of galaxies does not perfectly trace the over-densities of the total matter field. Therefore, a galaxy bias factor is usually introduced to correct for the difference between the observed galaxy densities and the theoretical expectation from overall density perturbations. In most analyses, this biasing factor is either assumed to be constant or to evolve proportionally to some power of the redshift. The presence of massive

neutrinos, however, introduces a scale-dependent growth which must be taken into account when modelling the galaxy bias. If not accounted for, this could lead to a bias in the inferred cosmological parameters and bounds on neutrino mass sum when using data from upcoming galaxy surveys [233, 234].

To conclude the section on neutrino masses, I want to stress a crucial point: all bounds on neutrino masses inferred from cosmology are highly model-dependent and should be interpreted as such. The model of $\nu\Lambda$CDM is based on several assumptions (see Chapter 2), all of which enter the calculation of theoretical predictions and, therefore, have the power to affect the results of parameter estimates. One example is the effect of non-standard momentum distributions of the cosmic neutrino background radiation. Allowing for deviations from a perfectly thermal distribution, the mass bounds can be loosened by a factor of two [235]. Motivations for these deviations are particle decays into neutrinos or vice versa [236–238], neutrino self-interactions [140, 239–241], or oscillations to sterile neutrinos [242–244]. Another example of the strong model dependency of neutrino mass bounds inferred from cosmology is modifications of the underlying theory of gravity. As we shall see later, in Sec. 4 of this chapter, replacing GR by a scalar-tensor theory of gravity can shift the allowed neutrino mass sum to a higher value, to obtain $\Sigma\, m_\nu > 0$ from CMB and BAO data at a more than $2\,\sigma$ significance [24]. Hence, constraints on the sum of neutrino masses arising from cosmological fits can serve as a consistency test of the underlying assumed cosmology but cannot replace direct, cosmology model-independent laboratory measurements.

3.3 Non-Standard Radiation Content

In the concordance model of ΛCDM, the radiation content of the Universe only receives two contributions: from photons and – as long as they are ultra-relativistic – from the three Standard Model neutrinos. Quantitatively, the energy density (derived in Sec. 2.4, Eq. 2.22) is given by

$$\rho_r(t) = \left[1 + N_{\rm ur}\frac{7}{8}\left(\frac{T_\nu^0}{T_\gamma^0}\right)^4\right]\rho_\gamma(t)\,, \tag{3.12}$$

for times after neutrino decoupling and before the heaviest neutrino becomes non-relativistic. In this case, $N_{\rm ur}$ is equal to 3.045 in ΛCDM [48, 49]. After the first neutrino becomes non-relativistic, it evolves as a non-cold dark matter component, resulting in a decrease of $N_{\rm ur}$ and an additional contribution to the radiation energy density, $\rho_{\rm ncdm}(t) = 3\,p_{\rm ncdm}(t)$.

Heuristic approaches modifying the radiation content (given in Eq. 3.12) are to *i)* alter the neutrino temperature T_ν or *ii)* allow extra contributions

from additional relativistic species, $\rho_{\rm dr}(t)$, i.e. so-called dark radiation. I will briefly discuss both options in the following.

3.3.1 Neutrino Temperature

Modifications of the neutrino temperature arise in many extensions of standard cosmology: any particle species that decays or annihilates after neutrino decoupling can transfer a fraction of its energy into the electron-photon plasma and another fraction into neutrinos. Concrete examples are, e.g. self-interacting DM models with light mediators [245–249].

Depending on the exact decay, energy can either be primarily injected into the electron-photon plasma or into the ultra-relativistic neutrino component. Such decays can, therefore, lead to a change in the temperature ratio T_ν^0/T_γ^0. While T_γ^0 is well constrained by CMB measurements, so far there is no measurement of the temperature of the cosmic neutrino background, T_ν^0, allowing for more freedom for non-standard values in this parameter.

One can parametrise non-standard values of the neutrino temperature by defining the ratio

$$r_\nu = \frac{T_\nu}{T_\nu^{\Lambda\rm CDM}} \,, \tag{3.13}$$

where $T_\nu^{\Lambda\rm CDM}$ is the neutrino temperature in ΛCDM, such that r_ν is equal to unity in standard ΛCDM. The simplest assumption is that r_ν is constant since neutrino decoupling. It is, however, also conceivable that the neutrino temperature changes after BBN, for example, due to the decays of a very long-lived exotic particle species [249–253]. In such a case one generally expects also the baryon-to-photon ratio $\eta_b = n_b/n_\gamma$ to differ between the epochs of BBN and CMB formation.

3.3.2 Additional Ultra-Relativistic Species

The energy density in radiation can be enhanced due to the presence of additional relativistic species. These could be for example sterile neutrinos [242, 244, 254], light, millicharged WIMPS [255, 256], or from a decoupled dark sector [250, 257, 258].

In analogy to the case of SM neutrinos, one parametrises the energy density of ultra-relativistic species in terms of the equivalent number of effective neutrinos:

$$N_{\rm ur} = \frac{\rho_{\rm ur}}{\frac{7}{8}\left(\frac{4}{11}\right)^{4/3}\rho_\gamma} \,. \tag{3.14}$$

Under the assumption that the additional radiation does not interact with any of the other particle species, its only effect is to increase the Hubble rate during

radiation domination. In particular, interactions between dark matter and dark radiation, which can lead to late kinetic decoupling and a suppression of small-scale structure [259–261], are not covered by the above parametrisation. The presence of additional relativistic particles in this parametrisation is hence largely equivalent to an increase in the neutrino temperature. It is important to note, however, that dark radiation always increases ρ_r, i.e. $N_{\rm ur} \geq 0$.

As for the neutrino temperature, it can be interesting to study scenarios in which $N_{\rm ur}$ varies with time. In particular, $N_{\rm ur}$ decreases whenever the temperature drops below the mass of one of the additional exotic particles [262]. Conversely, an increase of $N_{\rm ur}$ can result from the annihilation or decay of other particle species, as in the case of the conversion of dark matter into dark radiation [263]. One can therefore introduce the two independent parameters $N_{\rm ur,BBN}$ and $N_{\rm ur,CMB}$, allowing $N_{\rm ur}$ to take different values today, at the time of recombination and during BBN.

With these newly introduced parameters, the effective number of relativistic degrees of freedom is given by

$$N_{\rm eff} = r_\nu^4 N_\nu + N_{\rm ur} \tag{3.15}$$

with $N_\nu = 3.045$ in the early Universe, where all three neutrino species are ultra-relativistic.

Note that in terms of observable signatures, the two scenarios parametrised here with r_ν and $N_{\rm ur}$ are completely degenerate. However, the underlying physical source for the modification does matter when it comes to parameter inference in a Bayesian framework as the prior ranges for the parameter must be chosen appropriately.[2]

3.3.3 Observable Signatures

Changing the energy density in radiation has different observable effects at different stages in the evolution of the Universe. In general, the radiation component is the dominant contributor to the energy budget of the Universe at early times. Hence, the effects of non-standard scenarios are more pronounced in observables from the early Universe.

- *Light element formation.* The addition of ultra-relativistic degrees of freedom and an increase of the neutrino temperature increase the Hubble rate at early times (see Eq. 2.18). An increased Hubble rate means that the various reactions relevant for BBN drop out of equilibrium at higher redshift, which leads to a decrease in the number of neutrons available for the formation of helium and hence, to a smaller helium abundance.

[2]See Sec. 5.1 for an introduction on Bayesian statistics and parameter inference.

- *Cosmic microwave background.* An increase of the energy density in radiation shifts the point of matter-radiation equality to a smaller redshift. Hence, gravitational potentials have more time to grow before recombination, the amplitude of the first peak in the CMB is enhanced, and its position θ^* is shifted towards smaller angular scales. While the latter effect can be compensated for by modifying other model parameters accordingly, $N_{\rm eff}$ also increases the damping length of fluctuations, resulting in a lower damping tail of the CMB, see, e.g. Refs. [264, 265]

- *Large scale structure.* A delay of matter-radiation equality by increasing the energy in the radiation component also delays the onset of structure formation. Modifications manifest as a change in the phase, and the amplitude of the BAOs imprinted in the matter power spectrum, see, e.g. Refs. [266, 267].

For more details on the effects of additional ultra-relativistic species on the cosmological evolution, refer to Refs. [220, 222, 256, 267].

3.4 Non-Standard Gravity: Galileon Cosmologies

Theories attempting to change the laws of gravity must alter the field equations of General Relativity (GR). As there are many ways to do so, it can be useful to tackle the problem with a systematic approach based on Lovelock's theorem [268, 269]. Lovelock's theorem states:

> *'The only second-order, local gravitational field equations derivable from an action containing solely the 4D metric tensor (plus related tensors) are the Einstein field equations with a cosmological constant.'*
>
> (Lovelock, 1971)

Therefore, any theory that aims to modify gravity by altering the laws of GR from an action-based approach must modify or break at least one of the requirements of Lovelock's theorem. This provides different ansatzes to write down extensions to GR by including

- non-local terms,
- higher dimensionality,
- higher order derivatives, and/or
- extra degrees of freedom.

Another approach would be to abandon the action principle and treat gravity as an emergent property, see, e.g. Refs. [270–272]. A sketch to give the reader a broad, non-exhaustive overview of the variety of different possible models is shown in Figure 3.1. For comprehensive reviews on modified gravity (MG) theories and their phenomenology, refer to Refs. [171–177].

In this work, I will focus on the extension of GR by an extra scalar degree of freedom. A large variety of these models are embedded in Horndeski's theory of gravity, the most general local, four-dimensional, Lorentz-invariant scalar-tensor theory of gravity that keeps the equations of motions at second order [273]. The Horndeski action reads

$$S = \int d^4x\sqrt{-g}\left[\mathcal{L}_M[g_{\mu\nu},\psi_{\rm m}] + \sum_{i=2}^{5}\mathcal{L}_i^{\rm H}[g_{\mu\nu},\phi] + \right], \tag{3.16}$$

with $\mathcal{L}_M[g_{\mu\nu},\psi_{\rm m}]$ being the Lagrangian of the matter fields $\psi_{\rm m}$, and the Lagrangian densities

$$\begin{aligned}
\mathcal{L}_2^{\rm H} &= K(\phi,X),\\
\mathcal{L}_3^{\rm H} &= -G_3(\phi,X)\,\Box\phi,\\
\mathcal{L}_4^{\rm H} &= G_4(\phi,X)\,R + G_{4,X}\left[(\Box\phi)^2 - \phi_{;\mu\nu}\phi^{;\mu\nu}\right],\\
\mathcal{L}_5^{\rm H} &= G_5(\phi,\,X)\,G_{\mu\nu}\phi^{;\mu\nu} - \frac{1}{6}\,G_{5,X}(\phi,\,X)\,\times\\
&\quad\times\left[(\Box\phi)^3 + 2\phi_{;\mu}{}^{\nu}\phi_{;\nu}{}^{\alpha}\phi_{;\alpha}{}^{\mu} - 3\phi_{;\mu\nu}\phi^{;\mu\nu}\Box\phi\right].
\end{aligned}$$

The extra scalar degree of freedom is given by ϕ and its standard kinetic term by $X \equiv -\partial_\mu\phi\,\partial^\mu\phi/2$. A Horndeski model is fully specified by the four arbitrary functions K, G_3, G_4 and G_5 of the scalar and its kinetic term. Here, $G_{i,X}$ indicates derivatives with respect to X, and I introduced the notation $\phi_{;\mu\nu} \equiv \nabla_\mu\nabla_\nu\phi$ and $\Box\phi \equiv \nabla_\mu\nabla^\mu\phi$. See Refs. [274, 275] for the equations of motion. To recover GR, one has to set $G_4(\phi,X)$ to $M_{\rm Pl}^2/2$ and all other Horndeski functions to zero.

Examples of well studied scalar-tensor theories belonging to the Horndeski class are quintessence [277, 278], k-essence [279, 280], $f(R)$ theories [281–283], covariant Galileons [21, 23], kinetic gravity braiding [128, 284, 285], or the fab four [286–289].

One of the results of this thesis is to show how a combination of cosmological and astrophysical observations can be used to rule out covariant Galileons as a viable alternative to GR. This section serves as a brief introduction to the model. I will first introduce the action of the model and discuss general properties, followed by a discussion of the background evolution and model parameters. Thereafter, I will comment on the imposed stability conditions

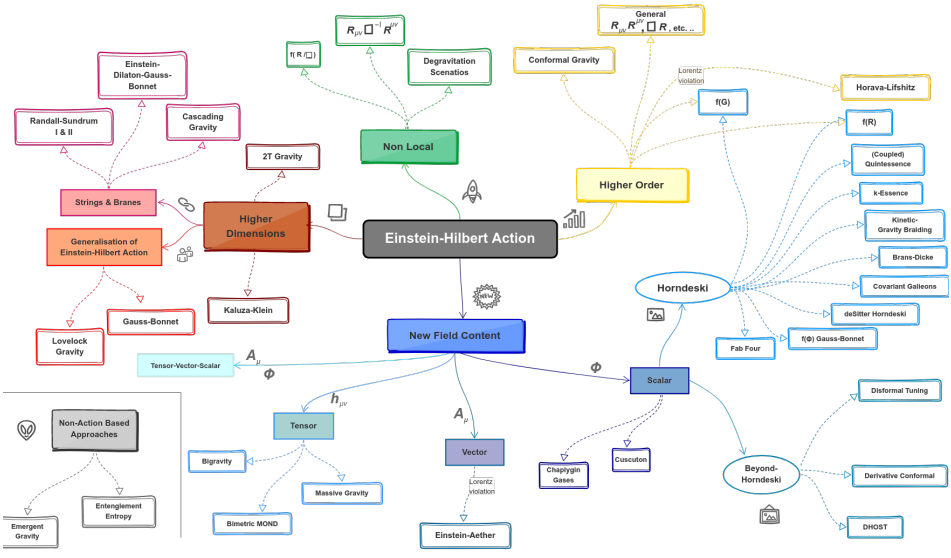

Figure 3.1: Incomplete overview of the landscape of modified gravity models. Covariant Galileons, the model investigated in more detail here, can be found on the right border in the middle as a sub-class of Horndeski models. Adapted with permission from Tessa Baker from Figure 3 in Ref. [276].

and important phenomenological properties of the minimally-coupled covariant Galileon model.

3.4.1 Action of the Covariant Galileon Model

The Galileon model was initially constructed by Nicolis *et al.* [21] such that in a flat space-time, up to total derivatives, the action is invariant under the shift symmetry of the gradient of the scalar field,

$$\partial_\mu \phi \to \partial_\mu \phi + b_\mu \,, \tag{3.17}$$

where b_μ is a constant vector. According to Ostrogradski's theorem [290], ghost instabilities can arise if higher than second-order derivatives are contained in the equations of motion.[3] To avoid these unphysical states, the additional terms allowed to enter the action are terms of the form [21]

$$\begin{aligned}
\mathcal{L}_1^{\rm Gal} &\propto -\phi \,, && (3.18)\\
\mathcal{L}_2^{\rm Gal} &\propto X \,, && (3.19)\\
\mathcal{L}_3^{\rm Gal} &\propto X \,\Box\, \phi, && (3.20)\\
\mathcal{L}_4^{\rm Gal} &\propto X \left[(\Box\phi)^2 - (\partial_\mu\partial_\nu\phi)^2\right], && (3.21)\\
\mathcal{L}_5^{\rm Gal} &\propto X \left[(\Box\phi)^3 - 3\Box\phi(\partial_\mu\partial_\nu\phi)^2 + 2(\partial_\mu\partial_\nu\phi)^3\right]. && (3.22)
\end{aligned}$$

Refer to [21] for the derivation of the equations of motion.

To generalise the model to non-flat space-times, a promotion of the partial derivatives to covariant derivatives is required. However, this leads to the presence of third-order derivatives in the equations of motion [22] and the potential presence of Ostrogradski ghosts [290]. One can avoid the occurrence of higher-order terms by introducing counter-terms that couple the Galileon field to the Einstein tensor and the Ricci scalar [22]. These counter-terms lead to an exact cancellation of the higher-order derivatives in curved space-times.[4] The action of the covariant Galileon is given by

$$S = \int \mathrm{d}^4x\,\sqrt{-g}\left[\frac{M_{\rm Pl}^2}{2}R + \sum_{i=1}^{5}\mathcal{L}_i^{\rm Gal}[g_{\mu\nu},\phi] \;+ \mathcal{L}_{\rm m}[g_{\mu\nu},\psi_{\rm m}]\right], \tag{3.23}$$

[3] I will comment in more detail on Ostrogradski ghosts and further instabilities in Sec. 3.4.3.

[4] Note that the inclusion of these counter-terms is sufficient but not necessary to obtain ghost-free scenarios [291–293]. Second-order equations of motion, and, therefore, healthy theories can also be obtained by imposing further constraints [291, 292, 294].

with the Lagrangian densities

$$\mathcal{L}_1^{\rm Cov} = -\frac{c_1 M^3}{2}\phi\,, \tag{3.24}$$

$$\mathcal{L}_2^{\rm Cov} = c_2\, X\,, \tag{3.25}$$

$$\mathcal{L}_3^{\rm Cov} = 2\frac{c_3}{M^3} X\,\Box\phi\,, \tag{3.26}$$

$$\mathcal{L}_4^{\rm Cov} = \frac{c_4}{M^6} X^2\, R + 2\frac{c_4}{M^6} X\left[(\Box\phi)^2 - \phi_{;\mu\nu}\phi^{;\mu\nu}\right]\,, \tag{3.27}$$

$$\mathcal{L}_5^{\rm Cov} = \frac{c_5}{M^9} X^2\, G_{\mu\nu}\phi^{;\mu\nu} - \frac{1}{3}\frac{c_5}{M^9} X\left[(\Box\phi)^3 + 2\phi_{;\mu}{}^{\nu}\phi_{;\nu}{}^{\alpha}\phi_{;\alpha}{}^{\mu} - 3\phi_{;\mu\nu}\phi^{;\mu\nu}\Box\phi\right]\,. \tag{3.28}$$

In this form, the standard term $M_{\rm Pl}^2/2$ from the Einstein-Hilbert action is separated from the Galileon specific terms. The coefficients c_i appearing in the Galileon terms are constants and the free parameters of the theory. The introduction of the mass scale $M^3 \equiv M_{\rm Pl}H_0^2$ ensures that the Galileon parameters are dimensionless. Note that the extra degrees of freedom are constants and not arbitrary functions of ϕ and X as in the general Horndeski Lagrangian. Further, there is no combination of the parameters c_i for which a ΛCDM limit is obtained [21].[5]

The couplings in $\mathcal{L}_4^{\rm Cov}$ and $\mathcal{L}_5^{\rm Cov}$ of the scalar field to the Ricci scalar and Einstein tensor, respectively, are the counter terms that ensure that the equations of motion are kept at second order. Furthermore, the theory contains derivative couplings, i.e. couplings between derivatives of the field and derivatives of the metric, for example, the term proportional to $X\,\Box\phi$ in $\mathcal{L}_3$. This mixing of the kinetic terms of the metric and the scalar field is commonly referred to as 'braiding'.

The coupling of gravity to matter in the action (Eq. 3.23) is explicitly assumed to be minimal; the matter Lagrangian only depends on the metric $g_{\mu\nu}$ and matter fields $\psi_{\rm m}$, and there is no explicit occurrence of the Galileon field ϕ. I will only discuss this minimally-coupled case in the present work. Examples with a non-minimal coupling to matter can be found, e.g. in Refs. [295, 296].

The action (3.23) can be divided into sub-classes of covariant Galileon models by consecutively including the densities $\mathcal{L}_i$. I will follow the standard terminology and refer to models that include contributions to the action up to the $\mathcal{L}_3$ term as cubic Galileons. Similarly, quartic and quintic Galileons stand for models including terms up to $\mathcal{L}_4$ and $\mathcal{L}_5$ respectively.

A noteworthy feature shared by the quartic and the quintic branch of the

[5] This is the case as the theory does not include a cosmological constant, i.e. $\Lambda = 0$. If ones adds a cosmological constant term, the ΛCDM limit is reached for $c_i \to 0$.

theory is that they predict an anomalous propagation speed of gravitational waves [297]. This can be easily seen when considering the effective field theory (EFT) formulation of Bellini and Sawicki [298]. Their formulation shows that the propagation speed of tensor modes is generally not equal to the speed of light in all Horndeski theories that include a coupling of the scalar to the Ricci and/or Einstein tensor via $\mathcal{L}_4$ and/or $\mathcal{L}_5$. Instead, tensor perturbations can propagate slower, or faster than the speed of light, and the propagation speed has a time dependences.

An appealing property of the covariant Galileon models is that they are self-accelerating, i.e. the late-time acceleration can be solely generated by the kinetics of the scalar field without the need for a potential term [21, 23, 299]. As these scenarios are the main ones of interest in the context of dark energy, I will set the coefficient of the potential term, c_1, to zero in the remainder of this work.

3.4.2 Background Evolution and Model Parameter Space

The study of the background evolution of covariant Galileons requires to solve the Friedmann equation (Eq. 2.18) and the equation of motion of the scalar field numerically. However, an analytical expression would be preferable as the numerical calculation can become computationally expensive. To calculate the background evolution, it is further necessary to specify an initial condition for the time derivative of the Galileon field, $\dot{\bar{\phi}} \equiv \mathrm{d}\bar{\phi}/\mathrm{d}t$.[6] It was shown that the Galileon background evolution can be described analytically if the evolution is chosen such that the product of the Hubble parameter and the time derivative of the Galileon field is constant at all times [299], i.e.

$$H\dot{\bar{\phi}} = \text{constant} \equiv \xi H_0^2, \tag{3.29}$$

where ξ is a dimensionless constant. This represents the so called 'tracker solution' [299].

Generally, cosmological solutions with different initial conditions (not captured by the tracker solution) yield different background evolution scenarios [299]. Nevertheless, these converge eventually all to a common trajectory described by Eq. (3.29) [299]. Furthermore, Barreira *et al.* [24, 300, 301] showed that if a Galileon model is required to be cosmologically viable, in the sense that it provides a good fit to the CMB temperature power spectrum, it must reach the tracker solution before the late-time acceleration sets in. The dynamics of the Galileon field only become relevant at late times, giving rise

[6] Recall that $\bar{\phi}$ indicates the spacial average of ϕ.

to the late-time acceleration. The modifications introduced at early times are negligible. Hence, one can assume that the evolution of the background follows the tracker solution at all times.

Assuming the tracker background evolution, one can derive an analytic expression for the Friedman equation [299, 302]. This is done by using Eq. (3.29) to replace $\dot{\bar{\phi}}$ in the Friedman equation (with $\Omega_\Lambda = 0$) to obtain

$$\begin{aligned} E^4(a) &= \left(\Omega_{r0}a^{-4} + \Omega_{m0}a^{-3} + \Omega_{\nu 0}\frac{\bar{\rho}_\nu(a)}{\bar{\rho}_{\nu 0}}\right) E^2(a) \\ &+ \frac{1}{6}c_2\xi^2 + 2c_3\xi^3 + \frac{15}{2}c_4\xi^4 + 7c_5\xi^5\,, \end{aligned} \tag{3.30}$$

where $E(a) = H(a)/H_0$ and $\Omega_{\nu 0}$ indicates the energy density of neutrinos today. Requiring that the Universe is flat gives the condition for the present day

$$\begin{aligned} \Omega_{\phi 0} &\equiv 1 - \Omega_{r0} - \Omega_{m0} - \Omega_{\nu 0} \\ &= \frac{1}{6}c_2\xi^2 + 2c_3\xi^3 + \frac{15}{2}c_4\xi^4 + 7c_5\xi^5\,, \end{aligned} \tag{3.31}$$

allowing us to fix one of the Galileon parameters. A second model parameter can be fixed by enforcing the tracker evolution in the background equations of motion of the Galileon field, leading to

$$c_2\xi^2 + 6c_3\xi^3 + 18c_4\xi^4 + 15c_5\xi^5 = 0\,. \tag{3.32}$$

With these constraints and the Friedman equation (Eq. 3.30), one obtains the two equations that fully specify the background evolution of the Galileon models [299, 301, 303]:

$$\dot{\bar{\phi}} = \xi\, H_0^2/H(a)\,, \tag{3.33}$$

$$\begin{aligned} \left(\frac{H(a)}{H_0}\right)^2 &= \frac{1}{2}\left[\left(\Omega_{r0}\, a^{-4} + \Omega_{m0}\, a^{-3} + \Omega_{\nu 0}\,\frac{\bar{\rho}_\nu(a)}{\bar{\rho}_{\nu 0}}\right)\right] + \\ &\quad \frac{1}{2}\left[\left(\Omega_{r0}\, a^{-4} + \Omega_{m0}\, a^{-3} + \Omega_{\nu 0}\,\frac{\bar{\rho}_\nu(a)}{\bar{\rho}_{\nu 0}}\right)^2 + 4\,\Omega_{\phi 0}\right]^{1/2}. \end{aligned} \tag{3.34}$$

It is worth noting that the Hubble rate only depends on the energy densities Ω_{i0}, but not on the Galileon parameters, c_i. Therefore, they cannot be constrained by observables that only rely on background quantities, such as BAO and SNe Ia data.

Galileon Parameter Space

The analytical expression for the background expansion of the model on the tracker solution (Eq. 3.34) considerably simplifies the numerical treatment. However, another problem occurs when trying to constrain the Galileon parameter space: there is a symmetry under redefinition of the dimensionless couplings [299, 301, 303],

$$\begin{aligned} c_2 &\longrightarrow c_2/B^2, \\ c_3 &\longrightarrow c_3/B^3, \\ c_4 &\longrightarrow c_4/B^4, \\ c_5 &\longrightarrow c_5/B^5, \\ \phi &\longrightarrow \phi B\,, \end{aligned} \tag{3.35}$$

where B is a constant real parameter. Owing to this degeneracy, any attempt to obtain constraints on the Galileon parameters with a Markov Chain Monte Carlo (MCMC) analysis leads to a stagnation of the likelihood in a region with infinitely long tails in the model parameter space, as shown in Ref. [301]. The authors suggest a solution, which is to fix one parameter to obtain scaling-invariant quantities for the others. In the accompanying Paper A we followed the approach of Ref. [24] and fixed the value of c_2 to -1.[7]

Hence, the five free Galileon parameters[8]

$$\{c_2, c_3, c_4, c_5, \xi\}\,, \tag{3.36}$$

are reduced to just two free parameters, c_4 and c_5, by *(i)* the closure relation requiring the Universe to be spatially flat (Eq. 3.31), *(ii)* assuming that the background evolution follows the tracker solution at all times (Eq. 3.29), and *(iii)* fixing c_2 to -1 to break the scaling degeneracy in the Galileon parameter space. To be explicit: this means that the cubic branch of the Galileon models has no more free parameters than ΛCDM, the quartic branch has one additional parameter (c_4) and the quintic branch two (c_4 and c_5).

[7]The reason to choose c_2 to fix over the other parameters is that in the test MCMC chains of Ref. [24] it turned out that c_2 does not change its sign, contrary to c_3, c_4 and c_5. Therefore, fixing the sign of c_3, c_4 or c_5 would exclude solutions that can fit the data. Hence, generality can be maintained by requiring c_2 to be negative. The exact numerical value of $c_2 < 0$ is arbitrary. One can simply rescale all parameters following Eq. (3.35) to obtain a projection into the rest of the parameter space.

[8]Recall that the coefficient of the potential term c_1 is set to 0, such that the late-time acceleration is driven by the dynamics of the Galileon field.

3.4.3 Stability Conditions

To be a viable alternative to GR, a theory should not suffer from pathologies like ghost or gradient instabilities. Ghost fields are instabilities that occur when a degree of freedom does not have a minimum energy state, i.e. the Hamiltonian is unbounded from below. Hence, ghost degrees of freedom can carry negative energies. The pair production of a ghost and an ordinary particle will, therefore, lead to a rapid decay of the vacuum state which is fatal for the viability of a theory. Gradient instabilities, on the other hand, arise when the background evolves into a regime where the squared speed of sound of perturbations is negative. This leads to unbounded exponential growth of the perturbations on small scales [173]. On the level of the Lagrangian, this can be avoided by requiring the spatial gradient of the extra field to have the correct sign, i.e. the opposite sign to that of the kinetic term.

One special case of ghost instabilities are Ostrogradski ghosts [290].[9] These linear instabilities arise from a non-degenerate Lagrangian[10] that depends on second (or higher) order time derivatives, in such a way that a partial integration cannot cancel this dependence in the Hamiltonian. Covariant Galileons are by construction free from the Ostrogradski ghosts as the couplings of the scalar to the Ricci scalar and Einstein tensor were introduced to keep the equations of motion at second order [22]. The authors of Refs. [297, 302, 305] derived the conditions to avoid ghost as well as gradient instabilities. The reader should refer to these works for the explicit expressions. A noticeable property of these expressions is that for covariant Galileon models (and also all other theories belonging to the Horndeski class), the conditions for avoiding ghost and gradient instabilities depend only on background quantities. Therefore, it is not necessary to solve the full perturbation equations to decide whether a given combination of model parameters leads to a stable solution or not. In the remainder of this work, I will only consider parameter combinations that pass these stability conditions.

3.4.4 Phenomenology of Covariant Galileon Cosmologies

Galileon cosmologies have been confronted with CMB, BAO and SNe Ia data to assess their cosmological viability, see, e.g. Refs. [24, 303, 306–309]. The models are a late-time modification of gravity and do not have a ΛCDM limit, so the cosmological best-fit parameters are generally not expected to be similar

[9] For a review of Ostrogradski's theorem, see [173, 304].

[10] A Lagrangian $L(\vec{x}, \dot{\vec{x}}, \ddot{\vec{x}})$ with $\vec{x} = (x_1, x_2, .., x_N)$ is non-degenerate if $\det\left(\frac{\partial^2 L}{\partial \ddot{x}_i \ddot{x}_j}\right) \neq 0$ holds.

to the ones of ΛCDM. I will briefly summarise the results of previous studies to provide an overview of the phenomenology of minimally-coupled covariant Galileon cosmologies:

- Quartic and quintic Galileons predict a propagation speed of tensor perturbations unequal to the speed of light [297, 308].
- The value of the Hubble constant inferred from the CMB is higher than the one in ΛCDM and in agreement with local measurements from type SNe Ia [11], as assessed in Ref. [24].
- A simultaneous fit to BAO and CMB data requires non-zero neutrino masses ($\Sigma\, m_\nu \gtrsim 0.3$ eV at $2\,\sigma$) [24].
- The time evolution of the lensing potential can differ considerably from the standard ΛCDM case: instead of a strict, scale-independent decrease of the potential after matter domination, the potential can grow, stay constant, decay, or show other non-trivial behaviours in Galileon models. This behaviour depends on the considered scale and model parameters [24].
- A statistical invalidation of covariant Galileon cosmologies solely by cosmological observations through a combination of CMB, BAO, SNe Ia, H_0 and weak lensing data has been reported [310].[11]

For further details and studies of solar system constraints and non-linear structure formation, refer to Refs. [21, 24, 297, 306, 308, 309, 311–313].

3.5 Cosmology with Cosmic Superstrings

String theory is a consistent framework to unify all of nature's known forces and matter contents. The basic idea of string theory is that the fundamental constituents of matter are neither point-like particles, nor quantum fields, but rather one-dimensional strings, appearing either open or as closed loops. To be consistent, the theory must be formulated in more than just four dimensions; to describe bosonic strings 26 dimensions are needed, for the description of superstrings, incorporating supersymmetry, ten dimensions are necessary.

To explain what we can observe in four dimensions, there are different mechanisms to achieve a *compactification* of the additional dimensions appearing

[11] This study was published after Paper A, and after the constraints on the models arising from the observation of a GW and its electromagnetic counterpart. I will discuss the latter two results in Sec. 4.1.

in string theory. These mechanisms typically create many *moduli*, appearing as scalar fields in the 4-dimensional, low-energy limit. For introductions on (super)string theory and details on compactification mechanisms, refer to textbooks and lecture notes [314–321]. For a clear conceptual introduction, see Ref. [322].

There are different types of string theories differing in their symmetry and compactification properties. In the following, we will consider type IIb superstring theory, a parity-violating theory with oriented strings.

Besides offering a theory of gravity valid beyond the Planck scale, string theory can also realise a phase of inflation in the early Universe. The moduli from compactification provide many natural candidates to act as inflaton fields. Heavy moduli with steep potentials reach their respective potential minima relatively quickly, while light moduli with flat potentials take more time to reach their respective minima. The modulus reaching its minimum last can, therefore, act as the inflaton. It can not only drive the accelerated expansion, but its potential can also fulfil the slow-roll conditions needed for inflation to last sufficiently long. It is further conceivable that not only the last modulus reaching its minimum acts as a single inflaton, but that the combination of several moduli leads to a realisation of inflation. Hence, string theory can provide explanations for the origins of inflation in single and multi-field scenarios. Refer to Ref. [323, 324] for more technical details on string theory and inflation.

Many inflation scenarios from string theory share a common prediction: the fundamental one-dimensional building blocks of string theory can get stretched out to macroscopic size during the rapid phase of expansion [325]. If produced towards the end of inflation, the superstrings start to form string networks, and can still be present on cosmological scales in today's Universe. These cosmic strings can leave observable signatures, opening a window to observationally test predictions of superstring theory.

The primary free parameter of cosmic strings is the dimensionless string tension, $G\mu/c^2$.[12] In analogy to strings in classical mechanics, the string tension quantifies the energy per unit length.

In the remainder of this chapter, I will first clarify the difference between cosmic strings and cosmic superstrings. After that, I will give an overview of the cosmological evolution of cosmic superstring networks, and the parameters governing this evolution. Finally, I will discuss observational signatures and current bounds on the model parameters of cosmic superstrings.

[12]To keep the discussion in line with the conventions in Paper B, I will use SI units in this section.

3.5.1 Cosmic Strings vs. Cosmic Superstrings

Cosmic strings can be produced by phase transitions in the early Universe. These phase transitions can occur when gauge symmetries are spontaneously broken. Examples of theories that exhibit such a symmetry breaking are grand unified theories (GUTs). Inspired by the unification of the weak and electromagnetic force above a certain energy scale, GUTs are built to unify the strong with the electroweak force above the so-called GUT scale ($\sim 10^{16}$ GeV). Once the energies in the early Universe fall below that scale, the symmetry all three forces share is spontaneously broken; the strong force decouples from the weak and electromagnetic force, resulting in a phase transition [326]. These phase transitions can result in the formation of classic, GUT-scale cosmic strings formed at the end of an inflationary phase [327]. Other phase transitions, not necessarily related to GUTs, can lead to the production of classic cosmic strings at other times with different, but fixed energy scales.

In contrast, cosmic superstrings are proposed to be the fundamental building blocks of the contents of the Universe, stretched out to macroscopic length scales. A difference compared to field-theoretic cosmic strings is that cosmic superstrings are produced with a spectrum of energies, and not at a fixed energy scale. Conceptually, this can be understood as follows: cosmic superstrings reside in throats of a warped, higher-dimensional manifold. Besides model-dependent production details, the string tension we would observe in our four dimensions depends on the exact location of the superstring in the throat. Usually, superstrings are confined at the bottom of the throat, but can move or oscillate around it [328–330]. These movements will cause the string tension to appear to vary in time and/or along the string when observed in $3 + 1$ dimensions.

The string tension of cosmic GUT-scale strings would be close to the Planck scale. The tension of CSSs, however, can be much smaller and can be anywhere between the Planck scale and experimental limits near the weak scale. Current observational constraints set the limits $G\mu/c^2 \lesssim 10^{-7}$. I will discuss where these limits arise from in Sec. 3.5.4.

3.5.2 Cosmological Evolution of Superstring Networks

The clustering properties of cosmic strings and cosmic superstrings are similar: the strings interact with each other, cluster and form networks. Strings that collide can either pass through each other or break and reconnect with intercommutation probability P_{int}. If a string collides with itself, it can form a string loop. These closed string loops will emit (gravitational) radiation and evaporate over time. A difference between networks composed of cosmic strings and cosmic superstrings (CSSs) lies in the intercommutation probabil-

ity. For classical strings, the intercommutation probability is equal to unity (see [331, 332]), while CSSs intercommute with $P_{\rm int} < 1$. The reduced rate of intercommutations has an important consequence: the number density of long string loops is higher in networks of CSSs compared to networks of classical strings.

Additionally, model-dependent factors can further increase the number density of CSSs. How large this enhancement is, is generally unknown. Chernoff & Tye [330] (referred to as CT18 in the following) incorporated the model-dependent uncertainties into the dimensionless factor

$$\mathcal{G} \equiv \frac{N_T\, N_s}{P_{\rm int}}\,, \tag{3.37}$$

where N_T is the effective number of throats in which CCSs reside, and N_s is the effective number of string species within a single throat. An interpretation of the parameter $\mathcal{G}$ is to think of it as the effective number of CSS species. It can range from unity to as high as 10^4. The best estimate quoted by CT18 is $\mathcal{G} = 100$.

The results of network simulations of cosmic strings all exhibit a self-similar scaling solution. The intercommutation, breaking and rejoining of CSSs proceeds with high efficiency, and the horizon scale is the only length scale that characterises the string network at any given time [333]. On scales larger than the horizon, long strings follow a random walk. Below the horizon scale, a fixed number of long strings exist, while small closed string loops dominate over long string segments [331, 334, 335]. The energy density of cosmic strings remains a fixed fraction of the total energy density of the Universe. The scaling solution does not depend crucially on the initial conditions. If more/fewer strings are present initially, the collision rate increases/decreases such that the number of strings per horizon volume reaches the scaling solution. Hence, the scaling solution acts as an attractor (see Refs. [314, 320, 321] for reviews).

The results of the network simulations show that closed loops dominate the number density of cosmic strings in volumes of astrophysical interest. Hence, these closed loops are the most important component when it comes to observational signatures. Therefore, the following discussion focuses on string loops.

The size of newly formed string loops is proportional to the scale of the horizon. The earlier string loops form, the smaller their size. After formation, closed loops start evaporating by emitting energy. This energy can either be exclusively in form of gravitational waves (GWs) or, depending on the model, also in form of axions or electromagnetic emissions. The parameter χ quantifies the fraction of gravitationally emitted energy. Assuming $\chi = 1$ in the following,

the lifetime of the loop is

$$t_{\rm life} = \frac{l/c}{\Gamma\, G\mu/c^2}\,, \tag{3.38}$$

where l is the invariant loop length, and Γ the dimensionless effective decay rate of string loops. CT18 perform numerical simulations and determine the value of Γ to be about 50. One can define the characteristic length $l_g = \Gamma\,(G\mu/c^2)\,c\,t_H$, where t_H indicates the age of the Universe. Any string loops born with a length l smaller than this characteristic length will have evaporated by today.

Internal motions of strings, like rotations, vibrations and oscillations, proceed with the internal velocity $v_{\rm i}$. Initially, after loop formation, the internal velocity is high, about $0.1 - 0.3\,c$, and decreases with time [334]. Hence, the earlier a string forms, the slower its internal motion will be today.

Table 3.1 provides a summary of all (derived) parameters and quantities important in this context for the derivation of the evolution of CSS networks in the Universe.

The dependence of the networking properties on the string tension is the following: strings of lower tension formed earlier, when the horizon was smaller. Therefore, strings with lower tension have a smaller invariant length l. Compared to strings with larger tensions, low tension strings have a higher number density today.

Assuming a cosmological model, the *homogeneous distribution* of cosmic string loops can be simulated. CT18 provide an analytical approximation to the distribution of the homogeneous number density of string loops per logarithmic interval of loop length, $(\mathrm{d}\,n/\mathrm{d}\ln l)_{\rm hom}$. It is

$$\left(\frac{\mathrm{d}\,n}{\mathrm{d}\ln l}\right)_{\rm hom} = 1.15\times10^{-6}\frac{x}{(1+x)^{5/2}}\frac{f_{0.2}\,\mathcal{G}\,\alpha_{0.1}^{1/2}}{\left(\chi\,\Gamma_{50}\,\mu_{-13}\right)^{3/2}}\ \mathrm{kpc}^{-3}\,, \tag{3.39}$$

with $x \equiv l\,/\,l_g$, $l_g = 0.026\,\chi\,\Gamma_{50}\,\mu_{-13}$, and the definitions

$$\mu_{-13} \equiv \frac{G\mu/c^2}{10^{-13}}\,, \quad \alpha_{0.1} \equiv \frac{\alpha}{0.1}\,, \quad f_{0.2} \equiv \frac{f}{0.2}\,, \quad \text{and} \quad \Gamma_{50} \equiv \frac{\Gamma}{50}\,. \tag{3.40}$$

The inferred values from the simulations are $\Gamma_{50} = \alpha_{0.1} = f_{0.2} = 1$. It is safe to ignore the numerical uncertainties on these values as they are small compared to uncertainties in $\mathcal{G}$, which range over several orders of magnitude.

Figure 3.2 shows the homogeneous distribution (Eq. 3.39) without superstring enhancement, i.e. $\mathcal{G} = 1$. The number density of string loops is highest at a loop length close to the characteristic length l_g. For string tensions $G\mu/c^2 \lesssim 10^{-9}$, the number density of string loops below galactic scales is not suppressed due to loop decays.

Parameter	Typical value/ Definition	Description
$G\mu/c^2$	$G\mu/c^2 \lesssim 10^{-7}$	Dimensionless string tension. Observationally constrained, see Sec. 3.5.4.
$\mathcal{G}$	$1 \leq \mathcal{G} \leq 10^4$	Dimensionless effective number of cosmic superstring species. Theoretical range from Ref. [330], with best estimate $\mathcal{G} = 100$.
v_i	$v_\mathrm{i} \sim 0.1 - 0.3\,c$	Initial internal velocity of oscillating strings after formation; typical value quoted for large loops after formation [334]. As the Universe expands v_i decreases.
α	$\alpha \sim 0.1$	Size of large strings relative to horizon size [330].
f	$0.05 \lesssim f \lesssim 0.2$	Fraction of strings forming large string loops of invariant size $l = \alpha\, c\, t$ at time t. Estimates from Refs. [336, 337].
χ	$\chi \leq 1$	Fraction of energy evaporating string loops emit into gravitational waves.
Γ	50	Effective dimensionless decay rate of loops in networks. Depends on the geometry and internal characteristics of the cosmic superstring. Typical value quoted for a string loop with $\chi = 1$ [330].
$\beta(\mu)$	$0 < \beta(\mu) < 0.46$	Fraction of strings clustering with DM. Strings with higher tension cluster less; hence, $\beta(\mu)$ decreases with increasing tension. Quoted typical values arise from numerical simulations of clustering properties, see [330].
P	$l\,/\,(2c)$	Fundamental loop period, where l is the invariant loop length.
t_life	$(l/c)\,/\,[\Gamma\,(G\mu/c^2)]$	Characteristic lifetime of cosmic superstrings.

Table 3.1: Relevant model parameters (*upper part*) and derived characteristics (*lower part*) of cosmic superstrings.

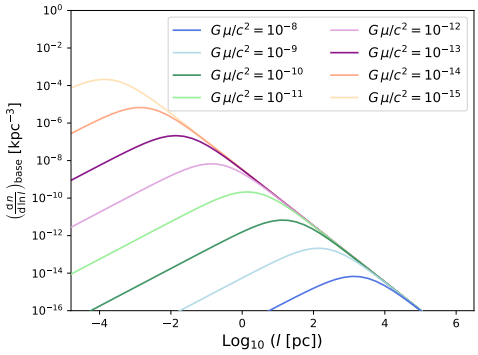

Figure 3.2: The number density of string loops per logarithmic interval of length, $(\mathrm{d}\, n/\mathrm{d}\ln l)_{\mathrm{base}}$, as a function of the loop length. This baseline distribution is given by the homogeneous distribution (Eq. 3.39) with $\mathcal{G} = 1$, meaning no superstring enhancement is taken into account. The number density is shown for different string tensions, from $G\mu/c^2 = 10^{-8}$ to 10^{-15} (bottom to top) in powers of 10^{-1}. The network simulations leading to these results are from Ref. [330], obtained by assuming a flat ΛCDM cosmology. Figure from Paper B.

Integrating the homogeneous distribution of string loops over all loop length l yields the homogeneous string loop density in the Universe. It is given by

$$\Omega_{\mathrm{loop}} = 2.4 \times 10^{-10} \left(\frac{\mathcal{G}\, f_{0.2}}{h^2}\right) \left(\frac{\alpha_{0.1}\, \mu_{-13}}{\Gamma_{50}}\right)^{1/2} , \tag{3.41}$$

with the Hubble constant $H_0 = 100\, h$ km/s/Mpc. The fact that the loop density Ω_{loop} is so low poses challenges to experimental searches.

The homogeneous distribution is a good proxy to describe the string distribution on large scales. However, on small scales corrections reflecting the actual clustering of matter must be taken into account. One can do this by introducing a factor $\mathcal{F}$ that parametrises the string density enhancement due to an enhancement in the DM density. The inhomogeneous density then reads

$$\left(\frac{\mathrm{d}\, n}{\mathrm{d}\ln l}\right)_{\mathrm{inhom}} = \mathcal{F} \left(\frac{\mathrm{d}\, n}{\mathrm{d}\ln l}\right)_{\mathrm{hom}} , \tag{3.42}$$

with

$$\mathcal{F} \equiv \beta(\mu)\, \mathcal{E} \equiv \beta(\mu)\, \frac{\rho_{\mathrm{DM,\,local}}}{\rho_{\mathrm{DM,\,cosmo}}} . \tag{3.43}$$

This includes the definition of $\mathcal{E}$ which is parametrising the enhancement of the local DM density ($\rho_{\mathrm{DM,\,local}}$) compared to the average DM density in the

Universe ($\rho_{\mathrm{DM,\,cosmo}}$). The factor $\beta(\mu)$ is a string tension-dependent quantity resulting from numerical simulations. CT18 determined it to be $0 < \beta(\mu) < 0.46$, where the highest value of ~ 0.46 occurs for small string tensions with $G\mu/c^2 = 10^{-15}$.

With these ingredients, one can compute the inhomogeneous string loop density (Eq. 3.43). This density distribution is important when searching for signatures of cosmic strings in the late Universe. We will now turn to the details of such an observable signature, microlensing sourced by cosmic strings.

3.5.3 Microlensing by Cosmic Superstrings

Imagine a long, thin string with cylindrical symmetry. If there are no internal motions of the string, the string is invariant under a Lorentz boost along its length. These properties give rise to an energy-momentum tensor of the object in which pressure and density have the same magnitude, but opposite signs. The tension acts as a negative pressure along the string length [338] leading to a locally flat space-time around the string. However, internal string motions break the Lorentz invariance. Globally, the internal movements and oscillations of the string induce a cone-shaped space-time carving out a deficit angle on a plane perpendicular to the cosmic string. This deficit angle, $\Delta\Theta$, depends on the string tension and is given by $8\pi G\mu/c^2$ (see, e.g. Refs. [314, 339]). When two photons on a parallel trajectory pass the string on either side, they are both deflected towards the string.

For the alignment of a point-like source and a string with typical tensions in the range $10^{-14} \lesssim G\mu/c^2 \lesssim 10^{-7}$, the deflection scale of the two photons is too small to resolved by an observer. The string induces a microlensing event where the flux measured by the observer appears instantaneously twice as high as the unlensed flux [338, 340, 341]. The geometry of this alignment is shown in the *left panel* of Figure 3.3.

Owing to the internal oscillations of a cosmic string loop, a geometrical alignment between observer, source, and the string does not give rise to just one, but several microlensing events. While the oscillation proceeds with the string's internal velocity, $v_{\mathrm{i}} \sim c$, the centre-of-mass motion of a string bound within a galaxy is about $v_{\mathrm{com}} \sim 300$ km/s. Hence, about $N_{\mathrm{rep}} = v_{\mathrm{i}}/v_{\mathrm{com}} \sim 1000$ repetitions of lensing events per alignment can occur during the time it takes the string to pass the source, $t_{\mathrm{pass}} \sim l/v_{\mathrm{com}}$. The *right panel* of Figure 3.3 shows the repetition of microlensing events as an oscillating string passes the source.

The feature that makes microlensing events sourced by cosmic strings unique compared to the lensing by other known sources, is the instantaneous increase of the flux. If the geometry allows one to approximate the source as

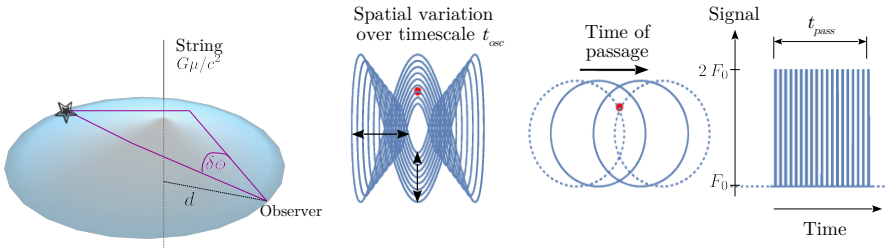

Figure 3.3: *Left panel*: Visualisation of an alignment between observer, cosmic string, and source leading to a microlensing event. The string carves out a space-time wedge of the disk perpendicular to the string with angle $\Delta\Theta = 8\pi G\mu/c^2$. The string is depicted by the black solid line, the blue shading represents the 3-dimensional space-time cone. For an observer in front of the string, there are two paths the photons emitted by a source within the deficit angle can take. For a string that lies at an angle $\theta_{\rm str}$ with respect to the line of sight, the observer will detect two images of the source separated by the angle $\delta\phi = \theta_{\rm str}\,\Delta\Theta\left(1 - \frac{d}{D}\right)$. Here, d is the distance between observer and string, and D is the distance between observer and source. *Right panel*: Sequence of microlensing events caused by a moving loop (*blue lines*) and a stationary source (*red dot*). The internal oscillations of the loop occurring on time-scale $t_{\rm osc}$ are shown on the left. The projection of the area that is covered by the string loop as it moves with its centre of mass velocity is shown in the middle. The time scale for the loop to pass the source is given by $t_{\rm pass}$. The dotted circles depict the beginning and end of the passing. The sequence of the induced microlensing events, as detected by the observer, are shown in the right picture. The bottom line indicates the unlensed flux F_0. The increased flux measurements lie exactly a factor of two above the unlensed values. Figure adapted from Paper B.

a point source, the flux is enhanced by precisely a factor of two. In contrast, a Newtonian mass acting as a lens leaves a different signal: if a string passes the line of sight to a source, an observer would see a gradual increase followed by a gradual decrease of the source's flux. The maximum flux enhancement depends on the mass of the lens, an exact factor of two is only a special case. Hence, an indication for the presence of a cosmic string would be given by the observation of an immediate doubling of the brightness of an object, and ideally a consecutive observation of a sudden decrease to the initially measured value.

The timescales on which microlensing events take place are important for estimating how feasible a detection of such events would be. The duration of one lensing event depends on the tension of the string acting as a lens and the geometry. In particular, on the distance between observer and source D, the distance between observer and string d, the string's velocity perpendicular to the line of sight $v_{\mathrm{com},\perp}$, and the angle of the string to the line of sight θ_{str}. From these quantities one can derive the lensing duration t_{lens}:

$$t_{\mathrm{lens}} = \frac{8\pi G\mu}{c^2}\,\sin\theta_{\mathrm{str}}\frac{d}{v_\perp}\left(1-\frac{d}{D}\right). \tag{3.44}$$

Fixing the distance between observer and source, D, the lensing duration takes its maximum value when the string is positioned directly in the middle, i.e. $d = 0.5\,D$, leading to maximum lensing time

$$t_{\mathrm{lens,\,max}} = \frac{8\pi G\mu}{c^2}\,\sin\theta_{\mathrm{str}}\frac{D}{4v_\perp}. \tag{3.45}$$

It is easy to see that lensing events last longer when sourced by strings with higher tensions. The further away a source is from the observer, the larger $t_{\mathrm{lens,\,max}}$, where the scaling with distance is linear. This yields $t_{\mathrm{lens,\,max}} \sim 1$ s for string tension $G\mu/c^2 = 10^{-13}$ when observing a source at ~ 10 kpc distance. For a string tension of 10^{-9} the corresponding maximum lensing time is $t_{\mathrm{lens,\,max}} \sim 2$ h. An order-of-magnitude estimate for the time between two microlensing events sourced by oscillations of a single string acting as a lens is $t_{\mathrm{osc}} \sim l\,/\,(2c) \sim 42\,\mu_{-13}$ days for $D \sim 10$ kpc.

Knowing the typical timescales of microlensing events, one can design experiments aiming to detect cosmic strings. Generally, the exposure time when observing a source should be shorter than the typical lensing duration. If the exposure time exceeds the duration of a lensing event, an observer can never see the flux enhancement by a factor of two. Further, when choosing a target, the string distribution along the line of sight should be as dense as possible to increase the change of a detection.

3.5.4 Observational Signatures

Both types of strings, cosmic strings and cosmic superstrings increase the energy content of the Universe and interact gravitationally. These properties can leave signatures in different observables, allowing us to test the existence of cosmic strings:

- *Light element abundances.* Cosmic strings are an additional contribution to the energy density in the Universe. As a direct consequence, the additional energy source increases the Hubble rate. If this increase is noticeable during the epoch of BBN, reactions governing the formation of light elements drop out of equilibrium at earlier times. Hence, the number of neutrons available for helium formation decreases, leading to a decrease in the predicted helium abundance. Measurements of the helium abundance, therefore, offer a probe for strings formed before the end of BBN. The exact inferred bound on the string tension depends on theoretical uncertainties like the intercommutation probability and details of the production mechanisms of string loops, see, e.g. Refs. [342, 343].

- *Effects on the CMB power spectrum.* Cosmic strings source tensor and vector perturbations. If present in the early Universe, these perturbations can be observed via B-mode polarisations of the CMB [344]. Further, cosmic strings generate line-like discontinuities in the CMB temperature map. This can be understood as follows: assume a string is moving transversely across the sky between an observer and the surface of last scattering with velocity v_{com}. Owing to the deficit angle in the metric of the cosmic string, photons passing behind this cosmic string will experience a blueshift, photons passing ahead of the string will be redshifted. These fluctuations would be of order $\delta T/T \sim G\mu/c^2\, v_{\mathrm{com}}$ [345]. The non-detection of this effect in the Planck CMB temperature map leads to the bound $G\mu/c^2 \lesssim 8 \times 10^{-7}$ at 95% confidence level [346].

- *Gravitational wave background.* Assuming cosmic strings emit the major fraction of their energy through gravitational radiation, they contribute to the gravitational wave background in the Universe. Hence, their parameter space can be probed by gravitational wave observatories such as LIGO. Refer to Ref. [343] for recent constraints as low as $G\mu/c^2 \lesssim 10^{-10}$. However, these bounds crucially depend on the precise modelling of the properties of cosmic strings. These uncertainties also make it questionable whether a signal should be expected within the much lower frequency range tested by LISA [347].

- *Millisecond pulsars.* Millisecond pulsars are spinning sources that emit pulses at precise time intervals. They can be used to search for passing cosmic strings as gravitational waves in the frequency range $10^9 - 10^7$ Hz in the line of sight would disturb the timing of the pulse, see, e.g. Refs. [348–351]. The undisturbed observation of a pulsar for more than twenty years leads to a stringent upper bound on the string tension of $G\mu/c^2 \lesssim 1.5 \times 10^{-11}$ at 95% confidence level [352, 353]. However, the theoretical estimation of these signals highly depends on the underlying assumptions about the gravitational wave emissions by cosmic superstrings. Hence, a bound inferred from observations not requiring these assumptions would be desirable in order to obtain an independent test.

- *Weak lensing.* Cosmic strings lead to the presence of vector perturbations in the early Universe. Today, these could be observable in weak lensing surveys, as vector modes would induce a rotation of the image of distant galaxies [354, 355].

- *Microlensing.* Cosmic strings produce a distinct microlensing signal: once a string passes the line of sight between an observer and a point-like source, the measured flux is instantaneously increased by a factor of two. Likewise, it decreases again to its original value once the string is no longer aligned with the source and observer [338, 340, 341]. These distinct microlensing signatures have been used to estimate constraints on the parameter space of cosmic strings that arise from, e.g. observing quasars and galaxies [356, 357], compact radio sources [358], and stars within our galaxy [359]. These constraints mainly rely on clustering properties of cosmic strings. Hence, microlensing searches can yield an independent confirmation of bounds depending on details of gravitational wave emission by cosmic strings. The expected constraints on the string tension yield $G\mu/c^2 \lesssim 10^{-9}$ with the observation of compact radio sources [358], and $G\mu/c^2 \lesssim 10^{-10}$ with the observation of galactic stars [359].

For more details on different possibilities to observe cosmic strings, I refer the reader to Sec. 4.3 of Ref. [360] and the review given in Ref. [361].

3.6 Connecting the Dots

To conclude this chapter about models going beyond the assumptions of ΛCDM, I will make a few general remarks on the bigger picture. At first glance, the different models and theories introduced here – inflation models, cosmological

signatures of BSM particle physics, modifications of gravity, and cosmologies with cosmic superstrings – might seem disconnected in form and/or nature.

However, this is not the case: superstring theory is a higher dimensional theory of gravity which can also realise a phase of inflation in the early Universe [e.g. 323, 324, 362]. Other approaches are to link the early and late epochs of accelerated expansion by attempts to realise inflation with early dark energy models [e.g. 363–368] or to find a connection between dark energy and string theory [147, 162, 163, 369–371]. More attempts to find a suitable candidate for the inflaton are suggested and realised by particle physics [372], for example through the Higgs sector [e.g. 367, 373–376], and axion monodromy models [e.g. 377–380]. Furthermore, by introducing new fields, for example in the form of axions or supersymmetric partners of SM particles, string theory may give rise to BSM phenomena, and has the potential to provide dark matter candidates [e.g. 162, 370, 381–384]. Yet another link between BSM physics and cosmology could be a connection of mass-varying neutrinos and dark energy [e.g. 385–388]. Another example highlighting the profound connections between the different fields are Standard Model–axion–seesaw–Higgs portal inflation (SMASH) models [160, 389, 390]. These models provide a dark matter candidate in form of the axion, explain neutrino flavour oscillations through the seesaw mechanism by introducing three right-handed neutrinos, and realise inflation through the Higgs portal. The models further address the lack of observations of strong CP violating processes and the matter anti-matter asymmetry in the Universe.

Besides potential theoretical connections, degeneracies between the effects of the different theories appear in their impact on observables. For example, modified gravity theories can predict an enhanced matter power spectrum on small scales compared to the standard ΛCDM scenario. Increasing the neutrino masses can counteract this effect, leading to predictions consistent with current observations [e.g. 391–397]. Beyond the degeneracy between modified gravity and the absolute mass scale of neutrinos, BSM particle physics has the potential to alter cosmological predictions. Non-standard neutrino interactions can raise the cosmological upper bound on neutrino masses (see Sec. 3.2), and the constraints on the spectral index if the additional interactions are active inflation [161]. Furthermore, decays of particles in the early Universe can decrease the temperature of neutrinos with respect to the photon temperature. This temperature decrease effectively reduces the number of relativistic degrees of freedom (see Sec. 3.3). Hence, such decays of exotic particles can open up the parameter space for the presence of an additional ultra-relativistic species like sterile neutrinos or radiation from the dark sector.

Therefore, it is crucial to be aware of the various connections and degeneracies between different non-standard (cosmological) models. Only considering

one extension at a time could hide important effects. A more complete approach to the open problems in the SM of particle physics and cosmology might help to find an answer to the long-standing question '*what are dark energy and dark matter?*'

Chapter 4

Summary of Included Papers

In this chapter, I will summarise those parts of the results of this thesis that are included as Paper A and Paper B. I will only discuss the main results, for all analysis details I refer the reader to the publications included in Part III.

4.1 Galileon Gravity in Light of ISW, CMB, BAO and H_0 Data

In the light of the remaining Hubble tension [10, 13, 16], covariant Galileons are an attractive alternative to ΛCDM: they are a self-accelerating model in which the inferred value of H_0 from fits to CMB and BAO data is naturally consistent with the value obtained by local measurements.

Luckily, the Galileon phenomenology differs much from that of ΛCDM (see Sec. 3.4.4), which means that its viability can be tested beyond just requiring that it fits CMB, BAO and SNe Ia data. For example, the fit to these datasets requires non-zero neutrino masses with a $\sim 5\,\sigma$ significance and a central value of $\Sigma\, m_\nu \sim 0.5$ eV. Hence, tighter limits on the upper bound on the sum of neutrino masses by future laboratory experiments (see Refs. [398–401]) can constrain or rule out the model. Further, the non-trivial evolution of the gravitational potentials allows us to test the theory's validity through measurements of the ISW amplitude in different redshift regions. Another option to test the model is to measure the propagation speed of gravitational waves (GWs) as tensor perturbations are expected to propagate anomalously in quartic and quintic Galileon models [297]. I will present details of how the latter two options can rule out the viability of the considered Galileon models in the remainder of this section.

In the following I summarise the results that my collaborators and I obtained in Paper A. Except where indicated, all results are taken from Paper A.

First, I discuss the constraints arising from fits to updated CMB and BAO datasets. Afterwards I present the main results of our work: how the cubic branch of Galileon cosmologies can be ruled out at $\sim 8\,\sigma$ significance. Further, we set additional constraints on the parameter space of the quartic and quintic models. We achieve this by making use of measurements of the ISW amplitude derived from the cross-correlation of the CMB temperature spectrum with foreground galaxies from the Wide-field Infrared Survey Explorer (WISE) survey [402]. The satellite scanned the whole sky and detected massive galaxies up to a redshift $z \sim 1$ with a peak of the distribution around $z \sim 0.3$ [403]. In this work, we use the ISW data determined by Ferraro *et al.* [404] from a sample containing $\sim$50 million galaxies.

Numerical Treatment

Before starting to present the results, I will briefly comment on the numerical treatment. We obtain all theoretical predictions for cosmological observables for the Galileon models by using the publicly available Boltzmann solver `hi_class` [405, 406]. This is an implementation of the linear perturbations of Horndeski's theory of gravity within the Cosmic Linear Anisotropy Solving System (CLASS) [225]. Bellini *et al.* [407] tested the implementation of covariant Galileons in `hi_class` and verified it against that in EFTCAMB [408, 409], and a private modification of CAMB [223, 224] from the authors of Ref. [24, 301]. The predictions form all codes are consistent, for more details refer to Ref. [407].

In `hi_class`, the background for the Galileon models is solved analytically via the tracker solution (see Sec. 3.4.2). The linear perturbations are derived by internally translating the Galileon model into the Bellini-Sawicki effective field theory formulation of Horndeski's theory [298]. The stability conditions then take the form of Eq. (3.13) and (3.14) of Ref. [298]. The linear perturbation equations as implemented into `hi_class` are given in Appendix A.2 of Ref. [405].

Fit to CMB and BAO Data

We perform a Monte Carlo Markov Chain (MCMC) analysis with CMB data from the Planck 2015 data release [17, 410] and with BAO data from the BAO13 compilation[1] to update the constraints on the cosmological and model parameters of covariant Galileons. Data from SNe Ia are not included in our

[1]Here and in Paper A the abbreviation 'BAO13' stands for the BAO scale measurements from 6dFGS [69], SDSS DR7 LRG [411] and BOSS DR9 CMASS [71], which were used in the Planck 2013 analysis [102].

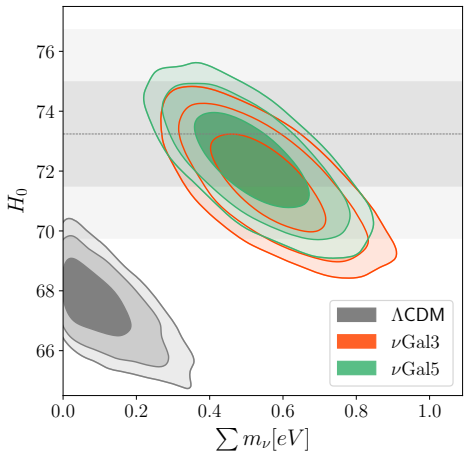

Figure 4.1: Marginalised constraints $(1-3\,\sigma)$ in the $H_0 - \Sigma\, m_\nu$ plane resulting from the MCMC analysis with CMB and BAO13 data for ΛCDM, cubic and quintic Galileons. The horizontal shaded region indicates the constraints on the Hubble constant from local measurements [11]. We excluded the quartic model from the figure as the constraints are indistinguishable from the quintic case. Plot from Paper A.

analysis as measurements of the BAO scale offer a higher constraining power. However, we explicitly verified that the inclusion of the SNe Ia Joint Light-Curve Analysis (JLA) sample [412] does not give rise to a tension with the other two datasets.

In our analysis, we treat the neutrino masses in ΛCDM as a free parameter, as opposed to the baseline model from the Planck analyses [10, 17, 102] (see Sec. 2.6). *A priori*, there is no motivation to fix the mass to one specific value within the allowed range ($0.06\ \text{eV} < \Sigma\, m_\nu < 6.6\ \text{eV}$ [218]). Hence, we only require the mass to be positive. Further, we assume three degenerate mass eigenstates for all models. To explicitly emphasise that $\Sigma\, m_\nu$ is a free parameter, cubic Galileons are abbreviated with νGal_3, quartic models with νGal_4 and quintic with νGal_5.

Our MCMC analysis from Paper A confirms the findings from the previous literature (e.g. Refs. [24, 306, 413]): Galileon cosmologies can fit CMB and background data from BAO measurements simultaneously if non-zero neutrino masses are allowed. The resulting value for H_0 is in agreement with the local measurement from SNe Ia data from Riess *et al.* [11, 13] without any additional prior. Figure 4.1 illustrates this by showing the two-dimensional marginalised constraints on $\Sigma\, m_\nu$ and H_0.

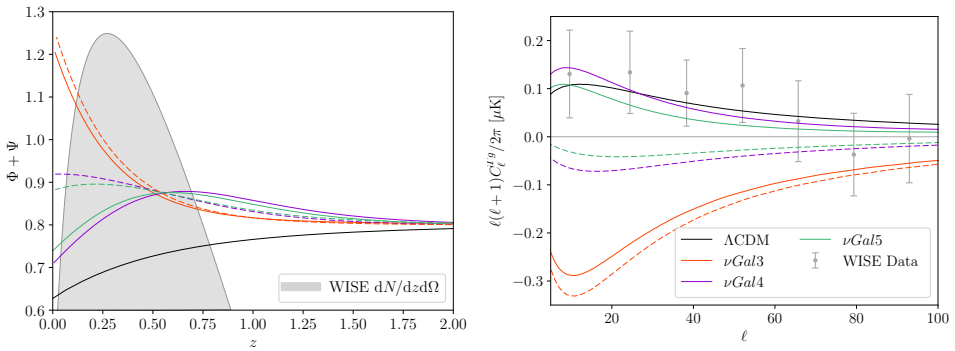

Figure 4.2: *Left panel*: Time evolution of the lensing potential (in arbitrary units) on the scale $k = 0.01$ Mpc for ΛCDM and Galileons. Galileon models with different model parameters are indicated with solid and dashed lines (see the label of the *right panel* for the colours of the different models). To visualise the region probed by the data, the redshift distribution function of the WISE galaxies is marked by the grey shaded region in the *left panel* (with adjusted offset and normalisation). The corresponding ISW signal from the cross-correlation of the CMB temperature anisotropies with WISE galaxies [402] as measured by Ferraro *et al.* [404] is shown in the *right panel*. Figures adapted from Paper A.

The BAO13 compilation that we used in this study does not include all up-to-date measurements. More recent measurements[2] exhibit a $\sim 2\,\sigma$ tension with Galileon models. As combining datasets that are in tension in a joint analysis can lead to inconsistent results [418], these newer results are not included in the MCMC analysis of Paper A. However, the significance of the tension is not sufficient to conclusively rule out Galileon cosmologies. For a more detailed discussion of the tension with the newer BAO measurements, the reader should refer to Sec. 5.4 of Paper A.

Constraints from Measurements of the ISW Amplitude

As discussed in Sec. 3.4.4, Galileon models can exhibit a non-trivial evolution of the lensing potential after matter domination. A suitable observable to probe this feature is the ISW effect. A strict increase of the lensing potential after matter domination would cause the expected ISW signal to have the opposite

[2]SDSS DR7 MGS [414], BOSS DR11 Lyα-auto [415], BOSS DR11 Lyα-cross [416] and BOSS DR12 Galaxy [417].

sign compared to ΛCDM.[3] As the amplitude of the ISW power spectrum has been measured to be positive at up to $\sim 4\,\sigma$ significance [404, 419–421], Galileon models predicting a negative sign can be ruled out.

Figure 4.2 shows the freedom of the exact time evolution of the lensing potential in Galileon models at a fixed scale. The plot displays the redshift-dependent evolution of the lensing potential and the corresponding expected ISW signal from WISE galaxies [404] for ΛCDM and different Galileon models. It is easy to see that the Galileon models have the potential to predict a different sign of the ISW amplitude within the redshift range of the WISE galaxies when compared to ΛCDM. In Paper A we set out to answer the question: *Are there regions in the Galileon parameter space that are compatible with CMB and BAO data, and at the same time pass the observational test posed by measurements of the ISW amplitude?*

To assess this, we post-processed the chains from the MCMC analysis with CMB and BAO data by calculating the predicted for ISW amplitude for WISE foreground galaxies, and compared it to the measured data from Ref. [404]. We assume that the measurement of CMB, BAO13 and ISW data are independent. The solid lines in Figure 4.2 correspond to this best-fitting Galileon models, while the dashed lines indicate the best fit to CMB+BAO13 data only. If the best-fitting model to all datasets does not provide an acceptable fit, a given Galileon branch can be discarded as a viable theory of gravity.

Our results from Paper A for the different Galileon branches are:

- *Cubic Galileons.* We showed that the cubic sector of the minimally coupled covariant Galileon model can be ruled out. We found no region in the parameter space predicting a positive ISW amplitude. The best-fitting case is in $7.8\,\sigma$ tension with the WISE measurement from Ref. [404]. This poor fit is the cubic model shown with a solid line in Figure 4.2. This strong tension dismisses the model as viable.

- *Quartic and quintic Galileons.* The models can be constrained but not ruled out by ISW measurements from WISE galaxies [404]. The extra couplings in the actions of the theories and the larger freedom in their model parameter spaces give the models more flexibility to fit the data. The best-fitting models to CMB+BAO data predict a negative ISW amplitude, in tension with observations. However, there is a region in the parameter space yielding positive amplitudes. This is shown in Figure 4.3, which presents the two-dimensional marginalised

[3]Recall from section 2.6 that the ISW amplitude is the integral of the time derivatives of the gravitational potentials. Hence, increasing instead of decreasing potentials cause a change of sign in the signal.

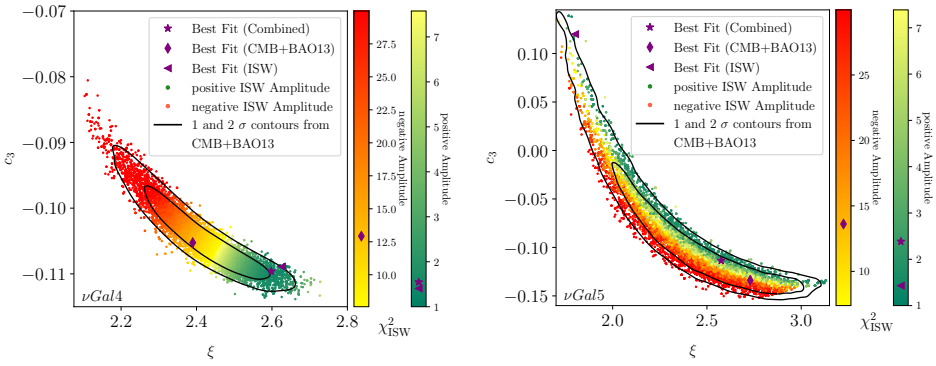

Figure 4.3: Marginalised 1 and $2\,\sigma$ constraints on the Galileon parameter space from CMB+BAO13 data for the quartic (*left panel*) and quintic (*right panel*) model. The goodness-of-fit of the corresponding ISW amplitude from the post-processed models are indicated via the coloured χ^2 values; orange/red dots correspond to negative, yellow/green dots to models with positive amplitudes. Further, models yielding the best fit to ISW data only are marked with a *triangle*, to CMB+BAO13 data with a *rhombus*, and to the combination of CMB+BAO13+ISW data with a *star*. The evolution of the potentials and the corresponding ISW amplitude of the last two cases are, respectively, displayed with the dashed and solid line in Figure 4.2. Figures from Paper A.

	$100\,\omega_b$	ω_{cdm}	H_0	$10^9 A_s$	n_s	τ_{reio}	$\Sigma\, m_\nu$	ξ	c_3
$\nu Gal4$	2.193	0.1195	73.08	2.04	0.957	0.0439	0.44	2.60	-0.11
$\nu Gal5$	2.204	0.1193	71.39	2.13	0.963	0.0647	0.63	2.58	-0.11

Table 4.1: Free cosmological and model parameters of the quartic and quintic Galileon which provide the best fit to the combination of CMB, BAO13 and ISW data. These models are indicated with a star in Figure 4.3; they lie within the $\sim 1\,\sigma$ confidence region arising from the MCMC constraints from CMB and BAO13 data. Table adapted from Paper A.

constraints on the Galileon parameter space from the MCMC analysis with CMB+BAO13 data. We indicate the expected ISW amplitude for each sampled point with colour. We mark the best-fitting models to CMB+BAO13 data and to the combination with ISW data in the parameter space. The quartic and quintic best-fit cases correspond to the solid lines shown in Figure 4.2. Table 4.1 lists the corresponding cosmological and Galileon parameters for these two best-fitting models. The WISE ISW measurement strongly constrains the valid parameter space of quartic and quintic models but does not rule the models out.

Propagation Speed of Gravitational Waves

This section contains a brief summary of studies that have been published since Paper A, leading to an invalidation of the quartic and quintic Galileon sector. The combination of the results from Paper A and the results from the first measurement of the propagation speed of tensor perturbations, discussed in the following, allows one to rule out all three branches of minimally-coupled covariant Galileons.

The announcement of the detection of a GW event from the merger of two neutron stars and the associated electromagnetic counterpart (EMC) [422–424] provided the first tight bound on the propagation speed of GWs, c_g. This bound leads to stringent constraints and the invalidation of several modified gravity models that predict an anomalous propagation speed of tensor perturbations (e.g. Refs. [425–430]).[4] The quartic and quintic covariant Galileons are among these theories, predicting a redshift dependent evolution of $c_g(z)$.

[4]Reviews on the consequences of this observation on a broader range of modified gravity theories can be found in Chapter 10 of Ref. [176] and in Ref. [177].

I will briefly discuss the consequences of the constraints on c_g on the viability of the models.

The signals from GW170817 and the EMC counterpart, GRB170817A, were detected with a time delay of 1.7 s [422–424]. With the event having taken place at a luminosity distance of ~ 40 Mpc at $z \sim 0.01$ [422–424], the allowed fractional deviation of c_g from the speed of light is constrained to be smaller than $\sim 9 \times 10^{-16}$ [426]. As the event has taken place fairly close to us, one can argue that strictly speaking $c_g = 1$ has only been determined to hold today, i.e. $c_{g0} = 1$.

The requirement that GWs propagate with the speed of light in today's Universe translates into a bound on the Galileon parameters, constraining $|c_4|$ and $|c_5|$ to be smaller than about 10^{-17} [426]. In comparison, the cosmological constraints arising from CMB, BAO and ISW in Paper A are at the order of $10^{-2} - 10^{-3}$.

Technically, this leaves a region in the Galileon parameters space that is in agreement with the constraints on c_{g0} and cosmological probes from CMB, BAO, H_0 and ISW data. However, this is not a favourable scenario compared to ΛCDM as it requires fine-tuning of two additional model parameters. More importantly, working around the GW speed constraint by requiring $c_{g0} = 1$ was shown not to be robust against perturbations. Small changes would reintroduce the speed difference [425, 426]. Hence, quartic and quintic Galileons do not provide a viable cosmological solution and can, therefore, be discarded as a cosmologically viable alternative to GR.[5]

4.2 Prospects of Cosmic Superstring Detection through Microlensing of Extragalactic Point-Like Sources

String theory is often criticised for not being verifiable or falsifiable due to a lack of observational signatures. The existence of cosmic superstrings, however, could open a potential window to the detection of distinct signatures of the theory. These cosmic superstrings are the one-dimensional fundamental building blocks of the theory stretched out to macroscopic lengths scales.

[5]Note, however, that it has been pointed out that the energy of GW170817 is close to the ultraviolet (UV) cut-off scale of Horndeski's theories of gravity [431]. This opens the possibility that a luminal propagation of GWs at the energy of GW170817 would not be in contradiction to an anomalous speed below the UV cut-off. Future measurements from, e.g. LISA [216], probe lower frequency ranges and can hence provide ultimate clarity on this matter.

Produced towards the of inflation, or shortly after it, these strings can have lengths scales of galaxy size and survive until the present day.

To date, the most stringent constraints on the tension of cosmic superstrings (CSSs) arise from the lack of detection of their gravitational-wave background radiation and the lack of time delays in signals from millisecond pulsars. Both of these techniques rely on the modelling of gravitational wave emission by CSSs. How much of their energy CSSs emit into gravitational waves is model dependent and comes along with many uncertainties [343, 352, 353, 432]. Thus, bounds not strongly relying on these assumptions could deliver an independent test.

An example of a detection method that does heavily rely on the modelling of evaporation channels, is the search for microlensing events by CSSs. One can uniquely distinguish these microlensing events from events by any other known source. Newtonian lenses cause a gradual increase and decrease of the measured flux as they move into and out of the line of sight. In contrast, microlensing by CSSs of point-like sources leads to an instantaneous doubling of the measured flux once the string is aligned with the observer and source. The main uncertainty of this method arises from the modelling of clustering properties of superstring networks.

In general, microlensing events from CSSs will be rare, as constraints from the CMB on additional energy content of the Universe set a tight bound on the allowed abundance of these objects. The number and energy density of CSSs are expected to be low: the latter is roughly 10^{-10} (depending on the string tension, see Eq. 3.41). Therefore, it is important to design any ML search for CSSs such that the number of strings that can act as a lens is maximised. To achieve that it is beneficial for experiments to

1. target regions with high DM density along the line of sight, as CSSs trace the DM distribution,
2. probe large volumes by choosing targets that are far away, and
3. have large statistics, through either a high number of observed sources and/or a long survey duration.

Studies of lensing events on CSSs have focused on the detection of events from sources within our own Galaxy [359], using compact radio sources [358], or extended sources like quasars [433]. In Paper B we estimate the event rates for extragalactic point-like sources in the optical. In particular, we consider targets that are *i)* stars in our neighbouring galaxy Andromeda (M31), and *ii)* distant Supernovae Type Ia (SNe Ia).

The benefits of using stars in M31 as a target are twofold. Firstly, one increases the probed volume with high densities compared to searches within the Milky Way (MW). Not only CSSs confined in the halo of the MW, but

also CSSs bound within the DM halo of M31 can cross the line of sight. This addresses point 1 above. Secondly, there are several billion stars in M31, out of which we can resolve about one million can as point sources. This addresses point 3 above.

The advantage of searching for CSSs with distant Supernovae Type Ia observations is the long line of sight. As SNe Ia can be several hundreds or even thousands of Mpc away, the probed volume is large. This addresses point 2 above. Furthermore, as we shall see below, the timescales of the ML events are such that usual observations of SNe Ia are sensitive to these events. In addition to that, the expected brightness of SNe Ia is well known. Hence, a flux enhancement of a factor of two is clearly noticeable. Consequently, no survey strategies need to be adopted and one can readily use the data taken, e.g. for supernova cosmology, to search for CSSs and constrain their parameter space. The disadvantage of this method is that the CSS density along the line of sight is relatively low. The strings acting as potential lenses move freely through the intergalactic medium (IGM) and are neither bound nor clustered within any halo. One goal of our analysis in Paper B was to assess whether the reduced string density can be outweighed by probing large volumes when it comes to detection rates.

Our resulting estimates for ML events sourced by CSSs do not crucially depend on the modelling of the exact evaporation channels of the strings, unlike GW background and millisecond pulsar timing constraints. Nevertheless, we must make simplifying assumptions concerning the string loop dynamics and parameters, as well as idealisations regarding observational technicalities. I will comment on these in more detail below when explaining our the simulation technique. Paper B provides an order-of-magnitude estimates of whether a detection of CSSs through ML events of extragalactic stars or SNe Ia is feasible. The goal was to gauge whether either current data can already set bounds on the parameter space of CSSs, or if a detection of CSSs in the currently unconstrained range of string tensions would be achievable with near-future technologies.

In the following, I present the results that my collaborators and I obtained in Paper B: an assessment of the prospect of the indirect detection of a CSSs through ML events of extragalactic point-like sources. I will first explain how we model the density profiles of DM and cosmic superstrings along the line of sight. After that, I will comment on the timescales of the events, followed by a discussion of the assumed survey setup, simulation technique and simplifying assumptions. I will conclude this chapter by presenting the results of the event rate simulations.

Modelling of String Loop Density along the Line of Sight

The density of cosmic superstrings must be estimated to assess how many strings an observer can expect to cross the line of sight to a source. We have seen in Sec. 3.5.2 that network evolution simulations allow us to infer the homogeneous distribution of cosmic strings (Eq. 3.39). Further simulations of the clustering properties of strings with DM enable one to determine the string loop distribution with knowledge of the DM density (Eq. 3.43). Hence, we need to model the DM density profile along the line of sight from observer to target. The choices that we make in Paper B are:

- *Stars in Andromeda.* When observing stars in M31 the line of sight passes through the dark matter halo of the MW and the halo of M31. To model this, we assume that both halos are spherical, where the density and mass of the profiles scale as $r^{-9/4}$ and $r^{3/4}$, respectively. We set the matching point of the two density profiles such that the total mass of M31 is twice as high as the mass of the MW. Further, we assume a rotation velocity of 220 km/s at radius $r = 8.5$ kpc in the MW and M31. Then, the DM density profile as a function of the distance r from the centre of the MW is given by
$$\rho_{\mathrm{MW-M31}} = \begin{cases} \frac{A}{r^{9/4}} & 0 < r < r_1 \\ \frac{2^{3/4}A}{(B-r)^{9/4}} & r_1 < r < B\,, \end{cases} \tag{4.1}$$
where $B = r_1 + r_2$ is the distance to M31, with $r_1 = 345$ kpc, $r_2 = 435$ kpc, $B = 780$ kpc [434]. Further, $A = 1.15 \times 10^9\ \mathrm{M}_\odot/\mathrm{kpc}^3$, such that the mass of the MW is $1.54 \times 10^{12}\ \mathrm{M}_\odot$ and the mass of M31 is $3.08 \times 10^{12}\ \mathrm{M}_\odot$.

- *Distant Supernovae.* Type Ia Supernovae are extremely bright sources and are visible up to high redshifts, currently up to $z \sim 2.2$ [435]. A redshift of 2.2 corresponds to a light-travel distance of about 3000 Mpc. Considering that the radius of the MW is about 17 kpc, the predominant part of this distance lies within the IGM. Hence, we ignore the DM enhancement within the MW and the host halo of the SNe Ia, and model the DM distribution along the line of sight by the constant homogeneous distribution:
$$\rho_{\mathrm{DM}}(r) = \Omega_{\mathrm{DM}}\,\bar{\rho}_{\mathrm{c}}\,, \tag{4.2}$$
with $\Omega_{\mathrm{DM}} = 0.25$, $\bar{\rho}_{\mathrm{c}} = 3\,H_0^2/(8\pi G)$, and $h = 0.7$.

After setting the DM density distribution $\mathcal{E} = \frac{\rho_{\mathrm{DM,\,local}}}{\rho_{\mathrm{DM,\,cosmo}}}$, we can calculate the string enhancement $\mathcal{F} = \mathcal{E}\,\beta(\mu)$ along the line of sight. Recall from Sec. 3.5.2 that $0 < \beta(\mu) \lesssim 0.46$ is a factor arising from simulations which assess how well strings of a given tension cluster with DM. Figure 4.4 shows the resulting DM and string distributions.

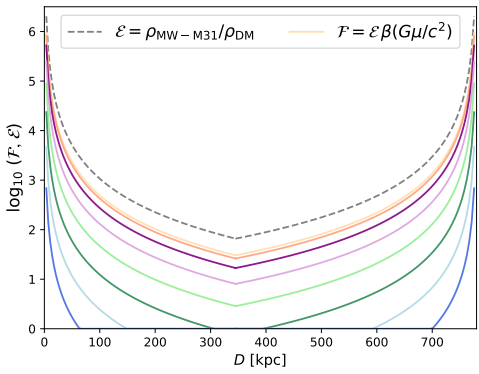

Figure 4.4: DM density profile ($\mathcal{E}$, dashed line) and string enhancement ($\mathcal{F} = \mathcal{E}\,\beta(\mu)$, solid lines) between the centre of the MW and the centre of M31. The results are shown for different string tensions from $G\mu/c^2 = 10^{-8}$ (*blue*, bottom) to $G\mu/c^2 = 10^{-15}$ (*beige*, top). Strings with lower tension cluster more with dark matter, and, therefore, trace the DM distribution better. The largest enhancement, about 10^5, is in the centre of the respective halos; the minimum value along the line of sight is $\mathcal{F} = 1$, the homogeneous limit. Figure from Paper B.

Timescales of Microlensing Events

The typical timescales of the ML events are a crucial factor when designing experiments searching for CSSs: an observer might overlook possible events if the exposure time (t_{obs}) is long compared to the lensing duration (t_{lens}). The observed flux magnification would be smaller than two, and not even detectable if $t_{\mathrm{lens}} \ll t_{\mathrm{obs}}$. On the other hand, lensing times could be much longer than the total survey duration (T_{obs}). In this case, the presence of the CSS could only be revealed if the source's brightness is known, as for SNe Ia. However, if the brightness of the observed object is unknown (as in the case of stars in M31), the magnification would not be noticed.

We calculate the maximum ML event duration for a fixed string tension given the distance between observer and source (see Sec. 3.5.3 Eq. 3.45). The *left panel* of Figure 4.5 shows these maximum timescales as a function of string tension for different source locations.

An observer only sees the flux enhancement for the maximum lensing time if a string is oriented perpendicular to the line of sight and is situated equidistant from observer and source. In case of observations of stars in M31, this is unlikely. The DM and string densities peak close to the centres of the MW and M31, therefore, it is more likely for a string to pass close to either observer

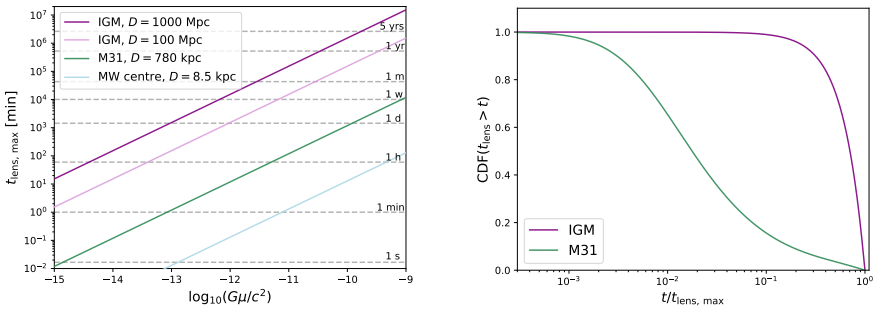

Figure 4.5: *Left panel:* The maximum duration of a microlensing event as a function of cosmic string tension. The time scales are shown for different distances D between observer and source. The *green line* is relevant for sources in M31, the *purple lines* show two representative distances of SNe Ia lensed by strings in the intergalactic medium (IGM). *Right panel*: Cumulative probability distribution function (CDF) for microlensing event durations for distant SNe Ia lensed by CSSs in the IGM (*purple line*), and stars in M31 (*green line*). We scale the CDF by the respective maximum possible lensing time, $t_{\mathrm{lens,\,max}}$. In the case of M31, we assumed the source is located 8 kpc in front of the galactic centre in M31. The scaled CDF is independent of the distance of the source for lensing by CSSs in the IGM. Figure from Paper B.

or source. To correct for this, we normalise the string density profile and interpret it as a probability distribution function for the position of the lens. Drawing sample positions from this, we calculate the ML event duration for each drawn string position. Repeating this for $\sim 10^6$ positions yields a cumulative probability distribution function (CDF) for the duration of the lensing events.

The *right panel* of Figure 4.5 shows the CDFs for the observation of stars in M31 and of distant SNe Ia. As expected, most lensing events of stars in M31 are much shorter than the maximum event duration, as most strings reside close to either observer or source. For a majority of the events $t_{\mathrm{lens}} < 0.01\, t_{\mathrm{lens,\,max}}$. Hence, most events will be shorter than 1 s for small string tensions, making them challenging to detect. In contrast, the CDF for the lensing of SNe Ia by strings in the IGM is relatively flat and events lasting $t_{\mathrm{lens}} \sim t_{\mathrm{lens,\,max}}$ are not unlikely. This is a reflection of the flat homogeneous density profile along the line of sight.

Survey Set-up, Observation Criteria & Event Rate Simulation

To simulate the rate of expected ML events, we must assume a specific survey strategy. I list our choices for source positions, exposure times, and survey durations in Table 4.2.

Also given in Table 4.2 are the detection criteria. These are needed to decide whether one classifies a measured flux as enhanced or not. For example, stars can have intrinsic brightness fluctuations which one should not count as flux enhancement when searching for CSSs. On the other hand, if the alignment of observer, CSS, and source happens during an exposure, the resulting flux measure will not yield a factor of two enhancement. Assuming that the alignment happened after 50% of the exposure time, and is not broken until the end, the observer will measure a flux enhancement of factor 1.5. Requiring a perfect sequence of zero enhancements, followed by a sequence of doubled flux measurements, which is then again followed by an unenhanced flux measurement, therefore, might be too stringent. Hence, we classify a flux measure F as not enhanced if it does not exceed $F\,(1+\delta_{\mathrm{min}})$. Likewise, a flux needs to exceed $F\,(1+\delta_{\mathrm{max}})$ to be classified as enhanced.

It is also likely that only one 'edge' of the ML event falls within the observation time. This means that the observer only detects a sudden flux increase (rising edge) or a sudden flux decrease (falling edge) in two consecutive observation windows. Such an observation would reduce the significance of a detection. We denote fully resolved events (detection of rising and falling edge) by n_{lens}, the number of detections of only one edge by n_{edge}.

Given that lensing events of distant sources can last several years, it is

	Stars in M31	Supernovae Ia
Source	star at 8 kpc distance from M31 centre	SNe at distances $100 - 2000$ Mpc
Survey	1 year, 2 hours/night repeated 1 s exposures separated by 0.01 s	3 months, 5 times/night repeated 30 s exposures separated by 1 h
Min./Max. flux variation for detection	$\delta_{\min} = \delta_{\max} = 30\ \%$	$\delta_{\min} = \delta_{\max} = 10\ \%$

Table 4.2: Our choices for the survey strategies used in the simulation of the expected number of ML event detections. The first column indicates the survey setup for the observation of stars in M31. The second column lists our choices for the observation of SNe Ia. I will refer to the exposure times as $t_{\rm obs}$, and the time span between the end and beginning of successive nightly exposures as $\Delta t_{\rm obs}$. The criteria we apply to classify a flux as enhanced or not are given by $\delta_{\min}$ and $\delta_{\max}$ (see main text for details). Table adapted from Paper B.

possible that a SN Ia is lensed during its entire observable lifetime of ~ 3 months. Such an observation can still be an indicator for the presence of a CSS as the theoretical brightness of SNe Ia is known. The number of these continuously lensed events is denoted by $n_{\rm CL}$.

We calculate the expected number of ML event detections per source as

$$n_{\rm lens} = \epsilon_{\rm lens}\, \tilde{\Gamma}\, T_{\rm obs}/N_\star\,, \tag{4.3}$$

where $\epsilon_{\rm lens}$ is the efficiency of a survey to detect ML events for a given string tension, $\tilde{\Gamma}$ is the rate at which lensing events occur, $T_{\rm obs}$ is the time between the first and last observation of a survey, and $N_\star$ is the number of sources. Similarly, one can calculate the number of expected detections of rising and falling edges, $n_{\rm edge}$, and the number of observations of continuously lensed objects, $n_{\rm CL}$.

We simulate the efficiency $\epsilon_{\rm lens}$ to detect an ML event sourced by a CSS for a given target at a distance D, a fixed string tension, and a set survey plan. To do so, we assume that during the entire survey, one alignment between observer, string and source takes place. The time at which this occurs, the position of the CSS, and its angle with respect to the line of sight are randomly

drawn. From these quantities, we can infer the duration of one lensing event with the help of the CDF for the lensing timescales (see Figure 4.5). This allows us to create a stream of the $N_{\rm rep}$ time intervals where the flux of the source appears enhanced.[6] Comparing the time intervals with enhanced fluxes to the exposure times of the survey yields the measured fluxes. We apply the defined observation criteria and count the number of rising and falling edges in the vector of flux measures. This counting results in the number of predicted observed events $n_{\rm lens}$, $n_{\rm edge}$ and $n_{\rm CL}$, given that a string crossed the line of sight. By repeating this $\mathcal{O}(10^5)$ times, we get an estimate of how efficient a survey is expected to be in detecting a microlensing event by a CSS.

The rate per second at which lensing events occur, $\tilde{\Gamma}$, can be calculated as

$$\tilde{\Gamma} = \int n_\star r^2 \,\mathrm{d}\,\Omega \,\mathrm{d}\, r \int \mathrm{d}\, r' \,\mathrm{d}\, l \left(\frac{\mathrm{d}\, n}{\mathrm{d}\, l}\right)' \left\langle \frac{\mathrm{d}\, A_\perp}{\mathrm{d}\, t} \right\rangle = N_\star \int_0^D \mathrm{d}\, r' \mathrm{d}\, l \left(\frac{\mathrm{d}\, n}{\mathrm{d}\, l}\right)' \left\langle \frac{\mathrm{d}\, A_\perp}{\mathrm{d}\, t} \right\rangle , \tag{4.4}$$

where $n_\star(r)$ is the density of stars, $N_\star$ the total number of sources within the probed volume, and $(\mathrm{d}\, n/\mathrm{d}\, l)'$ the length spectrum of loops. The observer is placed at the origin and strings acting as a lens lie between the observer and source ($0 < r' < r$). The quantity $\mathrm{d}\, A_\perp/\mathrm{d}\, t$ denotes the rate at which a string loop covers an area perpendicular to the line of sight; it is averaged over the orientation and motion of the loop in space-time, as well as over the characteristic trajectories traced by different loops. The second equality holds when assuming that the sources are confined within a narrow cone at fixed distance D. With this rate $\tilde{\Gamma}$ and the simulated efficiency, we can calculate the number of expected events given in Eq. (4.3).

In all calculations and simulations, we assume that $\mathcal{G}$, the factor parametrising string theory unknowns regarding the number density of CSSs, is equal to 100. This assumption is based on the estimate from Ref. [336]. However, in principle, $\mathcal{G}$ could be unity, or as large as $10,000$. The uncertainty in this parameter, therefore, dominates all given estimates. However, the results can be easily rescaled to any value of $\mathcal{G}$, as the event rates are linear in $\mathcal{G}$, i.e. $\mathcal{G} \propto n_{\rm lens}$.

In the analysis, we made several simplifying assumptions. We did not account for uncertainties in the DM density distribution. Additionally, we fix parameters of CSSs describing their clustering properties to their best fit values from network simulations, instead of varying and marginalising over them. Further, we assumed that different ML events are uncorrelated. This

[6] Recall from Sec. 3.5.3 that owing to internal oscillations of CSSs, one alignment can lead to $N_{\rm rep} = v_{\rm i}/v_{\rm com} \sim 1000$ microlensing events. Here $v_{\rm i}$ and $v_{\rm com}$ are, respectively, the internal and centre-of-mass velocities of the string. For strings within the MW and M31, we assume $v_{\rm com} = 220$ km/s, while strings moving in the IGM are assumed to move with $v_{\rm com} = 600$ km/s.

means we did not take into account that a CSS that aligns with one star could move on and give rise to another ML event of a neighbouring star. We ignored cosmological effects in the event rate analysis for distant sources, such as the increase of the DM and string loop densities with increasing redshift. The latter two assumptions, neglecting event correlations and the cosmological evolution, make our results more conservative. From a technical point of view, we neglected detector and photon noise, extinction effects of the signal, and the effects of sources being not perfectly point-like.[7] For a full list of the underlying assumptions, I refer the reader to Appendix B of Paper B.

Results

Figure 4.6 summarises our main results. It shows the simulated number of detections per point-like source depending on the string tension for two stars located at different positions within M31, and for different distances of sources lensed by CSSs in the IGM. One can understand the trends as follows:

- *Sources in M31.* Strings with high tension have a low number density and do not strongly trace the DM abundance (see Figure 4.4). Therefore, the abundance of these strings is too low to yield seizable lensing rates. The rates increase with decreasing string tension, up until the timescales of the events are too small to be captured by a survey with an observation window of 1 s. This turnover happens at string tension $G\mu/c^2 = 10^{-13}$. If one considers an idealised survey, i.e. continuous monitoring of the source with arbitrarily small time resolution, the theoretical detection rate keeps increasing with decreasing string tension.

  The rates for a source located 8 kpc behind the centre of M31 can be more than two orders of magnitude higher compared to the rates for a source located at 8 kpc distance to the centre on a plane perpendicular to the line of sight. This is the case as the line of sight of the former passes through the high-density core of M31. Hence, especially for low tension strings, the string number density is higher when observing a source behind M31's centre, leading to higher detection rates.

- *Distant SNe Ia.* High tension strings give rise to longer lensing time scales. For sources at distance 1000 Mpc, events can last longer than a few decades for $G\mu/c^2 \gtrsim 10^{-9}$. Hence, the higher the string tension, the higher the probability of seeing a SNe Ia which is lensed during

[7] If the point-source approximation does not hold, the string only partially covers the object. This partial coverage means only a fraction of the source is lensed, and the measured flux enhancement is lower than a factor of two.

its entire observable period of ~ 3 months. Therefore, the detection rate of continuously lensed sources n_{CL} increases with increasing string tension. However, n_{CL} vanishes as soon as the total observation time $T_{\mathrm{obs}} = 3$ months becomes larger than the event duration. In turn, the chance of detecting the beginning or end of an alignment, quantified through n_{edge}, decreases with increasing lensing duration, i.e. increasing tension.

We derive the constraints on the string tension that arises from a non-detection of a factor of two flux enhancement in the Pantheon dataset, containing 1048 SNe Ia. The resulting constraints are indicated in Figure 4.6.

Based on the results from our simulations we can draw the following conclusions: firstly, no available dataset of stars in neighbouring galaxies, or SNe Ia, can constrain so far unprobed regions of the parameter space of cosmic superstrings.

When observing stars in nearby galaxies short exposure times, and short separations of observation windows, are beneficial. With current technologies, exposure times of 1 s separated by just 0.01 s can be achieved. This would require the observation of about 10^5 stars over the course of 1 year to constrain string tensions of $G\mu/c^2 \sim 10^{-13}$, where this survey is most sensitive. With a sample of about one million stars, the probed tension range expands to $10^{-13.5} < G\mu/c^2 < 10^{-11.5}$.

The observation of distant SNe Ia is less promising for a possible detection of ML events by CSSs. Our estimate shows that one would only expect about one event in $10^7 - 10^8$ observations. These large numbers are not expected to be reached with near-future surveys. However, a potential ML event sourced by a cosmic string would clearly be visible in the standard observations of SNe Ia. Hence, no adaption of survey strategies for the search for cosmic superstrings is needed, and the possibility of a detection by chance remains.

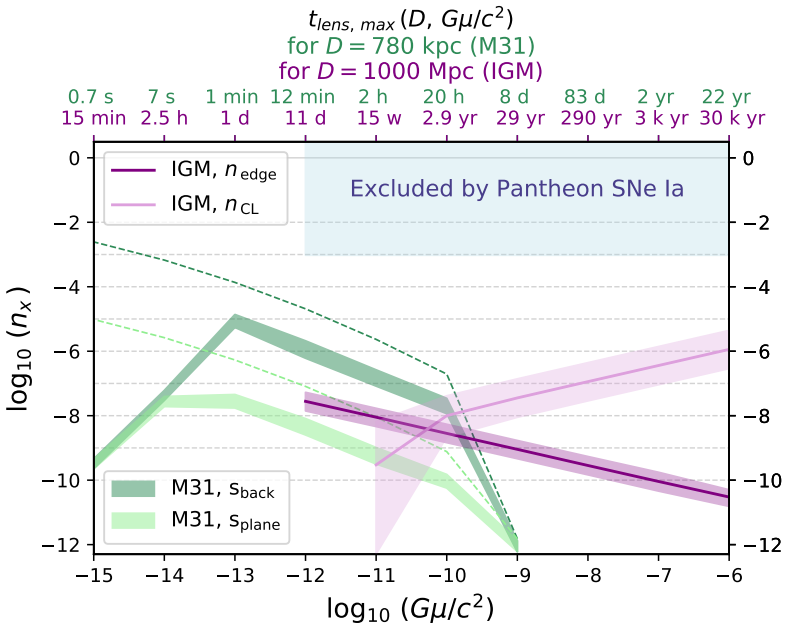

Figure 4.6: Simulated number of expected detections of microlensing (ML) events sourced by cosmic superstrings (CSSs) as a function of string tension for different source locations. *Green lines* refer to stars in Andromeda (M31), *purple lines* to distant sources lensed by CSSs in the intergalactic medium (IGM). The lower x-axis indicates the string tension, and the upper axis gives the respective maximum lensing durations for a given source distance. *Green* values apply to stars in M31, *purple* values to a source at $D = 1000$ Mpc. **M31:** shaded bands indicate the event rates for a star located behind the centre of M31 (*dark green*) and a star located in the plane perpendicular to the line of sight (*light green*), both 8 kpc from M31's centre. The lower borders correspond to detecting a fully resolved ML event ($n_{\rm lens}$); the upper borders give the rates for detecting only a rising or falling edge of the flux increase ($n_{\rm edge}$). Dotted lines indicate the number of events that could theoretically be detected by an ideal survey with arbitrarily small time resolution. **IGM:** expected number of detections for two different detection criteria. Firstly, $n_{\rm edge}$, the detection of a rising or falling edge of the flux increase. Secondly, $n_{\rm CL}$, the observation of a constantly lensed object. Central line stands for a source located at $D = 1000$ Mpc, the respective lower and upper border indicate the numbers for sources located at 500 Mpc and 2000 Mpc, respectively. Figure from Paper B.

Chapter 5

Statistical Inference and the Global and Modular Beyond-the-Standard-Model Inference Tool (GAMBIT)

One goal in fundamental research is to find models that reliably predict observed phenomena. In this quest, one can ask different questions to gain more information about the underlying laws dictating the outcome of observations. Firstly, is a given hypothesis, for example, the existence of a new particle, consistent with the data? This concerns *hypothesis testing*. Secondly, if a model has free parameters, which combination of these parameters describes the observed data best? This question relates to *parameter inference*. And thirdly, given several models, do observations prefer one of them over the other? The answer to this requires the performance of *model comparison*.

All of the techniques mentioned above are commonly applied in particle physics and cosmology. These statistical analyses typically require the use of computational tools. One example of such a software tool is GAMBIT, the Global and Modular Beyond-the-Standard-Model Inference Tool. It is an open-source software package designed to conduct parameter inference and model comparison. A wide range of Beyond-the-Standard-Model (BSM) theories are readily implemented in GAMBIT and can be confronted with a variety of experimental datasets from different fields of physics.

In will start this chapter by giving a brief introduction to methods for parameter inference used in the context of GAMBIT in Sec. 5.1. Sec. 5.2 provides an overview of the models and likelihoods available for use within GAMBIT. I will explain the key concepts of GAMBIT's technical design in Sec. 5.3.

5.1 Statistical Methods for Parameter Inference

To investigate statistical questions, one can follow two distinct philosophies: frequentist or Bayesian statistics. The frequentist approach to statistics interprets probability in terms of the frequency of the occurrence of events. Take the example of tossing a coin, where the outcome can either be heads H or tails T. The estimate for the probability of the event H happening, i.e. $P(H)$, is then

$$P(H) = \frac{n_H}{N}\,, \tag{5.1}$$

where n_H is the number of times the coin landed on heads, and N is the total number of coin tosses. Observing $n_H = 30$ when tossing the coin 100 times, a frequentist will make a point estimate for $P(H)$ of 0.3 based on this data. In contrast, in the Bayesian approach, one defines a probability as the degree of belief in a hypothesis. Before performing any experiment, one quantifies a prior expectation of the outcome. In the case of flipping a coin, one could – based on the geometry – assume that $P(H)$ follows, e.g. a Gaussian distribution centred around 0.5. Alternatively, if there was a reason to believe that the coin is biased in either way, one could adopt an uninformative prior by assuming that it is equally likely that $P(H)$ takes any value between 0 and 1. After performing the experiment, the Bayesian will update their degree of belief in the given hypothesis. In general, this can lead to prior-dependent results.

In both the Bayesian and frequentist frameworks, probabilities obey Kolmogorov's three axioms [436]. These axioms are *i)* probabilities are non-negative and real numbers, *ii)* the probability of at least one of the possible outcomes happening is 1, and *iii)* the probability of several disjoint events occurring at once is equal to the sum of the probabilities of the occurrence of each event. What differs, however, are important points when it comes to the interpretation of probabilities and what kind of information one can extract from data.

One crucial difference between the frequentist and Bayesian schools of thought follows from the interpretation of probability. Frequentist probabilities can only be used for statements about outcomes of processes that are, at least in principle, repeatable. Bayesian probability, on the other hand, can be used to express one's degree of belief in *any* statement.

In the following, I will give a brief introduction to the methods of parameter inference in both the frequentist and the Bayesian framework. For in-depth textbook introductions and methods for hypothesis testing and model comparison, see, e.g. Refs. [437–440]. For discussions of statistical methods in the context of cosmology refer to Refs. [418, 441–446].

An important definition in parameter inference is the *likelihood*. Consider

a model $\mathcal{M}$ with a set of n continuous variables, $\bar{\theta}_n = \{\theta_1, \theta_2, \ldots, \theta_n\}$. Let $\mathbf{D}$ denote the outcome of an experiment in the form of a dataset. One defines the likelihood function as the probability of observing the data $\mathbf{D}$ given a set of parameters $\bar{\theta}_n$ of the model $\mathcal{M}$. It is usually denoted as

$$\mathcal{L}(\mathbf{D}|\mathcal{M}, \bar{\theta}_n)\,. \tag{5.2}$$

In a frequentist approach the combination of parameters $\bar{\theta}_n$ that shows the best agreement with the data is inferred by searching for the combination $\{\theta_1, \theta_2, \ldots, \theta_n\}$ that maximises the likelihood in the multi-dimensional parameter space. If a set of secondary, or *nuisance*, parameters is involved, one usually reports the *profile likelihood*. Nuisance parameters are not of direct interest in the analysis; for example they can parametrise calibration uncertainties of a detector. To obtain the profile likelihood, one maximises the likelihood function over the nuisance parameters, $\bar{\alpha}_m$, i.e.

$$\hat{\mathcal{L}}(\mathbf{D}|\mathcal{M}, \bar{\theta}_n) = \max_{\bar{\alpha}_m} \mathcal{L}(\mathbf{D}|\mathcal{M}, \bar{\theta}_n, \bar{\alpha}_m)\,. \tag{5.3}$$

In the Bayesian approach the values for the preferred model parameters $\bar{\theta}_n$ from a set of data $\mathbf{D}$ are inferred from the *posterior distribution*. It is given by

$$p(\bar{\theta}_n|\mathcal{M}, \mathbf{D}) = \frac{\mathcal{L}(\mathbf{D}|\mathcal{M}, \bar{\theta}_n)\,\mathcal{P}(\bar{\theta}_n|\mathcal{M})}{\mathcal{E}(\mathbf{D}|\mathcal{M})}\,, \tag{5.4}$$

where $\mathcal{P}(\bar{\theta}_n|\mathcal{M})$ is the prior, and $\mathcal{E}(\mathbf{D}|\mathcal{M})$ is the evidence. The prior encodes the prior knowledge about the probability of the value of a parameter θ_i. This information can come from previously performed experiments or from physical constraints, e.g. requiring that the mass of a particle cannot be negative. The evidence follows from the requirement that the posterior is a probability distribution. To ensure that the posterior obeys Kolmogorov's second axiom, the integral $\int p(\bar{\theta}_n|\mathcal{M}, \mathbf{D})\,\mathrm{d^n}\bar{\theta}_n$ must be equal to unity. The expression for the evidence then follows from Eq. 5.4:

$$\mathcal{E}(\mathbf{D}|\mathcal{M}) = \int \mathcal{L}(\mathbf{D}|\mathcal{M}, \bar{\theta}_n)\,\mathcal{P}(\bar{\theta}_n|\mathcal{M})\,\mathrm{d^n}\bar{\theta}_n\,. \tag{5.5}$$

The Bayesian equivalent to the profile likelihood, where the effect of nuisance parameters is incorporated into the estimate of the statistic of interest in terms of the primary parameters, is the *marginalised posterior*. To obtain the marginalised posterior one simply integrates the full posterior over the nuisance parameters to obtain the posterior distribution for the parameters of interest. To visualise the results of a parameter inference analysis, it is common to integrate over all but one or two model parameters, to show the 1- or

2-dimensional marginalised constraints in terms of a specific parameter of pair of parameters.

Beyond point estimates of the set of best-fitting model parameters, parameter inference techniques can also provide measures for the uncertainty of the results. Frequentists quote maximum likelihood values with $X\%$ *confidence intervals*. The interpretation of this is that when repeating the experiment multiple times, $X\%$ of the time the data will be such that the true value of a model parameter will lie within the confidence interval inferred from the data. Bayesians indicate uncertainties with *credible regions* of $X\%$. These regions contain $X\%$ of the probability associated with the possible values of a model parameter.

To sum up: in frequentist parameter inference analyses, one is interested in maximizing the likelihood with respect to a set of model parameters. In Bayesian analyses, the posterior distribution, proportional to the product of likelihood and prior, is the quantity of interest. These differences have direct consequences for the type of sampling algorithms that one needs to employ in parameter inference. In the frequentist approach it is important to perform fast optimisations to find the maximum of the multi-dimensional likelihood function efficiently. In the Bayesian framework, one is interested in obtaining a sample of the likelihood function across the parameter space to infer the posterior.

5.2 GAMBIT Models, Modules and Likelihoods

GAMBIT offers a framework to confront different models with experimental data by performing parameter inference and model comparison in Bayesian and frequentist statistical frameworks. The design of GAMBIT is modular to provide maximum flexibility when it comes to including additional models, likelihoods, and external libraries for the calculation of observables or likelihoods. In the current public release v1.4.4, the implemented models and likelihoods are mainly related to particle physics. I will present the extension of this database to cosmological models and likelihoods in Chapter 6 of this thesis. In principle, however, the framework of GAMBIT can be extended to confront arbitrary models with data, even those not necessarily related to physics. The source is available for download from `http://gambit.hepforge.org` under the 3-clause BSD license.

The general idea of GAMBIT is not to reproduce already existing codes to perform observable and likelihood calculations, but to make use of well-tested, existing tools as external libraries and to combine them in a consistent framework. These external libraries are called *backends*. While GAMBIT is

written in C++11, backends can be implemented in different languages. GAMBIT supports interfaces to codes written in Python, Mathematica, Fortran and C.

The model database GAMBIT provided in release 1.4.4 contains different types of models. These are the Standard Model (SM) of particle physics, models incorporating nuclear uncertainties of the SM, the extension of the neutrino sector of the SM to right-handed neutrinos, models for the shape of dark matter (DM) halos, axions and axion-like particles, Higgs portal models, SM effective field theories, and supersymmetric extensions of the SM encoded in the Minimal Supersymmetric Standard Model (MSSM). Family trees connect all related models; for example, the Constrained Minimal Supersymmetric Standard Model (CMSSM) is a special case of the most general implemented MSSM model. Hence, the MSSM is a 'parent' model of the CMSSM, and a translation function maps the parameters from the child model to the more general case.

The different physics modules are responsible for calculating model predictions, observables and/or likelihoods. For example, the module DarkBit includes all computations related to calculating the relic density of a DM particle, relevant cross-sections, and direct and indirect detection likelihoods. The modules included in GAMBIT 1.4.4 are:

- SpecBit [447]: computation of masses and couplings of all SM and BSM particles included in the theory under investigation. In terms of likelihoods, the vacuum stability of a theory can be assessed.
- DecayBit [447]: calculation of particle decay widths and branching ratios of all particles, including calculations thereof for BSM states. The module offers likelihoods for the decay widths of SM particles to test the predictions of a theory.
- PrecisionBit [447]: calculation of precision observables, for example, the fine-structure constant, the strong coupling constant, or the Higgs mass. Further, PrecisionBit includes likelihoods to compare these predictions to experimental data.
- FlavBit [448]: computation of predictions and likelihoods of flavour physics processes, for example, B meson decays or muon to electron conversion inside nuclei.
- ColliderBit [449]: offers a range of likelihoods from the Large Hadron Collider (LHC) and the Large Electron-Positron collider (LEP). For example, from searches for supersymmetric particles, Higgs searches, and missing energy searches for DM particles.
- DarkBit [450]: calculation of relic density of a DM particle and likelihoods for laboratory (direct) as well as astrophysical (indirect) DM searches.

- NeutrinoBit [451]: observable and likelihood calculation for constraints on (extensions of) the neutrino sector of the SM.

In addition to physics modules, GAMBIT also has a module that is responsible for all tasks related to parameter sampling, ScannerBit [452]. It has all tools for sampling the likelihood and computing associated posterior weights. Model comparison analyses in the frequentist approach, by performing simulations, and the Bayesian approach, through the calculation of the evidence, are also supported. ScannerBit offers the user a choice between different built-in and external sampling algorithms. For example, a regular Markov Chain Monte Carlo (MCMC) algorithm (GreAT [453]), an ensemble MCMC algorithm (T-Walk [452]), nested samplers (MultiNest [454, 455] and polychord [456]), and a differential evolution optimiser (Diver [452]).

For more details, refer to the GAMBIT manual [457], the recent GAMBIT review [458], and the respective module papers, Refs. [447–451]. For global fit results obtained with GAMBIT, see Ref. [459] for an analysis of different Higgs Portal models, Ref. [460] for a study of axions and axion-like particles, Ref. [451] for right-handed neutrinos, Ref. [461, 462] for scalar singlet DM models, Ref. [463–465] for studies of supersymmetric extensions of the SM, or Ref. [466] for lepton-universal effective field theory fits to anomalies in B meson decays.

5.3 Design Principles of GAMBIT

With GAMBIT the user can freely choose which model they want to constrain with which combination of likelihoods. This flexibility poses several challenges: on the one hand, one must ensure that model-dependent assumptions and calculations are only used for models that they apply to. On the other hand, to keep the code maintainable, no equation or calculation should appear multiple times. Hence, the design of the framework must offer maximum flexibility and minimum ambiguity at the same time.

The design of GAMBIT addresses the challenge of maximising flexibility and re-usability by introducing the concept of *capabilities* and *dependencies*. Each capability provides the result of a self-contained sub-calculation. For example, this can be the mass or lifetime of a given particle, different interaction cross-sections, or the DM relic density. If the result from another capability is needed in the calculation, it can be accessed via a dependency on the required capability. For example, the calculation of the relic density requires the knowledge of the masses and lifetimes of a number of particles.

Every capability can be provided by one or more *module functions*, which contain the actual implementation of the calculation. While all module func-

tions of a capability provide in principle the same result, e.g. the DM relic density, the calculations given in the different module functions differ. The results can either be obtained using different calculation techniques (e.g. analytical versus numerical computation) or be valid for different models. In the latter case, the module function has a tag that indicates for which model(s) it is valid.

Which module function is activated to provide a given capability in a specific run is automatically determined by GAMBIT's internal *dependency resolver*. At the beginning of each run, the dependency resolver works out which capabilities need to be evaluated to compute the chosen likelihoods and observables from the model parameters. In this process, the dependency resolver automatically respects the model dependency of functions, and it only activates functions if they are consistent with the given choice of models. If ambiguities exist, or if dependencies cannot be resolved, e.g. due to a missing external library, the dependency resolver will exit with an informative error message. All inputs for a GAMBIT run, such as likelihoods, models, scan settings are specified in a YAML file.[1]

For an overview of how a GAMBIT run proceeds conceptually, see Figure 5.1. Figure 5.2 shows a simple example of a dependency tree of a GAMBIT run using only the module CosmoBit. I will present the models and likelihoods introduced by the new module CosmoBit in the next chapter.

[1] YAML (YAML Ain't Markup Language) is a data serialisation language developed to be easily readable and writeable by humans.

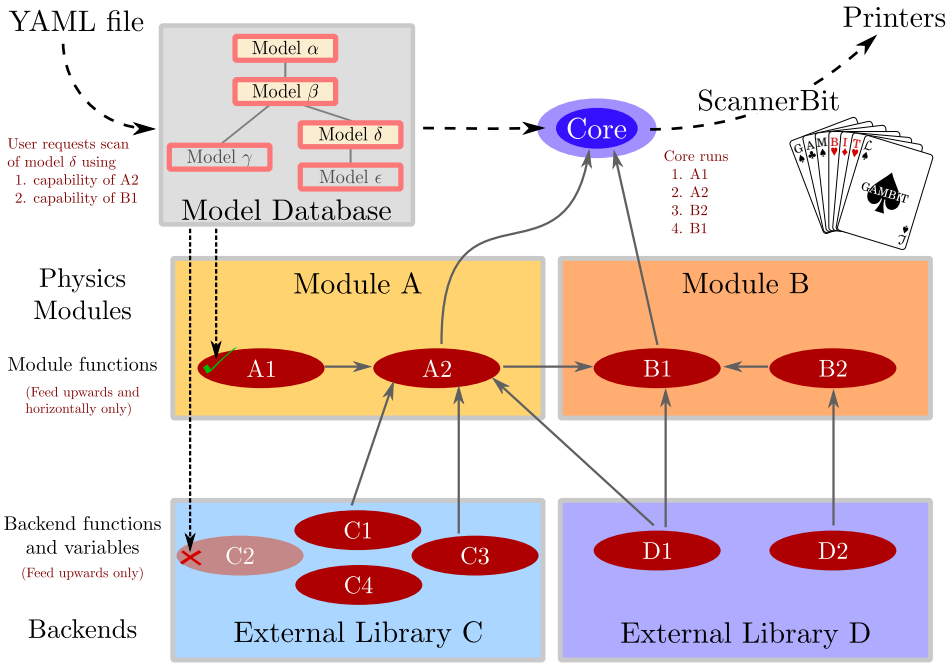

Figure 5.1: A conceptual overview of a GAMBIT run: based on the models, likelihoods and scan settings specified in the YAML file, the dependency resolver assesses which module functions and which calculations from external libraries need to be evaluated in which order. The results of the likelihood evaluations for one parameter point are passed through the core to ScannerBit, which controls the model parameter values for each evaluation according to the sampling algorithm chosen by the user. Figure from Ref. [457], used with permission.

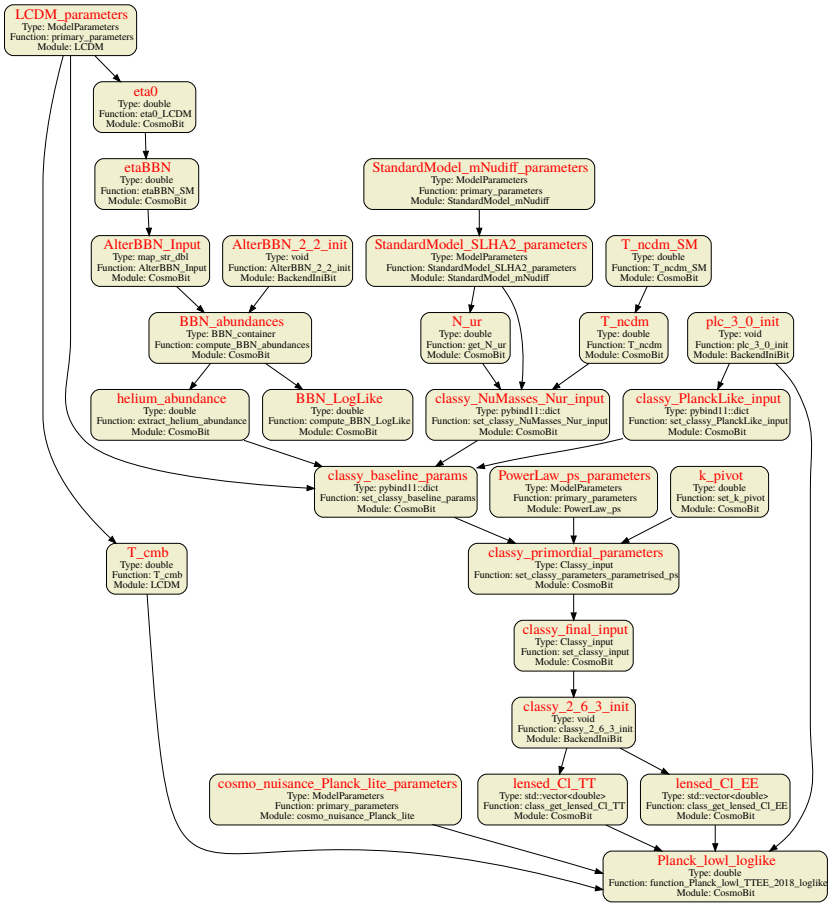

Figure 5.2: Dependency tree of a simple GAMBIT run. The boxes stand for the capabilities that are evaluated. Below the capability names (printed in *red*), the return type, the function used to provide the capability, and the module it is implemented in are indicated. The evaluation order follows the arrows. The arrows also show the different dependencies: for example, the function compute_BBN_LogLike, providing capability BBN_LogLike, has a dependency on the capability BBN_abundances. In this specific example, GAMBIT evaluates the Planck CMB likelihood (Planck_lowl_loglike) and the BBN likelihood using abundance measurement of light elements (compute_BBN_LogLike) to constrain the model parameters of ΛCDM and the SM neutrino masses (StandardModel_mNudiff_parameters). Note that CosmoBit passes the computed primordial helium abundance (here calculated by the backend AlterBBN [467, 468]) consistently to the Boltzmann solver (CLASS [225, 226] in this example).

Chapter 6

CosmoBit: A GAMBIT Module for Computing Cosmological Observables and Likelihoods

The practice of carrying out combined likelihood analyses of multiple datasets to compare models and estimate their parameters is well established, both in cosmology and particle physics. Packages such as CosmoMC [469, 470], MontePython [471, 472], and Cosmosis [473] provide the ability to use combinations of observables from, e.g. large-scale structure (LSS), Supernovae Type Ia (SN Ia), Big Bang Nucleosynthesis (BBN) and the cosmic microwave background (CMB) to constrain a number of different cosmological models. These range from the canonical ΛCDM cosmology, to theories of inflation, dark energy, additional neutrinos, exotic energy injection, and many others.

On the particle physics side, 'global fitting' frameworks such as GAMBIT [457, 458], MasterCode [474] and HEPFit [475] allow phenomenologists to carry out combined fits to data from the Large Hadron Collider (LHC), direct and indirect dark matter searches, flavour physics, precision Standard Model (SM) measurements, and neutrino physics. These have been applied to a number of different theories for physics beyond the SM (BSM), ranging from supersymmetry [463–465, 476, 477] to extended Higgs sectors [459, 461, 462, 478, 479], axions [460] and additional neutrinos [451]. Many of these BSM scenarios have additional cosmological implications not accounted for in the particle physics fits. Examples are inflationary implications of different axion theories, impacts on BBN of decaying heavy relics, and effects of neutrinos on the power spectrum of cosmological perturbations at small scales. Likewise, most beyond-ΛCDM theories are effective theories describing the impacts of new states on cosmology, with completions in terms of concrete BSM models leading to a host of potential signals in traditional particle physics experiments.

To date, no package has been developed for combining the wealth of cosmological and particle physics datasets available, to constrain theories from both sides simultaneously. In this chapter, I present CosmoBit, the first development in this direction. CosmoBit is a cosmology module within GAMBIT, providing observable and likelihood calculations for BBN, the CMB, LSS, SNe Ia and other cosmological probes. When combined with existing GAMBIT modules specialised for neutrino [451], collider [449], flavour [448], dark matter [450] and precision [447] physics — as well as a host of advanced statistical sampling algorithms accessible via the ScannerBit module [452] — CosmoBit allows one to use GAMBIT to perform joint cosmological and particle global fits.

CosmoBit is open source and will be part of the GAMBIT 1.5 release, available to download from `http://gambit.hepforge.org`. Note that while the majority of the development has been finished at the time of writing, we have not release the code yet. In the following, I will describe the code in its current state. Even though we do not plan to make further essential changes, the reader should be aware that design revisions (e.g. changes in naming conventions or interfaces) could be made before the initial release. Therefore, I recommend that the reader consults – once published – the CosmoBit module paper for the final technicalities. CosmoBit will be released under the terms of the standard 3-clause BSD license.[1]

This comprehensive chapter starts with an executive summary given in Sec. 6.1. The summary provides a broad conceptual overview of the models, likelihoods and external libraries that, in combination, form the heart of CosmoBit. I will then discuss the details of each of these points individually. Sec. 6.2 addresses all models introduced with CosmoBit, Sec. 6.3 observable and likelihood calculations, and Sec. 6.4 technical details about the implementation and use of external libraries. In the end, I will present validation analyses and first results in Sec. 6.5.

6.1 Executive Summary

CosmoBit introduces a range of new models, likelihoods and interfaces to external libraries (*backends*). Before going into details, I will give an executive summary of the newly introduced features. For each of these points, I provide a reference to the specific section where the respective details are covered.

The different *models* the user can test with CosmoBit are organised in different family trees and model groups. These are:

- Cosmological models defining the cosmological baseline parameters of

[1] http://opensource.org/licenses/BSD-3-Clause.

ΛCDM. *[Definitions → Sec. 6.2.1]*

- Inflation models dictating the shape of the primordial power spectrum. *[Definitions → Sec.6.2.2]*

- Neutrino mass parameters to include massive neutrinos with realistic mass splitting. *[Definitions → Sec. 6.2.3]*

- Additional energy in radiation allowing the user to vary the baryon-to-photon ratio and the effective number of relativistic degrees of freedom at different times. *[Definitions → Sec. 6.2.4]*

- Energy injection into the primordial plasma in the early Universe by annihilating or decaying dark matter models. *[Definitions → Sec. 6.2.5]*

- Cosmological nuisance parameters needed if likelihoods with nuisance parameters are in use. *[Definitions → Sec. 6.2.6]*

Figure 6.1 gives an overview of these model groups. The user can easily infer which backend they need to install for scans of a specific model (group) from the graphic.

The *likelihoods* the user can employ to test the implemented models range from probes of the early Universe to tests of the late Universe. The options in CosmoBit are not limited to the standard combination of CMB, BAO and SNe Ia likelihoods. Further options like measurements of light element abundances probing the epoch of BBN, weak lensing and galaxy clustering measurements are also available for use. To avoid simply re-implementing existing likelihood calculations, we utilise two external libraries:

- plc: the official Planck likelihood code [480, 481]. Serves to compute CMB likelihoods for the temperature, polarisation, and lensing spectra. *[Likelihoods → Sec. 6.3.2; technical details → Sec. 6.4.7]*

- MontePython: a parameter inference package for cosmology [471, 472]. Provides access to an extensive database of different cosmological likelihoods. *[Likelihoods → Sec. 6.3.3; technical details → Sec. 6.4.5]*

Refer to Sec. 6.3 for more details on the exact datasets used for the likelihood calculations.

To calculate the likelihoods mentioned above, the computation of *theoretical predictions* for the respective observables is required. We obtain these from well-tested, public external codes:

- MultiModeCode: a tool to compute the primordial power spectrum (PPS) for different (multi-field) inflation models [482, 483]. The PPS encodes the initial spectrum of perturbations in the early Universe which can leave observable signatures on cosmological observables. *[Technical details → Sec. 6.4.6]*

- AlterBBN: a code to compute the abundances of light elements formed during BBN for different non-standard physics scenarios [467, 468]. *[Likelihood calculation → Sec. 6.3.1; technical details → Sec. 6.4.2]*

- CLASS: the Cosmic Linear Anisotropy Solving System [225, 226]. CLASS solves the Boltzmann equation in order to determine the evolution of the linear power spectrum, primarily during the recombination epoch. This is required for predicting various cosmological observables. *[Technical details → Sec. 6.4.3]*

- ExoCLASS: an extension of CLASS incorporating exotic electromagnetic energy injection into the CMB [484]. These effects can be sourced by annihilating or decaying DM models and would leave signatures in CMB spectra. The technical details and usage are analogous to the CLASS interface.

- DarkAges: a tool to compute the efficiency of energy injection by exotic particle decays or annihilations [484]. The computed efficiencies are an input required for ExoCLASS to compute cosmological observables. *[Technical details → Sec. 6.4.4]*

Table 6.1 provides an overview of the different backends and their purposes. Note, however, that the modularity of GAMBIT allows the user to replace any of these backends by a different external library of their choice. For example, instead of using CLASS for the computation of cosmological observables, one could implement an interface to CAMB [223, 224]. Likewise, the calculation of the primordial element abundances can be provided by, e.g. PArthENoPE [485, 486] instead of AlterBBN.

Some backends can help to decrease the runtime of a fit if a scanner supporting the use of *fast-slow* parameters is employed. This functionality allows different sets of parameters to be changed with a different frequency, such that 'fast' (typically nuisance) parameters – used for calculations that evaluate quickly – are changed far more frequently than 'slow' parameters necessary for calculations requiring longer runtime. If from one point in parameter-space to the next no parameter changing the outcome of a calculation is modified, GAMBIT skips the computation; instead, it reports the previously-computed

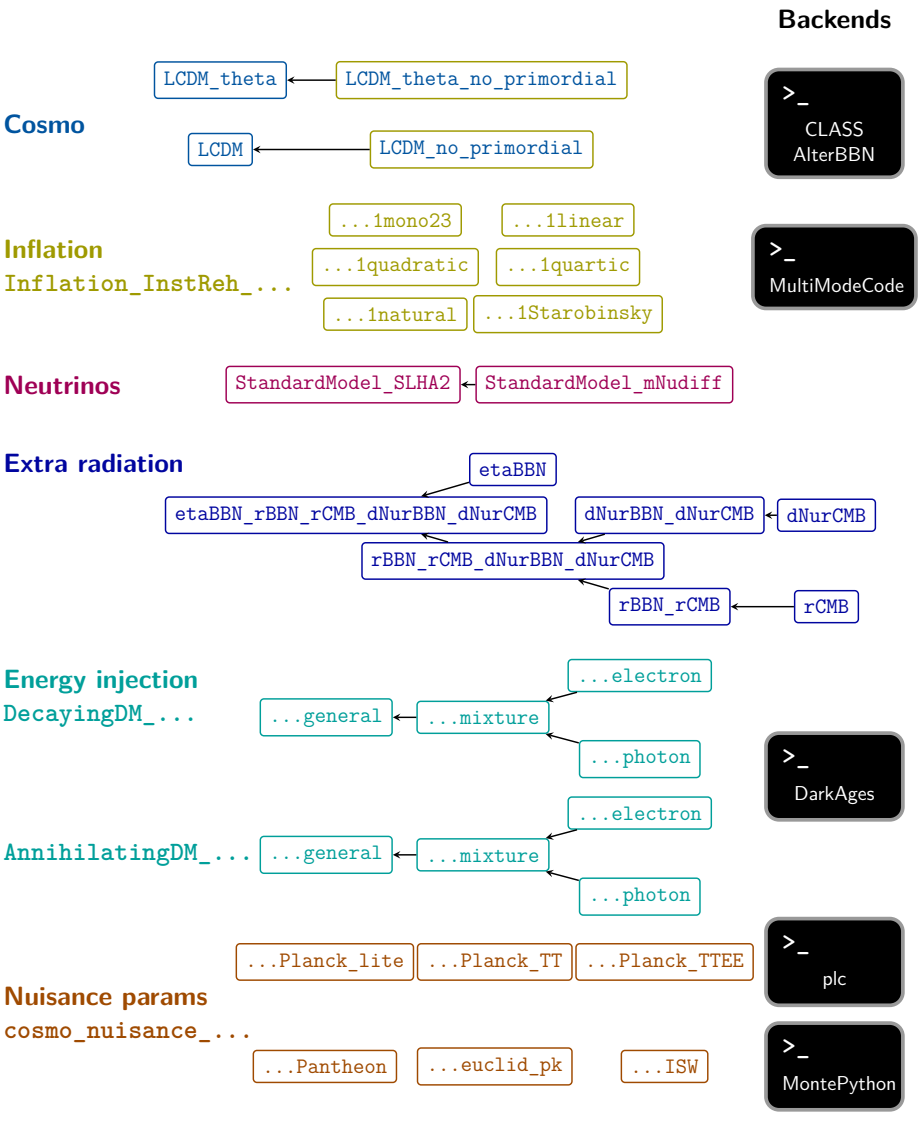

Figure 6.1: Overview of all models relevant to the use of CosmoBit. Arrows mark child-to-parent relations from child models to their parents. Models are grouped into different categories indicated by different colours. Besides the use of a cosmological model (*blue*), the inclusion of all other models is optional. The black boxes indicate which external library (*backend*) the user needs to install for the respective model choice.

Backend	Capabilities & Purpose	F/S	Allowed Models
AlterBBN	Calculate light element abundances → Helium abundance for CLASS run → BBN Likelihood	✓	LCDM, LCDM_theta, extra_radiation, StandardModel_mNudiff
CLASS	Calculate cosmological observables → Planck likelihoods → MontePython likelihoods	✓	LCDM, LCDM_theta, extra_radiation, StandardModel_mNudiff
ExoCLASS	As CLASS but can also be used with annihilating and decaying DM models	✓	+AnnihilatingDM_general, +DecayingDM_general
DarkAges	Calculate spectrum & efficiency of energy injection into CMB → passed to ExoCLASS	✓	AnnihilatingDM_general, DecayingDM_general
MontePython	Calculate cosmological likelihoods	✗	cosmo_nuisance.., except cosmo_nuisance_Planck..
MultiMode	Calculate primordial power spectrum → passed to CLASS	✗	Inflation_..
plc	Calculate Planck likelihoods	✗	LCDM, LCDM_theta, cosmo_nuisance_Planck..

Table 6.1: Overview of the roles and capabilities of the backends interfaced with CosmoBit. The table also indicates which backends can exploit the use of *fast-slow* (F/S) parameters by skipping their respective calculation if no input parameter has changed from one point to the next in parameter space. The last column provides a list of models that are allowed to be used with the respective backend. The model extra_radiation is an abbreviation for the model etaBBN_rBBN_rCMB_dNurBBN_dNurCMB.

results. Currently, only computations provided by AlterBBN, CLASS, ExoCLASS and DarkAges support this feature. We plan to support the fast-slow functionality natively in a future release of GAMBIT, such that it is employed in all likelihood calculations.

In the following sections I will give more details about the implemented models and their parameters, the implemented likelihoods, and the technical details concerning the backend interfaces.

6.2 Cosmological Models in CosmoBit

In this section, I will move through the different model groups in the sequence cosmological models, inflationary models, neutrino mass treatment, additional radiation, and nuisance parameters.

When using GAMBIT in practice, the user can obtain information about each model and its parameters by typing `./gambit <model_name>`.

6.2.1 Standard Cosmology – LCDM

The concordance model of ΛCDM traditionally has six free parameters. In CosmoBit, we include a seventh parameter: the temperature of the CMB as measured today, $T_{\rm CMB}$.

The inclusion of the CMB temperature as a fundamental parameter gives the user full flexibility in the exact treatment of $T_{\rm CMB}$. It is common to fix $T_{\rm CMB}$ to the mean value inferred from the COBE/FIRAS measurement, $T_{\rm CMB} = 2.72548 \pm 0.00057$ K [487]. However, with the increased precision of future surveys, this treatment can lead to a bias in the estimates for other cosmological parameters from parameter inference [103]. Hence, we choose an implementation that provides the freedom to fix $T_{\rm CMB}$, use a Gaussian prior or likelihood arising from the monopole measurement, or to vary $T_{\rm CMB}$ independently from any prior measurement.

Further, we provide the option to use the angular acoustic scale of the first CMB peak ($\theta^\star$) as a free parameter instead of H_0. In terms of physics, these models are equivalent. It is left to the user to choose their preference.

Without any further specification, the treatment of neutrino masses will default to a simplified model: one massive neutrino with the minimum required mass of $\Sigma\, m_\nu = 0.06$ eV. This default behaviour is consistent with the 'baseline' model of the Planck 2015 & 2018 analyses [10, 17]. In this case, no additional ultra-relativistic species are considered, so a photon-to-neutrino temperature ratio of 0.71611 is assumed, and $N_{\rm ur}$ takes the value of 2.0328. These choices lead to the standard scenario of $N_{\rm eff} = 3.046$ in the early Universe, and $\Sigma\, m_\nu/\Omega_{\nu 0} = 93.14\, h^2$ eV [48]. To avoid this simplified treatment, the

user can include the model StandardModel_mNudiff in the scan. The model parameters are the neutrino mass splittings and the mass of the lightest neutrino; refer to Sec. 6.2.3 for details on this model.

The implemented cosmological models and their parameters are:

LCDM: `T_cmb, omega_b, omega_cdm, H0, tau_reio, n_s, ln10A_s`.

Standard ΛCDM with 7 free parameters: the temperature of the CMB as measured today, `T_cmb`, the rescaled baryon energy density today, `omega_b`, the rescaled energy density of cold dark matter today, `omega_cdm`, the Hubble rate today in km /(s Mpc), `H0`, the optical depth to reionisation, `tau_reio`, and the tilt and amplitude of the scalar primordial power spectrum, `n_s` and `ln10A_s`, respectively.

LCDM_no_primordial: `T_cmb, omega_b, omega_cdm, H0, tau_reio`.

As LCDM but without any information about the primordial power spectrum. To be scanned in conjunction with an inflationary model, which provides the primordial power spectrum to pass to CLASS.

LCDM_theta: `T_cmb, omega_b, omega_cdm, 100theta_s, tau_reio, n_s, ln10A_s`.

As LCDM but replacing the free parameter H_0 with $\theta^\star = r^\star/d_A^\star$, the angular acoustic scale of the CMB multiplied by a factor of 100.

LCDM_theta_no_primordial: `T_cmb, omega_b, omega_cdm, 100theta_s, tau_reio`.

As LCDM_no_primordial but using $\theta^\star = r^\star/d_A^\star$ instead of H_0.

6.2.2 Inflationary Models and Parameters

This section introduces models supported in CosmoBit that go beyond a simple parametrisation of the PPS with A_s and n_s. These inflationary models include natural and Starobinsky inflation, plus various versions of single-field inflation with a monomial potential,

$$V(\phi) = \lambda\, M_\mathrm{Pl}^{4-n}\, \frac{\phi^n}{n}\,. \tag{6.1}$$

Currently, only single-field inflation models assuming instant reheating are implemented. This makes N_pivot, the number of e-folds over which inflation occurs, a derived parameter (via its relation to instant reheating, as in Ref. [488]). In CosmoBit, we use the MultiModeCode to compute the PPS. It can solve equations of motion for multi-field models and non-instantaneous reheating scenarios, but the first release of CosmoBit will not support these features.

There is one important thing to note: whenever an inflationary model is used the cosmological model may not include any assumptions regarding the

shape of the PPS. Instead, the inflation model and its respective parameters dictate the form of the PPS. Hence, the inclusion of an inflation model requires the use of a cosmological model without primordial parameters. These models are LCDM_no_primordial and LCDM_theta_no_primordial, which correspond to the baseline ΛCDM model without the two parameters A_s and n_s.

The supported inflationary models are:

Inflation_InstReh_1mono23: `lambda`.

A single-field model with monomial potential, with $n = 2/3$ in eq. (6.1).

Inflation_InstReh_1linear: `lambda`.

Single-field inflation with a linear potential, with $n = 1$ in eq. (6.1).

Inflation_InstReh_1quadratic: `m_phi`.

Single-field inflation with a quadratic potential, with $n = 2$ and $\lambda M_{\rm Pl}^2 \to m_\phi^2$ in Eq. (6.1).

Inflation_InstReh_1quartic: `lambda`.

Single-field inflation with a quartic potential, with $n = 4$ in eq. (6.1).

Inflation_InstReh_1natural: `lambda, f_phi`.

Natural inflation, in which the inflaton is a pseudo Nambu-Goldstone boson of a broken global symmetry [489, 490] resulting in a potential of the form $V(\phi) = \lambda^4 M_{\rm Pl}^4 [1 + \cos(\phi/f_\phi)]$.

Inflation_InstReh_1Starobinsky: `lambda`.

Starobinsky inflation results from adding an R^2 term to the Einstein-Hilbert action, which is generically expected to appear due to corrections arising from quantum gravity [187]. When transformed to the Einstein frame, this corresponds to a single-field inflation model with potential $V(\phi) = \lambda^4 M_{\rm Pl}^4 \left[1 - e^{-\sqrt{2/3}\phi/M_{\rm Pl}}\right]^2$.

6.2.3 Neutrino Masses

The user can choose to consider a realistic treatment of neutrino masses by including the model StandardModel_mNudiff in the scan. This inclusion disables the simplified default assumptions made in the baseline ΛCDM model.

In the absence of any non-standard energy injection or radiation content, the number of ultra-relativistic species today, $N_{\rm ur}$, is set to 0.00641, and the temperature ratio between photons and neutrinos is not modified. This leads to the standard value of $N_{\rm eff} = 3.046$ in the early Universe.

StandardModel_mNudiff: `mNu_light, dmNu21, dmNu31`.

A realistic model of all three Standard Model neutrinos parametrised by the mass of the lightest neutrino, `mNu_light`, the squared mass splitting from the second to first (`dmNu21`) and third to the lightest neutrino (`dmNu31`) in eV^2.

By fixing the sign of `dmNu31`, one can choose the neutrino mass hierarchy: for a scan only considering the normal (inverted) hierarchy `dmNu31` should be strictly positive (negative).

6.2.4 Non-Standard Radiation Content

We include a general model which captures extensions related to a non-standard value of ΔN_{eff} and a non-standard baryon-to-photon ratio at the epoch of BBN. The model is called etaBBN_rBBN_rCMB_dNurBBN_dNurCMB. The modifications to N_{eff} can arise from either changing the temperature ratio between photons and neutrinos or from introducing additional ultra-relativistic species (see Sec. 3.3 for details). Whenever a model parameter name of the most general model does not appear in the name of a child, the parameter value takes its respective standard value from ΛCDM, as described below.

etaBBN_rBBN_rCMB_dNurBBN_dNurCMB: `eta_BBN, r_BBN,r_CMB, dNur_BBN, dNur_CMB`.

Most general model allowing modifications to the baryon-to-photon-ratio at the end of BBN (`eta_BBN`), introducing additional ultra-relativistic degrees of freedom during BBN and CMB release (`dNur_BBN` and `dNur_CMB`), and changing the neutrino temperature, parametrised by the temperature ratio $r_{\mathrm{BBN(CMB)}} = T_\nu^{\mathrm{BSM}}/T_\nu^{\mathrm{SM}}$ at BBN (recombination).

rBBN_rCMB_dNurBBN_dNurCMB: `r_BBN, r_CMB, dNur_BBN, dNur_CMB`.

As etaBBN_rBBN_rCMB_dNurBBN_dNurCMB but with η_{BBN} set equal to the value at recombination, encoded in ω_b (equal to η_0 in ΛCDM).

dNurBBN_dNurCMB: `dNur_BBN, dNur_CMB`.

As rBBN_rCMB_dNurBBN_dNurCMB but with no BSM modifications of the temperature of neutrinos, $r_{\mathrm{CMB}} = r_{\mathrm{BBN}} = 1$.

rBBN_rCMB: `r_BBN, r_CMB`.

As rBBN_rCMB_dNurBBN_dNurCMB but with no extra ultra-relativistic degrees of freedom at either BBN or recombination, this means that $\Delta N_{\mathrm{ur,CMB}} = \Delta N_{\mathrm{ur,BBN}} = 0$.

rCMB: `r_CMB`.

As rBBN_rCMB but with the same ratio of neutrino temperatures at the end of BBN and at recombination, $r_{\rm CMB} = r_{\rm BBN}$.

dNurCMB: `dNur_CMB`.

As dNurBBN_dNurCMB but with a constant number of extra ultra-relativistic degrees of freedom between the end of BBN and at recombination, $\Delta N_{\rm ur,CMB} = \Delta N_{\rm ur,BBN}$.

etaBBN: `eta_BBN`.

As etaBBN_rBBN_rCMB_dNurBBN_dNurCMB but with no contribution to $\Delta N_{\rm eff}$ from neither ultra-relativistic species nor a change of the neutrino temperatures, i.e. $r_{\rm CMB} = r_{\rm BBN} = 1$ and $\Delta N_{\rm ur,CMB} = \Delta N_{\rm ur,BBN} = 0$.

6.2.5 Energy Injection

The first version of CosmoBit allows the user to consider two common scenarios of energy injection into the CMB: energy injection through s-wave annihilating dark matter or energy injection through a decaying subcomponent of dark matter. The parameters describing these scenarios are the dark matter mass m_χ, the fractional abundance ξ, and either the thermally-averaged cross-section $\langle\sigma v\rangle$ (for annihilating DM) or the particle lifetime τ (for decaying DM).

Further model-specific dependencies are the spectrum of injected electromagnetic particles and the resulting dimensionless *efficiency functions* $f_c(z, x_e)$. The efficiency functions link the energy injection rate per unit time and volume $\left(\frac{\mathrm{d}^2E}{\mathrm{d}V\,\mathrm{d}t}\Big|_{\rm dep,c}\right)$ to the energy deposition rate $\left(\frac{\mathrm{d}^2E}{\mathrm{d}V\,\mathrm{d}t}\Big|_{\rm inj}\right)$ via

$$\left.\frac{\mathrm{d}^2E}{\mathrm{d}V\,\mathrm{d}t}\right|_{\rm dep,c}(z, x_e) = f_c(z, x_e) \cdot \left.\frac{\mathrm{d}^2E}{\mathrm{d}V\,\mathrm{d}t}\right|_{\rm inj}(z)\,. \tag{6.2}$$

Here, z denotes a given redshift, x_e the free electron fraction, and the subscript c indicates through which channel – ionisation, excitation, or heat – energy is deposited into the primordial plasma. For each given model, we must evaluate the functions $f_c(z, x_e)$. In CosmoBit, we employ the code DarkAges for the calculation of $f_c(z, x_e)$ (see Sec. 6.4.4). The backend ExoCLASS [484] is responsible for calculating the predictions for cosmological observables taking these types of early-time energy injections into account.

The models implemented in the first release of CosmoBit and their respective parameters are:

AnnihilatingDM_general: `mass, sigmav`.

Most general scenario of energy injection by s-wave annihilating dark matter. The `mass` is given in GeV and the thermal averaged cross-section `sigmav` $= \langle \sigma v \rangle$ in cm^3/s. This scenario implicitly assumes that the particle in question constitutes all of dark matter. The fractional abundance ξ is, therefore, implicitly assumed to be equal to unity. For scenarios where the annihilating species is a fraction of dark matter, the cross-section should be scaled by ξ^2.

AnnihilatingDM_mixture: `mass, sigmav, BR`.

Dark matter annihilates into electron-positron pairs with a given branching ratio `BR`. The kinetic energy of the products is $m_\chi - m_e$, annihilation into photon pairs proceeds with branching ratio (1−`BR`). The kinetic energy of the resulting photons is m_χ. No radiative corrections are assumed.

AnnihilatingDM_photon: `mass, sigmav`.

Child of AnnihilatingDM_mixture where dark matter annihilates exclusively into a photon pair, i.e. `BR` $= 0$.

AnnihilatingDM_electron: `mass, sigmav`.

Child of AnnihilatingDM_mixture where dark matter annihilates exclusively into an electron-positron pair, i.e. `BR` $= 1$.

DecayingDM_general: `mass, lifetime, fraction`.

Most general scenario of energy injection by a decaying subcomponent of dark matter. The mass is given in GeV and the lifetime in seconds. The fractional abundance ξ is the value at production, before any decays have taken place.

DecayingDM_mixture: `mass, lifetime, fraction, BR`.

Dark matter subcomponent decaying into electron-positron pairs with a given branching ratio `BR`. The kinetic energy of the products is $\frac{m_\chi}{2} - m_e$, decay into photon pairs proceeds with branching ratio (1−`BR`). The kinetic energy of the resulting photons is $\frac{m_\chi}{2}$. No radiative corrections are assumed.

DecayingDM_photon: `mass, lifetime, fraction`.

Child of DecayingDM_mixture where the dark matter subcomponent decays exclusively into a photon pair, i.e. `BR` $= 0$.

DecayingDM_electron: `mass, lifetime, fraction`.

Child of DecayingDM_mixture where the dark matter subcomponent decays exclusively into an electron-positron pair, i.e. `BR` $= 1$.

6.2.6 Cosmological Nuisance Parameters

Various cosmological likelihoods require the inclusion of additional nuisance parameters in the scan. We implement these as separate models. As a classic example, consider a study including CMB, BAO scale and SNe Ia likelihoods. Among these three likelihoods, two come with nuisance parameters: the Planck 2018 CMB likelihoods [10], and the Pantheon dataset comprising the redshift and light-curve parameters of 1048 SNe Ia [491]. The two nuisance parameter models and their respective parameters are:

cosmo_nuisance_Pantheon: `M`.

Nuisance parameter for the Pantheon likelihood [491], where `M` is the absolute magnitude of a Type Ia Supernova.

cosmo_nuisance_Planck_lite: `A_planck`.

Nuisance parameter for Planck 'lite' CMB likelihoods with marginalised foregrounds; this requires only the use of one nuisance parameter encoding the absolute calibration, A_{Planck}.

All other nuisance parameter models implemented in CosmoBit are listed in Table 6.2. See the following section, 6.3, for more details on the respective likelihoods.

Model Name cosmo_nuisance_..	Number of Parameters	Likelihood Name(s)
[Provided by plc]:		
..Planck_TTTEEE	34	Planck CMB TT-TE-EE
..Planck_TT	16	Planck CMB TT
..Planck_lite	1	Planck lite
[Provided by MontePython]:		
..JLA	4	JLA
..Pantheon	1	JLA_simple, Pantheon
..BK14	10	BK14
..ISW	16	ISW
..ska	10	ska1_lensing, ska1_pk, ska2_lensing, ska2_pk, ska1_IM_band1, ska1_IM_band2
..euclid_pk	4	euclid_pk
..euclid_lensing	1	euclid_lensing
..CFHTLens_correlation	1	CFHTLens_correlation
..kids450_qe_likelihood_public	7	kids450_qe_likelihood_public
..dummy	10	

Table 6.2: List of all implemented cosmological nuisance parameter models, the number of free parameters they each possess, and the name of the likelihood they appear in. The backend plc provides the likelihoods in the upper part of the table; the backend MontePython [471, 472] provides the likelihood calculations in the lower part. To obtain detailed information about the model parameters and their physical meanings, use the command `./gambit <model_name>`. We provide the model cosmo_nuisance_dummy as an example for the user of how to add a new nuisance parameter model. All new functions and files associated with these examples contain detailed comments and instructions for potential developers.

6.3 Likelihoods in CosmoBit

In this section, I present the likelihoods currently available for use in CosmoBit. These likelihoods probe a range of different cosmological epochs. I will discuss likelihoods probing the phase of BBN by measurements of light element abundances first. After that, I will turn to the included CMB likelihoods, followed by an overview of likelihoods made available through the interface to MontePython. I provide a summary of the most important likelihoods in Table 6.3. The reader should refer to the references in this table for details regarding the original studies and likelihood calculations.

6.3.1 Light Elements from Big Bang Nucleosynthesis

To obtain theoretical predictions for the light element abundances, we use the software tool AlterBBN [467, 468]. It allows the user to vary, e.g. the baryon-to-photon ratio, the number of ultra-relativistic degrees of freedom, and the neutron lifetime. Other modifications available for use include a modified expansion rate sourced by, e.g. early DE, additional entropy injection from non-standard particle decays, and decaying scalar fields. AlterBBN evaluates a nuclear reaction network containing 100 different reactions and computes the abundances of all light elements from hydrogen up to oxygen (^{16}O), as well as the full covariance matrix arising from correlated theoretical uncertainties of the different abundances. The inclusion of these theoretical uncertainties is essential for the likelihood calculation.

The likelihood function arising from the abundances of n different species is

$$\log \mathcal{L} = -\frac{1}{2}\left[(\mathbf{t}-\mathbf{d})\, C_{\mathrm{tot}}^{-1}\, (\mathbf{t}-\mathbf{d})^{\mathrm{T}} + (2\pi)^n \det C_{\mathrm{tot}}\right] . \tag{6.3}$$

Here, $\mathbf{d}$ and $\mathbf{t}$ are the vectors of length n containing the measured and the theoretically predicted abundances, respectively; $\det C_{\mathrm{tot}}$ denotes the determinate of the total covariance matrix C_{tot}. The covariance matrix is composed of contributions from theoretical and observational uncertainties, $C_{\mathrm{tot}} = C_{\mathrm{obs}} + C_{\mathrm{theo}}$. Note that C_{obs} is a diagonal matrix as the measurements are uncorrelated. The diagonal elements are the squares of the respective $1\,\sigma$ uncertainties.

The user can choose which light element abundance measurement(s) they want to include in likelihood calculation. A valid choice is any (sub)set of deuterium, helium-3, helium-4, and lithium-7. The default treatment is to include only deuterium and helium-4. The central values and their respective $1\,\sigma$ uncertainties normalised to the hydrogen abundance are $\mathrm{D/H} = (2.547 \pm 0.025) \times 10^{-5}$, and $\mathrm{He4/H} = 0.245 \pm 0.003$ (recommended values from the Particle Data Group [498]). See Sec. 6.4.2 how to customise this choice.

Likelihood	Brief Description	Nuisance Params	External Library
BBN	Light element abundance measurements for D, ^{4}He, ^{3}He and ^{7}Li, see Sec. 6.4.2.	0	AlterBBN
CMB			
BK14	Likelihoods from BICEP2/KECK array (2014) [492].	10	MP
Planck	Planck 2018 [481] and 2015 [480]:		
Low-ℓ	*Planck low-ℓ* likelihood, TT, EE, TTEE.	1	plc
High-ℓ	*Planck high-ℓ* likelihood, TT, (TTTEEE).	16 (34)	plc
High-ℓ 'lite'	*Planck high-ℓ* lite likelihood, TT, (TT-TEEE).	1	plc
lensing	*Planck* lensing likelihoods.	1	plc
SNe Ia			
Pantheon	Pantheon sample including 1048 SNe Ia [491].	1	MP
BAO scale			MP
WiggleZ	Likelihood from the WiggleZ dark energy survey reconstruction of the baryon acoustic feature [493].	0	
BOSS	Baryon Oscillation Spectroscopic Survey (BOSS), CMASS and LOWZ DR10 & 11 [71], Lymann alpha DR 10 & 11 [416], combined DR 12 sample [417].	0	MP
Weak lensing			
KiDS	Tomographic weak lensing Kilo-Degree Survey (KiDS) likelihood from [122].	6	MP
CFTHLenS	Likelihood from the Canada-France-Hawaii Telescope Legacy Survey (CFHTLenS) [494].	1	MP
Galaxy clusters			
SDSS	Likelihoods based on the Sloan Digital Sky Survey (SDSS) DR 4 [495] and DR 7 [496].	0	MP
WiggleZ	Likelihood from the WiggleZ dark energy survey power spectrum analysis [497].	0	MP

Table 6.3: Table with a selection of available likelihoods in CosmoBit. For details on how to include likelihoods in the scan, refer to Sec. 6.4.1. Beyond the here listed likelihoods, all likelihoods implemented in MontePython 3.3 are available for use in CosmoBit. See Sec. 6.4.5 for the description of the MontePython interface with GAMBIT.

6.3.2 Anisotropies in the Cosmic Microwave Background

To calculate likelihoods related to the CMB spectra, we use the `Plik` likelihoods published within the Planck Likelihood Code (plc) [480, 481]. Using plc, we gain access to the full set of the Planck 2015 and 2018 likelihoods, i.e. the low-ℓ and high-ℓ likelihoods for the temperature and polarisation spectra, as well as the lensing likelihood constraining the CMB lensing potential.

The Planck likelihoods contain nuisance parameters to account for uncertainties related to the instrument calibration and signal contamination. There are 34 extra parameters when using high-ℓ polarisation likelihoods and 16 when employing only the temperature anisotropies. To reduce the number of dimensions in a parameter scan, the plc package also contains a *lite* (lightweight) version of the high-ℓ likelihoods. In this lite likelihood, the foregrounds are already marginalised over, meaning that only one nuisance parameter remains: A_{Planck}, the absolute calibration.

Note that the Planck marginalised lite likelihoods was constructed to reduce the number of nuisance parameters involved in the likelihood calculation for a standard ΛCDM model. It should, therefore, be used with care when considering extensions to ΛCDM or alternative theories, as *a priori*, it is not given that this simplification is a valid approximation for any given model.

Refer to Refs. [480, 481] for details on the likelihood calculation. I provide a documentation of the plc usage within GAMBIT in Sec. 6.4.7.

6.3.3 Overview of Likelihoods Available via MontePython

To provide a variety of additional, well-tested cosmological likelihoods, CosmoBit interfaces to MontePython [471, 472]. MontePython is a tool to perform parameter scans of cosmological models. It allows the user to choose between different sampling algorithms and offers an extensive library of cosmological likelihoods. Within CosmoBit, we are only interested in the latter feature, the likelihood calculations and not in the sampling functionality. Likelihoods that are entirely implemented in MontePython can be used out-of-the-box within CosmoBit.[2]

This interface provides access to various probes of the Universe: the user can include probes of the background evolution through measurements of recession velocities of SNe Ia, and the BAO scale. The inclusion of weak lensing and galaxy clustering data offer probes of the linear matter power spectrum. Measurements of the ISW effect through cross-correlations of the CMB tem-

[2]This excludes the Planck and WMAP CMB likelihoods as they require the installation of additional libraries. The Planck CMB likelihoods are made available within CosmoBit through the interface to plc.

perature spectrum with foreground galaxies probe the time evolution of gravitational potentials. Table 6.3 provides an incomplete selection of likelihoods and datasets included in MontePython.

Besides testing a model against already available datasets, MontePython also allows the user to forecast the sensitivity of future experiments. Examples of this are cosmic shear and galaxy clustering forecasts for Euclid and the Square Kilometer Array (SKA) [499, 500].

For an up-to-date compilation of all available likelihoods, I refer the reader to the MontePython website.[3] I describe how we extract the likelihoods from MontePython, and how the user can include the likelihoods in an analysis with GAMBIT in Sec. 6.4.5

6.4 Practical Usage and Interfaces to External Libraries

In this section, I aim to give the reader practical instructions on how to use the features of CosmoBit within GAMBIT. I will start with a quick-start guide for the installation and a simple first run. I then detail the interfaces to the different backends in alphabetical order (AlterBBN, CLASS, DarkAges, MontePython, MultiModeCode, plc). I will provide practical usage information for all of these backends, and technical details primarily for the parts where I have been one of the leading contributors to the implementation.

6.4.1 Quickstart

In the following, I provide a quick-start guide for a simple test run of CosmoBit with the example YAML file `$GAMBIT/yaml_files/CosmoBit_quickStart.yaml`. This includes an explanation of the configure and installation steps for GAMBIT, how to install all backends relevant for running CosmoBit, and how to start the scan. The example YAML file includes additional comments on each of its entries. The user can find a more detailed explanation of all the features that CosmoBit introduces in `CosmoBit_tutorial.yaml`.

To run the example provided in `CosmoBit_quickStart.yaml` one must first configure and build GAMBIT. After downloading GAMBIT, run the following command from the GAMBIT base directory:

```
mkdir build
cd build
cmake -D WITH_MPI=ON ..
```

[3] https://brinckmann.github.io/montepython_public/

```
# n = number of cores to use for build
make -jn scanners
cmake ..
# n = number of cores to use for build
make -jn gambit
```

The flag `-D WITH_MPI=ON` enables parallel computation with several MPI processes. The step `make -jn scanners` will install all available scanners that are implemented in the ScannerBit module [452].

The user can download and build all external codes interfaced with CosmoBit by executing

```
make alterbbn classy darkages montepythonlike multimodecode plc
```

in the build directory. This command will download the default version of each backend. The user can choose different versions by adding the version number, for example, with `make classy_exo_2.7.2` to build ExoCLASS version 2.7.2.

To start a scan with, e.g. two MPI processes running in parallel use the command

```
mpirun -N 2 ./gambit -f yaml_files/CosmoBit_quickStart.yaml
```

6.4.2 Interface to AlterBBN

AlterBBN is used to compute the relic abundance of light elements from BBN. Currently, in CosmoBit the primoridal element abundances are used for two purposes: *i)* to pass the helium abundance, which is an initial condition for reionisation calculations, to CLASS, and *ii)* to provide the theoretical predictions and errors for the BBN likelihood if requested.

Practical Usage

The user can choose to include the calculation of the BBN likelihood with the following entries in the YAML file:

```
ObsLikes:

  # Likelihood from light element abundances from BBN,
  # isotopes to include can be specified in the Rules
  # section as shown below
  - purpose: LogLike
    capability: BBN_LogLike
    module: CosmoBit

  # (optional): add element abundance + error to output
  - purpose: Observable
```

```
  capability: Deuterium_abundance

- purpose: Observable
  capability: Helium_abundance

- purpose: Observable
  capability: Helium3_abundance

- purpose: Observable
  capability: Lithium7_abundance

- purpose: Observable
  capability: Beryllium7_abundance


Rules:

  # (optional): choose which light element abundance measurements
  # are used for the likelihood calculation,
  # all values given relative to the Hydrogen abundance
  # and passed with [<mean>, <1 sigma uncertainty>]
  - capability: BBN_LogLike
    options:
      Yp: [0.245, 0.003]  # default value
      H2: [2.547e-5, 0.025e-5] # default value
      Li7: [1.6e-10, 0.30e-10] # not included by default
```

The rule sets which element abundances are to be used for the likelihood calculation by the capability *BBN_LogLike*. If this rule does not exist, the default behaviour is to include deuterium and helium with the values indicated in the example. These default values are the recommended values from the Particle Data Group [498]. In principle, the user can also include the helium-3 measurements in the likelihood calculation. However, owing to difficulties in inferring the primordial value from today's measurements, the use of helium-3 is not recommended for cosmological tests [498].

Technical Details

AlterBBN stores all settings and assumptions relevant to the primordial elemental abundance calculation within the C structure named `relicparam`. It contains the values of any (model) parameters needed for the abundance calculation. Examples of cosmological model-dependent parameters are the baryon-to-photon ratio after BBN (`eta0`), the number of ultra-relativistic degrees of freedom (`dNu`), or density and temperature of an additional dark component. Examples of technical settings are, e.g. related to numerical integration methods (`failsafe`), or different methods for the theoretical error calculation (`err`).

To have access to these settings, we make the `relicparam` structure available for use within GAMBIT by including it as a backend type.[4]

The interface between CosmoBit and AlterBBN is set-up as follows:

1) **Set AlterBBN input parameters**, `capability` *AlterBBN_Input*.
`Function` *AlterBBN_Input*, `type: map_str_dbl`. All parameters and settings to be passed to AlterBBN are collected in a map from parameter name to the respective value. Currently, these are `eta0`, `dNnu`, and `Nnu`, the effective number of SM Neutrinos. Additionally the user can pass values for the precision parameters `err` and `failsafe` as run options. The default values are 1, and 0, respectively.
[*Note for developers:* to add a new model that requires additional input settings implement these changes here. Location: `CosmoBit.cpp`, header definition in `CosmoBit_rollcall.hpp`.]

2) **Get primordial element abundances**, `capability` *BBN_abundances*.
`Function` *compute_BBN_abundances*, `type: BBN_Container`. Gains access to the AlterBBN input through a dependency on *AlterBBN_Input* (step 1). The resulting input map is passed as an argument to the backend requirement *calc_nucl_err* (step 3). Through this call to *calc_nucl_err* the vector `BBN_abund` and matrix `BBN_covmat` storing the primordial element abundances and their covariances are filled. These results are stored within the type `BBN_Container` (see Table 6.4) such that they are accessible for other capabilities within GAMBIT.
[*Note for developers:* model independent. Location: `CosmoBit.cpp`, header definition in `CosmoBit_rollcall.hpp`.]

3) **AlterBBN function to compute relic density abundances**.
`BE_CONVINIENCE_FUNCTION` *calc_nucl_err* `(map_str_dbl &, double*, double*)`.
Receives the AlterBBN input map, the unfilled abundance vector `BBN_abund` and covariance matrix `BBN_covmat` as input arguments. An instance of the `relicparam` structure is created and passed together with the input map to the backend convenience function *fill_cosmomodel* (step 4). The latter function handles the model-dependent setting of input arguments. After that, the AlterBBN internal routine *nucl_err* is called to fill `BBN_abund` and `BBN_covmat` with the predicted element abundances and their covariances. Returns 0 if the calculation was successful, 1 if unsuccessful.
[*Note for developers:* model independent. Location: `AlterBBN_2.X.cpp`, header definition in `AlterBBN_2.X.hpp`.]

[4] In `Backends/include/gambit/Backends/backend_types/AlterBBN.hpp`.

4) **Pass input parameters to AlterBBN.**
`BE_CONVINIENCE_FUNCTION` *fill_cosmomodel* `(relicparam*, map_str_dbl &)`. This function takes an instance of the `relicparam` structure and the input map created in *AlterBBN_Input* (step 1) as argument. All parameter values contained in the input map will overwrite the defaults of the corresponding `relicparam` structure members.
[*Note for developers:* if the user would like use any additional AlterBBN features, the rules to pass the corresponding settings must be added here. Location: `AlterBBN_2.X.cpp`, header definition in `AlterBBN_2.X.hpp`.]

5) **Compute BBN likelihood**, `capability` *BBN_LogLike*.
`Function` *compute_BBN_LogLike*, `type: double`. Has a dependency on the BBN abundance calculation (step 2). Through this dependency we gain access to the abundance calculation results stored in the `BBN_Container`. From these results, we calculate the BBN likelihood as described in Sec. 6.3.1.
[*Note for developers:* model independent. Location: `CosmoBit.cpp`, header definition in `CosmoBit_rollcall.hpp`.]

Additionally, we provide capabilities to compute the deuterium abundance (called *Deuterium_abundance*), helium abundances, (*Helium_abundance* for helium-4 and *Helium3_abundance* for helium-3), lithium (*Lithium7_abundance*), and beryllium (*Beryllium7_abundance*). They each have a dependency on the capability *BBN_abundances* and provide a vector with the calculated mean (first entry) and the uncertainty (second entry) of the respective abundance.

6.4.3 Interface to CLASS

We implement the interface between GAMBIT and CLASS using the Python wrapper for CLASS, called classy.[5] We chose this over the option of a direct interface to the relevant C structures and functions through shared libraries. The C interface would allow GAMBIT full access to all structures and their members, as well as the control to run every single CLASS module.[6] While this access and control is not possible through the Python interface, using the Python wrapper comes with other significant advantages: firstly, it makes the interface version-independent. This version independence means that if

[5]Hence, the `make` target to build the interface to CLASS is called classy. This is to be explicit about our use of the Python wrapper for the interface.

[6]CLASS is separated into different modules, each responsible for different physics. For example, the `background` module solves the background equations, and the spectra are computed in the `spectra` module.

Type	Name	Purpose
`BBN_Container`		
`int`	`NNUC`	`private`, number of element abundances computed by AlterBBN
`vec<double>`	`BBN_abund`	`private`, vector of length `NNUC+1` to be filled with element abundances
`vec<vec<double>>`	`BBN_covmat`	`private`, covariance matrix of element abundances with dimension `NNUC+1` × `NNUC+1`
`map_str_int`	`abund_map`	`private`, map from element name to the respective position in `BBN_abund` vector, e.g. 'H2' → 3
`double`	*get_BBN_abund*(`int i`)	`return` the i^{th} element of `BBN_abund`
`double`	*get_BBN_covmat*(`int i`, `int j`)	`return` the $(i,j)^{th}$ element of `BBN_covmat`

Table 6.4: Members and attributes of the type `BBN_Container`. The main purpose is to store the results of AlterBBN in a type accessible to module functions in CosmoBit. The member `abund_map` is a hard-coded map between the name of an element and its position in the abundance vector and covariance matrix. This is to avoid mistakes when accessing the result for a particular element and to make the code more explicit.

relevant input parameters of a given CLASS version are known to its Python wrapper, no new code needs to be produced to interface this alternative CLASS version with GAMBIT. This makes it easy to use (privately) developed extensions of CLASS for non-standard physics scenarios. Secondly, the use of the Python wrapper provides the possibility to easily use cosmological likelihoods implemented in MontePython (see Sec. 6.4.5 for the usage and technical details.)

The CLASS versions interfaced in GAMBIT 1.5 are CLASS 2.6.3, 2.9.3, and ExoCLASS 2.7.2.

At the moment, CLASS is the only Boltzmann solver interfaced with GAMBIT. However, our design of the interface is such that all CLASS-specific capabilities and functions are clearly separated from capabilities that could, in principle, be resolved by a different source code. Hence, the set up allows for the possibility to implement interfaces to other Boltzmann solvers, e.g. CAMB [223, 224] with minimum effort.

In the following, I will first give some practical usage information. After

that, I provide a user guide on how to interface a new version of CLASS and instructions on how to pass input parameters for a new model to CLASS. I will then give details on the patches we apply to CLASS and finally explain technicalities of the interface to CosmoBit.

Practical Usage

GAMBIT's dependency resolution automatically takes care of creating a dictionary containing all input parameters for CLASS. These input parameters depend on the settings specified in the YAML file: on the one hand, the included models decide which model parameters CosmoBit passes CLASS; on the other hand, the chosen likelihoods dictate the run-specific settings (e.g. which spectra need to be computed). As CosmoBit sets and passes these values automatically, in practice, the user does not need to know about any CLASS specific syntax, settings or functions.

The only likelihood-dependent setting that the user needs to set themselves is the information whether they want to include MontePython likelihoods in the scan or not (see Sec. 6.4.5 for more details on the MontePythonLike interface). This is done by choosing which function is used to pass CLASS input parameters from CosmoBit to the CLASS frontend. The `Rules` section in the YAML file must contain one of the following two options:

```
Rules:

  # Initialisation of input arguments for CLASS if no
  # MontePython likelihoods are in use
  - capability: classy_final_input
    function: set_classy_input

 # .. OR ..

 # Initialisation of input arguments for CLASS if
 # MontePython likelihoods are in use
  - capability: classy_final_input
    function: set_classy_input_with_MPLike
```

The latter ensures sure that CosmoBit passes potential run options required by the chosen MontePython likelihoods to CLASS. If the user chooses the wrong function to resolve this capability, GAMBIT will inform them which choice is the right one in the context of their specific YAML file.

If the user wishes to pass any additional settings to CLASS, they can achieve this specifying the settings in the `Rules` sections of the input YAML file – for example, the entries

```
Rules:
```

```
# Pass additional run options to CLASS
- capability: classy_baseline_params
  function: set_classy_baseline_params
  options:
    classy_dict:
      back_integration_stepsize : 7.e-3
      tol_background_integration : 1.e-2
```

result in a CLASS run with increased precision for the background integration. The user can pass any input parameter that is understood by the respective CLASS version's Python wrapper through this option. If one specifies conflicting values for a parameter, CosmoBit will exit with an error identifying any problematic entries. Such a conflict can occur if, for example, the user tries to overwrite a model parameter, or passes an option that conflicts with a setting required by one of the likelihoods in use.

Adding a New CLASS Version

CLASS is under continual development, and new versions with new features are regularly released. Several forks of CLASS, including more non-standard cosmological scenarios and models have been developed.[7] To make it easy for the user to use these extensions with GAMBIT, I will explain how to add an interface to a new CLASS version. I recommend implementing any version — even if forked and extended with respect to the public CLASS repository — as a different version of the classy backend. For example, we implement ExoCLASS 2.7.2 as version `exo_2.7.2`, and my_CLASS version 4.2.0 should be implemented as classy version `my_4.2.0`.

The steps to be followed are:

1) Set the **default backend location**. This is done by adding an entry for the new version to `config/backend_locations.yaml.default`:

```
classy:
  2.6.3:
      ./Backends/installed/classy/2.6.3/lib/classy_2_6_3.py
  my_4.2.0:
      ./Backends/installed/classy/my_2.4.0/lib/classy_my_4_2_0.py
```

2) Add the **download and installation commands** for CLASS version `my_4.2.0` to `cmake/backends.cmake`. Copy the ExoCLASS example and replace the version name, download link, and `md5` checksum. Remove all

[7] Just a few examples are ExoCLASS [484], `hi_class` [405, 406], and CLASS-PT [501].

commands related to patches if you do not need to use any feature requiring a CLASS patch. If patches are required, the user must provide these.

3) Create a **header and source file** for the frontend interface to the new CLASS version.[8] Simply copy and rename the file for the default classy version and replace the version name. The source file is entirely version-independent, only the version numbers in the header file must be modified, these are the last two lines of:

```
#define BACKENDNAME classy
#define BACKENDLANG Python
#define VERSION my_4.2.0
#define SAFE_VERSION my_4_2_0
```

After rerunning CMake, the user can build their CLASS version by typing `make classy_my_4.2.0` in the build directory. All structure members, input parameters and methods that are known to the Python wrapper of the new version will be automatically available for use within GAMBIT.

Setting CLASS Input for a New Model

If the user wishes to implement a new cosmological model, they must pass the corresponding parameters and settings to CLASS. In this section, I will give an outline of how to do this. I will use the example of a new model called DE_model with two model parameters: `w0_fld` and `wa_fld`. These are commonly used to parametrise the time evolution of the equation of state of a perfect fluid modelling DE.

1) Add a **capability to set all model-dependent parameters** for the CLASS run (here: *classy_parameters_DE_model*). The header definition to be added to `Cosmobit_rollcall.hpp` reads:

```
#define CAPABILITY classy_parameters_DE_model
START_CAPABILITY
  #define FUNCTION set_classy_parameters_DE_model
   START_FUNCTION(pybind11::dict)
   ALLOW_MODELS(DE_model)
  #undef FUNCTION
#undef CAPABILITY
```

Note that the macro `ALLOW_MODEL(DE_model)` allows the user to access the model parameters DE_model through the `*Param` dictionary.

[8] The header files are in `Backends/include/gambit/Backends/frontends/`, source files in `Backends/src/frontends/` .

2) Implement the **module function** *set_classy_parameters_DE_model* which provides the capability defined in step 1). To do so add the following lines to `CosmoBit.cpp`:

```
void set_classy_parameters_DE_model(pybind11::dict &result)
{

    using namespace Pipes::set_classy_parameters_DE_model;

    // make sure that nothing is retained from the previous
    // parameter combination
    result.clear();

    // add model-specific CLASS settings to input dictionary:
    // set energy density of cosmological constant to 0 ..
    // .. and let CLASS infer the energy density of the
    // perfect fluid
    result["Omega_Lambda"] = 0;
    result["Omega_fld"] = -1;

    // set model parameters for parametrised time evolution of w
    result["w0_fld"] = *Param["w0_fld"];
    result["wa_fld"] = *Param["wa_fld"];
}
```

3) Give the function that collects all input parameters for CLASS **access to the new input parameters** which were set in step 2). One can achieve this by adding a `MODEL_CONDITIONAL_DEPENDENCY` to the function *set_classy_baseline_params*. This requires the addition of the line

```
MODEL_CONDITIONAL_DEPENDENCY(classy_parameters_DE_model,
                             pybind11::dict, DE_model)
```

to the declaration of *set_classy_baseline_params* in `CosmoBit_rollcall.hpp`.

4) **Add the new input parameters** to the CLASS input dictionary composed in the function *set_classy_baseline_params*. The user can acomplish this by adding the following lines to the source code of the function in `CosmoBit.cpp`:

```
// if the model is in use ..
if (ModelInUse("DE_model"))
{
  // .. add additional entries to dict passed to CLASS
  // the dictionary result contains all previously added
  // parameter values.
  // (input consistency checks only executed in first run)
  merge_pybind_dicts(result,*Dep::classy_parameters_DE_model,
```

```
                                first_run);
}
```

Patches Applied to CLASS

In the first release of CosmoBit, there are two scenarios in which we need to apply patches to CLASS: whenever working with *i)* inflationary models for which an external source provides the primordial power spectrum, or *ii)* annihilating or decaying DM models injecting energy into the CMB. The former requires us to pass the primordial power spectrum, the latter to pass annihilation coefficients in form of arrays to CLASS. In both of these scenarios we pass pointers to the respective arrays to CLASS. The patches that we apply to accomplish that are:

- **Additional primordial spectrum type** `pointer_to_Pk`. In the standard version of CLASS, the user can choose different options for how to compute the primordial power spectrum. This is done by setting the input parameter `P_k_ini type` to the desired option (e.g. `analytic_Pk`, `inflation_H`, ..). We add the additional option `pointer_to_Pk`. If this option is chosen, CLASS skips the computation of the primordial power spectrum.[9] Instead, three arrays are passed to CLASS with the new options `k_array`, `pks_array`, and `pkt_array`, holding values of the wavenumber k, the amplitude of scalar modes, and tensor modes respectively. Additionally, the length of the arrays needs to be passed through the new input parameter `lnk_size`.

  This patch is needed whenever the user scans LCDM_no_primordial in combination with any Inflation_.. model.

- **Additional energy injection coefficient types** `pointer_to_fz_channel` **and** `pointer_to_fz_eff`. ExoCLASS provides different options for the calculation of the efficiency functions of energy injection into the CMB by decay or annihilation of exotic components. The user can choose the calculation mode with the input parameter `energy_deposition_function`. We add two additional options for this parameter: `pointer_to_fz_channel` and `pointer_to_fz_eff`. If a decaying or annihilating DM model depositing energy into the CMB is scanned, CosmoBit automatically passes one of these options to ExoCLASS. Which option CosmoBit chooses depends

[9] This calculation is done in the function *primordial_init* in the CLASS source file `source/primordial.c`.

on the operation mode of DarkAges.[10] In any case, the relevant energy efficiency functions are passed to ExoCLASS and stored internally.

This patch only applies to ExoCLASS and is needed whenever the user scans a decaying or annihilating DM model (DecayingDM_general or AnnihilatingDM_general) in combination with a cosmological model.

- **Passing arrays to CLASS**. Both of the additional CLASS input options described above make it necessary to pass arrays computed within GAMBIT to CLASS. As we use the Python wrapper for the interface to CLASS, every entry that is included in the Python input dictionary will be converted to a string with a pre-defined maximum length before being passed to (the C code) CLASS. To avoid problems associated with potentially exceeding this limit we pass pointers directly to CLASS. To achieve this, we convert the memory address of the array's first element to a string, pass it to CLASS through the Python dictionary, and then convert the string back to a memory address within CLASS. We copy the entries of the passed arrays to the entries of the respective arrays within CLASS. The creation of these hard copies is necessary to avoid interfering with any of the code's internal memory management and to avoid double free corruptions.

  This patch is needed whenever one of the two functionalities mentioned above is in use.

Technical Details

The Python wrapper for CLASS is implemented in the Python package classy. This package provides a Python class *named* `Class`. It is common, to instantiate the object as `cosmo` in CLASS examples; I refer to this object as `cosmo` for clarity in the following section. The object `cosmo` provides all necessary functions to run CLASS. For communication between C++ and Python within GAMBIT, we use pybind11.[11]

The first important part of the CLASS the interface to GAMBIT is that CosmoBit must create a CLASS input dictionary reflecting all model- and likelihood-dependent choices. To achieve this, we implement several different capabilities, each gathering the relevant input parameters for different models and storing them in Python dictionaries. These dictionaries map the parameter names in CLASS syntax to the corresponding input values. The capabilities created to set CLASS input parameters are:

[10] Refer to Sec. 6.4.4 for an explanation of the two different operation modes.

[11] `https://github.com/pybind/pybind11`

- *classy_NuMasses_Nur_input* to set parameters related to neutrinos and ultra-relativistic species,
- *classy_primordial_parameters* to set the primordial helium abundance abundance and parameters related to the primordial power spectrum,
- *classy_baseline_params* for model parameters of LCDM_no_primodial, and
- *classy_PlanckLike_input* for the correct CLASS settings if any of the Planck likelihoods are in use.

CosmoBit composes the final input dictionary for CLASS, `input_dict`, in the function providing the capability *classy_final_input*. We store the `input_dict` as a member of the type `Classy_input` which provides some useful methods for convenience. See Table 6.5 for details on this type.

The second important part is the classy frontend. Here, the `static` object `cosmo` provides all necessary functions to steer CLASS: setting the input parameters (`cosmo.set(input_dict)`), running CLASS (`cosmo.compute()`), cleaning the structures (`cosmo.struct_cleanup()`), and requesting computed quantities (e.g. `cosmo.lensed_cl()` for the lensed CMB spectra). We implemented backend convenience functions to return relevant CLASS outputs. Besides the CMB spectra, these convenience functions return, e.g. the angular and luminosity distances to a given redshift, or the linear growth rate.

The CLASS call is initiated in the backend initialisation function. This initialisation function has a dependency on the capability *classy_final_input*, through which we gain access to the input dictionary created within CosmoBit. Note that unless CLASS is called for the first time during a scan, CosmoBit compares the current values of the input parameters to the ones used in the previous CLASS call. If the contained parameter values are equal, CosmoBit skips the CLASS run. To fully exploit the time one can save through this feature, the scanner in use must support to sample 'fast' (usually nuisance) parameters before changing 'slow' cosmological parameters.

6.4.4 Interface to DarkAges

To compute the efficiency of energy injection into the CMB, we provide an interface to DarkAges. Refer to Ref. [484] for a detailed description of the code.

In the regular usage of ExoCLASS, DarkAges 1.0 is called internally at runtime. To allow for more flexibility and modularity, we employ DarkAges as a standalone code and use the results as external inputs for ExoCLASS. The code calculates the efficiency functions $f_c(z, x_e)$ (Eq. 6.2) by means of the convolution of the particle spectra of injected photons, electrons, and positrons.

Type	Name	Purpose
`Classy_Input`		
pyDict	`input_dict`	`private`, dictionary filled with all inputs to be passed to CLASS
pyDict	*get_input_dict* ( )	return `input_dict`
string	*print_entries_to_logger* ( )	return string with all entries of `input_dict` to be sent to logger
string	*add_dict* (pyDict `add_dict`)	add all elements from `add_dict` to `input_dict`, return string with duplicated keys for cross-checks
void	*clear* ( )	clear all entries from `input_dict`
bool	*has_key* (string `key`)	check if `key` is already contained in `input_dict`
void	*add_entry* (string `key`, string `val`)	add `key` and `val` pair to `input_dict`, overloaded with types `double`, `int` and `vector<double>` for `val`
void	*merge_input_dict* (pyDict `extra_dict`)	merge entries from `extra_dict` into `input_dict`

Table 6.5: Members and attributes of the type `Classy_Input`. The main purpose is to fill the member `input_dict` with all settings and parameters that need to be passed to CLASS. An instance of this type is created in CosmoBit and the entries from different (model-dependent) functions can add and merge values into it. This is done by using the function *add_entry* or *merge_input_dict*. Note that the latter function contains CLASS specific rules about how to treat duplicated entries.

In version 1.0 of DarkAges, the table of channel-dependent efficiency functions $f_c(z)$ is derived by using the transfer functions of Slatyer *et al.* [502]. In this calculation, the redshift-dependent ionisation fraction x_e is assumed to evolve as in the standard ΛCDM case without additional energy injection. This assumption can lead to an underestimation of the effect on the IGM temperature in cases where the modifications in x_e deviate from the canonical value [503]. One can circumvent this problem by assuming that the efficiency function factorises as

$$f_c(z, x_e) = \chi_c(x_e) \cdot f_{\text{eff}}(z)\,, \tag{6.4}$$

where $\chi_c(x_e)$ is the fraction of energy deposited into each of the deposition channels as a function of the ionisation fraction [502]. Release 1.2 of Dark-

Ages contains this improved factorised approach. This version is available in CosmoBit such that the user can choose between calculating $f_c(z, x_e)$ from the transfer functions or with the factorised approach.

DarkAges is written in Python, and the interfaced version works with Python 2 and 3. In the following, I provide a practical usage guide.

Practical Usage

The interface to DarkAges is very compact and requires no additional YAML input. The dependency resolver will automatically enable the use of DarkAges whenever a model injecting energy into the CMB is in use. The energy injection efficiency needed by ExoCLASS for the calculation of the CMB spectrum is calculated automatically. By default, DarkAges will calculate the table of energy injection efficiencies separated into the five deposition channels considered in Ref. [502]. If the user wishes to use the effective efficiency function $f_{\text{eff}}(z)$ instead, the input option `f_eff_mode` can be set accordingly in the `Rules` section of the YAML-file.

The available options are:

```
Rules:

  # (optional): additional options for DarkAges
  # all set to their respective default value
  - capability: DarkAges_1_2_0_init
    options:
      f_eff_mode : false # true to calculate f_eff(z) rather then f_c(z)
      print_table : false # print the table to stdout. Useful for debugging
      z_max : 1.e7 # Continue the efficiency table up to given redshift
```

6.4.5 Interface to MontePython

GAMBIT has its own dedicated scanning module, ScannerBit. Hence, the CosmoBit interface to MontePython serves to make use of MontePython's extensive bank of likelihoods. We do not use any of the sampling machinery MontePython offers. The interface has the sole purpose of enabling the user to use public or private MontePython likelihoods out-of-the-box when performing parameter scans with GAMBIT.

We designed the interface such that GAMBIT loads all MontePython likelihoods at runtime. This means that if the user implements a new MontePython likelihood, there is no need to re-compile or add any new code to GAMBIT. I will first provide a practical usage guide and comment on more technical details after that.

Practical Usage

Like all GAMBIT likelihoods, the MontePythonLike likelihoods to be used for a scan must be specified via the YAML file. In the current implementation of the interface, all MontePython log-likelihoods are summed up in the capability *MP_combined_LogLike* and treated as one contribution to the total likelihood. To use MontePython likelihoods, the `ObsLikes` section in the YAML file must contain the entries:

```
ObsLikes:

  # Use MontePython likelihoods in scan
  - capability: MP_combined_LogLike
    purpose: LogLike

  # (optional, but recommended): print a breakdown of each likelihood
  # component in the above total lnL to the output file
  - purpose: Observable
    capability: MP_LogLikes
    type: map_str_dbl
```

The capability *MP_Observables* provides the possibility to compute and store likelihood values that GAMBIT does not add to the total likelihood (which drives the parameter sampling). This feature can, for example, be useful to test how the scanned model performs when compared to a dataset that is not independent of a dataset already used for driving the parameter scan. The specification for this `ObsLikes` entry is similar to the likelihoods:

```
ObsLikes:

  # Add these lines to compute MontePython likelihoods
  # which are not to be added to the total LogLike
  # => these do not drive the scan
  - purpose: Observable
    capability: MP_Observables
    type: map_str_dbl
```

The user must specify which exact likelihoods shall be used in the `Rules` section:

```
Rules:

  # Choose which MontePython likelihoods are computed
  - capability: MP_experiment_names
    function: set_MP_experiment_names
    options:
      # Likelihoods that drive the scan
      Likelihoods:
        Pantheon: default
        bao_smallz_2014: default
```

```
    # (optional): compute likelihoods that do not contribute to lnL;
    # they will only be printed
    Observables:
      hst: path/to/custom/settings/for/hst_likelihood.data

# Add likelihood-specific input arguments to CLASS input
- capability: get_classyInput
  function: init_classyInput_with_MPLike
  module: CosmoBit
```

The value *default* for the chosen likelihoods means that the MontePython default `.data` settings file is used.[12] If the user wishes to use non-standard settings, they can specify a path relative to the GAMBIT installation directory to a custom settings file for the respective likelihood.

In the second setting, choosing the function *init_classyInput_with_MPLike* for the capability *get_classyInput* is essential for every run in which MontePython likelihoods are used in conjunction with CLASS. It ensures that GAMBIT adds likelihood-dependent input settings to the input arguments for CLASS. Hence, the user does not need to specify which spectra or quantities must be computed by CLASS for the likelihood calculations.

The user must ensure that all nuisance parameters needed for a specific likelihood are scanned over as well. These nuisance parameters are included by including pre-defined models with the corresponding parameters in the scan. The naming convention is such that the nuisance parameters used by example_like are defined in the model cosmo_nuisance_example_like. To increase user friendliness, GAMBIT automatically checks if this is the case and exits with an error message indicating the missing parameter and which model needs to be included. Similarly, if the user requests a likelihood that does not exist in the MontePython installation folder at run time, CosmoBit will exit with an error and print all currently available likelihoods to the terminal.

Technical Details

To maintain the modularity of GAMBIT, MontePython is neither allowed to control the parameter sampling nor to execute a call to CLASS internally. All information is centrally stored and administrated by CosmoBit. To achieve this, we have modified the `Likelihood` and `Data` classes implemented in MontePython. When executing the download and build step for MontePython, GAMBIT copies the alternative implementations to the installation directory

[12] The default settings are saved within the folder `Backends/installed/montepythonlike/3.3.0/montepython/likelihoods/<likelihood_name>/<likelihood_name>.data`.

and applies a patch. This patch replaces the import of the original MontePython `Likelihood` class by our alternative definition. Note that a result of this patching procedure is that the specific installation of MontePython in the GAMBIT backends directory cannot be used as a standalone program.

Let me briefly explain the purpose of the two MontePython objects that we use within CosmoBit:

- `Data` class. In its original version this class centrally manages various information, e.g. related to parameter sampling, MontePython run options, and the likelihood calculations. Out of these, we only need the latter feature within CosmoBit. The initialised `Data` object is passed to every `Likelihood` initialisation function and collects all likelihood-dependent input parameters for CLASS. Examples of such likelihood-dependent inputs are the calculation of the matter power spectrum at a specific redshift or a minimum number of computed multipoles in the CMB spectra. MontePython stores these input options for CLASS within the Python dictionary `cosmo_arguments`, which is a member of the `Data` object. Further, the `Data` object contains a dictionary storing all current values of cosmological nuisance parameters (`mcmc_parameters`).

- `Likelihood` class. For each MontePython likelihood a derived class that inherits from the `Likelihood` class is implemented. The name of this class matches the likelihood name. To be more explicit: for the calculation of the likelihood *boss_bao* the class `boss_bao` is implemented. Each of these `Likelihood` classes has an initialisation function and a function called *loglike()*. Both of these take an instance of the `Data` object as an input argument. In the initialisation step, potential data files are read in, and if the calculation of the likelihood requires any specific CLASS settings, these are added to the `cosmo_arguments` dictionary of the `Data` object. The *loglike()* function computes and returns the logarithm of the likelihood, *LogLike*. In addition to the `Data` object, the function *loglike()* takes the results of a CLASS run stored in the global `cosmo` Python object as an input argument. The `cosmo` object provides access to all theoretically-predicted observables computed by CLASS.

The patch for these two objects for the use within GAMBIT removes all dependencies on MontePython command-line arguments, input and output streams, as well as calls to CLASS. These MontePython features are not needed as all input settings, writing of output files and calls to other backends are managed by GAMBIT.

The individual steps executed in GAMBIT when MontePython likelihoods are used are:

1) **Set likelihood names**, `capability` *MP_experiment_names*.
`Function` *set_MP_experiment_names*, `type: map_str_map_str_str`. Create a map from the YAML file input mapping all likelihood names in use to *i)* their `purpose`, *LogLike* to drive scan or *Observable* to just compute and report the value, and *ii)* to the path to the `.data` file containing the MontePython settings for the likelihoods in use. This step is only executed once, before the first parameter point is calculated.

2) **Set nuisance parameter values**, `capability` *parameter_dict_for_MPLike*.
`Function` *pass_empty_parameter_dict_for_MPLike*, `type: pyDict`. If none of the active likelihoods requires the use of extra nuisance parameters, the dependency resolver will automatically choose this function to satisfy the capability. It simply passes an empty dictionary.
`Function` *set_parameter_dict_for_MPLike*, `type: pyDict`. Save the current value of all nuisance parameters to the dictionary `mcmc_parameters` managed by the `Data` object. The function has access to all nuisance parameters through the `ALLOW_MODELS` macro in the rollcall header definition.
[*Note for developers:* to implement a new nuisance parameter model for a MontePython likelihood, it must be added to the list of allowed models for this capability in the header. Location: `CosmoBit.cpp`, header definition in `CosmoBit_rollcall.hpp`.]

3) **Get CLASS input settings**, `capability` *cosmo_args_from_MPLike*.
`Function` *init_cosmo_args_from_MPLike*, `type: pyDict`. Get all arguments for a CLASS run required by the active likelihoods in the form of a Python dictionary. We do this by initialising the `Data` object and all requested `Likelihood` objects by using the list of all active likelihood names obtained in step 1). After all likelihoods are initialised, the dictionary *cosmo_arguments* of the `Data` object contains all the necessary run options. This step is only executed once, before the first likelihood calculation of the first parameter point.

4) **Pass settings to CLASS**, `capability` *classy_final_input*.
`Function` *set_classy_input_with_MPLike*, `type: pyDict`. Add all likelihood-specific input arguments to the input dictionary passed to CLASS. The likelihood-specific input arguments obtained in step 3) are merged into the input dictionary containing all other CLASS input parameters.

5) **Calculate individual likelihoods**, `capability` *calc_MP_LogLikes*.
`Function` *calc_MP_LogLikes*, `type: MPLike_result_container`. During the first run, GAMBIT creates a `static const` object of the custom type `MPLike_data_container`. We define this type to store the initialised `Data` object and a map from likelihood name to respective `Likelihood` object,

see Table 6.6 for more details. The `Data` and `Likelihood` objects are only initialised once and saved during the entire GAMBIT run. CosmoBit then iterates over the requested MontePython likelihoods and queries the *LogLike* value for each likelihood separately. We obtain these results by a call to the `BE_CONVINIENCE_FUNCTION` *get_MP_loglike* (step 6). The individual likelihood values are added to a map from likelihood name to the respective calculated *LogLike* value. This map is stored within the type `MPLike_result_container`.

6) **MontePython likelihood calculation**, `capability` *calc_MP_LogLikes*. `BE_CONVINIENCE_FUNCTION double` *get_MP_LogLike* `(MPLike_data_container, ↪pyObj &, str)`. The three arguments of the function are an instance of the object `MPLike_data_container`, the `cosmo` instance of CLASS's Python object, and the likelihood name `like_name`. The `Data` and the `Likelihood` object can be extracted from the `MPLike_data_container` with the help of `like_name`. We can then calculate the likelihood in one line:[13]

```
double LogLike = <likelihood_object>.loglkl(cosmo, mplike.data);
```

7) **Calculate combined likelihood**, `capability` *MP_Combined_LogLike*. `Function` *calc_MP_combined_LogLike*, `type: double`. Finally, all individual *LogLike* values contained in the `like_name`-to-*LogLike* map constructed in step 5) are added up. This sum is the combined likelihood contribution from all MontePython likelihoods included in the scan.

6.4.6 Interface to MultiModeCode

The shape of the primordial power spectrum parametrised by A_s and n_s, and typically adopted with ΛCDM is purely phenomenological. In CosmoBit, we allow the user to either scan phenomenological parameters of the parametrised primordial power spectrum, or an inflationary sector given a concrete inflation model. When considering an inflationary model, it is not meaningful to scan over the parameters A_s and n_s. Therefore, any scans of an inflationary scenario must be performed in combination with the GAMBIT model LCDM_no_primordial.[14] See Sec. 6.2 for details on the cosmological and inflationary models within GAMBIT.

To compute the primordial power spectra, CosmoBit provides an interface to the inflationary solver MultiModeCode [483]. It is a Fortran 95/2000 package capable of solving equations of motion of the background, and first-order

[13] For the sake of clarity I exclude some additional necessary pybind11-related syntax.

[14] Alternatively, the user can scan LCDM_theta_no_primordial.

Type	Name	Purpose
`MPLike_data_container`		
`pyObj`	`data`	Python object storing an instance of the MontePython `Data` object
`map_str_pyobj`	`likelihoods`	a map from likelihood name to the initialised MontePython `Likelihood` object
`MPLike_result_container`		
`map_str_dbl`	`logLike_results`	`private` map from likelihood name to *LogLike* value. Contains all likelihoods driving the scan
`map_str_dbl`	`obs_results`	`private` map from likelihood name to *LogLike* value. Contains all likelihoods treated as observables, these are not added to the total *LogLike* driving the scan
`void`	*add_logLike* (`string like`, `double logLike`)	add key `like` with value `logLike` to `logLike_results` map
`void`	*add_obs* (`string obs`, `double logLike`)	add key `obs` with value `logLike` to `obs_results` map
`map_str_dbl`	*get_logLike_results* ( )	`return` member `logLike_results`
`map_str_dbl`	*get_obs_results* ( )	`return` member `obs_results`

Table 6.6: Members and attributes of the types `MPLike_data_container` and `MPLike_result_container`. The former is initialised as `const static` and stores the MontePython `Data` object and a map from likelihood name to the respective MontePython `Likelihood` objects during the entire GAMBIT run. The type `MPLike_result_container` is for storing and accessing the likelihoods and observables computed with MontePython in the form of a map from likelihood/observable name to *LogLike* value.

CosmoBit type	Member variable and description	C++ Type
Primordial_ps	k, wavenumbers k	std::vector<double>
	P_s, scalar power spectrum $P_s(k)$	std::vector<double>
	P_t, tensor power spectrum $P_t(k)$	std::vector<double>
Parametrised_ps	A_s, amplitude of scalar perturbations A_s	double
	n_s, scalar spectral tilt n_s	double
	r, scalar to tensor ratio r	double
	N_pivot, number of e-folds	double

Table 6.7: Table describing the member variables of the classes Primordial_ps and Parametrised_ps. Each variable has a corresponding getter and setter function, get_<variable> and set_<variable>.

perturbations for single and multi-field inflation models with canonical kinetic terms and minimal coupling to gravity. MultiModeCode is an improvement of the single-field inflationary solver ModeCode [482], which is also implemented in CLASS.

Practical Usage

When scanning an inflationary model, the user has the option of returning either the full power spectrum to CosmoBit (to pass to CLASS) or parameters describing the shape of the power spectrum. These are governed by the types Primordial_ps and Parametrised_ps, respectively. The names of the member variables for both power spectrum classes in CosmoBit are detailed in Table 6.7. Given the parametrised form of the power spectrum, CLASS will recompute the full power spectrum internally. Therefore, to avoid computing the power spectrum twice, we recommend passing the full power spectrum to CLASS. Furthermore, passing the full power spectrum contains physics not captured by the parametrised spectrum, such as the running of the spectral index. Hence, if the user wishes to explore the full phenomenology of a given inflationary model — specifically models beyond slow-roll — passing the full power spectrum is advised.

The Primordial_ps type hold vectors of k values with corresponding values of $P(k)$ for scalar and tensor perturbations.[15] The user must set the following

[15]For the single-field inflation models included in this release of CosmoBit, isocurvature modes do not exist. Isocurvature modes can become important in multi-field inflationary scenarios and should be passed to both Primordial_ps and CLASS if considered.

YAML entries to select the full power spectrum:

```
Rules:

  # Pass arrays (k, P(k)) to CLASS
  - capability: classy_primordial_parameters
    function: set_classy_parameters_primordial_ps
```

Alternatively, for the parametrised version of the power spectrum, the appropriate YAML entries are:

```
Rules:

  # Pass A_s, n_s and r to CLASS
  - capability: classy_primordial_parameters
    function: set_classy_parameters_parametrised_ps
```

6.4.7 Interface to plc

The plc backend makes the Planck 2015 and 2018 likelihoods available for use within CosmoBit. Running the command `make plc` in the GAMBIT build directory will download and configure plc 3.0. The commands `make plc_data_3.0` and `make plc_data_2.0` will lead to an automatic download of the Planck 2018 and 2015 data, respectively.

The relevant YAML settings in the to use the likelihoods are:

```
ObsLikes:

  # Choose which Planck likelihoods to use in scan
  # and which function shall be used to satisfy it
  - purpose: LogLike
    capability: Planck_lowl_loglike
    function: function_Planck_lowl_TTEE_2018_loglike

  - purpose: LogLike
    capability: Planck_highl_loglike
    function: function_Planck_highl_TTTTEE_2018_loglike

  - purpose: LogLike
    capability: Planck_lensing_loglike
    function: function_Planck_lensing_2018_loglike
```

The different Planck likelihoods for high and low-ℓ as well as lensing can be fulfilled by different module functions, depending on which exact combination of data the user wants to include. See Table 6.8 for all available options.

Capability	Available Functions Planck_..	Nuisance Parameters
Planck_lowl_loglike	..lowl_TT_2015_loglike	1
	..lowl_TEB_2015_loglike	1
	..lowl_TT_2018_loglike	1
	..lowl_EE_2018_loglike	1
	..lowl_TTEE_2018_loglike	1
Planck_highl_loglike	..highl_TTTEEE_2015_loglike	34
	..highl_TTTEEE_2018_loglike	34
	..highl_TTTEEE_lite_2015_loglike	1
	..highl_TTTEEE_lite_2018_loglike	1
	..highl_TT_2015_loglike	16
	..highl_TT_2018_loglike	16
	..highl_TT_lite_2015_loglike	1
	..highl_TT_lite_2018_loglike	1
Planck_highl_loglike	..lensing_2015_loglike	1
	..lensing_2018_loglike	1
	..lensing_marged_2018_loglike	1

Table 6.8: Overview of capabilities and functions to compute CMB likelihoods published by the Planck collaboration. Likelihoods with TEB in the name include measurements of the CMB E- and/or B-mode polarisations. The lowl likelihoods cover the multipole range $2 \leq \ell \leq 29$, and highl the range $30 \leq \ell \leq 2508$. For details on the 2015 likelihoods, see Ref. [480], for the 2018 likelihoods, see Ref. [481].

6.5 Validation and Results

6.5.1 Validation

To validate our implementation, we reproduce the results obtained and published by the Planck collaboration [10]. The constraints we reproduce are on the ΛCDM *baseline* model arising from different combinations of CMB and BAO scale likelihoods. In the baseline model the six standard parameters of ΛCDM are varied, the CMB temperature today is fixed to 2.7255 K [76], the neutrino mass sum is fixed to 0.06 eV, and one assumes that there is only one massive neutrino species, i.e. $\Sigma\, m_\nu = m_\nu = 0.06$ eV.

The Planck likelihoods we use in the validation analysis are from the temperature anisotropy spectrum, E-mode polarisation, and CMB lensing. The

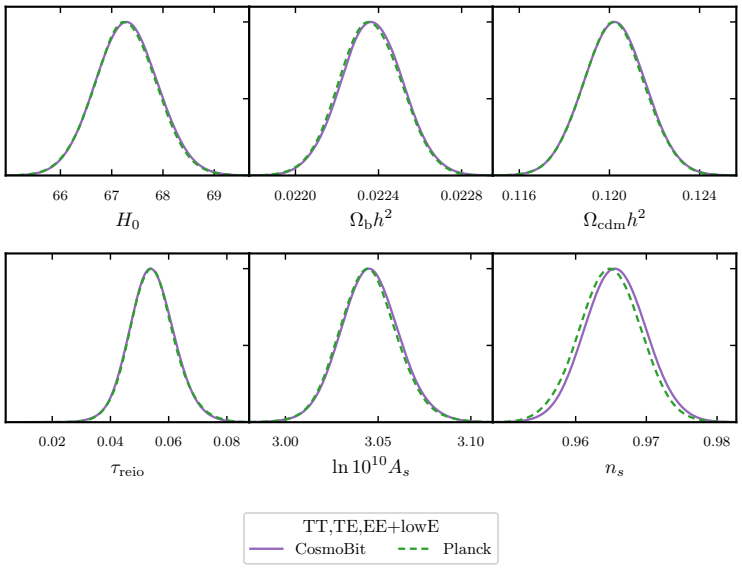

Figure 6.2: Comparison of one-dimensional marginalised constraints on ΛCDM baseline model ($\Sigma m_\nu = 0.06$) as published by the Planck collaboration, Ref. [10, Table 1], and the results obtained with CosmoBit. The datasets included in this analysis are CMB lite TT,TE,EE+lowE likelihoods involving one nuisance parameter.

BAO scale measurements are from the 6dF galaxy survey [69], the SDSS main galaxy sample (MGS) [414] and the BOSS DR12 anisotropic consensus results [417]. These analyses validate our interface to plc used for the CMB likelihood calculations, the interface to CLASS used for the computation of the predicted evolution of cosmological distances and CMB spectra, and to MontePython through the use of the BAO likelihoods.

In Figure 6.2, I show the one-dimensional marginalised posterior distributions for all six model parameters, comparing the results from Planck [10] and CosmoBit for an analysis including CMB temperature and polarisation data. Table 6.9 provides an overview of the resulting constraints on the ΛCDM model parameters for several different likelihood combinations. All results agree well within their 68% error margins.

Parameter	TT+lowE	TT,TE,EE +lowE	TT,TE,EE +lowE+lensing	TT,TE,EE+lowE +lensing+BAO
H_0^{CB}	67.01 ± 0.91	67.39 ± 0.61	67.37 ± 0.54	67.68 ± 0.42
H_0^{Pl}	66.88 ± 0.92	67.27 ± 0.60	67.36 ± 0.54	67.66 ± 0.42
$100\,\omega_{\mathrm{b}}^{\mathrm{CB}}$	2.215 ± 0.021	2.237 ± 0.015	2.238 ± 0.014	2.243 ± 0.014
$100\,\omega_{\mathrm{b}}^{\mathrm{Pl}}$	2.212 ± 0.022	2.236 ± 0.015	2.237 ± 0.015	2.242 ± 0.014
$100\,\omega_{\mathrm{cdm}}^{\mathrm{CB}}$	12.04 ± 0.21	12.02 ± 0.14	12.01 ± 0.12	11.936 ± 0.094
$100\,\omega_{\mathrm{cdm}}^{\mathrm{Pl}}$	12.06 ± 0.21	12.02 ± 0.14	12.00 ± 0.12	11.933 ± 0.091
$100\,\tau_{\mathrm{reio}}^{\mathrm{CB}}$	5.22 ± 0.80	5.43 ± 0.78	5.44 ± 0.75	5.63 ± 0.72
$100\,\tau_{\mathrm{reio}}^{\mathrm{Pl}}$	5.22 ± 0.80	$5.44^{+0.70}_{-0.81}$	5.44 ± 0.73	5.61 ± 0.71
$\ln\left(10^{10}\,A_s\right)^{\mathrm{CB}}$	3.041 ± 0.016	3.046 ± 0.016	3.045 ± 0.014	3.048 ± 0.014
$\ln\left(10^{10}\,A_s\right)^{\mathrm{Pl}}$	3.040 ± 0.016	3.045 ± 0.016	3.044 ± 0.014	3.047 ± 0.014
$100\,n_s^{\mathrm{CB}}$	9.64 ± 0.56	9.66 ± 0.43	9.66 ± 0.41	9.68 ± 0.37
$100\,n_s^{\mathrm{Pl}}$	9.63 ± 0.57	9.65 ± 0.44	9.65 ± 0.42	9.67 ± 0.38

Table 6.9: Validation of CosmoBit results. A comparison of the official Planck results and the results obtained with CosmoBit for the 68% confidence intervals of the six ΛCDM baseline model parameters with fixed $\Sigma\, m_\nu = 0.06$ eV. We show the constraints on the six ΛCDM model parameters obtained with CosmoBit (upper rows, marked with superscript CB) and the corresponding results published by the Planck collaboration [10, Table 2] (lower rows, marked with superscript Pl). The constraints arise from a combination of different CMB likelihoods (column $1-3$) and the combination of CMB and BAO data (column 4). The BAO compilation consists of the measurements of the BAO scale by the 6dF galaxy survey [69], the SDSS main galaxy sample (MGS) [414], and the BOSS DR12 anisotropic consensus results [417].

6.5.2 Results

As a first application, I use CosmoBit to set constraints on the lightest neutrino mass using data from cosmology and particle physics. In addition to the six free parameters of ΛCDM, I also vary the lightest neutrino mass and the two neutrino mass splittings. In CosmoBit this corresponds to a scan including the two models LCDM and StandardModel_mNudiff. I perform two analyses, one assuming a normal neutrino mass hierarchy (NH), and one an inverted hierarchy (IH). The CMB temperature is fixed to the monopole measurement of $T_{\mathrm{CMB}} = 2.72548$ K [76].

The likelihoods I use in this fit are:

- *Neutrino oscillation data.* One-dimensional $\Delta\chi^2$ tables for the normal and inverted mass hierarchy from the NuFit collaboration (release 3.2 [504]). Their results are obtained from fits to data from solar, atmospheric, reactor, and accelerator experiments. Refer to Ref. [504] for the full list of experimental data included, and Ref. [505] for details on the likelihood calculations.

- *Primordial element abundances.* Abundance measurements of deuterium and helium as probes of BBN. I use $Y_{\rm He} = 0.245 \pm 0.003$ for the helium [506] and $\mathrm{D} = (2.527 \pm 0.030) \times 10^{-5}$ for the deuterium abundance [507], where both values are normalised to the hydrogen abundance.

- *CMB spectra.* Planck lite high and low ℓ temperature and polarisation data as well as CMB lensing [481].

- *BAO scale.* Measurements from the 6dF galaxy survey [69], the SDSS main galaxy sample (MGS) [414], the BOSS DR12 anisotropic consensus results [417] and the measurement at redshift $z = 0.73$ from the WiggleZ survey [493]. The two WiggleZ measurements at $z = 0.44$ and $z = 0.60$ are excluded to avoid overlap with the volume probed by the BOSS DR12 sample, covering redshift $z = 0.38$, 0.51 and 0.61.

- *Supernovae Ia.* Pantheon compilation [491] including 1048 SNe Ia.

Table 6.10 shows the prior ranges as used in the scan.

The likelihoods listed above, in combination with the prior choices, lead to the following constraints: the upper bound on the lightest neutrino mass assuming a standard ΛCDM cosmology is $m_{\nu,\,\rm light} < 0.055$ eV at 95% confidence level for a normal mass hierarchy. For an inverted hierarchy, the mass bound is $m_{\nu,\,\rm light} < 0.056$ eV at 95% confidence level. Figure 6.3 shows the one- and two-dimensional marginalised constraints on the Hubble constant H_0 and the neutrino mass parameters.

The bounds presented here are tighter than the ones obtained in a similar analysis by Loureiro *et al.* [508] (referred to as L19 in the following). The authors of L19 also combine neutrino oscillation data from NuFit with cosmological probes from BBN, CMB, BAO and SNe Ia data to obtain an upper bound on the lightest neutrino mass. Their result is $m_{\nu,\,\rm light} < 0.085$ eV ($m_{\nu,\,\rm light} < 0.078$ eV) at 95% confidence level assuming a normal (inverted) mass hierarchy. In their analysis, L19 fixed the neutrino mass splittings to their respective central value from particle physics constraints. As this removes two degrees of freedom in the parameter space, one would naively expect the

Model	Parameter	Range	Prior Type
ΛCDM	H_0	[50, 80]	flat
	$\omega_{\rm b}$	[0.020, 0.024]	flat
	$\omega_{\rm cdm}$	[0.10, 0.15]	flat
	$(10^{10}\, A_s)$	[2.5, 3.5]	flat
	n_s	[0.90, 1.10]	flat
	$\tau_{\rm reio}$	[0.004, 0.20]	flat
ν-masses	$m_{\nu,\,\rm light}$	$[10^{-5}, 10]$	log
	Δm^2_{21}	$[5 \times 10^{-5}, 10 \times 10^{-5}]$	flat
(NH)	$\Delta m^2_{3\ell}$	[0.002,0.003]	flat
(IH)	$\Delta m^2_{3\ell}$	[-0.003,-0.002]	flat
Nuisance	$A_{\rm Planck}$	[0.9,1.1]	flat
	M	[-20, -18]	flat

Table 6.10: Parameter ranges and prior types used in the analysis to obtain an upper bound on the lightest neutrino mass. The ranges for the neutrino mass splitting $\Delta m^2_{3\ell}$ are given assuming a normal mass hierarchy (NH), and an inverted (IH), respectively. The nuisance parameters are the absolute calibration for the Planck 'lite' CMB likelihoods, $A_{\rm Planck}$, and the absolute magnitude of SNe Ia.

results of L19 to be more stringent than ours. However, there are two differences in the choice of data. While I use the same BBN and SNe Ia data as L19 in my analysis, the CMB and BAO datasets differ.

- *CMB spectra.* L19 used the CMB temperature, lensing and polarisation likelihoods from the Planck 2015 data release [480]. I performed the analysis with CosmoBit using likelihoods from the 2018 data release [481], offering more constraining power.

- *BAO data.* In the analysis with CosmoBit, I used the geometrical constraints from BAOs through measurements of the BAO scale at different redshifts. L19 used a re-analysis of the BOSS DR12 data leading to constraints on the angular power spectrum of galaxy number counts (GNCs) in 13 different redshift bins [509]. In contrast to the geometrical BAO probes, the GNC power spectrum carries information about the full shape of the matter power spectrum. However, in the process of the data analysis, several uncertainties need to be modelled, and cuts need to be made. Uncertainties that require modelling are, for example, the galaxy

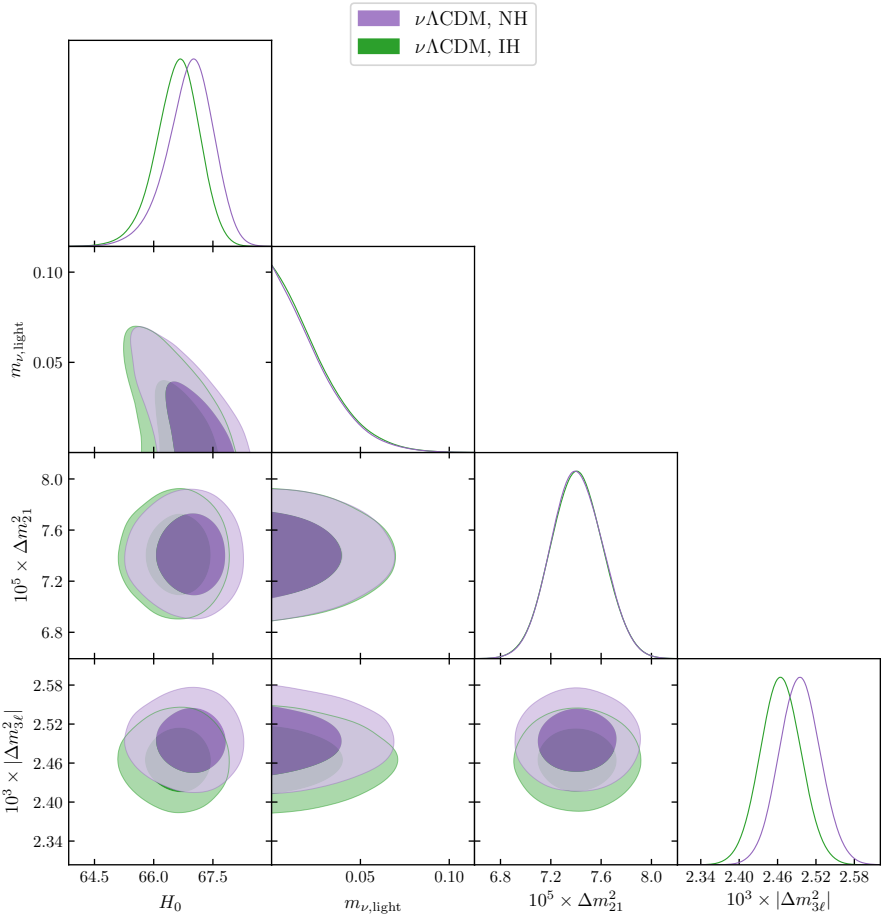

Figure 6.3: Constraints on H_0, the lightest neutrino mass $m_{\nu,\,\mathrm{light}}$, the neutrino mass splitting Δm^2_{21} and the absolute value of $\Delta m^2_{3\ell}$. Results for a normal mass hierarchy are shown in *purple*, and results for an inverted mass hierarchy in *green*. The constraints arise from a parameter scan including likelihoods from neutrino oscillation experiments provided by the NuFit collaboration [505], the abundances of helium and deuterium from BBN, CMB temperature anisotropies, lensing and polarisation data [481], BAO scale measurements [69, 414, 417, 493], and SNe Ia data [491].

bias, redshift error dispersions, or spectroscopic redshift errors. To take uncertainties regarding these factors into account, nuisance parameters must be added. In total, the BAO likelihood from Ref. [509] that L19 used introduced 28 additional nuisance parameters. In addition to that, cuts that remove non-linear scales from the data were made. In principle, non-linear scales provide the most constraining power on neutrino mass parameters. However, the removal of these non-linearities from the data is necessary as the signal in non-linear regimes is dominated by shot noise. Hence, with current data and analysis techniques, the use of BAO scale measurements, as I have done here, adds more constraining power to neutrino mass parameters than the use of data encoding the full shape of the matter power spectrum. See, e.g. Ref [510] for a direct comparison of constraints on the sum of neutrino masses arising from BAO scale measurements and full power spectrum probes.

Owing to these differences in the likelihood choice, the results obtained with CosmoBit provide a more stringent upper bound on the mass of the lightest neutrino than the results from Loureiro *et al.* [508].

Chapter 7

Conclusions

> *'If simple perfect laws uniquely rule the universe, should not pure thought be capable of uncovering this perfect set of laws without having to lean on the crutches of tediously assembled observations? True, the laws to be discovered may be perfect, but the human brain is not. Left on its own, it is prone to stray, as many past examples sadly prove. In fact, we have missed few chances to err until new data freshly gleaned from nature set us right again for the next steps. Thus pillars rather than crutches are the observations on which we base our theories;'*
> (Martin Schwarzschild, 1958 in Structure and Evolution of Stars [511])

From its infancy, modern cosmology has been driven by data. In the last century, the concordance model of cosmology has undergone two groundbreaking changes of direction triggered by experimental data. The first was the observation of galaxy rotation curves, which led to the realisation that the mass of galaxies is dominated by an invisible component called *dark matter* [512–516]. The second game-changing finding was the discovery that the expansion of the Universe is neither slowing down, nor constant, but in fact, accelerating. This discovery was made by combining the measurements of recession velocities of Type Ia supernovae (SNe Ia) with data from the cosmic microwave background (CMB) and baryonic acoustic oscillations (BAOs) [8, 9]. Only the combination of these three independent datasets could provide convincing evidence for the late-time acceleration of the Universe, and lead to yet another addition to the cosmological model: a contribution labelled *dark energy* responsible for driving the accelerated expansion.

The discovery of dark matter and dark energy has led to the formulation of the concordance model of cosmology, ΛCDM. Together these dark components contribute about 95% of the energy content of the Universe but are only included in ΛCDM as effective descriptions lacking a consistent theoreti-

cal origin. Since the formulation of the concordance model we have gathered a wealth of data, not only to probe and constrain the parameter space of ΛCDM but also to test concrete alternative theories that provide possible explanations for dark matter or dark energy. This has allowed us to narrow down such possible alternative models, to slowly get to the bottom of the fundamental theories governing our Universe and the mystery surrounding its dominating dark components.

In this work, I presented two concrete examples of how one can use observables from different underlying physical phenomena, and different epochs of the evolution of the Universe, to probe or even rule out models involving non-standard physics. Paper A shows how a modified gravity model can be ruled out. In Paper B, we investigate the prospects of detecting cosmic superstrings through microlensing of extra-galactic stellar sources. In Chapter 6, I presented the first tool to test models beyond the concordance model of cosmology and theories beyond the Standard Model of particle physics, using cosmological and particle physics data simultaneously.

Firstly, I showed how minimally-coupled covariant Galileons can be invalidated as a viable alternative to GR. Covariant Galileons [21–23] extend GR by introducing an extra scalar degree of freedom. The kinematics of this scalar can give rise to an accelerated late-time expansion of the Universe without the need to include a fine-tuned cosmological constant. Galileon models do not have a GR limit and, therefore, yield different cosmological parameter values compared to ΛCDM when confronted with data. If massive neutrinos are allowed, Galileon cosmologies provide a fit comparable to ΛCDM to CMB and BAO data, and the value inferred for the Hubble constant is consistent with local measurements [24].

Covariant Galileons are divided into cubic, quartic and quintic branches, in increasing complexity. The simplest, cubic, branch introduces in addition to the kinetic term of the scalar a derivative coupling between the scalar field and the metric. Quartic models add a coupling of the scalar to the Ricci scalar and quintic models to the Einstein tensor. The latter two models share the phenomenological property of predicting an anomalous propagation speed of gravitational waves, c_g [297]. Another difference between Galileon models and ΛCDM is given by the non-trivial time evolution of the lensing potential after matter domination. While the potential decreases in ΛCDM on all scales, the behaviour is scale-dependent in covariant Galileon models, allowing for a deepening of the potential at late times on small scales [24].

In Paper A, we utilised the behaviour of the lensing potential in covariant Galileons at late times to test the viability of these models. An observable that directly probes the time evolution of the potential is the amplitude of the integrated Sachs-Wolfe effect (ISW). Using the cross-correlation of the CMB

temperature spectrum and galaxy number counts, the ISW amplitude has been measured to be positive at $\sim 4\,\sigma$ significance [404, 419–421]. This result is in agreement with the prediction from ΛCDM, as the decreasing lensing potential after matter domination gives rise to a positive signal. Hence, models with rising potentials — predicting a negative ISW amplitude — are in strong tension with observations. This is the case for cubic Galileon models. My collaborators and I showed in Paper A that cubic Galileon models that fit CMB and BAO data are in tension with the measurement of the ISW effect at more than $7\,\sigma$. The constraints arising from ISW measurements are not as stringent for quartic and quintic Galileons: their parameter space can only be constrained. Viable regions remain that fit ISW as well as CMB and BAO measurements.

Quartic and quintic Galileon models share the phenomenological property of predicting an anomalous propagation speed of gravitational waves, c_g [297]. This deviation of the propagation speed of gravitational waves (GWs) disqualifies the models as cosmologically viable [308, 425–430, 517, 518]. The tight constraints on the measurement of c_g from a neutron star merger and its associated electromagnetic counterpart [422–424] make the theories inconsistent with observations. Hence, all three branches of the minimally-coupled covariant Galileon can be considered ruled out.

Secondly, I discussed the results obtained in Paper B. In this study, my collaborators and I assessed the prospects of the detection of cosmic superstrings (CSSs) by the observation of extragalactic point-like sources. CSSs are the theoretical one-dimensional constituents of superstring theories stretched out to galactic scales. These objects leave a distinct microlensing signature when crossing the line of sight between an observer and a point-like source: as long as all three are aligned, the observed flux is an exact factor of two larger than the unlensed flux. The increase and decrease at the beginning and end of the alignment happen instantaneously, and not gradually as with Newtonian lenses. No other known astrophysical object produces a microlensing signal similar to the immediate factor-of-two enhancement caused by a CSS acting as a lens. The detection of such a signal, or a lack thereof, can, therefore, be used to probe the existence and parameter space of CSSs.

In Paper B, we estimated the expected detection rate of microlensing events by CSSs when observing two different types of targets: *i)* stars in Andromeda, and *ii)* distant SNe Ia. The allowed energy density of CSSs can be constrained by the remaining parameter space that CMB measurements leave for the presence of additional energy contents in the early Universe. In general, CSSs are expected to cluster with DM but are also present in the intergalactic medium (IGM) with lower number densities. To maximise the chances of detection, one should design searches to target sources where the number of CSSs along

the line of sight is as high as possible. We try to achieve this by

i) increasing the part of the line of sight that passes through dense, galactic halos. This applies to the observation of extragalactic stars, as the line of sight passes through the Milky Way and the halo of the host galaxy.

ii) increasing the absolute length of the line of sight. We aim to achieve this by considering SNe Ia, which we can observe at distances of order 1000 Mpc.

One result of our analysis is that existing observations of extragalactic stars or SNe Ia catalogues cannot constrain the parameter space of CSSs. In the case of *i)* extragalactic stars, the timescales of the ML event are expected to be much shorter ($\lesssim \mathcal{O}(1\,\mathrm{s})$) than the exposure times of typical surveys ($\gtrsim \mathcal{O}(10\,\mathrm{s})$). This mismatch of timescales leads to a dilution of the enhanced signal. We estimated the number of expected detections for a survey with a shorter exposure time, which increases the sensitivity for the detection of a microlensing event by a CSS. We assume observation windows of 1 s separated by 0.01 s. If observations with such a survey are made for two hours per night over the course of a year, the observation of one million stars will probe string tensions in the CSS tension range $10^{-13.5} < G\mu/c^2 < 10^{11.5}$. When considering *ii)* standard strategies for the observation of SNe Ia, the timescales of the microlensing events and the survey strategy match. However, the statistics of current and future datasets are not high enough. Sample sizes of $10^7 - 10^8$ would be needed to probe string tensions in the range $10^{-12} \lesssim G\mu/c^2 \lesssim 10^{-6}$. These large sample sizes are not expected to be reached with future facilities like the LSST [519].

I have shown examples of how one can use cosmological and astrophysical to test signatures of non-standard physics phenomena. However, there is still a variety of different models of dark energy [171–177], dark matter and/or physics beyond the Standard Model (BSM) [2, 520–524], that has not been confronted with all available data yet, or can only be constrained by them. In the near future we will gain access to new cosmological data from, e.g. upcoming surveys like DESI, WFIRST, Euclid, SKA or the LSST [519, 525–528], future GW detectors (e.g. IndIGO, KAGRA, LISA [216, 529, 530]), or improved measurements of the CMB [531–534]. Additionally, particle physics experiments also offer a source of information relevant for cosmology: direct [e.g. 535–539] and indirect [e.g. 540–545] searches for DM, missing energy searches at particle colliders [e.g. 546–548], and laboratory measurements of neutrino masses and their properties [e.g. 218, 398, 549–556].

Many non-standard particle physics phenomena probed in laboratory and indirect searches also leave signatures in cosmological observables. For example, non-standard neutrino self-interactions during inflation can affect the

shape of the primordial power spectrum. Another example is the existence of light right-handed neutrinos, which can be tested with probes from Big Bang Nucleosynthesis (BBN) and the CMB, as they would manifest as additional ultra-relativistic species in the early Universe. A third example that is relevant in cosmology and particle physics is the set of models of dark matter particles that decay or annihilate in the early Universe. If these decays/annihilations take place during the epoch of BBN or recombination, they provide an additional source of energy and can leave imprints in today's observables of light element abundances and the CMB. These links between cosmology and particle physics show that tests of non-standard physical phenomena benefit from the combination of probes from both fields.

In Part II of this thesis, I presented the first tool that allows one to test a variety of non-standard physics scenarios against likelihoods from cosmology, astrophysics, and particle physics simultaneously. We achieved this by developing CosmoBit: a module to compute cosmological observables and likelihoods within the framework of the Global and Modular Beyond-the-Standard-Model Inference Tool (GAMBIT). GAMBIT is a tool that provides different scanning algorithms to perform parameter inference and model comparison for a wide range of BSM models. The different modules of GAMBIT offer access to observables and likelihoods from different fields of physics: while CosmoBit is responsible for cosmology-related calculations, DarkBit [450] computes observables and likelihoods relevant for dark matter searches, NeutrinoBit for neutrino experiments [451], ColliderBit [449] for collider searches, and FlavBit [448] for flavour experiments. PrecisionBit, SpecBit, and DecayBit [447] serve to provide predictions for precision observables, spectra & branching fractions, and decay widths, respectively.

The module CosmoBit adds several groups of new models and likelihoods to the framework of GAMBIT. Besides the addition of the standard ΛCDM model, the user can also test several extensions thereof:

- inflation models predicting the shape of primordial curvature and density fluctuations,
- neutrino mass models consistent with results from neutrino oscillation measurements,
- models that include additional energy content in the form of radiation in the early Universe, and
- annihilating and decaying dark matter models.

These modifications can leave imprints on cosmological observables from different epochs of the Universe. The cosmological likelihoods provided by CosmoBit are

- probes of the phase of BBN, ~ 3 minutes after the Big Bang, through measurements of light element abundances,
- probes of the epoch of recombination, $\sim 380,000$ years after the Big Bang, through measurements of anisotropies in the CMB, and
- late-time probes from observations of for example galaxy clusters, or recession velocities of SNe Ia.

The computation of cosmological observables and likelihoods are not directly implemented in CosmoBit. To avoid replicating existing code, and to minimise the possibility of errors, we make use of well-tested and established external libraries. We use CLASS [33, 226] for the computation of cosmological observables like the CMB spectra, AlterBBN [467, 468] to calculate the prediction for primordial light element abundances, and plc [480, 481] for the computation of CMB likelihoods using data from the Planck satellite. Additionally, we provide an interface to MontePython [471, 472] which gives access to an extensive database of cosmological likelihoods. These likelihoods include weak lensing probes [122, 494, 557], galaxy clustering analyses [495, 497], and measurements of the BAO scale [71, 417, 493, 558, 559].

As the first application of CosmoBit, I set constraints on the mass of the lightest neutrino using cosmological data and data from neutrino oscillation experiments. In this analysis, I use the neutrino oscillation likelihoods from the NuFit collaboration [504, 505]. The included cosmological likelihoods are probes from abundance measurements of helium and deuterium, CMB temperature, lensing and polarisation data from Planck 2018 [481], SNe Ia data from the Pantheon compilation [491], and measurements of the BAO scale and the growth of structure [417, 497]. Assuming a normal mass hierarchy, the result is $m_{\nu,\,\text{light}} < 0.055$ eV at 95% confidence level. For an inverted mass hierarchy, I obtain $m_{\nu,\,\text{light}} < 0.056$ eV at 95% confidence level.

Beyond the constraint on neutrino masses, CosmoBit offers a lot of exciting applications. Non-standard neutrino self-interactions not only leave signatures in laboratory probes [e.g. 218, 549–556], but also on the primordial power spectrum [161], the formation of light elements during BBN, the CMB, and the temperature of the cosmic neutrino background today [140, 143]. By combining likelihoods made available through CosmoBit and NeutrinoBit [451], one can perform a joint analysis of these constraints. Similarly, the user can probe the parameter space of axion-like particles (ALPs). Depending on the lifetime and production mechanism, ALPs can have impacts on cosmological and astrophysical probes: they can inject energy during BBN, affecting the formation of light elements, or during recombination, leaving imprints on the CMB. From an astrophysical perspective, ALPs can cause photon bursts in SNe explosions, alter the transparency of the IGM, and the course of stellar evolution. These

astrophysical likelihoods are available in DarkBit [450, 460] and can easily be combined in an analysis with the cosmological probes provided by CosmoBit.

In the future, GAMBIT will also support the addition of new models through a Lagrangian level tool, GUM (GAMBIT Universal Models) [560]. This means that the user will be able to add any model to GAMBIT by simply specifying the Lagrangian of the theory. All calculations and code for likelihood evaluations of direct and indirect dark matter experiments, collider searches and energy injection into the CMB will be produced automatically. This will open up the possibility to easily test various dark matter models against data from cosmology and particle physics simultaneously.

Cosmic late-time acceleration and the nature of dark matter remain two of the biggest mysteries in physics. New generations of experiments, designed to shed light on these strange phenomena, will start operating in the near future. These experiments are diverse and probe many different underlying physical phenomena, as well as energy, length and time scales. Some of these experiments hold the potential for a definite direct detection of, e.g. a dark matter particle. Other probes can only tighten error bars to constrain or rule out alternative theories. A measurement of a statistical anomaly in one of these experiments would not be particularly meaningful. However, this can change if different independent experiments, potentially even from various fields of physics, show anomalies in favour of the same theory. Hence, we can only extract the full wealth of information held by available datasets when the problem is approached from a global perspective: through the inclusion of all relevant datasets in parameter estimation and model comparison. Considering only a limited range of experimental data could let us overlook important new features. Hence, in case of a continued lack of any direct detection of non-standard physics, the performance of global fits with the right tools could provide what we have been searching for in recent decades: a guidepost to understanding the dark components of our Universe.

References

[1] L. Bergström, *Nonbaryonic dark matter: Observational evidence and detection methods*, *Rept. Prog. Phys.* **63** (2000) 793, [hep-ph/0002126].

[2] J. Silk et al., *Particle Dark Matter: Observations, Models and Searches*. Cambridge Univ. Press, Cambridge, 2010, 10.1017/CBO9780511770739.

[3] K. Freese, *Review of Observational Evidence for Dark Matter in the Universe and in upcoming searches for Dark Stars*, *EAS Publ. Ser.* **36** (2009) 113–126, [0812.4005].

[4] G. Bertone and D. Hooper, *History of dark matter*, *Rev. Mod. Phys.* **90** (2018) 045002, [1605.04909].

[5] J. de Swart, G. Bertone and J. van Dongen, *How Dark Matter Came to Matter*, *Nature Astron.* **1** (2017) 0059, [1703.00013].

[6] D. Huterer and D. L. Shafer, *Dark energy two decades after: Observables, probes, consistency tests*, *Rept. Prog. Phys.* **81** (2018) 016901, [1709.01091].

[7] P. Brax, *What makes the Universe accelerate? A review on what dark energy could be and how to test it*, *Rept. Prog. Phys.* **81** (2018) 016902.

[8] Supernova Search Team collaboration, A. G. Riess et al., *Observational evidence from supernovae for an accelerating universe and a cosmological constant*, *Astron. J.* **116** (1998) 1009–1038, [astro-ph/9805201].

[9] Supernova Cosmology Project collaboration, S. Perlmutter et al., *Measurements of Omega and Lambda from 42 high redshift supernovae*, *Astrophys. J.* **517** (1999) 565–586, [astro-ph/9812133].

[10] Planck collaboration, N. Aghanim et al., *Planck 2018 results. VI. Cosmological parameters*, 1807.06209.

[11] A. G. Riess et al., *A 2.4% Determination of the Local Value of the Hubble Constant*, *Astrophys. J.* **826** (2016) 56, [1604.01424].

[12] A. G. Riess, S. Casertano, W. Yuan, L. Macri, J. Anderson, J. W. MacKenty et al., *New parallaxes of galactic cepheids from spatially scanning the hubble space telescope : Implications for the hubble constant*, *Astrophys. J.* **855** (2018) 136, [1801.01120].

[13] A. G. Riess et al., *Milky Way Cepheid Standards for Measuring Cosmic Distances and Application to Gaia DR2: Implications for the Hubble Constant*, *Astrophys. J.* **861** (2018) 126, [1804.10655].

[14] S. Suyu et al., *H0licow – i. h0 lenses in cosmograil's wellspring: program overview*, *Mon. Not. Roy. Astron. Soc.* **468** (2017) 2590–2604, [1607.00017].

[15] V. Bonvin et al., *H0licow – v. new cosmograil time delays of he 0435-1223: h_0 to 3.8 per cent precision from strong lensing in a flat Λcdm model*, *Mon. Not. Roy. Astron. Soc.* **465** (2017) 4914–4930, [1607.01790].

[16] A. G. Riess, S. Casertano, W. Yuan, L. M. Macri and D. Scolnic, *Large Magellanic Cloud Cepheid Standards Provide a 1% Foundation for the Determination of the Hubble Constant and Stronger Evidence for Physics beyond ΛCDM*, *Astrophys. J.* **876** (2019) 85, [1903.07603].

[17] Planck collaboration, P. A. R. Ade et al., *Planck 2015 results. XIII. Cosmological parameters*, *Astron. Astrophys.* **594** (2016) A13, [1502.01589].

[18] Super-Kamiokande collaboration, Y. Fukuda et al., *Evidence for oscillation of atmospheric neutrinos*, *Phys. Rev. Lett.* **81** (1998) 1562–1567, [hep-ex/9807003].

[19] SNO collaboration, Q. R. Ahmad et al., *Measurement of the rate of $\nu_e + d \to p + p + e^-$ interactions produced by ^8B solar neutrinos at the Sudbury Neutrino Observatory*, *Phys. Rev. Lett.* **87** (2001) 071301, [nucl-ex/0106015].

[20] SNO collaboration, Q. R. Ahmad et al., *Direct evidence for neutrino flavor transformation from neutral current interactions in the Sudbury Neutrino Observatory*, *Phys. Rev. Lett.* **89** (2002) 011301, [nucl-ex/0204008].

[21] A. Nicolis, R. Rattazzi and E. Trincherini, *The Galileon as a local modification of gravity*, *Phys. Rev.* **D79** (2009) 064036, [0811.2197].

[22] C. Deffayet, S. Deser and G. Esposito-Farese, *Generalized Galileons: All scalar models whose curved background extensions maintain second-order field equations and stress-tensors*, *Phys. Rev.* **D80** (2009) 064015, [0906.1967].

[23] C. Deffayet, G. Esposito-Farese and A. Vikman, *Covariant Galileon*, *Phys. Rev.* **D79** (2009) 084003, [0901.1314].

[24] A. Barreira, B. Li, C. Baugh and S. Pascoli, *The observational status of Galileon gravity after Planck*, *JCAP* **1408** (2014) 059, [1406.0485].

[25] S. Weinberg, *Gravitation and cosmology: principles and applications of the general theory of relativity*, vol. 1. Wiley New York, 1972.

[26] P. J. E. Peebles, *Principles of physical cosmology*. Princeton university press, 1993.

[27] J. A. Peacock, *Cosmological physics*. Cambridge university press, 1999.

[28] S. Dodelson, *Modern cosmology*. Elsevier, 2003.

[29] J. B. Hartle, *Gravity: An introduction to einstein's general relativity*, 2003.

[30] S. M. Carroll, *Spacetime and geometry: An introduction to general relativity*. Addison-Wesley, 2004.

[31] L. Bergström and A. Goobar, *Cosmology and particle astrophysics*. Springer Science & Business Media, 2006.

[32] B. Schutz, *A first course in general relativity*. Cambridge university press, 2009.

[33] J. Lesgourgues, *An Overview of cosmology*, astro-ph/0409426.

[34] L. A. Anchordoqui, *Lectures on astronomy, astrophysics, and cosmology*, 0706.1988.

[35] O. F. Piattella, *Lecture Notes in Cosmology*. UNITEXT for Physics. Springer, Cham, 2018, 10.1007/978-3-319-95570-4.

[36] M. Bartelmann, *Cosmology lecture notes*, . Available at https://heibox.uni-heidelberg.de/f/e1e57faba9a44eb88692/ (accessed March 23, 2020).

[37] E. Papantonopoulos, *The Physics of the Early Universe*. Lecture Notes in Physics. Springer Berlin Heidelberg, 2005.

[38] D. H. Lyth and A. R. Liddle, *The primordial density perturbation: Cosmology, inflation and the origin of structure*. 2009.

[39] D. Gorbunov and V. Rubakov, *Introduction to the Theory of the Early Universe: Hot Big Bang Theory*. World Scientific, 2017.

[40] P. Di Bari, *Cosmology and the Early Universe*. Series in Astronomy and Astrophysics. CRC Press, 2018.

[41] M. Hashimoto, R. Nakamura, E. Thushari and K. Arai, *Big-Bang Nucleosynthesis: Thermonuclear History in the Early Universe*. SpringerBriefs in Physics. Springer Singapore, 2018.

[42] S. Weinberg, *Cosmology*. OUP Oxford, 2008.

[43] G. Steigman, *Primordial alchemy: From the Big Bang to the present universe*, astro-ph/0208186.

[44] J. Garcia-Bellido, *Cosmology and astrophysics*, in *2004 European School of High-Energy Physics, Sant Feliu de Guixols, Spain, 30 May - 12 June 2004*, pp. 267–342, astro-ph/0502139.

[45] K. A. Olive, *Primordial big bang nucleosynthesis*, in *NATO Advanced Study Institute: Summer School on Theoretical and Observational Cosmology*, astro-ph/9901231.

[46] F. Iocco, G. Mangano, G. Miele, O. Pisanti and P. D. Serpico, *Primordial Nucleosynthesis: from precision cosmology to fundamental physics*, *Phys. Rept.* **472** (2009) 1–76, [0809.0631].

[47] L. Husdal, *On Effective Degrees of Freedom in the Early Universe*, *Galaxies* **4** (2016) 78, [1609.04979].

[48] G. Mangano, G. Miele, S. Pastor, T. Pinto, O. Pisanti and P. D. Serpico, *Relic neutrino decoupling including flavor oscillations*, *Nucl. Phys.* **B729** (2005) 221–234, [hep-ph/0506164].

[49] P. F. de Salas and S. Pastor, *Relic neutrino decoupling with flavour oscillations revisited*, *JCAP* **1607** (2016) 051, [1606.06986].

[50] Particle Data Group collaboration, M. Tanabashi, K. Hagiwara, K. Hikasa, K. Nakamura, Y. Sumino, F. Takahashi et al., *Review of particle physics*, *Phys. Rev.* **D98** (2018) 030001.

[51] U. LeVerrier, *Lettre de m. le verrier à m. faye sur la théorie de mercure et sur le mouvement du périhélie de cette planète*, *Comptes rendus hebdomadaires des séances de l'Académie des sciences* **49** (1859) 379–383.

[52] A. Einstein, *Die grundlage der allgemeinen relativitätstheorie (the foundation of the general theory of relativity)*, *Annalen der Physik* **354** (1916) 769–822.

[53] A. Einstein, *Explanation of the perihelion motion of mercury from the general theory of relativity*, *Sitzungsber. Preuss. Akad. Wiss. Berlin (Math. Phys.)* **831** (1915) .

[54] J. Renn, *The genesis of general relativity*, in *The Eleventh Marcel Grossmann Meeting: On Recent Developments in Theoretical and Experimental General Relativity, Gravitation and Relativistic Field Theories (In 3 Volumes)*, pp. 532–542, World Scientific, 2008.

[55] R. A. d'Inverno, *Introducing Einstein's relativity*. Clarendon Press, 1992.

[56] S. D. Majumdar, *A class of exact solutions of einstein's field equations*, *Physical Review* **72** (1947) 390.

[57] D. Kramer, H. Stephani, M. MacCallum and E. Herlt, *Exact solutions of einstein's field equations*, *Berlin* (1980) .

[58] H. Stephani, D. Kramer, M. MacCallum, C. Hoenselaers and E. Herlt, *Exact solutions of Einstein's field equations*. Cambridge University Press, 2009.

[59] M. S. R. Delgaty and K. Lake, *Physical acceptability of isolated, static, spherically symmetric, perfect fluid solutions of Einstein's equations*, *Comput. Phys. Commun.* **115** (1998) 395–415, [gr-qc/9809013].

[60] M. Ishak, L. Chamandy and K. Lake, *Exact solutions with w modes*, *Phys. Rev.* **D64** (2001) 024005, [gr-qc/0007073].

[61] K. Schwarzschild, *On the gravitational field of a sphere of incompressible fluid according to Einstein's theory*, *Sitzungsber. Preuss. Akad. Wiss. Berlin (Math. Phys.)* **1916** (1916) 424–434, [physics/9912033].

[62] R. P. Kerr, *Gravitational field of a spinning mass as an example of algebraically special metrics*, *Phys. Rev. Lett.* **11** (1963) 237–238.

[63] A. Friedmann, *Über die krümmung des raumes*, *Zeitschrift fur Physik* **10** (1922) 377–386.

[64] G. Lemaître, *Expansion of the universe, the expanding universe*, *Mon. Not. Roy. Astron. Soc.* **91** (1931) 490–501.

[65] H. P. Robertson, *Kinematics and world-structure*, *Astrophys. J.* **82** (1935) 284.

[66] A. G. Walker, *On milne's theory of world-structure*, *Proceedings of the London Mathematical Society* **2** (1937) 90–127.

[67] D. W. Hogg, *Distance measures in cosmology*, `astro-ph/9905116`.

[68] S. Cole, W. J. Percival, J. A. Peacock, P. Norberg, C. M. Baugh, C. S. Frenk et al., *The 2df galaxy redshift survey: power-spectrum analysis of the final data set and cosmological implications*, *Mon. Not. Roy. Astron. Soc.* **362** (2005) 505–534, [`astro-ph/0501174`].

[69] F. Beutler, C. Blake, M. Colless, D. H. Jones, L. Staveley-Smith, L. Campbell et al., *The 6df galaxy survey: baryon acoustic oscillations and the local hubble constant*, *Mon. Not. Roy. Astron. Soc.* **416** (2011) 3017–3032, [`1106.3366`].

[70] C. Blake, T. Davis, G. B. Poole, D. Parkinson, S. Brough, M. Colless et al., *The wigglez dark energy survey: testing the cosmological model with baryon acoustic oscillations at z= 0.6*, *Mon. Not. Roy. Astron. Soc.* **415** (2011) 2892–2909, [`1105.2862`].

[71] L. Anderson, E. Aubourg, S. Bailey, D. Bizyaev, M. Blanton, A. S. Bolton et al., *The clustering of galaxies in the sdss-iii baryon oscillation spectroscopic survey: baryon acoustic oscillations in the data release 9 spectroscopic galaxy sample*, *Mon. Not. Roy. Astron. Soc.* **427** (2012) 3435–3467, [`1203.6594`].

[72] D. H. Weinberg, M. J. Mortonson, D. J. Eisenstein, C. Hirata, A. G. Riess and E. Rozo, *Observational probes of cosmic acceleration*, *Physics reports* **530** (2013) 87–255, [`1201.2434`].

[73] J. C. Mather et al., *A Preliminary measurement of the Cosmic Microwave Background spectrum by the Cosmic Background Explorer (COBE) satellite*, *Astrophys. J.* **354** (1990) L37–L40.

[74] J. C. Mather et al., *Measurement of the Cosmic Microwave Background spectrum by the COBE FIRAS instrument*, *Astrophys. J.* **420** (1994) 439–444.

[75] D. J. Fixsen, E. S. Cheng, J. M. Gales, J. C. Mather, R. A. Shafer and E. L. Wright, *The Cosmic Microwave Background spectrum from the full COBE FIRAS data set*, *Astrophys. J.* **473** (1996) 576, [astro-ph/9605054].

[76] D. J. Fixsen, *The Temperature of the Cosmic Microwave Background*, *Astrophys. J.* **707** (2009) 916–920, [0911.1955].

[77] C. L. Bennett et al., *Cosmic temperature fluctuations from two years of COBE differential microwave radiometers observations*, *Astrophys. J.* **436** (1994) 423–442, [astro-ph/9401012].

[78] C. L. Bennett, A. Banday, K. M. Gorski, G. Hinshaw, P. Jackson, P. Keegstra et al., *Four year COBE DMR cosmic microwave background observations: Maps and basic results*, *Astrophys. J.* **464** (1996) L1–L4, [astro-ph/9601067].

[79] POLARBEAR collaboration, P. A. R. Ade et al., *A Measurement of the Cosmic Microwave Background B-Mode Polarization Power Spectrum at Sub-Degree Scales with POLARBEAR*, *Astrophys. J.* **794** (2014) 171, [1403.2369].

[80] M. Kamionkowski and E. D. Kovetz, *The Quest for B Modes from Inflationary Gravitational Waves*, *Ann. Rev. Astron. Astrophys.* **54** (2016) 227–269, [1510.06042].

[81] W. Hu, N. Sugiyama and J. Silk, *The Physics of microwave background anisotropies*, *Nature* **386** (1997) 37–43, [astro-ph/9604166].

[82] W. Hu and S. Dodelson, *Cosmic microwave background anisotropies*, *Ann. Rev. Astron. Astrophys.* **40** (2002) 171–216, [astro-ph/0110414].

[83] D. Wands, O. F. Piattella and L. Casarini, *Physics of the Cosmic Microwave Background Radiation*, *Astrophys. Space Sci. Proc.* **45** (2016) 3–39, [1504.06335].

[84] Topical Conveners: K.N. Abazajian, J.E. Carlstrom, A.T. Lee collaboration, K. N. Abazajian et al., *Neutrino Physics from the Cosmic Microwave Background and Large Scale Structure*, *Astropart. Phys.* **63** (2015) 66–80, [1309.5383].

[85] K. N. Abazajian et al., *Inflation Physics from the Cosmic Microwave Background and Large Scale Structure*, *Astropart. Phys.* **63** (2015) 55–65, [1309.5381].

[86] R. Minkowski, *Spectra of Supernovae*, *PASP* **53** (1941) 224.

[87] J. C. Wheeler and R. Levreault, *The peculiar Type I supernova in NGC 991*, *Astrophys. J.* **294** (1985) L17–L20.

[88] J. H. Elias, K. Matthews, G. Neugebauer and S. E. Persson, *Type I supernovae in the infrared and their use as distance indicators.*, *Astrophys. J.* **296** (1985) 379–389.

[89] P. Schneider, G. Meylan, C. Kochanek, P. Jetzer, P. North and J. Wambsganss, *Gravitational Lensing: Strong, Weak and Micro: Saas-Fee Advanced Course 33*. Saas-Fee Advanced Course. Springer Berlin Heidelberg, 2006.

[90] S. Refsdal, *On the possibility of determining hubble's parameter and the masses of galaxies from the gravitational lens effect*, *Mon. Not. Roy. Astron. Soc.* **128** (1964) 307.

[91] S. Birrer et al., *H0licow – ix. cosmographic analysis of the doubly imaged quasar sdss 1206+4332 and a new measurement of the hubble constant*, *Mon. Not. Roy. Astron. Soc.* **484** (2019) 4726, [1809.01274].

[92] J. Tyson, R. Wenk and F. Valdes, *Detection of systematic gravitational lens galaxy image alignments - Mapping dark matter in galaxy clusters*, *Astrophys. J. Lett.* **349** (1990) L1–L4.

[93] T. G. Brainerd, R. D. Blandford and I. Smail, *Measuring galaxy masses using galaxy - galaxy gravitational lensing*, *Astrophys. J.* **466** (1996) 623, [astro-ph/9503073].

[94] R. K. Sachs and A. M. Wolfe, *Perturbations of a cosmological model and angular variations of the microwave background*, *Astrophys. J.* **147** (1967) 73–90. [Gen. Rel. Grav.39,1929(2007)].

[95] M. J. Rees and D. W. Sciama, *Large scale Density Inhomogeneities in the Universe*, *Nature* **217** (1968) 511–516.

[96] R. G. Crittenden and N. Turok, *Looking for a Cosmological Constant with the Rees-Sciama Effect*, *Phys. Rev. Lett.* **76** (1996) 575–578, [astro-ph/9510072].

[97] W. Hu, *Dark synergy: Gravitational lensing and the CMB*, *Phys. Rev.* **D65** (2002) 023003, [astro-ph/0108090].

[98] S. Boughn and R. Crittenden, *A Correlation of the cosmic microwave sky with large scale structure*, *Nature* **427** (2004) 45–47, [astro-ph/0305001].

[99] A. Coc and E. Vangioni, *Primordial nucleosynthesis*, *Int. J. Mod. Phys. E* **26** (2017) 1741002, [1707.01004].

[100] S. Deguchi and W. D. Watson, *Excitation of the hyperfine transitions of atomic hydrogen, deuterium, and ionized helium 3 by Lyman-alpha radiation*, *Astrophys. J.* **290** (1985) 578–586.

[101] F. Spite and M. Spite, *Abundance of lithium in unevolved halo stars and old disk stars: Interpretation and consequences*, *Astron. Astrophys.* **115** (1982) 357–366.

[102] Planck collaboration, P. A. R. Ade et al., *Planck 2013 results. XVI. Cosmological parameters*, *Astron. Astrophys.* **571** (2014) A16, [1303.5076].

[103] J. Yoo, E. Mitsou, Y. Dirian and R. Durrer, *Background photon temperature $\bar{T}$: A new cosmological Parameter?*, *Phys. Rev.* **D100** (2019) 063510, [1905.09288].

[104] Particle Data Group collaboration, C. Patrignani et al., *Review of Particle Physics*, *Chin. Phys.* **C40** (2016) 100001.

[105] Planck collaboration, Y. Akrami et al., *Planck 2018 results. I. Overview and the cosmological legacy of Planck*, *Astron. Astrophys.* **Forthcoming article** (2018) , [1807.06205].

[106] L. Sbordone, P. Bonifacio, E. Caffau, H.-G. Ludwig, N. T. Behara, J. I. González Hernández et al., *The metal-poor end of the spite plateau*, *Astronomy & Astrophysics* **522** (2010) A26, [1003.4510].

[107] B. D. Fields, K. A. Olive, T.-H. Yeh and C. Young, *Big-bang nucleosynthesis after planck*, *JCAP* **03** (2020) 010, [1912.01132].

[108] R. H. Cyburt, B. D. Fields and K. A. Olive, *An Update on the big bang nucleosynthesis prediction for Li-7: The problem worsens*, *JCAP* **0811** (2008) 012, [0808.2818].

[109] B. D. Fields, *The primordial lithium problem*, *Ann. Rev. Nucl. Part. Sci.* **61** (2011) 47–68, [1203.3551].

[110] B. Moore, *Evidence against dissipationless dark matter from observations of galaxy haloes*, *Nature* **370** (1994) 629.

[111] A. A. Klypin, A. V. Kravtsov, O. Valenzuela and F. Prada, *Where are the missing Galactic satellites?*, *Astrophys. J.* **522** (1999) 82–92, [astro-ph/9901240].

[112] M. Boylan-Kolchin, J. S. Bullock and M. Kaplinghat, *Too big to fail? The puzzling darkness of massive Milky Way subhaloes*, *Mon. Not. Roy. Astron. Soc.* **415** (2011) L40, [1103.0007].

[113] D. H. Weinberg, J. S. Bullock, F. Governato, R. Kuzio de Naray and A. H. G. Peter, *Cold dark matter: controversies on small scales*, *Proc. Nat. Acad. Sci.* **112** (2015) 12249–12255, [1306.0913].

[114] A. Del Popolo and M. Le Delliou, *Small scale problems of the ΛCDM model: a short review*, *Galaxies* **5** (2017) 17, [1606.07790].

[115] J. S. Bullock and M. Boylan-Kolchin, *Small-Scale Challenges to the ΛCDM Paradigm*, *Ann. Rev. Astron. Astrophys.* **55** (2017) 343–387, [1707.04256].

[116] H. K. Eriksen, F. K. Hansen, A. J. Banday, K. M. Gorski and P. B. Lilje, *Asymmetries in the Cosmic Microwave Background anisotropy field*, *Astrophys. J.* **605** (2004) 14–20, [astro-ph/0307507]. [Erratum: Astrophys. J.609,1198(2004)].

[117] C. L. Bennett et al., *Seven-Year Wilkinson Microwave Anisotropy Probe (WMAP) Observations: Are There Cosmic Microwave Background Anomalies?*, *Astrophys. J. Suppl.* **192** (2011) 17, [1001.4758].

[118] Planck collaboration, P. A. R. Ade et al., *Planck 2013 results. XXIII. Isotropy and statistics of the CMB*, *Astron. Astrophys.* **571** (2014) A23, [1303.5083].

[119] Planck collaboration, P. A. R. Ade et al., *Planck 2015 results. XVI. Isotropy and statistics of the CMB*, *Astron. Astrophys.* **594** (2016) A16, [1506.07135].

[120] D. J. Schwarz, C. J. Copi, D. Huterer and G. D. Starkman, *CMB Anomalies after Planck*, *Class. Quant. Grav.* **33** (2016) 184001, [1510.07929].

[121] H. Hildebrandt et al., *KiDS-450: Cosmological parameter constraints from tomographic weak gravitational lensing*, *Mon. Not. Roy. Astron. Soc.* **465** (2017) 1454, [1606.05338].

[122] F. Köhlinger et al., *KiDS-450: The tomographic weak lensing power spectrum and constraints on cosmological parameters*, *Mon. Not. Roy. Astron. Soc.* **471** (2017) 4412–4435, [1706.02892].

[123] DES collaboration, T. M. C. Abbott et al., *Dark Energy Survey year 1 results: Cosmological constraints from galaxy clustering and weak lensing*, *Phys. Rev.* **D98** (2018) 043526, [1708.01530].

[124] M. Raveri and W. Hu, *Concordance and Discordance in Cosmology*, *Phys. Rev.* **D99** (2019) 043506, [1806.04649].

[125] DES collaboration, M. A. Troxel et al., *Survey geometry and the internal consistency of recent cosmic shear measurements*, *Mon. Not. Roy. Astron. Soc.: Letters* (2018) , [1804.10663].

[126] DES collaboration, T. M. C. Abbott et al., *Dark Energy Survey Year 1 Results: Cosmological Constraints from Cluster Abundances and Weak Lensing*, 2002.11124.

[127] LSST collaboration, A. Nicola et al., *Tomographic galaxy clustering with the Subaru Hyper Suprime-Cam first year public data release*, *JCAP* **03** (2020) 044, [1912.08209].

[128] C. Deffayet, O. Pujolàs, I. Sawicki and A. Vikman, *Imperfect dark energy from kinetic gravity braiding*, *JCAP* **10** (2010) 026, [1008.0048].

[129] G. Addison, Y. Huang, D. Watts, C. Bennett, M. Halpern, G. Hinshaw et al., *Quantifying discordance in the 2015 Planck CMB spectrum*, *Astrophys. J.* **818** (2016) 132, [1511.00055].

[130] D. N. Spergel, R. Flauger and R. Hložek, *Planck Data Reconsidered*, *Phys. Rev.* **D91** (2015) 023518, [1312.3313].

[131] Planck collaboration, N. Aghanim et al., *Planck intermediate results. LI. Features in the cosmic microwave background temperature power spectrum and shifts in cosmological parameters*, *Astron. Astrophys.* **607** (2017) A95, [1608.02487].

[132] G. Efstathiou, *H0 Revisited*, *Mon. Not. Roy. Astron. Soc.* **440** (2014) 1138–1152, [1311.3461].

[133] W. Cardona, M. Kunz and V. Pettorino, *Determining H_0 with Bayesian hyper-parameters*, *JCAP* **1703** (2017) 056, [1611.06088].

[134] B. R. Zhang, M. J. Childress, T. M. Davis, N. V. Karpenka, C. Lidman, B. P. Schmidt et al., *A blinded determination of H_0 from low-redshift Type Ia supernovae, calibrated by Cepheid variables*, *Mon. Not. Roy. Astron. Soc.* **471** (2017) 2254–2285, [1706.07573].

[135] B. Follin and L. Knox, *Insensitivity of the distance ladder Hubble constant determination to Cepheid calibration modelling choices*, *Mon. Not. Roy. Astron. Soc.* **477** (2018) 4534–4542, [1707.01175].

[136] A. Cuceu, J. Farr, P. Lemos and A. Font-Ribera, *Baryon Acoustic Oscillations and the Hubble Constant: Past, Present and Future*, *JCAP* **1910** (2019) 044, [1906.11628].

[137] N. Schöneberg, J. Lesgourgues and D. C. Hooper, *The BAO+BBN take on the Hubble tension*, *JCAP* **10** (2019) 029, [1907.11594].

[138] R. J. Wilkinson, C. Boehm and J. Lesgourgues, *Constraining Dark Matter-Neutrino Interactions using the CMB and Large-Scale Structure*, *JCAP* **05** (2014) 011, [1401.7597].

[139] M. Archidiacono, S. Gariazzo, C. Giunti, S. Hannestad, R. Hansen, M. Laveder et al., *Pseudoscalar—sterile neutrino interactions: reconciling the cosmos with neutrino oscillations*, *JCAP* **1608** (2016) 067, [1606.07673].

[140] I. M. Oldengott, T. Tram, C. Rampf and Y. Y. Y. Wong, *Interacting neutrinos in cosmology: exact description and constraints*, *JCAP* **1711** (2017) 027, [1706.02123].

[141] E. Di Valentino, C. Bøehm, E. Hivon and F. R. Bouchet, *Reducing the H_0 and σ_8 tensions with Dark Matter-neutrino interactions*, *Phys. Rev.* **D97** (2018) 043513, [1710.02559].

[142] M. Park, C. D. Kreisch, J. Dunkley, B. Hadzhiyska and F.-Y. Cyr-Racine, *ΛCDM or self-interacting neutrinos: How CMB data can tell the two models apart*, *Phys. Rev.* **D100** (2019) 063524, [1904.02625].

[143] N. Blinov, K. J. Kelly, G. Z. Krnjaic and S. D. McDermott, *Constraining the Self-Interacting Neutrino Interpretation of the Hubble Tension*, *Phys. Rev. Lett.* **123** (2019) 191102, [1905.02727].

[144] E. Mörtsell and S. Dhawan, *Does the Hubble constant tension call for new physics?*, *JCAP* **09** (2018) 025, [1801.07260].

[145] V. Poulin, T. L. Smith, T. Karwal and M. Kamionkowski, *Early Dark Energy Can Resolve The Hubble Tension*, *Phys. Rev. Lett.* **122** (2019) 221301, [1811.04083].

[146] M.-X. Lin, G. Benevento, W. Hu and M. Raveri, *Acoustic Dark Energy: Potential Conversion of the Hubble Tension*, *Phys. Rev.* **D100** (2019) 063542, [1905.12618].

[147] S. Alexander and E. McDonough, *Axion-Dilaton Destabilization and the Hubble Tension*, *Phys. Lett.* **B797** (2019) 134830, [1904.08912].

[148] N. Khosravi, S. Baghram, N. Afshordi and N. Altamirano, H_0 *tension as a hint for a transition in gravitational theory*, *Phys. Rev.* **99** (2019) 103526, [1710.09366].

[149] R. C. Nunes, *Structure formation in $f(T)$ gravity and a solution for H_0 tension*, *JCAP* **05** (2018) 052, [1802.02281].

[150] H. Desmond, B. Jain and J. Sakstein, *Local resolution of the Hubble tension: The impact of screened fifth forces on the cosmic distance ladder*, *Phys. Rev.* **D100** (2019) 043537, [1907.03778]. [Erratum: Phys.Rev.D 101, 069904 (2020)].

[151] A. Linde, *Inflationary Cosmology after Planck 2013*, in *100e Ecole d'Ete de Physique: Post-Planck Cosmology*, pp. 231–316, 2015, 1402.0526.

[152] J. Martin, C. Ringeval and V. Vennin, *Encyclopaedia Inflationaris*, *Phys. Dark Univ.* **5-6** (2014) 75–235, [1303.3787].

[153] J. Martin, C. Ringeval, R. Trotta and V. Vennin, *The Best Inflationary Models After Planck*, *JCAP* **1403** (2014) 039, [1312.3529].

[154] V. Vennin, K. Koyama and D. Wands, *Inflation with an extra light scalar field after planck*, *JCAP* **03** (2016) 024, [1512.03403].

[155] B. A. Bassett, S. Tsujikawa and D. Wands, *Inflation dynamics and reheating*, *Rev. Mod. Phys.* **78** (2006) 537–589, [astro-ph/0507632].

[156] D. Wands, *Multiple field inflation*, *Lect. Notes Phys.* **738** (2008) 275–304, [astro-ph/0702187].

[157] K.-Y. Choi, J.-O. Gong and D. Jeong, *Evolution of the curvature perturbation during and after multi-field inflation*, *JCAP* **02** (2009) 032, [0810.2299].

[158] C. T. Byrnes and K.-Y. Choi, *Review of local non-gaussianity from multi-field inflation*, *Adv. Astron.* **2010** (2010) 724525, [1002.3110].

[159] VIRGO Consortium collaboration, R. E. Smith, J. A. Peacock, A. Jenkins, S. D. M. White, C. S. Frenk, F. R. Pearce et al., *Stable clustering, the halo model and nonlinear cosmological power spectra*, *Mon. Not. Roy. Astron. Soc.* **341** (2003) 1311, [astro-ph/0207664].

[160] G. Ballesteros, J. Redondo, A. Ringwald and C. Tamarit, *Unifying Inflation with the Axion, Dark Matter, Baryogenesis, and the Seesaw Mechanism*, *Phys. Rev. Lett.* **118** (2017) 071802, [1608.05414].

[161] G. Barenboim, P. B. Denton and I. M. Oldengott, *Constraints on inflation with an extended neutrino sector*, *Phys. Rev.* **D99** (2019) 083515, [1903.02036].

[162] A. Arvanitaki, S. Dimopoulos, S. Dubovsky, N. Kaloper and J. March-Russell, *String Axiverse*, *Phys. Rev.* **D81** (2010) 123530, [0905.4720].

[163] M. Kamionkowski, J. Pradler and D. G. E. Walker, *Dark energy from the string axiverse*, *Phys. Rev. Lett.* **113** (2014) 251302, [1409.0549].

[164] D. J. E. Marsh, *Axion Cosmology*, *Phys. Rept.* **643** (2016) 1–79, [1510.07633].

[165] P. Ciarcelluti, *Cosmology with mirror dark matter*, *Int. J. Mod. Phys. D* **19** (2010) 2151–2230, [1102.5530].

[166] N. E. Mavromatos, C. R. Argüelles, R. Ruffini and J. A. Rueda, *Self-interacting dark matter*, *Int. J. Mod. Phys. D* **26** (2016) 1730007.

[167] S. Tulin and H.-B. Yu, *Dark Matter Self-interactions and Small Scale Structure*, *Phys. Rept.* **730** (2018) 1–57, [1705.02358].

[168] A. Ibarra, D. Tran and C. Weniger, *Indirect Searches for Decaying Dark Matter*, *Int. J. Mod. Phys. A* **28** (2013) 1330040, [1307.6434].

[169] J. A. S. Lima, *Alternative dark energy models: An Overview*, *Braz. J. Phys.* **34** (2004) 194–200, [astro-ph/0402109].

[170] J. Yoo and Y. Watanabe, *Theoretical Models of Dark Energy*, *Int. J. Mod. Phys. D* **21** (2012) 1230002, [1212.4726].

[171] J. Frieman, M. Turner and D. Huterer, *Dark Energy and the Accelerating Universe*, *Ann. Rev. Astron. Astrophys.* **46** (2008) 385–432, [0803.0982].

[172] T. Clifton, P. G. Ferreira, A. Padilla and C. Skordis, *Modified Gravity and Cosmology*, *Phys. Rept.* **513** (2012) 1–189, [1106.2476].

[173] A. Joyce, B. Jain, J. Khoury and M. Trodden, *Beyond the Cosmological Standard Model*, *Phys. Rept.* **568** (2015) 1–98, [1407.0059].

[174] K. Koyama, *Cosmological Tests of Modified Gravity*, *Rept. Prog. Phys.* **79** (2016) 046902, [1504.04623].

[175] L. Heisenberg, *A systematic approach to generalisations of General Relativity and their cosmological implications*, *Phys. Rept.* **796** (2019) 1–113, [1807.01725].

[176] M. Ishak, *Testing General Relativity in Cosmology*, *Living Rev. Rel.* **22** (2019) 1, [1806.10122].

[177] J. M. Ezquiaga and M. Zumalacárregui, *Dark Energy in light of Multi-Messenger Gravitational-Wave astronomy*, *Front. Astron. Space Sci.* **5** (2018) 44, [1807.09241].

[178] D. Baumann, *Inflation*, in *Physics of the large and the small, TASI 09, proceedings of the Theoretical Advanced Study Institute in Elementary Particle Physics, Boulder, Colorado, USA, 1-26 June 2009*, pp. 523–686, 2011, 0907.5424.

[179] D. Langlois, *Lectures on inflation and cosmological perturbations*, *Lect. Notes Phys.* **800** (2010) 1–57, [1001.5259].

[180] S. Clesse, *An introduction to inflation after Planck: from theory to observations*, in *Proceedings, 10th Modave Summer School on Mathematical Physics: Modave, Belgium, September 1-5, 2014*, 2015, 1501.00460.

[181] J. A. Vazquez, L. E. Padilla and T. Matos, *Inflationary Cosmology: From Theory to Observations*, 1810.09934.

[182] Planck collaboration, P. Ade et al., *Planck 2013 results. XXII. Constraints on inflation*, *Astron. Astrophys.* **571** (2014) A22, [1303.5082].

[183] Planck collaboration, P. Ade et al., *Planck 2015 results. XX. Constraints on inflation*, *Astron. Astrophys.* **594** (2016) A20, [1502.02114].

[184] Planck collaboration, Y. Akrami et al., *Planck 2018 results. X. Constraints on inflation*, 1807.06211.

[185] A. R. Liddle and D. H. Lyth, *The Cold dark matter density perturbation*, *Phys. Rep.* **231** (1993) 1–105, [astro-ph/9303019].

[186] A. R. Liddle and S. M. Leach, *How long before the end of inflation were observable perturbations produced?*, *Phys. Rev.* **D68** (2003) 103503, [astro-ph/0305263].

[187] A. A. Starobinsky, *A New Type of Isotropic Cosmological Models Without Singularity*, *Phys. Lett.* **91B** (1980) 99–102. [Adv. Ser. Astrophys. Cosmol. 3, 130 (1987); 771 (1980)].

[188] D. Kazanas, *Dynamics of the Universe and Spontaneous Symmetry Breaking*, *Astrophys. J.* **241** (1980) L59–L63.

[189] A. H. Guth, *The Inflationary Universe: A Possible Solution to the Horizon and Flatness Problems*, *Phys. Rev.* **D23** (1981) 347–356. [Adv. Ser. Astrophys. Cosmol. 3, 139 (1987)].

[190] K. Sato, *Cosmological Baryon Number Domain Structure and the First Order Phase Transition of a Vacuum*, *Phys. Lett.* **99B** (1981) 66–70. [Adv. Ser. Astrophys. Cosmol. 3, 134 (1987)].

[191] V. F. Mukhanov and G. V. Chibisov, *Quantum Fluctuations and a Nonsingular Universe*, *JETP Lett.* **33** (1981) 532–535. [Pisma Zh. Eksp. Teor. Fiz. 33, 549 (1981)].

[192] A. D. Linde, *A New Inflationary Universe Scenario: A Possible Solution of the Horizon, Flatness, Homogeneity, Isotropy and Primordial Monopole Problems*, *Phys. Lett.* **108B** (1982) 389–393. [Adv. Ser. Astrophys. Cosmol. 3, 149 (1987)].

[193] A. Albrecht and P. J. Steinhardt, *Cosmology for Grand Unified Theories with Radiatively Induced Symmetry Breaking*, *Phys. Rev. Lett.* **48** (1982) 1220–1223. [Adv. Ser. Astrophys. Cosmol. 3, 158 (1987)].

[194] A. H. Guth and S. Y. Pi, *Fluctuations in the New Inflationary Universe*, *Phys. Rev. Lett.* **49** (1982) 1110–1113.

[195] J. M. Bardeen, P. J. Steinhardt and M. S. Turner, *Spontaneous creation of almost scale - free density perturbations in an inflationary universe*, *Phys. Rev.* **D28** (1983) 679.

[196] A. D. Linde, *Chaotic inflation*, *Phys.Lett.B* **129** (1983) 177–181.

[197] A. Vilenkin, *The Birth of Inflationary Universes*, *Phys. Rev.* **D27** (1983) 2848.

[198] A. H. Guth and S.-Y. Pi, *The Quantum Mechanics of the Scalar Field in the New Inflationary Universe*, *Phys. Rev.* **D32** (1985) 1899–1920.

[199] A. D. Linde, *ETERNAL CHAOTIC INFLATION*, *Mod. Phys. Lett.* **A1** (1986) 81.

[200] A. D. Linde, *Eternally Existing Selfreproducing Chaotic Inflationary Universe*, *Phys. Lett.* **B175** (1986) 395–400.

[201] A. A. Starobinsky, *STOCHASTIC DE SITTER (INFLATIONARY) STAGE IN THE EARLY UNIVERSE*, *Lect. Notes Phys.* **246** (1986) 107–126.

[202] K. Freese, J. A. Frieman and A. V. Olinto, *Natural inflation with pseudo - Nambu-Goldstone bosons*, *Phys. Rev. Lett.* **65** (1990) 3233–3236.

[203] F. C. Adams, J. Bond, K. Freese, J. A. Frieman and A. V. Olinto, *Natural inflation: Particle physics models, power law spectra for large scale structure, and constraints from cobe*, *Phys. Rev.* **D47** (1993) 426–455, [hep-ph/9207245].

[204] K. Freese and W. H. Kinney, *Natural inflation: Consistency with cosmic microwave background observations of planck and bicep2*, *JCAP* **03** (2015) 044, [1403.5277].

[205] M. Czerny and F. Takahashi, *Multi-natural inflation*, *Phys.Lett.B* **733** (2014) 241–246, [1401.5212].

[206] N. Makino and M. Sasaki, *The Density perturbation in the chaotic inflation with nonminimal coupling*, *Prog. Theor. Phys.* **86** (1991) 103–118.

[207] K. Nakayama, F. Takahashi and T. T. Yanagida, *Polynomial Chaotic Inflation in the Planck Era*, *Phys. Lett. B* **725** (2013) 111–114, [1303.7315].

[208] L. Boubekeur and D. H. Lyth, *Hilltop inflation*, *JCAP* **0507** (2005) 010, [hep-ph/0502047].

[209] K. Kohri, C.-M. Lin and D. H. Lyth, *More hilltop inflation models*, *JCAP* **12** (2007) 004, [0707.3826].

[210] K. Tzirakis and W. H. Kinney, *Inflation over the hill*, *Phys. Rev.* **D75** (2007) 123510, [astro-ph/0701432].

[211] D. Coone, D. Roest and V. Vennin, *The hubble flow of plateau inflation*, *JCAP* **11** (2015) 010, [1507.00096].

[212] LIGO Scientific, Virgo collaboration, B. P. Abbott et al., *Search for Tensor, Vector, and Scalar Polarizations in the Stochastic Gravitational-Wave Background*, *Phys. Rev. Lett.* **120** (2018) 201102, [1802.10194].

[213] LIGO Scientific, Virgo collaboration, B. P. Abbott et al., *Search for the isotropic stochastic background using data from Advanced LIGO's second observing run*, *Phys. Rev.* **D100** (2019) 061101, [1903.02886].

[214] S. Phinney, P. Bender, R. Buchman, R. Byer, N. Cornish, P. Fritschel et al., *The big bang observer: direct detection of gravitational waves from the birth of the universe to the present*, *NASA Mission Concept Study* (2004) .

[215] V. Corbin and N. J. Cornish, *Detecting the cosmic gravitational wave background with the big bang observer*, *Class. Quant. Grav.* **23** (2006) 2435–2446, [gr-qc/0512039].

[216] P. Amaro-Seoane, H. Audley, S. Babak, J. Baker, E. Barausse, P. Bender et al., *Laser Interferometer Space Antenna*, *ArXiv e-prints* (2017) , [1702.00786].

[217] N. Bartolo et al., *Science with the space-based interferometer LISA. IV: Probing inflation with gravitational waves*, *JCAP* **1612** (2016) 026, [1610.06481].

[218] KATRIN collaboration, M. Aker et al., *Improved Upper Limit on the Neutrino Mass from a Direct Kinematic Method by KATRIN*, *Phys. Rev. Lett.* **123** (2019) 221802, [1909.06048].

[219] A. D. Dolgov, *Neutrinos in cosmology*, *Phys. Rept.* **370** (2002) 333–535, [hep-ph/0202122].

[220] J. Lesgourgues and S. Pastor, *Massive neutrinos and cosmology*, *Phys. Rept.* **429** (2006) 307–379, [astro-ph/0603494].

[221] Y. Y. Y. Wong, *Neutrino mass in cosmology: status and prospects*, *Ann. Rev. Nucl. Part. Sci.* **61** (2011) 69–98, [1111.1436].

[222] M. Lattanzi and M. Gerbino, *Status of neutrino properties and future prospects - Cosmological and astrophysical constraints*, *Front.in Phys.* **5** (2018) 70, [1712.07109].

[223] A. Lewis, A. Challinor and A. Lasenby, *Efficient computation of CMB anisotropies in closed FRW models*, *Astrophys. J.* **538** (2000) 473–476, [astro-ph/9911177].

[224] A. Lewis and S. Bridle, *Cosmological parameters from CMB and other data: A Monte Carlo approach*, *Phys. Rev.* **D66** (2002) 103511, [astro-ph/0205436].

[225] J. Lesgourgues, *The Cosmic Linear Anisotropy Solving System (CLASS) I: Overview*, *ArXiv e-prints* (2011) , [1104.2932].

[226] D. Blas, J. Lesgourgues and T. Tram, *The Cosmic Linear Anisotropy Solving System (CLASS). Part II: Approximation schemes*, *JCAP* **2011** (2011) 034, [1104.2933].

[227] R. Takahashi, M. Sato, T. Nishimichi, A. Taruya and M. Oguri, *Revising the Halofit Model for the Nonlinear Matter Power Spectrum*, *Astrophys. J.* **761** (2012) 152, [1208.2701].

[228] S. Bird, M. Viel and M. G. Haehnelt, *Massive Neutrinos and the Non-linear Matter Power Spectrum*, *Mon. Not. Roy. Astron. Soc.* **420** (2012) 2551–2561, [1109.4416].

[229] E. Semboloni, H. Hoekstra, J. Schaye, M. P. van Daalen and I. J. McCarthy, *Quantifying the effect of baryon physics on weak lensing tomography*, *Mon. Not. Roy. Astron. Soc.* **417** (2011) 2020, [1105.1075].

[230] J. Harnois-Déraps, L. van Waerbeke, M. Viola and C. Heymans, *Baryons, Neutrinos, Feedback and Weak Gravitational Lensing*, *Mon. Not. Roy. Astron. Soc.* **450** (2015) 1212–1223, [1407.4301].

[231] A. Schneider, R. Teyssier, J. Stadel, N. E. Chisari, A. M. C. Le Brun, A. Amara et al., *Quantifying baryon effects on the matter power spectrum and the weak lensing shear correlation*, *JCAP* **1903** (2019) 020, [1810.08629].

[232] N. E. Chisari et al., *Modelling baryonic feedback for survey cosmology*, *Open J. Astrophys.* (2019) , [1905.06082].

[233] A. Raccanelli, L. Verde and F. Villaescusa-Navarro, *Biases from neutrino bias: to worry or not to worry?*, *Mon. Not. Roy. Astron. Soc.* **483** (2019) 734–743, [1704.07837].

[234] S. Vagnozzi, T. Brinckmann, M. Archidiacono, K. Freese, M. Gerbino, J. Lesgourgues et al., *Bias due to neutrinos must not uncorrect'd go*, *JCAP* **1809** (2018) 001, [1807.04672].

[235] I. M. Oldengott, G. Barenboim, S. Kahlen, J. Salvado and D. J. Schwarz, *How to relax the cosmological neutrino mass bound*, *JCAP* **1904** (2019) 049, [1901.04352].

[236] M. C. Gonzalez-Garcia, V. Niro and J. Salvado, *Dark Radiation and Decaying Matter*, *JHEP* **04** (2013) 052, [1212.1472].

[237] S. Hannestad, *Probing neutrino decays with the cosmic microwave background*, *Phys. Rev.* **D59** (1999) 125020, [astro-ph/9903475].

[238] M. Kaplinghat, R. E. Lopez, S. Dodelson and R. J. Scherrer, *Improved treatment of cosmic microwave background fluctuations induced by a late decaying massive neutrino*, *Phys. Rev.* **D60** (1999) 123508, [astro-ph/9907388].

[239] K. C. Y. Ng and J. F. Beacom, *Cosmic neutrino cascades from secret neutrino interactions*, *Phys. Rev.* **D90** (2014) 065035, [1404.2288]. [Erratum: Phys. Rev.D90,no.8,089904(2014)].

[240] F. Forastieri, M. Lattanzi and P. Natoli, *Cosmological constraints on neutrino self-interactions with a light mediator*, *Phys. Rev.* **D100** (2019) 103526, [1904.07810].

[241] C. D. Kreisch, F.-Y. Cyr-Racine and O. Doré, *The Neutrino Puzzle: Anomalies, Interactions, and Cosmological Tensions*, 1902.00534.

[242] J. Kopp, P. A. N. Machado, M. Maltoni and T. Schwetz, *Sterile Neutrino Oscillations: The Global Picture*, *JHEP* **05** (2013) 050, [1303.3011].

[243] K. Abazajian, N. F. Bell, G. M. Fuller and Y. Y. Y. Wong, *Cosmological lepton asymmetry, primordial nucleosynthesis, and sterile neutrinos*, *Phys. Rev.* **D72** (2005) 063004, [astro-ph/0410175].

[244] A. Boyarsky, O. Ruchayskiy and M. Shaposhnikov, *The Role of sterile neutrinos in cosmology and astrophysics*, *Ann. Rev. Nucl. Part. Sci.* **59** (2009) 191–214, [0901.0011].

[245] E. D. Carlson, M. E. Machacek and L. J. Hall, *Self-interacting dark matter*, *Astrophys. J.* **398** (1992) 43–52.

[246] M. R. Buckley and P. J. Fox, *Dark Matter Self-Interactions and Light Force Carriers*, *Phys. Rev. D* **D81** (2010) 083522, [0911.3898].

[247] K. Kainulainen, K. Tuominen and V. Vaskonen, *Self-interacting dark matter and cosmology of a light scalar mediator*, *Phys. Rev.* **D93** (2016) 015016, [1507.04931]. [Erratum: Phys.Rev.D 95, 079901 (2017)].

[248] T. Bringmann, F. Kahlhoefer, K. Schmidt-Hoberg and P. Walia, *Strong constraints on self-interacting dark matter with light mediators*, *Phys. Rev. Lett.* **118** (2017) 141802, [1612.00845].

[249] M. Hufnagel, K. Schmidt-Hoberg and S. Wild, *BBN constraints on MeV-scale dark sectors. Part II. Electromagnetic decays*, *JCAP* **11** (2018) 032, [1808.09324].

[250] M. Hufnagel, K. Schmidt-Hoberg and S. Wild, *BBN constraints on MeV-scale dark sectors. Part I. Sterile decays*, *JCAP* **02** (2018) 044, [1712.03972].

[251] M. Escudero, *Neutrino decoupling beyond the Standard Model: CMB constraints on the Dark Matter mass with a fast and precise $N_{\rm eff}$ evaluation*, *JCAP* **1902** (2019) 007, [1812.05605].

[252] P. F. Depta, M. Hufnagel, K. Schmidt-Hoberg and S. Wild, *BBN constraints on the annihilation of MeV-scale dark matter*, *JCAP* **1904** (2019) 029, [1901.06944].

[253] N. Sabti, J. Alvey, M. Escudero, M. Fairbairn and D. Blas, *Refined Bounds on MeV-scale Thermal Dark Sectors from BBN and the CMB*, *JCAP* **2001** (2020) 004, [1910.01649].

[254] A. D. Dolgov and F. L. Villante, *BBN bounds on active sterile neutrino mixing*, *Nucl. Phys.* **B679** (2004) 261–298, [hep-ph/0308083].

[255] K. M. Nollett and G. Steigman, *BBN And The CMB Constrain Light, Electromagnetically Coupled WIMPs*, *Phys. Rev.* **D89** (2014) 083508, [1312.5725].

[256] G. Steigman and K. M. Nollett, *Light WIMPs, Equivalent Neutrinos, BBN, and the CMB*, *Mem. Soc. Ast. It.* **85** (2014) 175, [1401.5488].

[257] J. L. Menestrina and R. J. Scherrer, *Dark Radiation from Particle Decays during Big Bang Nucleosynthesis*, *Phys. Rev.* **D85** (2012) 047301, [1111.0605].

[258] A. Berlin, D. Hooper and G. Krnjaic, *Thermal Dark Matter From A Highly Decoupled Sector*, *Phys. Rev.* **D94** (2016) 095019, [1609.02555].

[259] L. G. van den Aarssen, T. Bringmann and C. Pfrommer, *Is dark matter with long-range interactions a solution to all small-scale problems of ΛCDM cosmology?*, *Phys. Rev. Lett.* **109** (2012) 231301, [1205.5809].

[260] F.-Y. Cyr-Racine, K. Sigurdson, J. Zavala, T. Bringmann, M. Vogelsberger and C. Pfrommer, *ETHOS—an effective theory of structure formation: From dark particle physics to the matter distribution of the Universe*, *Phys. Rev.* **D93** (2016) 123527, [1512.05344].

[261] M. Vogelsberger, J. Zavala, F.-Y. Cyr-Racine, C. Pfrommer, T. Bringmann and K. Sigurdson, *ETHOS – an effective theory of structure formation: dark matter physics as a possible explanation of the small-scale CDM problems*, *Mon. Not. Roy. Astron. Soc.* **460** (2016) 1399–1416, [1512.05349].

[262] M. Blennow, E. Fernandez-Martinez, O. Mena, J. Redondo and P. Serra, *Asymmetric Dark Matter and Dark Radiation*, *JCAP* **1207** (2012) 022, [1203.5803].

[263] T. Bringmann, F. Kahlhoefer, K. Schmidt-Hoberg and P. Walia, *Converting nonrelativistic dark matter to radiation*, *Phys. Rev.* **D98** (2018) 023543, [1803.03644].

[264] Z. Hou, R. Keisler, L. Knox, M. Millea and C. Reichardt, *How Massless Neutrinos Affect the Cosmic Microwave Background Damping Tail*, *Phys. Rev.* **D87** (2013) 083008, [1104.2333].

[265] Z. Hou, R. Keisler, L. Knox, M. Millea and C. Reichardt, *How massless neutrinos affect the cosmic microwave background damping tail*, *Phys. Rev.* **D87** (Apr., 2013) 083008, [1104.2333].

[266] Z. Hou, C. L. Reichardt, K. T. Story, B. Follin, R. Keisler, K. A. Aird et al., *Constraints on Cosmology from the Cosmic Microwave*

Background Power Spectrum of the 2500 deg^2 SPT-SZ Survey, *Astrophys. J.* **782** (2014) 74, [1212.6267].

[267] Topical Conveners: K.N. Abazajian, J.E. Carlstrom, A.T. Lee collaboration, K. Abazajian et al., *Neutrino Physics from the Cosmic Microwave Background and Large Scale Structure*, *Astropart. Phys.* **63** (2015) 66–80, [1309.5383].

[268] D. Lovelock, *The einstein tensor and its generalizations*, *Journal of Mathematical Physics* **12** (1971) 498–501.

[269] D. Lovelock, *The four-dimensionality of space and the einstein tensor*, *Journal of Mathematical Physics* **13** (1972) 874–876.

[270] T. Nishioka, S. Ryu and T. Takayanagi, *Holographic Entanglement Entropy: An Overview*, *J. Phys.* **A42** (2009) 504008, [0905.0932].

[271] T. Faulkner, M. Guica, T. Hartman, R. C. Myers and M. Van Raamsdonk, *Gravitation from Entanglement in Holographic CFTs*, *JHEP* **03** (2014) 051, [1312.7856].

[272] E. P. Verlinde, *Emergent Gravity and the Dark Universe*, *SciPost Phys.* **2** (2017) 016, [1611.02269].

[273] G. W. Horndeski, *Second-order scalar-tensor field equations in a four-dimensional space*, *Int. J. Theor. Phys.* **10** (1974) 363–384.

[274] C. Deffayet, X. Gao, D. A. Steer and G. Zahariade, *From k-essence to generalised Galileons*, *Phys. Rev.* **D84** (2011) 064039, [1103.3260].

[275] T. Kobayashi, M. Yamaguchi and J. Yokoyama, *Generalized G-inflation: Inflation with the most general second-order field equations*, *Prog. Theor. Phys.* **126** (2011) 511–529, [1105.5723].

[276] P. Bull et al., *Beyond ΛCDM: Problems, solutions, and the road ahead*, *Phys. Dark Univ.* **12** (2016) 56–99, [1512.05356].

[277] B. Ratra and P. J. E. Peebles, *Cosmological consequences of a rolling homogeneous scalar field*, *Phys. Rev.* **D37** (1988) 3406–3427.

[278] C. Wetterich, *Cosmology and the fate of dilatation symmetry*, *Nuclear Physics B* **302** (1988) 668 – 696.

[279] C. Armendariz-Picon, T. Damour and V. F. Mukhanov, *k - inflation*, *Phys. Lett.* **B458** (1999) 209–218, [hep-th/9904075].

[280] C. Armendariz-Picon, V. F. Mukhanov and P. J. Steinhardt, *Essentials of k essence*, *Phys. Rev.* **D63** (2001) 103510, [astro-ph/0006373].

[281] S. M. Carroll, V. Duvvuri, M. Trodden and M. S. Turner, *Is cosmic speed - up due to new gravitational physics?*, *Phys. Rev.* **D70** (2004) 043528, [astro-ph/0306438].

[282] I. H. Brevik, S. Nojiri, S. D. Odintsov and L. Vanzo, *Entropy and universality of Cardy-Verlinde formula in dark energy universe*, *Phys. Rev.* **D70** (2004) 043520, [hep-th/0401073].

[283] S. Nojiri and S. D. Odintsov, *Modified gravity with negative and positive powers of the curvature: Unification of the inflation and of the cosmic acceleration*, *Phys. Rev.* **D68** (2003) 123512, [hep-th/0307288].

[284] T. Kobayashi, M. Yamaguchi and J. Yokoyama, *G-inflation: Inflation driven by the Galileon field*, *Phys. Rev. Lett.* **105** (2010) 231302, [1008.0603].

[285] O. Pujolàs, I. Sawicki and A. Vikman, *The imperfect fluid behind kinetic gravity braiding*, *Journal of High Energy Physics* **11** (2011) 156, [1103.5360].

[286] C. Charmousis, E. J. Copeland, A. Padilla and P. M. Saffin, *General second order scalar-tensor theory, self tuning, and the Fab Four*, *Phys. Rev. Lett.* **108** (2012) 051101, [1106.2000].

[287] C. Charmousis, E. J. Copeland, A. Padilla and P. M. Saffin, *Self-tuning and the derivation of a class of scalar-tensor theories*, *Phys. Rev.* **D85** (2012) 104040, [1112.4866].

[288] J.-P. Bruneton, M. Rinaldi, A. Kanfon, A. Hees, S. Schlogel and A. Fuzfa, *Fab Four: When John and George play gravitation and cosmology*, *Adv. Astron.* **2012** (2012) 430694, [1203.4446].

[289] E. J. Copeland, A. Padilla and P. M. Saffin, *The cosmology of the Fab-Four*, *JCAP* **1212** (2012) 026, [1208.3373].

[290] M. V. Ostrogradski, *Memoires sur les equations differentielles relatives au probleme des isoperimetres*, *Mem. Acad. St. Petersbourg VI 4* (1850) 385.

[291] M. Zumalacárregui and J. García-Bellido, *Transforming gravity: From derivative couplings to matter to second-order scalar-tensor theories beyond the Horndeski Lagrangian*, *Phys. Rev.* **D89** (2014) 064046, [1308.4685].

[292] J. Gleyzes, D. Langlois, F. Piazza and F. Vernizzi, *New Class of Consistent Scalar-Tensor Theories*, *Phys. Rev. Lett.* **114** (2015) 211101, [1404.6495].

[293] D. Langlois and K. Noui, *Degenerate higher derivative theories beyond Horndeski: evading the Ostrogradski instability*, *JCAP* **1602** (2016) 034, [1510.06930].

[294] J. Gleyzes, D. Langlois, F. Piazza and F. Vernizzi, *Exploring gravitational theories beyond Horndeski*, *JCAP* **1502** (2015) 018, [1408.1952].

[295] D. Bettoni and S. Liberati, *Disformal invariance of second order scalar-tensor theories: Framing the Horndeski action*, *Phys. Rev.* **D88** (2013) 084020, [1306.6724].

[296] J. M. Ezquiaga, J. García-Bellido and M. Zumalacárregui, *Field redefinitions in theories beyond Einstein gravity using the language of differential forms*, *Phys. Rev.* **D95** (2017) 084039, [1701.05476].

[297] A. De Felice and S. Tsujikawa, *Conditions for the cosmological viability of the most general scalar-tensor theories and their applications to extended Galileon dark energy models*, *JCAP* **1202** (2012) 007, [1110.3878].

[298] E. Bellini and I. Sawicki, *Maximal freedom at minimum cost: linear large-scale structure in general modifications of gravity*, *JCAP* **1407** (2014) 050, [1404.3713].

[299] A. de Felice and S. Tsujikawa, *Cosmology of a Covariant Galileon Field*, *Phys. Rev. Lett.* **105** (2010) 111301, [1007.2700].

[300] A. Barreira, B. Li, C. M. Baugh and S. Pascoli, *Linear perturbations in Galileon gravity models*, *Phys. Rev.* **D86** (2012) 124016, [1208.0600].

[301] A. Barreira, B. Li, A. Sanchez, C. M. Baugh and S. Pascoli, *Parameter space in Galileon gravity models*, *Phys. Rev.* **D87** (2013) 103511, [1302.6241].

[302] A. De Felice and S. Tsujikawa, *Generalized Galileon cosmology*, *Phys. Rev.* **D84** (2011) 124029, [1008.4236].

[303] S. Nesseris, A. De Felice and S. Tsujikawa, *Observational constraints on Galileon cosmology*, *Phys. Rev.* **D82** (2010) 124054, [1010.0407].

[304] R. P. Woodard, *Ostrogradsky's theorem on Hamiltonian instability*, *Scholarpedia* **10** (2015) 32243, [1506.02210].

[305] S. Appleby and E. V. Linder, *The Paths of Gravity in Galileon Cosmology*, *JCAP* **1203** (2012) 043, [1112.1981].

[306] N. Chow and J. Khoury, *Galileon Cosmology*, *Phys. Rev.* **D80** (2009) 024037, [0905.1325].

[307] D. F. Mota, M. Sandstad and T. Zlosnik, *Cosmology of the selfaccelerating third order Galileon*, *JHEP* **12** (2010) 051, [1009.6151].

[308] P. Brax, C. Burrage and A.-C. Davis, *The Speed of Galileon Gravity*, *JCAP* **1603** (2016) 004, [1510.03701].

[309] J. Neveu, V. Ruhlmann-Kleider, P. Astier, M. Besançon, J. Guy, A. Möller et al., *Constraining the ΛCDM and Galileon models with recent cosmological data*, *Astron. Astrophys.* **600** (2017) A40, [1605.02627].

[310] S. Peirone, N. Frusciante, B. Hu, M. Raveri and A. Silvestri, *Do current cosmological observations rule out all Covariant Galileons?*, *Phys. Rev.* **D97** (2018) 063518, [1711.04760].

[311] C. Burrage and D. Seery, *Revisiting fifth forces in the Galileon model*, *JCAP* **1008** (2010) 011, [1005.1927].

[312] B. Li, A. Barreira, C. M. Baugh, W. A. Hellwing, K. Koyama et al., *Simulating the quartic Galileon gravity model on adaptively refined meshes*, *JCAP* **1311** (2013) 012, [1308.3491].

[313] A. Barreira, B. Li, C. M. Baugh and S. Pascoli, *Spherical collapse in Galileon gravity: fifth force solutions, halo mass function and halo bias*, *JCAP* **1311** (2013) 056, [1308.3699].

[314] L. Perivolaropoulos, *Cosmic string theory: The Current status*, in *ICTP Summer School in High-energy Physics and Cosmology*, pp. 0204–270, 1994, astro-ph/9410097.

[315] J. Polchinski, *String theory: Volume 1, an introduction to the bosonic string*. Cambridge university press, 1998.

[316] A. Vilenkin and E. S. Shellard, *Cosmic Strings and Other Topological Defects*. Cambridge University Press, 2000.

[317] J. Polchinski, *Introduction to cosmic F- and D-strings*, in *String theory: From gauge interactions to cosmology. Proceedings, NATO Advanced Study Institute, Cargese, France, June 7-19, 2004*, pp. 229–253, 2004, hep-th/0412244.

[318] K. Becker, M. Becker and J. H. Schwarz, *String theory and M-theory: A modern introduction*. Cambridge University Press, 2006.

[319] M. Sakellariadou, *Cosmic Strings and Cosmic Superstrings*, *Nucl. Phys. B Proc. Suppl.* **192-193** (2009) 68–90, [0902.0569].

[320] C. Ringeval, *Cosmic strings and their induced non-Gaussianities in the cosmic microwave background*, *Adv. Astron.* **2010** (2010) 380507, [1005.4842].

[321] M. Hindmarsh, *Signals of Inflationary Models with Cosmic Strings*, *Prog. Theor. Phys. Suppl.* **190** (2011) 197–228, [1106.0391].

[322] E. J. Copeland and T. Kibble, *Cosmic Strings and Superstrings*, *Proc. Roy. Soc. Lond. A* **A466** (2010) 623–657, [0911.1345].

[323] D. Baumann and L. McAllister, *Inflation and String Theory*. Cambridge Monographs on Mathematical Physics. Cambridge University Press, 2015, 10.1017/CBO9781316105733.

[324] D. F. Chernoff and S. H. H. Tye, *Inflation, string theory and cosmic strings*, *Int. J. Mod. Phys.* **D24** (2015) 1530010, [1412.0579].

[325] E. Witten, *Cosmic Superstrings*, *Phys. Lett. B* **153** (1985) 243–246.

[326] U. Amaldi, W. de Boer, P. H. Frampton, H. Furstenau and J. T. Liu, *Consistency checks of grand unified theories*, *Phys. Lett. B* **281** (1992) 374–382.

[327] R. Jeannerot, J. Rocher and M. Sakellariadou, *How generic is cosmic string formation in SUSY GUTs*, *Phys. Rev.* **D68** (2003) 103514, [hep-ph/0308134].

[328] A. Avgoustidis, *Cosmic String Dynamics and Evolution in Warped Spacetime*, *Phys. Rev.* **D78** (2008) 023501, [0712.3224].

[329] A. Avgoustidis, S. Chadburn and R. Gregory, *Cosmic superstring trajectories in warped compactifications*, *Phys. Rev.* **D86** (2012) 063516, [1204.0973].

[330] D. F. Chernoff and S. H. H. Tye, *Detection of Low Tension Cosmic Superstrings*, *JCAP* **1805** (2018) 002, [1712.05060].

[331] E. Shellard, *Cosmic String Interactions*, *Nucl. Phys. B* **283** (1987) 624–656.

[332] R. A. Matzner, *Interaction of U(1) cosmic strings: Numerical intercommutation*, *Computers in Physics* **2** (1988) 51–64.

[333] A. Albrecht and N. Turok, *Evolution of Cosmic Strings*, *Phys. Rev. Lett.* **54** (1985) 1868–1871.

[334] D. P. Bennett and F. R. Bouchet, *The Two Point Correlation Function of Cosmic String Loops*, *Phys. Rev. Lett.* **63** (1989) 1334.

[335] B. Allen and E. Shellard, *Cosmic string evolution: a numerical simulation*, *Phys. Rev. Lett.* **64** (1990) 119–122.

[336] D. F. Chernoff, *Clustering of Superstring Loops*, 0908.4077.

[337] J. J. Blanco-Pillado, K. D. Olum and B. Shlaer, *The number of cosmic string loops*, *Phys. Rev.* **D89** (2014) 023512, [1309.6637].

[338] A. Vilenkin, *Gravitational Field of Vacuum Domain Walls and Strings*, *Phys. Rev.* **D23** (1981) 852–857.

[339] M. Hindmarsh and T. Kibble, *Cosmic strings*, *Rept. Prog. Phys.* **58** (1995) 477–562, [hep-ph/9411342].

[340] A. Vilenkin, *Cosmic strings as gravitational lenses*, *Astrophys. J.* **282** (1984) L51–L53.

[341] A. Vilenkin, *Looking for cosmic strings*, *Nature* **322** (1986) 613–614.

[342] X. Siemens, V. Mandic and J. Creighton, *Gravitational wave stochastic background from cosmic (super)strings*, *Phys. Rev. Lett.* **98** (2007) 111101, [astro-ph/0610920].

[343] LIGO Scientific, Virgo collaboration, B. P. Abbott et al., *Constraints on cosmic strings using data from the first Advanced LIGO observing run*, *Phys. Rev.* **D97** (2018) 102002, [1712.01168].

[344] L. Pogosian and M. Wyman, *B-modes from cosmic strings*, *Phys. Rev.* **D77** (2008) 083509, [0711.0747].

[345] R. J. Danos and R. H. Brandenberger, *Searching for Signatures of Cosmic Superstrings in the CMB*, *JCAP* **02** (2010) 033, [0910.5722].

[346] Planck collaboration, P. A. R. Ade et al., *Planck 2013 results. XXV. Searches for cosmic strings and other topological defects*, *Astron. Astrophys.* **571** (2014) A25, [1303.5085].

[347] J. Polchinski, *Cosmic String Loops and Gravitational Radiation*, in *Recent developments in theoretical and experimental general relativity, gravitation and relativistic field theories. Proceedings, 11th Marcel Grossmann Meeting, MG11, Berlin, Germany, July 23-29, 2006. Pt. A-C*, pp. 105–125, 2007, 0707.0888.

[348] S. L. Detweiler, *Pulsar timing measurements and the search for gravitational waves*, *Astrophys. J.* **234** (1979) 1100–1104.

[349] M. V. Sazhin, *Opportunities for detecting ultralong gravitational waves*, *Soviet Ast.* **22** (1978) 36–38.

[350] B. Bertotti, B. J. Carr and M. J. Rees, *Limits from the timing of pulsars on the cosmic gravitational wave background.*, *Mon. Not. Roy. Astron. Soc.* **203** (1983) 945–954.

[351] R. S. Foster and D. C. Backer, *Constructing a Pulsar Timing Array*, *Astrophys. J.* **361** (1990) 300.

[352] J. J. Blanco-Pillado and K. D. Olum, *Stochastic gravitational wave background from smoothed cosmic string loops*, *Phys. Rev.* **D96** (2017) 104046, [1709.02693].

[353] J. J. Blanco-Pillado, K. D. Olum and X. Siemens, *New limits on cosmic strings from gravitational wave observation*, *Phys. Lett.* **B778** (2018) 392–396, [1709.02434].

[354] D. B. Thomas, C. R. Contaldi and J. Magueijo, *Rotation of galaxies as a signature of cosmic strings in weak lensing surveys*, *Phys. Rev. Lett.* **103** (2009) 181301, [0909.2866].

[355] D. Yamauchi, T. Namikawa and A. Taruya, *Weak lensing generated by vector perturbations and detectability of cosmic strings*, *JCAP* **1210** (2012) 030, [1205.2139].

[356] A. A. de Laix, L. M. Krauss and T. Vachaspati, *Gravitational Lensing Signature of Long Cosmic Strings*, *Phys. Rev. Lett.* **79** (1997) 1968–1971, [astro-ph/9702033].

[357] K. Kuijken, X. Siemens and T. Vachaspati, *Microlensing by cosmic strings*, *Mon. Not. Roy. Astron. Soc.* **384** (2008) 161–164.

[358] K. J. Mack, D. H. Wesley and L. J. King, *Observing cosmic string loops with gravitational lensing surveys*, *Phys. Rev.* **D76** (2007) 123515, [astro-ph/0702648].

[359] D. F. Chernoff and S. H. H. Tye, *Cosmic String Detection via Microlensing of Stars*, 0709.1139.

[360] R. C. Myers and M. Wyman, *Cosmic superstrings*, *Superstring cosmology: modern string theory concepts from the Big Bang to cosmic structure, ed. J. Erdmenger, Wiley* **19** (2009) .

[361] E. J. Copeland, L. Pogosian and T. Vachaspati, *Seeking String Theory in the Cosmos*, *Class. Quant. Grav.* **28** (2011) 204009, [1105.0207].

[362] S. Kachru, R. Kallosh, A. D. Linde, J. M. Maldacena, L. P. McAllister and S. P. Trivedi, *Towards inflation in string theory*, *JCAP* **10** (2003) 013, [hep-th/0308055].

[363] C. Wetterich, *Cosmology and the Fate of Dilatation Symmetry*, *Nucl. Phys. B* **302** (1988) 668–696, [1711.03844].

[364] J. Sola, *Dark energy: A Quantum fossil from the inflationary Universe?*, *J. Phys.* **A41** (2008) 164066, [0710.4151].

[365] C. Ringeval, T. Suyama, T. Takahashi, M. Yamaguchi and S. Yokoyama, *Dark energy from primordial inflationary quantum fluctuations*, *Phys. Rev. Lett.* **105** (2010) 121301, [1006.0368].

[366] J. Garcia-Bellido, J. Rubio, M. Shaposhnikov and D. Zenhausern, *Higgs-Dilaton Cosmology: From the Early to the Late Universe*, *Phys. Rev.* **D84** (2011) 123504, [1107.2163].

[367] F. Bezrukov, G. K. Karananas, J. Rubio and M. Shaposhnikov, *Higgs-Dilaton Cosmology: an effective field theory approach*, *Phys. Rev.* **D87** (2013) 096001, [1212.4148].

[368] S. Casas, G. K. Karananas, M. Pauly and J. Rubio, *Scale-invariant alternatives to general relativity. III. The inflation-dark energy connection*, *Phys. Rev.* **D99** (2019) 063512, [1811.05984].

[369] R. Sundrum, *Towards an effective particle string resolution of the cosmological constant problem*, *JHEP* **07** (1999) 001, [hep-ph/9708329].

[370] D. J. Marsh, *The Axiverse Extended: Vacuum Destabilisation, Early Dark Energy and Cosmological Collapse*, *Phys. Rev.* **D83** (2011) 123526, [1102.4851].

[371] P. Berglund, T. Hübsch and D. Minić, *Dark Energy and String Theory*, *Phys. Lett.* **B798** (2019) 134950, [1905.08269].

[372] A. Mazumdar and J. Rocher, *Particle physics models of inflation and curvaton scenarios*, *Phys. Rept.* **497** (2011) 85–215, [1001.0993].

[373] A. De Simone, M. P. Hertzberg and F. Wilczek, *Running Inflation in the Standard Model*, *Phys. Lett. B* **678** (2009) 1–8, [0812.4946].

[374] A. Barvinsky, A. Kamenshchik and A. Starobinsky, *Inflation scenario via the Standard Model Higgs boson and LHC*, *JCAP* **11** (2008) 021, [0809.2104].

[375] O. Lebedev and H. M. Lee, *Higgs Portal Inflation*, *Eur. Phys. J.* **C71** (2011) 1821, [1105.2284].

[376] V. V. Khoze, *Inflation and Dark Matter in the Higgs Portal of Classically Scale Invariant Standard Model*, *JHEP* **11** (2013) 215, [1308.6338].

[377] E. Silverstein and A. Westphal, *Monodromy in the CMB: Gravity Waves and String Inflation*, *Phys. Rev.* **D78** (2008) 106003, [0803.3085].

[378] L. McAllister, E. Silverstein and A. Westphal, *Gravity Waves and Linear Inflation from Axion Monodromy*, *Phys. Rev.* **D82** (2010) 046003, [0808.0706].

[379] N. Kaloper, A. Lawrence and L. Sorbo, *An Ignoble Approach to Large Field Inflation*, *JCAP* **1103** (2011) 023, [1101.0026].

[380] R. Blumenhagen, A. Font, M. Fuchs, D. Herschmann, E. Plauschinn, Y. Sekiguchi et al., *A Flux-Scaling Scenario for High-Scale Moduli Stabilization in String Theory*, *Nucl. Phys. B* **897** (2015) 500–554, [1503.07634].

[381] P. Svrcek and E. Witten, *Axions In String Theory*, *JHEP* **06** (2006) 051, [hep-th/0605206].

[382] B. S. Acharya, G. Kane and P. Kumar, *Compactified String Theories – Generic Predictions for Particle Physics*, *Int. J. Mod. Phys. A* **27** (2012) 1230012, [1204.2795].

[383] F. Quevedo, *Local String Models and Moduli Stabilisation*, *Mod. Phys. Lett. A* **30** (2015) 1530004, [1404.5151].

[384] A. Dashko and R. Dick, *The shadow of dark matter as a shadow of string theory*, *Eur. Phys. J. C* **79** (2019) 312, [1809.01089].

[385] R. Fardon, A. E. Nelson and N. Weiner, *Dark energy from mass varying neutrinos*, *JCAP* **10** (2004) 005, [astro-ph/0309800].

[386] C. Wetterich, *Growing neutrinos and cosmological selection*, *Phys. Lett. B* **655** (2007) 201–208, [0706.4427].

[387] A. Brookfield, C. van de Bruck, D. Mota and D. Tocchini-Valentini, *Cosmology with massive neutrinos coupled to dark energy*, *Phys. Rev. Lett.* **96** (2006) 061301, [astro-ph/0503349].

[388] G. La Vacca and D. F. Mota, *Mass-Varying Neutrino Cosmologies in light of CMB and Weak Lensing measurements*, *Astron. Astrophys.* **560** (2013) A53, [1205.6059].

[389] G. Ballesteros, J. Redondo, A. Ringwald and C. Tamarit, *Standard Model—axion—seesaw—Higgs portal inflation. Five problems of particle physics and cosmology solved in one stroke*, *JCAP* **8** (2017) 001, [1610.01639].

[390] G. Ballesteros, J. Redondo, A. Ringwald and C. Tamarit, *Several Problems in Particle Physics and Cosmology Solved in One SMASH*, *Front. Astron. Space Sci.* **6** (2019) 55, [1904.05594].

[391] H. Motohashi, A. A. Starobinsky and J. Yokoyama, *Matter power spectrum in f(R) gravity with massive neutrinos*, *Prog. Theor. Phys.* **124** (2010) 541–546, [1005.1171].

[392] M. Baldi, F. Villaescusa-Navarro, M. Viel, E. Puchwein, V. Springel and L. Moscardini, *Cosmic degeneracies – I. Joint N-body simulations of modified gravity and massive neutrinos*, *Mon. Not. Roy. Astron. Soc.* **440** (2014) 75–88, [1311.2588].

[393] B. Hu, M. Raveri, A. Silvestri and N. Frusciante, *Exploring massive neutrinos in dark cosmologies with EFTCAMB/ EFTCosmoMC*, *Phys. Rev.* **D91** (2015) 063524, [1410.5807].

[394] A. Barreira, B. Li, C. Baugh and S. Pascoli, *Modified gravity with massive neutrinos as a testable alternative cosmological model*, *Phys. Rev.* **D90** (2014) 023528, [1404.1365].

[395] N. Bellomo, E. Bellini, B. Hu, R. Jimenez, C. Pena-Garay and L. Verde, *Hiding neutrino mass in modified gravity cosmologies*, *JCAP* **02** (2017) 043, [1612.02598].

[396] S. Hagstotz, M. Gronke, D. Mota and M. Baldi, *Breaking cosmic degeneracies: Disentangling neutrinos and modified gravity with kinematic information*, *Astron. Astrophys.* **629** (2019) A46, [1902.01868].

[397] B. S. Wright, K. Koyama, H. A. Winther and G.-B. Zhao, *Investigating the degeneracy between modified gravity and massive neutrinos with redshift-space distortions*, *JCAP* **06** (2019) 040, [1902.10692].

[398] KATRIN collaboration, A. Osipowicz et al., *KATRIN: A Next generation tritium beta decay experiment with sub-eV sensitivity for the electron neutrino mass. Letter of intent*, hep-ex/0109033.

[399] G. Drexlin, V. Hannen, S. Mertens and C. Weinheimer, *Current direct neutrino mass experiments*, *Adv. High Energy Phys.* **2013** (2013) 293986, [1307.0101].

[400] S. Mertens, *Direct Neutrino Mass Experiments*, *J. Phys. Conf. Ser.* **718** (2016) 022013, [1605.01579].

[401] Project 8 collaboration, A. Ashtari Esfahani et al., *Determining the neutrino mass with cyclotron radiation emission spectroscopy—Project 8*, *J. Phys.* **G44** (2017) 054004, [1703.02037].

[402] E. L. Wright et al., *The Wide-field Infrared Survey Explorer (WISE): Mission Description and Initial On-orbit Performance*, *Astron. J.* **140** (2010) 1868, [1008.0031].

[403] L. Yan et al., *Characterizing the Mid-IR Extragalactic Sky with WISE and SDSS*, *Astron. J.* **145** (2013) 55, [1209.2065].

[404] S. Ferraro, B. D. Sherwin and D. N. Spergel, *WISE measurement of the integrated Sachs-Wolfe effect*, *Phys. Rev.* **D91** (2015) 083533, [1401.1193].

[405] M. Zumalacárregui, E. Bellini, I. Sawicki, J. Lesgourgues and P. G. Ferreira, *hi_class: Horndeski in the Cosmic Linear Anisotropy Solving System*, *JCAP* **1708** (2017) 019, [1605.06102].

[406] E. Bellini, I. Sawicki and M. Zumalacárregui, *hi_class: Background Evolution, Initial Conditions and Approximation Schemes*, *JCAP* **2002** (2020) 008, [1909.01828].

[407] E. Bellini et al., *Comparison of Einstein-Boltzmann solvers for testing general relativity*, *Phys. Rev.* **D97** (2018) 023520, [1709.09135].

[408] B. Hu, M. Raveri, N. Frusciante and A. Silvestri, *Effective Field Theory of Cosmic Acceleration: an implementation in CAMB*, *Phys. Rev.* **D89** (2014) 103530, [1312.5742].

[409] M. Raveri, B. Hu, N. Frusciante and A. Silvestri, *Effective Field Theory of Cosmic Acceleration: constraining dark energy with CMB data*, *Phys. Rev.* **D90** (2014) 043513, [1405.1022].

[410] Planck collaboration, R. Adam et al., *Planck 2015 results. I. Overview of products and scientific results*, *Astron. Astrophys.* **594** (2016) A1, [1502.01582].

[411] N. Padmanabhan, X. Xu, D. J. Eisenstein, R. Scalzo, A. J. Cuesta, K. T. Mehta et al., *A 2 per cent distance to z= 0.35 by reconstructing baryon acoustic oscillations–i. methods and application to the sloan digital sky survey*, *Mon. Not. Roy. Astron. Soc.* **427** (2012) 2132–2145, [1202.0090].

[412] M. e. a. Betoule, R. Kessler, J. Guy, J. Mosher, D. Hardin, R. Biswas et al., *Improved cosmological constraints from a joint analysis of the sdss-ii and snls supernova samples*, *Astronomy & Astrophysics* **568** (2014) A22, [1401.4064].

[413] C. de Rham, *Galileons in the Sky*, *Comptes Rendus Physique* **13** (2012) 666–681, [1204.5492].

[414] A. J. Ross, L. Samushia, C. Howlett, W. J. Percival, A. Burden and M. Manera, *The clustering of the SDSS DR7 main Galaxy sample – I. A 4 per cent distance measure at $z = 0.15$*, *Mon. Not. Roy. Astron. Soc.* **449** (2015) 835–847, [1409.3242].

[415] T. Delubac, J. E. Bautista, N. G. Busca, J. Rich, D. Kirkby, S. Bailey et al., *Baryon acoustic oscillations in the Lyα forest of BOSS DR11 quasars*, *AAP* **574** (2015) A59, [1404.1801].

[416] BOSS collaboration, A. Font-Ribera et al., *Quasar-Lyman α Forest Cross-Correlation from BOSS DR11 : Baryon Acoustic Oscillations*, *JCAP* **1405** (2014) 027, [1311.1767].

[417] BOSS collaboration, S. Alam et al., *The clustering of galaxies in the completed SDSS-III Baryon Oscillation Spectroscopic Survey: cosmological analysis of the DR12 galaxy sample*, *Mon. Not. Roy. Astron. Soc.* **470** (2017) 2617–2652, [1607.03155].

[418] L. Verde, *Statistical methods in cosmology*, *Lect. Notes Phys.* **800** (2010) 147–177, [0911.3105].

[419] Planck collaboration, P. A. R. Ade et al., *Planck 2013 results. XIX. The integrated Sachs-Wolfe effect*, *Astron. Astrophys.* **571** (2014) A19, [1303.5079].

[420] Planck collaboration, P. A. R. Ade et al., *Planck 2015 results. XXI. The integrated Sachs-Wolfe effect*, *Astron. Astrophys.* **594** (2016) A21, [1502.01595].

[421] A. J. Shajib and E. L. Wright, *Measurement of the integrated Sachs-Wolfe effect using the AllWISE data release*, *Astrophys. J.* **827** (2016) 116, [1604.03939].

[422] Virgo, LIGO Scientific collaboration, B. Abbott et al., *GW170817: Observation of Gravitational Waves from a Binary Neutron Star Inspiral*, *Phys. Rev. Lett.* **119** (2017) 161101, [1710.05832].

[423] Virgo, Fermi-GBM, INTEGRAL, LIGO Scientific collaboration, B. P. Abbott et al., *Gravitational Waves and Gamma-rays from a Binary Neutron Star Merger: GW170817 and GRB 170817A*, *Astrophys. J.* **848** (2017) L13, [1710.05834].

[424] GROND, SALT Group, OzGrav, DFN, INTEGRAL, Virgo, Insight-Hxmt, MAXI Team, Fermi-LAT, J-GEM, RATIR, IceCube, CAASTRO, LWA, ePESSTO, GRAWITA, RIMAS, SKA South Africa/MeerKAT, H.E.S.S., 1M2H Team, IKI-GW Follow-up, Fermi GBM, Pi of Sky, DWF (Deeper Wider Faster Program), Dark Energy Survey, MASTER, AstroSat Cadmium Zinc Telluride Imager Team, Swift, Pierre Auger, ASKAP, VINROUGE, JAGWAR, Chandra Team at McGill University, TTU-NRAO, GROWTH, AGILE Team, MWA, ATCA, AST3, TOROS, Pan-STARRS, NuSTAR, ATLAS Telescopes, BOOTES, CaltechNRAO, LIGO Scientific, High Time Resolution Universe Survey, Nordic Optical Telescope, Las Cumbres Observatory Group, TZAC Consortium, LOFAR, IPN, DLT40, Texas Tech University, HAWC, ANTARES, KU, Dark Energy Camera GW-EM, CALET, Euro VLBI Team, ALMA collaboration, B. P. Abbott et al., *Multi-messenger Observations of a Binary Neutron Star Merger*, *Astrophys. J.* **848** (2017) L12, [1710.05833].

[425] P. Creminelli and F. Vernizzi, *Dark Energy after GW170817 and GRB170817A*, *Phys. Rev. Lett.* **119** (2017) 251302, [1710.05877].

[426] J. M. Ezquiaga and M. Zumalacárregui, *Dark Energy After GW170817: Dead Ends and the Road Ahead*, *Phys. Rev. Lett.* **119** (2017) 251304, [1710.05901].

[427] J. Sakstein and B. Jain, *Implications of the Neutron Star Merger GW170817 for Cosmological Scalar-Tensor Theories*, *Phys. Rev. Lett.* **119** (2017) 251303, [1710.05893].

[428] H. Wang et al., *The GW170817/GRB 170817A/AT 2017gfo Association: Some Implications for Physics and Astrophysics*, *Astrophys. J.* **851** (2017) L18, [1710.05805].

[429] L. Amendola, M. Kunz, I. D. Saltas and I. Sawicki, *Fate of Large-Scale Structure in Modified Gravity After GW170817 and GRB170817A*, *Phys. Rev. Lett.* **120** (2018) 131101, [1711.04825].

[430] D. Langlois, R. Saito, D. Yamauchi and K. Noui, *Scalar-tensor theories and modified gravity in the wake of GW170817*, *Phys. Rev.* **D97** (2018) 061501, [1711.07403].

[431] C. de Rham and S. Melville, *Gravitational Rainbows: LIGO and Dark Energy at its Cutoff*, *Phys. Rev. Lett.* **121** (2018) 221101, [1806.09417].

[432] F. A. Jenet, G. B. Hobbs, W. van Straten, R. N. Manchester, M. Bailes, J. P. W. Verbiest et al., *Upper bounds on the low-frequency stochastic gravitational wave background from pulsar timing observations: Current limits and future prospects*, *Astrophys. J.* **653** (2006) 1571–1576, [astro-ph/0609013].

[433] K. Kuijken, X. Siemens and T. Vachaspati, *Microlensing by cosmic strings*, *Mon. Not. Roy. Astron. Soc.* **384** (2008) 161–164, [0707.2971].

[434] K. Z. Stanek and P. M. Garnavich, *Distance to M31 with the Hubble Space Telescope and HIPPARCOS Red Clump Stars*, *Astrophys. J. Lett.* **503** (1998) L131–L134, [astro-ph/9802121].

[435] S. A. Rodney et al., *Two Type Ia Supernovae at Redshift 2 : Improved Classification and Redshift Determination with Medium-band Infrared Imaging*, *Astron. J.* **150** (2015) 156, [1508.03100]. [Astron. J.151,47(2016)].

[436] N. Andrei, *Kolmogorov. foundations of the theory of probability*, 1950.

[437] G. Cowan, *Statistical Data Analysis*. Oxford science publications. Clarendon Press, 1998.

[438] F. J. Samaniego, *A comparison of the Bayesian and frequentist approaches to estimation*. Springer Science & Business Media, 2010.

[439] C. Bailer-Jones, *Practical Bayesian Inference: A Primer for Physical Scientists*. Cambridge University Press, 2017.

[440] J. Stanton, *Reasoning with Data: An Introduction to Traditional and Bayesian Statistics Using R*. Guilford Publications, 2017.

[441] L. Verde, *A practical guide to Basic Statistical Techniques for Data Analysis in Cosmology*, 0712.3028.

[442] R. Trotta, *Bayes in the sky: Bayesian inference and model selection in cosmology*, *Contemp. Phys.* **49** (2008) 71–104, [0803.4089].

[443] V. J. Martinez, E. Saar, E. M. Gonzales and M. J. Pons-Borderia, *Data Analysis in Cosmology*, vol. 665. Springer, 2009.

[444] A. Heavens, *Statistical techniques in cosmology*, 0906.0664.

[445] Ž. Ivezić, A. Connolly, J. VanderPlas and A. Gray, *Statistics, Data Mining, and Machine Learning in Astronomy: A Practical Python Guide for the Analysis of Survey Data*. Princeton Series in Modern Observational Astronomy. Princeton University Press, 2014.

[446] R. Trotta, *Bayesian Methods in Cosmology*, 2017, 1701.01467.

[447] GAMBIT Models Workgroup collaboration, P. Athron, C. Balázs, L. A. Dal, J. Edsjö, B. Farmer, T. E. Gonzalo et al., *SpecBit, DecayBit and PrecisionBit: GAMBIT modules for computing mass spectra, particle decay rates and precision observables*, *Eur. Phys. J. C* **78** (2018) 22, [1705.07936].

[448] GAMBIT Flavour Workgroup collaboration, F. U. Bernlochner, M. Chrząszcz, L. A. Dal, B. Farmer, P. Jackson, A. Kvellestad et al., *FlavBit: A GAMBIT module for computing flavour observables and likelihoods*, *Eur. Phys. J. C* **77** (2017) 786, [1705.07933].

[449] GAMBIT Collider Workgroup collaboration, C. Balázs, A. Buckley, L. A. Dal, B. Farmer, P. Jackson, A. Krislock et al., *ColliderBit: a GAMBIT module for the calculation of high-energy collider observables and likelihoods*, *Eur. Phys. J. C* **77** (2017) 795, [1705.07919].

[450] GAMBIT Dark Matter Workgroup collaboration, T. Bringmann, J. Conrad, J. M. Cornell, L. A. Dal, J. Edsjö, B. Farmer et al., *DarkBit: A GAMBIT module for computing dark matter observables and likelihoods*, *Eur. Phys. J. C* **77** (2017) 831, [1705.07920].

[451] M. Chrzaszcz, M. Drewes, T. Gonzalo, J. Harz, S. Krishnamurthy and C. Weniger, *A frequentist analysis of three right-handed neutrinos with GAMBIT*, 1908.02302.

[452] GAMBIT Scanner Workgroup collaboration, G. D. Martinez, J. McKay, B. Farmer, P. Scott, E. Roebber, A. Putze et al., *Comparison of statistical sampling methods with ScannerBit, the GAMBIT scanning module*, *Eur. Phys. J. C* **77** (2017) 761, [1705.07959].

[453] A. Putze and L. Derome, *The Grenoble Analysis Toolkit (GreAT)-A statistical analysis framework*, *Physics of the Dark Universe* **5** (2014) 29–34.

[454] F. Feroz and M. Hobson, *Multimodal nested sampling: an efficient and robust alternative to MCMC methods for astronomical data analysis*, *Mon.Not.Roy.Astron.Soc.* **384** (2008) 449, [0704.3704].

[455] F. Feroz, M. Hobson and M. Bridges, *MultiNest: an efficient and robust Bayesian inference tool for cosmology and particle physics*, *Mon.Not.Roy.Astron.Soc.* **398** (2009) 1601–1614, [0809.3437].

[456] W. J. Handley, M. P. Hobson and A. N. Lasenby, *POLYCHORD: next-generation nested sampling*, *Mon. Not. Roy. Astron. Soc.* **453** (2015) 4384–4398, [1506.00171].

[457] GAMBIT collaboration, P. Athron, C. Balázs, T. Bringmann, A. Buckley, M. Chrząszcz, J. Conrad et al., *GAMBIT: The Global and Modular Beyond-the-Standard-Model Inference Tool*, *Eur. Phys. J. C* **77** (2017) 784, [1705.07908]. Addendum in [561].

[458] A. Kvellestad, P. Scott and M. White, *GAMBIT and its Application in the Search for Physics Beyond the Standard Model*, *to appear in Prog. Part. Nuc. Phys.* (2020) , [1912.04079].

[459] GAMBIT collaboration, P. Athron et al., *Global analyses of Higgs portal singlet dark matter models using GAMBIT*, *Eur. Phys. J. C* **79** (2019) 38, [1808.10465].

[460] S. Hoof, F. Kahlhoefer, P. Scott, C. Weniger and M. White, *Axion global fits with Peccei-Quinn symmetry breaking before inflation using GAMBIT*, *JHEP* **03** (2019) 191, [1810.07192].

[461] GAMBIT collaboration, P. Athron, C. Balázs, T. Bringmann, A. Buckley, M. Chrząszcz, J. Conrad et al., *Status of the scalar singlet dark matter model*, *Eur. Phys. J. C* **77** (2017) 568, [1705.07931].

[462] P. Athron, J. M. Cornell, F. Kahlhoefer, J. McKay, P. Scott and S. Wild, *Impact of vacuum stability, perturbativity and XENON1T on global fits of $\mathbb{Z}_2$ and $\mathbb{Z}_3$ scalar singlet dark matter*, *Eur. Phys. J. C* **78** (2018) 830, [1806.11281].

[463] GAMBIT collaboration, P. Athron, C. Balázs, T. Bringmann, A. Buckley, M. Chrząszcz, J. Conrad et al., *A global fit of the MSSM with GAMBIT*, *Eur. Phys. J. C* **77** (2017) 879, [1705.07917].

[464] GAMBIT collaboration, P. Athron, C. Balázs, T. Bringmann, A. Buckley, M. Chrząszcz, J. Conrad et al., *Global fits of GUT-scale SUSY models with GAMBIT*, *Eur. Phys. J. C* **77** (2017) 824, [1705.07935].

[465] GAMBIT collaboration, P. Athron et al., *Combined collider constraints on neutralinos and charginos*, *Eur. Phys. J. C* **79** (2019) 395, [1809.02097].

[466] J. Bhom, M. Chrzaszcz, F. Mahmoudi, M. Prim, P. Scott and M. White, *A model-independent analysis of $b \to s\mu^+\mu^-$ transitions with GAMBIT's FlavBit*, 2006.03489.

[467] A. Arbey, *AlterBBN: A program for calculating the BBN abundances of the elements in alternative cosmologies*, *Comput. Phys. Commun.* **183** (2012) 1822–1831, [1106.1363].

[468] A. Arbey, J. Auffinger, K. P. Hickerson and E. S. Jenssen, *AlterBBN v2: A public code for calculating Big-Bang nucleosynthesis constraints in alternative cosmologies*, *Comput. Phys. Commun.* **248** (2020) 106982, [1806.11095].

[469] A. Lewis and S. Bridle, *Cosmological parameters from CMB and other data: A Monte Carlo approach*, *Phys. Rev.* **D66** (2002) 103511, [astro-ph/0205436].

[470] A. Lewis, *Efficient sampling of fast and slow cosmological parameters*, *Phys. Rev.* **D87** (2013) 103529, [1304.4473].

[471] B. Audren, J. Lesgourgues, K. Benabed and S. Prunet, *Conservative Constraints on Early Cosmology: an illustration of the Monte Python cosmological parameter inference code*, *JCAP* **1302** (2013) 001, [1210.7183].

[472] T. Brinckmann and J. Lesgourgues, *MontePython 3: boosted MCMC sampler and other features*, *Phys. Dark Univ.* **24** (2019) 100260, [1804.07261].

[473] J. Zuntz, M. Paterno, E. Jennings, D. Rudd, A. Manzotti, S. Dodelson et al., *CosmoSIS: modular cosmological parameter estimation*, *Astron. Comput.* **12** (2015) 45–59, [1409.3409].

[474] O. Buchmueller, R. Cavanaugh, D. Colling, A. de Roeck, M. J. Dolan, J. R. Ellis et al., *Frequentist analysis of the parameter space of minimal supergravity*, *Eur. Phys. J. C* **71** (2011) 1583, [1011.6118].

[475] J. De Blas et al., *HEPfit: a Code for the Combination of Indirect and Direct Constraints on High Energy Physics Models*, *Eur. Phys. J. C* **80** (2019) 456, [1910.14012].

[476] E. Bagnaschi et al., *Likelihood Analysis of the pMSSM11 in Light of LHC 13-TeV Data*, *Eur. Phys. J. C* **78** (2018) 256, [1710.11091].

[477] J. C. Costa et al., *Likelihood Analysis of the Sub-GUT MSSM in Light of LHC 13-TeV Data*, *Eur. Phys. J. C* **78** (2018) 158, [1711.00458].

[478] D. Chowdhury and O. Eberhardt, *Update of Global Two-Higgs-Doublet Model Fits*, *JHEP* **05** (2018) 161, [1711.02095].

[479] C.-W. Chiang, G. Cottin and O. Eberhardt, *Global fits in the Georgi-Machacek model*, *Phys. Rev.* **D99** (2019) 015001, [1807.10660].

[480] Planck collaboration, N. Aghanim et al., *Planck 2015 results. XI. CMB power spectra, likelihoods, and robustness of parameters*, *Astron. Astrophys.* **594** (2016) A11, [1507.02704].

[481] Planck collaboration, N. Aghanim et al., *Planck 2018 results. V. CMB power spectra and likelihoods*, 1907.12875.

[482] M. J. Mortonson, H. V. Peiris and R. Easther, *Bayesian Analysis of Inflation: Parameter Estimation for Single Field Models*, *Phys. Rev.* **D83** (2011) 043505, [1007.4205].

[483] L. C. Price, J. Frazer, J. Xu, H. V. Peiris and R. Easther, *MultiModeCode: An efficient numerical solver for multifield inflation*, *JCAP* **1503** (2015) 005, [1410.0685].

[484] P. Stöcker, M. Krämer, J. Lesgourgues and V. Poulin, *Exotic energy injection with ExoCLASS: Application to the Higgs portal model and evaporating black holes*, *JCAP* **1803** (2018) 018, [1801.01871].

[485] O. Pisanti, A. Cirillo, S. Esposito, F. Iocco, G. Mangano, G. Miele et al., *PArthENoPE: Public Algorithm Evaluating the Nucleosynthesis of Primordial Elements*, *Comput. Phys. Commun.* **178** (2008) 956–971, [0705.0290].

[486] R. Consiglio, P. de Salas, G. Mangano, G. Miele, S. Pastor and O. Pisanti, *PArthENoPE reloaded*, *Comput. Phys. Commun.* **233** (2018) 237–242, [1712.04378].

[487] D. J. Fixsen, *The Temperature of the Cosmic Microwave Background*, *Astrophys. J.* **707** (2009) 916–920, [0911.1955].

[488] R. Easther and H. V. Peiris, *Bayesian analysis of inflation. II. Model selection and constraints on reheating*, *Phys. Rev.* **D85** (2012) 103533, [1112.0326].

[489] K. Freese, J. A. Frieman and A. V. Olinto, *Natural inflation with pseudo nambu-goldstone bosons*, *Phys. Rev. Lett.* **65** (1990) 3233–3236.

[490] F. C. Adams, J. R. Bond, K. Freese, J. A. Frieman and A. V. Olinto, *Natural inflation: Particle physics models, power-law spectra for large-scale structure, and constraints from the cosmic background explorer*, *Phys. Rev. D* **47** (1993) 426.

[491] D. M. Scolnic et al., *The Complete Light-curve Sample of Spectroscopically Confirmed SNe Ia from Pan-STARRS1 and Cosmological Constraints from the Combined Pantheon Sample*, *Astrophys. J.* **859** (2018) 101, [1710.00845].

[492] BICEP2, Keck Array collaboration, P. A. R. Ade et al., *Improved Constraints on Cosmology and Foregrounds from BICEP2 and Keck Array Cosmic Microwave Background Data with Inclusion of 95 GHz Band*, *Phys. Rev. Lett.* **116** (2016) 031302, [1510.09217].

[493] E. A. Kazin et al., *The WiggleZ Dark Energy Survey: improved distance measurements to $z = 1$ with reconstruction of the baryonic*

acoustic feature, *Mon. Not. Roy. Astron. Soc.* **441** (2014) 3524–3542, [1401.0358].

[494] C. Heymans et al., *CFHTLenS tomographic weak lensing cosmological parameter constraints: Mitigating the impact of intrinsic galaxy alignments*, *Mon. Not. Roy. Astron. Soc.* **432** (2013) 2433, [1303.1808].

[495] SDSS collaboration, M. Tegmark et al., *Cosmological Constraints from the SDSS Luminous Red Galaxies*, *Phys. Rev.* **D74** (2006) 123507, [astro-ph/0608632].

[496] B. A. Reid et al., *Cosmological Constraints from the Clustering of the Sloan Digital Sky Survey DR7 Luminous Red Galaxies*, *Mon. Not. Roy. Astron. Soc.* **404** (2010) 60–85, [0907.1659].

[497] D. Parkinson et al., *The WiggleZ Dark Energy Survey: Final data release and cosmological results*, *Phys. Rev.* **D86** (2012) 103518, [1210.2130].

[498] Particle Data Group collaboration, M. Tanabashi et al., *Review of Particle Physics*, *Phys. Rev.* **D98** (2018) 030001.

[499] B. Audren, J. Lesgourgues, S. Bird, M. G. Haehnelt and M. Viel, *Neutrino masses and cosmological parameters from a Euclid-like survey: Markov Chain Monte Carlo forecasts including theoretical errors*, *JCAP* **2013** (2013) 026, [1210.2194].

[500] T. Sprenger, M. Archidiacono, T. Brinckmann, S. Clesse and J. Lesgourgues, *Cosmology in the era of Euclid and the Square Kilometre Array*, *JCAP* **2019** (2019) 047, [1801.08331].

[501] A. Chudaykin, M. M. Ivanov and M. Simonović, *CLASS-PT: non-linear perturbation theory extension of the Boltzmann code CLASS*, 2004.10607.

[502] T. R. Slatyer, *Indirect Dark Matter Signatures in the Cosmic Dark Ages II. Ionization, Heating and Photon Production from Arbitrary Energy Injections*, *Phys. Rev.* **D93** (2016) 023521, [1506.03812].

[503] H. Liu, G. W. Ridgway and T. R. Slatyer, *Code package for calculating modified cosmic ionization and thermal histories with dark matter and other exotic energy injections*, *Phys. Rev.* **D101** (2020) 023530, [1904.09296].

[504] I. Esteban, M. C. Gonzalez-Garcia, M. Maltoni, I. Martinez-Soler and T. Schwetz, *NuFit 3.2*, . http://www.nu-fit.org (accessed June 04, 2020).

[505] I. Esteban, M. C. Gonzalez-Garcia, M. Maltoni, I. Martinez-Soler and T. Schwetz, *Updated fit to three neutrino mixing: exploring the accelerator-reactor complementarity*, *JHEP* **01** (2017) 087, [1611.01514].

[506] Particle Data Group collaboration, K. A. Olive et al., *Review of Particle Physics*, update to Ref. [562] (2017) .

[507] R. J. Cooke, M. Pettini and C. C. Steidel, *One Percent Determination of the Primordial Deuterium Abundance*, *Astrophys. J.* **855** (2018) 102, [1710.11129].

[508] A. Loureiro et al., *On The Upper Bound of Neutrino Masses from Combined Cosmological Observations and Particle Physics Experiments*, *Phys. Rev. Lett.* **123** (2019) 081301, [1811.02578].

[509] A. Loureiro et al., *Cosmological measurements from angular power spectra analysis of BOSS DR12 tomography*, *Mon. Not. Roy. Astron. Soc.* **485** (2019) 326–355, [1809.07204].

[510] S. Vagnozzi, E. Giusarma, O. Mena, K. Freese, M. Gerbino, S. Ho et al., *Unveiling ν secrets with cosmological data: neutrino masses and mass hierarchy*, *Phys. Rev.* **D96** (2017) 123503, [1701.08172].

[511] M. Schwarzschild, *Structure and Evolution of Stars*. Princeton Legacy Library. Princeton University Press, 2015.

[512] V. C. Rubin and W. K. Ford, Jr., *Rotation of the Andromeda Nebula from a Spectroscopic Survey of Emission Regions*, *Astrophys. J.* **159** (1970) 379–403.

[513] V. C. Rubin, W. K. Ford, Jr. and N. Thonnard, *Extended rotation curves of high-luminosity spiral galaxies. IV. Systematic dynamical properties, Sa through Sc*, *Astrophys. J.* **225** (1978) L107–L111.

[514] V. C. Rubin, N. Thonnard and W. K. Ford, Jr., *Rotational properties of 21 SC galaxies with a large range of luminosities and radii, from NGC 4605 /R = 4kpc/ to UGC 2885 /R = 122 kpc/*, *Astrophys. J.* **238** (1980) 471.

[515] V. C. Rubin, W. K. Ford, Jr., N. Thonnard and D. Burstein, *Rotational properties of 23 SB galaxies*, *Astrophys. J.* **261** (1982) 439.

[516] V. C. Rubin, D. Burstein, W. K. Ford, Jr. and N. Thonnard, *Rotation velocities of 16 SA galaxies and a comparison of Sa, Sb, and SC rotation properties*, *Astrophys. J.* **289** (1985) 81.

[517] L. Lombriser and A. Taylor, *Breaking a Dark Degeneracy with Gravitational Waves*, *JCAP* **1603** (2016) 031, [1509.08458].

[518] D. Bettoni, J. M. Ezquiaga, K. Hinterbichler and M. Zumalacárregui, *Speed of Gravitational Waves and the Fate of Scalar-Tensor Gravity*, *Phys. Rev.* **D95** (2017) 084029, [1608.01982].

[519] LSST Science, LSST Project collaboration, P. A. Abell et al., *LSST Science Book, Version 2.0*, 0912.0201.

[520] H. Baer, K.-Y. Choi, J. E. Kim and L. Roszkowski, *Dark matter production in the early Universe: beyond the thermal WIMP paradigm*, *Phys. Rept.* **555** (2015) 1–60, [1407.0017].

[521] M. Klasen, M. Pohl and G. Sigl, *Indirect and direct search for dark matter*, *Prog. Part. Nucl. Phys.* **85** (2015) 1–32, [1507.03800].

[522] P. W. Graham, I. G. Irastorza, S. K. Lamoreaux, A. Lindner and K. A. van Bibber, *Experimental Searches for the Axion and Axion-Like Particles*, *Ann. Rev. Nucl. Part. Sci.* **65** (2015) 485–514, [1602.00039].

[523] G. Bertone and M. Tait, Tim, *A new era in the search for dark matter*, *Nature* **562** (2018) 51–56, [1810.01668].

[524] I. G. Irastorza and J. Redondo, *New experimental approaches in the search for axion-like particles*, *Prog. Part. Nucl. Phys.* **102** (2018) 89–159, [1801.08127].

[525] DESI collaboration, M. Levi et al., *The DESI Experiment, a whitepaper for Snowmass 2013*, 1308.0847.

[526] D. Spergel, N. Gehrels, C. Baltay, D. Bennett, J. Breckinridge, M. Donahue et al., *Wide-field infrarred survey telescope-astrophysics focused telescope assets wfirst-afta 2015 report*, 1503.03757.

[527] Euclid collaboration, R. Laureijs, J. Amiaux, S. Arduini, J.-L. Augueres, J. Brinchmann et al., *Euclid Definition Study Report*, 1110.3193.

[528] SKA Cosmology SWG collaboration, R. Maartens, F. B. Abdalla, M. Jarvis and M. G. Santos, *Overview of Cosmology with the SKA*, *PoS* **AASKA14** (2015) 016, [1501.04076].

[529] B. Iyer, T. Souradeep, C. Unnikrishnan, S. Dhurandhar, S. Raja, A. Sengupta et al., *Ligo-india, Report No. LIGO-M1100296 (Indian Initiative in Gravitational-wave Observations, 2011)* (2011) .

[530] KAGRA collaboration, K. Somiya, *Detector configuration of KAGRA: The Japanese cryogenic gravitational-wave detector*, *Class. Quant. Grav.* **29** (2012) 124007, [1111.7185].

[531] CMB-S4 collaboration, K. N. Abazajian et al., *CMB-S4 Science Book, First Edition*, 1610.02743.

[532] CMB-S4 collaboration, M. H. Abitbol et al., *CMB-S4 Technology Book, First Edition*, 1706.02464.

[533] K. Abazajian et al., *CMB-S4 Science Case, Reference Design, and Project Plan*, 1907.04473.

[534] K. Abazajian et al., *CMB-S4 Decadal Survey APC White Paper*, *Bull. Am. Astron. Soc.* **51** (2019) 209, [1908.01062].

[535] EDELWEISS collaboration, Q. Arnaud et al., *Optimizing EDELWEISS detectors for low-mass WIMP searches*, *Phys. Rev.* **D97** (2018) 022003, [1707.04308].

[536] PandaX collaboration, H. Zhang et al., *Dark matter direct search sensitivity of the PandaX-4T experiment*, *Sci. China Phys. Mech. Astron.* **62** (2019) 31011, [1806.02229].

[537] DEAP collaboration, R. Ajaj et al., *Search for dark matter with a 231-day exposure of liquid argon using DEAP-3600 at SNOLAB*, *Phys. Rev.* **D100** (2019) 022004, [1902.04048].

[538] LUX collaboration, D. Akerib et al., *Results of a Search for Sub-GeV Dark Matter Using 2013 LUX Data*, *Phys. Rev. Lett.* **122** (2019) 131301, [1811.11241].

[539] XENON collaboration, E. Aprile et al., *Dark Matter Search Results from a One Ton-Year Exposure of XENON1T*, *Phys. Rev. Lett.* **121** (2018) 111302, [1805.12562].

[540] VERITAS collaboration, J. Holder et al., *The first VERITAS telescope*, *Astropart. Phys.* **25** (2006) 391–401, [astro-ph/0604119].

[541] Fermi-LAT collaboration, W. Atwood et al., *The Large Area Telescope on the Fermi Gamma-ray Space Telescope Mission*, *Astrophys. J.* **697** (2009) 1071–1102, [0902.1089].

[542] HESS collaboration, A. Abramowski et al., *Search for a Dark Matter annihilation signal from the Galactic Center halo with H.E.S.S*, *Phys. Rev. Lett.* **106** (2011) 161301, [1103.3266].

[543] PAMELA collaboration, O. Adriani et al., *Cosmic-Ray Positron Energy Spectrum Measured by PAMELA*, *Phys. Rev. Lett.* **111** (2013) 081102, [1308.0133].

[544] AMS collaboration, M. Aguilar et al., *Electron and Positron Fluxes in Primary Cosmic Rays Measured with the Alpha Magnetic Spectrometer on the International Space Station*, *Phys. Rev. Lett.* **113** (2014) 121102.

[545] IceCube collaboration, M. Aartsen et al., *PINGU: A Vision for Neutrino and Particle Physics at the South Pole*, *J. Phys. G* **44** (2017) 054006, [1607.02671].

[546] F. Kahlhoefer, *Review of LHC Dark Matter Searches*, *Int. J. Mod. Phys. A* **32** (2017) 1730006, [1702.02430].

[547] B. Penning, *The pursuit of dark matter at colliders—an overview*, *J. Phys. G* **45** (2018) 063001, [1712.01391].

[548] A. Boveia and C. Doglioni, *Dark Matter Searches at Colliders*, *Ann. Rev. Nucl. Part. Sci.* **68** (2018) 429–459, [1810.12238].

[549] MiniBooNE collaboration, A. Aguilar-Arevalo et al., *A Combined $\nu_\mu \to \nu_e$ and $\bar{\nu}_\mu \to \bar{\nu}_e$ Oscillation Analysis of the MiniBooNE Excesses*, 2012, 1207.4809.

[550] M. Agostini et al., *Background-free search for neutrinoless double-β decay of ^{76}Ge with GERDA*, *Nature* **544** (2017) 47, [1703.00570].

[551] PIENU collaboration, M. Aoki et al., *Search for Massive Neutrinos in the Decay $\pi \to e\nu$*, *Phys. Rev.* **D84** (2011) 052002, [1106.4055].

[552] KamLAND-Zen collaboration, A. Gando et al., *Search for Majorana Neutrinos near the Inverted Mass Hierarchy Region with KamLAND-Zen*, *Phys. Rev. Lett.* **117** (2016) 082503, [1605.02889]. [Addendum: Phys. Rev. Lett.117,no.10,109903(2016)].

[553] CUORE collaboration, C. Alduino et al., *First Results from CUORE: A Search for Lepton Number Violation via $0\nu\beta\beta$ Decay of ^{130}Te*, *Phys. Rev. Lett.* **120** (2018) 132501, [1710.07988].

[554] NEXT collaboration, J. Renner et al., *Initial results on energy resolution of the NEXT-White detector*, *JINST* **13** (2018) P10020, [1808.01804].

[555] NEMO-3 collaboration, R. Arnold et al., *Search for neutrinoless quadruple-β decay of ^{150}Nd with the NEMO-3 detector*, *Phys. Rev. Lett.* **119** (2017) 041801, [1705.08847].

[556] EXO-200 collaboration, G. Anton et al., *Search for Neutrinoless Double-β Decay with the Complete EXO-200 Dataset*, *Phys. Rev. Lett.* **123** (2019) 161802, [1906.02723].

[557] S. Joudaki et al., *KiDS-450: Testing extensions to the standard cosmological model*, *Mon. Not. Roy. Astron. Soc.* (2016) , [1610.04606].

[558] A. Font-Ribera, P. McDonald, N. Mostek, B. A. Reid, H.-J. Seo and A. Slosar, *DESI and other dark energy experiments in the era of neutrino mass measurements*, *JCAP* **05** (2014) 023, [1308.4164].

[559] BOSS collaboration, L. Anderson et al., *The clustering of galaxies in the SDSS-III Baryon Oscillation Spectroscopic Survey: baryon acoustic oscillations in the Data Releases 10 and 11 Galaxy samples*, *Mon. Not. Roy. Astron. Soc.* **441** (2014) 24–62, [1312.4877].

[560] S. Bloor, T. E. Gonzalo and P. Scott, *GAMBIT Universal Models: Interfacing GAMBIT with Lagrangian level tools*, *in preparation* (2020) .

[561] GAMBIT collaboration, P. Athron, C. Balázs, T. Bringmann, A. Buckley, M. Chrząszcz, J. Conrad et al., *GAMBIT: The Global and Modular Beyond-the-Standard-Model Inference Tool. Addendum for GAMBIT 1.1: Mathematica backends, SUSYHD interface and updated likelihoods*, *Eur. Phys. J. C* **78** (2018) 98, [1705.07908]. Addendum to [457].

[562] Particle Data Group collaboration, C. Patrignani et al., *Review of Particle Physics*, *Chin. Phys. C* **40** (2016) 100001.